2014

DEPARTAMENTO DE CIÊNCIAS DA VIDA

FACULDADE DE CIÊNCIAS E TECNOLOGIA
UNIVERSIDADE DE COIMBRA

The role of the Ubiquitin-Proteasome system and Autophagy in Tau clearance in primary neurons

The role of the Ubiquitin-Proteasome system and Autophagy in Tau clearance in primary neurons

Marcos Schaan Profes

2014

Marcos Schaan Profes

DEPARTAMENTO DE CIÊNCIAS DA VIDA

FACULDADE DE CIÊNCIAS E TECNOLOGIA
UNIVERSIDADE DE COIMBRA

The role of the Ubiquitin-Proteasome system and Autophagy in Tau clearance in primary neurons

Dissertação apresentada à Universidade de Coimbra para o cumprimento dos requisitos necessários à obtenção do grau de Mestre em Biologia Celular e Molecular, realizada sob a orientação científica do Doutor Diederik Moechars (Janssen Pharmaceutica NV) e da Professora Doutora Ana Luisa Carvalho (Universidade de Coimbra)

Marcos Schaan Profes

2014

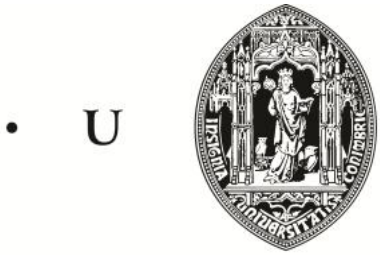

The work presented in this thesis resulted from a partnership between the University of Coimbra and Janssen. All experimental activities were performed at Janssen Beerse I, a Johnson & Johnson pharmaceutical research and development facility in Beerse, Belgium, under the supervision of Dr. Diederik Moechars, Dr. Agnieszka Sadowska and Dr. Ana Luisa Carvalho.

Beerse, 2014

Acknowledgments

I would like to thank Dieder, for giving me the opportunity to join his group and for the effort to make this possible since I was in Portugal. Additionally, I appreciate the enthusiasm, support and scientific discussions. It was a pleasure and a very rewarding opportunity to me to learn from you.

Aga, thanks for sharing this project with me and for the guidance. I'll never forget how it was to work with you.

To all the members of Tau group, thank you for all the scientific support, as well all the help and the availability that you gave me. I would especially like to thank to Guy and Marc for everything. If it weren't you for sure this thesis wouldn't be finished as it is.

A special thanks to my parents, that since I was born made a huge effort to put me where I am now. If weren't for you, for sure, I wouldn't accomplish and be half of what I already did and am.

Lastly, Isy, thanks for sharing my dreams with me. If weren't for your support, joy, friendship and love, I would never have the motivation to go further and further. There are no words to proper thank you for your influence in my life!

Thank you all!

RESUMO

A acumulação intraneuronal e dendrítica da proteína associada aos microtúbulos Tau é uma característica proeminente de múltiplas desordens do sistema nervoso central, entre as quais a doença de Alzheimer, demência frontotemporal com parkinsonismo -17 e a doença de Pick [1-3]. Durante a progressão dessas doenças, normalmente a proteína Tau solúvel se combina formando oligômeros, que por sua vez se agregam formando os insolúveis emaranhados neurofibrilares e filamentos do neurópilo [1-3]. A ocorrência de inclusões fibrilares intraneurais de Tau nessas doenças sugere que elas possuam um papel nos sintomas clínicos e patologias observados, indicando um possível uso para terapias com a finalidade de degradar espécias tóxicas ou patológicas da Tau [1-3].

As células são equipadas com dois principais mecanismos para degradação protéica: o proteassoma e a autofagia [4-7]. Proteínas destinadas à degradação pelo proteassoma são ubiquitinadas e subsequentemente degradadas [8]. Estudos demonstraram que ambos o preteassoma completo 26S e o núcelo ativo 20S do proteassoma podem degradar a Tau recombinante [6, 9]. Além disto, atividade reduzida do proteassoma foi associada com envelhecimento e é comum em doenças neurodegenerativas [10].

Alternativamente, as células podem degradar proteínas e outros materiais celulares pela autofagia [7]. Proteínas degradadas pela autofagia são encapsuladas em autofagossomas, que são subsequentemente fundidos com lisossomas, culminando com degradação do seu conteúdo [7]. Há evidências de que agregados de Tau podem ser degradados pela autofagia, e a inibição desse processo resulta em níves de agregados de Tau aumentados, assim como toxicidade neuronal [6]. Consequentemente, a avaliação dos papéis do proteassoma e da autofagia na degradação de agregados da Tau *in vitro* é de grande importância.

No presente estudo, nós otimizamos um modelo celular de agregação de Tau em neurônios no qual fibrilas pré-agregadas sinteticamente produzidas a partir de Tau recombinante (K18P301L) introduzidas nas células podem recrutar a Tau solúvel endógena transformando-a em agregados insolúveis, resultando em um modelo mais adequado a triagens de alta produtividade. Este modelo foi então utilizado como plataforma para caracterizar cineticamente as atividades do proteassoma e da autofagia em culturas primárias de neurônios mediante a indução da agregação da proteína Tau. Como resultado, nós demonstramos que a agregação da Tau induz ativação dependente do tempo do proteassoma e autofagia. Além da caracterização mencionada, os papéis do proteassoma e da autofagia foram avaliados a partir do uso de compostos de referência que inibem a atividade do proteassoma e induzem a atividade da autofagia, nomeadamente: MG132, Lactacistina e Rapamicina. A partir dessa abordagem farmacológica foi possível observar que a autofagia, quando induzida antes da indução da aggregação da proteína Tau, parece ter um papel importante na degradação da forma solúvel da Tau. Nossos resultados também sugerem que o proteassoma parece ser secundário na degradaçãdo da Tau, mas, apesar disso, pode estar trabalhando em conjunto com a autofagia, resultando na degradação de agregados da Tau. Essas observações são baseadas nos fatos de que a inibição do proteassoma não resultou em acumulação da Tau e de que a indução da autofagia resultou em degradação dos aggregados de Tau somente na presença de um proteassoma funcional. Por último, os nossos resultados preliminares da regulação negativa das enzimas OTUB1, USP5 e USP7, as quais interagem com a proteína Tau no cérebro de camundongo [11], indicam que nem a OTUB1 nem a USP5 parecem influenciar os níveis da Tau *in vitro*. Por outro lado, a regulação negativa da USP7 resultou em aumento da agregação da Tau, o que indica um possível papel dessa enzima de deubiquitinação na regulação da degradação da proteína Tau em culturas primárias de neurônios.

Apesar de esse estudo ter sido um passo inicial importante para entender o papel do proteassoma e da autofagia na degradação da Tau *in vitro*, estudos adicionais para melhor mensurar a contribuição desses mecanismos de degradação são necessários. Considerando isso, estudos *in vitro,* nos quais as variáveis podem ser rigorosamente controladas, serão instrumentais devido à complexidade do ambiente celular. Fundamentalmente, uma compreensão mais completa da contribuição de cada um dos mecanismos de

degradação protéica resultará em novas oportunidades para lidar terapeuticamente com a patologia da proteína Tau associada com a neurodegeneração em Tauopatias.

Key words: Tau, proteassoma, autofagia, degradação, culturas primárias de neurônios, Tauopatia.

ABSTRACT

Intraneuronal and dendritic accumulation of the microtubule-associated protein Tau is a prominent characteristic of multiple CNS disorders including Alzheimer's disease, frontotemporal dementia with Parkinsonism -17 (FTDP-17) and Pick's disease [1-3]. During the progression of these diseases, normally soluble Tau combines to form oligomers, which then aggregate to form insoluble neurofibrillary tangles (NFTs) and neuropil threads [1-3]. The occurrence of intraneuronal fibrillar Tau inclusions in these diseases suggests they play a role in the observed clinical symptoms and pathology, and implies that therapies aimed at degrading toxic or pathologic Tau species may be of potential use [1-3].

Cells are equipped with two general mechanisms to degrade proteins: the ubiquitin–proteasome system and autophagy [4-7]. Proteins that are destined for degradation via the proteasome are ubiquitinated and subsequently broken down [8]. Previous studies have shown that both the complete 26S proteasome as well as the active 20S proteasome core can degrade recombinant Tau [6, 9]. Moreover, reduced proteasome activity is associated with aging and is common in neurodegenerative diseases [10].

Alternatively, cells may degrade proteins and cellular material via the process of autophagy [7]. Proteins targeted for degradation via autophagy are encapsulated in autophagosomes that are subsequently fused to lysosomes with their degradation as a final outcome [7]. There is evidence that Tau aggregates can be cleared through autophagy, and inhibition of autophagy leads to an increased level of aggregated Tau as well as neurotoxicity [6]. . Consequently evaluating the roles of the ubiquitin-proteasome system and autophagy in the clearance of aggregated Tau *in vitro* is of major importance.

In this study, we optimized a neuronal Tau aggregation cellular model wherein synthetic pre-aggregated fibrils made from recombinant protein (K18P301L) introduced into cells can recruit soluble endogenous Tau into insoluble fibrillar aggregates, making it more suitable for future High Throughput Screens. Such model was then used as a platform to kinetically characterize the UPS and autophagy activities in primary neurons upon Tau aggregation. Interestingly, we showed that Tau aggregation induce temporal-dependent UPS and autophagy. We further validated the role of UPS and autophagy in Tau clearance by means of use of reference compounds known to inhibit UPS activity and to induce autophagy activity namely: MG132, Lactacystin and Rapamycin. By such pharmacological approach we could observe that autophagy seems to play a pivotal role in clearing soluble Tau species when induced, before Tau aggregation induction. Our results also suggest that UPS seems to be a secondary player in Tau clearance, but might be working together with autophagy resulting in aggregates clearance. Such observation is based on the results that upon UPS inhibition Tau accumulation did not occur and by the fact that only in the presence of a functional UPS induction of autophagy was able to clear aggregated Tau. Lastly, by knockingdown the deubiquitinating enzymes OTUB1, USP5 and USP7 that were shown to interact with Tau in the mouse brain [11], our preliminary results indicate that neither OTUB1 nor USP5 seem to influence Tau levels *in vitro*. On the other hand, USP7 ablation resulted in further Tau aggregation indicating a possible role of such DUB in regulating Tau degradation in primary neurons *in vitro*.

Although this study made an important initial step toward elucidating the role of UPS and autophagy in Tau degradation *in vitro*, further studies that better gauge the contribution of each degradative pathway will be necessary. In view of this observation, *in vitro* studies that can tightly control for variables including Tau modifications and proteolytic pathway function will likely be instrumental due to the complexity of the cellular environment. Fundamentally, a more complete understanding of the differential contribution of various proteolytic and degradative pathways will provide critical opportunities for therapeutically addressing the Tau pathology associated with neurodegeneration in tauopathies.

Key words: Tau, UPS, autophagy, clearance, primary neurons, Tauopathy.

INDEX

ABBREVIATION LIST

3-MA – 3-methyladenine

AAV6hTauP301L – adenoassociated virus serotype 6 encoding human full-lenght Tau containing P301L mutation under the synapsin 1 promoter

AD – Alzheimer's disease

AGE – Advanced Glycation end-product

Akt – Akt kinase or protein kinase B

α7nAChR – α7 nicotinic acetylcholine receptor

ALS - amyotrophic lateral sclerosis

AMPA - -amino-3-hydroxy-5-methyl-4-isoxazole propionic acid)-type glutamate receptors

ANOVA – Analysis of variance

APOE - apolipoprotein

APP - amyloid precursor protein

ATP – adenosine tri-phosphate

Aβ – amyloid beta

B27 – serum free suplement

BCA assay – bicinchoninic acid assay

Bis-Tris – 2-Bis(2-hydroxyethyl)amino-2-(hydroxymethyl)-1,3-propanediol. Bis(2- hydroxyethyl)amino-tris(hydroxymethyl)methane

BSA – bovine serum albumin

CAT – cationic amphiphilic tracer

CBD - corticobasal degeneration

CdK5 – cyclin-dependent kinase 5

CFS – cerebrospinal fluid

CHIP - carboxyl terminus of the Hsc70-interacting protein

CHMP2B - multivesicular body protein 2B

CMA – chaperone mediated autophagy

CNS – central nervous system

COS7 - Monkey Kidney Cells

DAS – day after seeding

DIV – day *in vitro*

DMSO – Dimethyl sulfoxide

DNA - Deoxyribonucleic acid

DUB – Deubiquitinating enzyme

E – embryonic day

ECL – enhanced chemiluminescence

EGF - epithelial growth factor

eGFP – enhanced green fluorescent protein

ELISA – Enzyme-Linked Immunosorbent Assay

ER – endoplasmic reticulum

FOXO – forkhead box O (FOXO) family of transcription factors

FPRL1 - formyl-peptide receptor-like-1

FRET - Fluorescence Resonance Energy Transfer

FTD - frontemporal lobe dementias

FTDP-17 - frontotemporal dementia with Parkinsonism -17

Fyn – Fyn kinase

GRN - progranulin

GSK3β - Glycogen synthase kinase bet

HBSS – Hank's Balanced Salt Solution

HEK293 –

HKGs – house keeping genes

HRP – hosedish peroxidase

Hsp70 - Heat shock protein 70

HSV – herpes simplex virus

HT7/hTau10 – alphaLISA antibody sandwich: biotinylated HT7/hTau10 conjugated to acceptor beads

hTau – human Tau

hTau10/hTau10 – alphaLISA antibody sandwich: biotinylated hTau10/hTau10 conjugated to acceptor beads

hTauP301L - human full-lenght Tau containing P301L mutation

hTauP301S – human full-lenght Tau containing P301S mutation

JIP1 - c-Jun-N-terminal kinase interacting protein 1

JNK - c-Jun N-terminal kinase

K18P301L - pre-fibrillized Tau seeds (truncated form of human Tau containing only the 4 MT- binding domains, K18, with a P301L point mutation)

LC3 – Microtubule-associated protein 1A/1B-light chain 3

LDS – lithium dodecyl sulfate

K – Lysine

M1/M3 - muscarinic M1/M3 receptors

MAP - Mitogen-activated protein

MAP-2 – Microtubule-associated protein 2

MAP1B - microtubule-associated protein 1B

MAPT – Tau gene

MARK - microtubule affinity regulating kinase

MEM – minimum essential media

MES buffer – MES electrophoretic buffer

MetOH – methanol

MOI – multiplicity of infection

MOPS buffer– MOPS electrophoretic buffer

MT – microtubule

mTOR – mammalian target of rapamycin

N – number of independent experiments

n – number of replicates

N2a – mouse Neuroblastoma derived cells

NFDM – non-fat dry milk

NFT – neurofibrillary tangle

NGF - nerve growth factor

NMDA - N-methyl D aspartate receptor

Nrf2 – factor-erythroid 2-related factor 2

OTUB - ovarian tumor proteases

OUTB1 - Ovarian tumor domain-containing ubiquitin aldehyde-binding protein 1

OXPHOS - Oxidative phosphorylation

P301L – Tau P301L mutation

P301S – Tau P301S mutation

p38 – p38 mitogen-activated protein kinase

PBS – Phosphate buffered saline

PBS-T – Phosphate Buffered Saline (PBS) solution with the detergent Tween® 20

PC-12 – PC-12ell line derived from a pheochromocytoma of the rat adrenal medulla

PCR – polymerase chain reaction

PET – positron emission tomography

PHF – paired helical filament

PiD – Pick's disease

Pin1 - peptidyl prolyl isomerase

PKA - cAMP-dependent protein kinase or protein kinase A

PLC γ - phospholipase C γ

PP2A - phosphatase 2A

PS19hTauP301S - transgenic mice overexpressing P301S human Tau (strain: B6;C3-Tg(Prnp-MAPT*P301S)PS19Vle/J)

Pro - proline

PSD-95 - postsynaptic density protein 95

PSEN1 - presenilin 1

PSEN2 - presenilin 2

PSP - Progressive supranuclear palsy

PTEN – Phosphatase and tensin homolog

RAGE - receptor for advanced glycation end products

RIPA buffer– Radio-Immunoprecipitation Assay Buffer

RNA - Ribonucleic acid

ROS – reactive oxygen species

rpm – rotations per minute

Sarkosyl – Sodium lauroyl sarcosinate

SDS-PAGE – sodium dodecyl sulfate polyacrylamide gel electrophoresis

Ser- serine

SH-SY5Y - neuroblastoma cell line

SH3 - SRC Homology 3 Domain

shRNA – short hairpin RNA

siRNA - Small interfering RNA

SYN1 – neuronal SYN1 promotor (synapsin 1)

TBS-T – Tris-Buffered Saline and Tween 20

Thr – threonine

TMB – 3,3',5,5'-tetramethylbenzidine

TNAP - tissue-non-specific alkaline phosphatase

UPS – ubiquitin-proteasome system

UPS5 - Ubiquitin-specific proteases 5 or isopeptidase T

UPS7 - Ubiquitin-specific peptidase 7

UPS9X - Ubiquitin Specific Peptidase 9, X-Linked

VCP - valosin containing protein gene

WT – wistar rat

β3-Tubulin – neuron specific Class III β-tubulin

ΔK280 – ΔK280 Tau mutation

1 INTRODUCTION

1.1 Neurodegenerative Tauopathies

Increased longevity and aging populations are a reality in western countries. As a consequence, incidences of age-related diseases are increasing substantially with high burdens for the individuals and for the society. Interestingly, the proportion of deaths resulting from diseases of age, like cancer, heart disease and stroke, have been lowered due to technological advances, whereas the proportion resulting from Alzheimer's disease (AD) increased 68% (from 2000 to 2010) [12]. Unfortunatelly, the current panorama and future perspectives regarding age-related dementias incidences are not good and it tends to soar [12].

Dementia syndrome is a highly prevalent neurodegenerative condition and it is seriously disabling for the carriers and it is often devastating for their caregivers and families [13, 14]. Alzheimer's disease and other dementia are exceptional in size, impact and costs, and thus leading with them is an actual global health challenge [12]. In 2010, 35.6 million of people worldwide were estimated to carry AD and related dementias [12, 15](Figure 1).

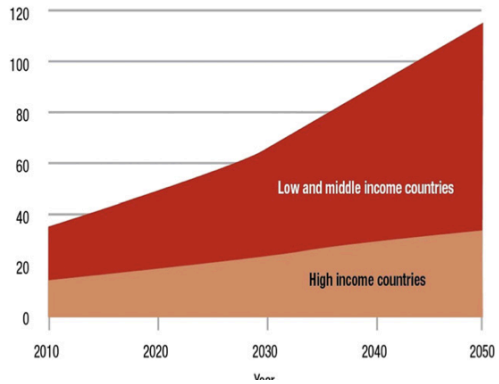

Figure 1: The growth in numbers of people with dementia (in milions) by country income. [15]

Over the last decades, progresses in histological and molecular methods have improved the understanding of these conditions and the mechanisms that lead to cell death [3]. It is now clear that many neurodegenerative disorders are characterized by intraneuronal deposition of insoluble proteins in addition to neuronal loss [2, 3, 16]. Thus, it is possible to classify these disorders by the characteristics of the insoluble proteins that accumulates within the neurons (and also glial and muscle cells), rather than just by their clinical and histological features [2, 3, 16]. Several intraneuronal inclusions have been described, such as Hirano bodies, Lewy bodies, Pick bodies, but neurofibrillary tangles (NFTs) are the most common [16]. NFTs, as it will be later described, are prominent intracellular accumulations of abnormal filaments formed by the microtubule-associated protein Tau (Tau) [1-3, 10, 16, 17] and their prominent appearance lead to the grouping of several heterogeneous dementias and movement disorders: the neurodegenerative Tauopathies [1-3, 16]. Of particular interest is that these inclusions are also seen, although in less extent, in the progression of normal aging [16]. This particular pathological feature is consistently found in the well characterized Alzheimer's disease (AD), progressive supranuclear palsy (PSP), corticobasal degeneration (CBD), Pick's disease (PiD), frontotemporal dementia and parkinsonism linked to chromosome 17 (FTDP-17), among others [2, 3, 16]. Tauopathies, despite having a diverse array of phenotypic manifestations, present brain dysfunction and degeneration linked to the progressive accumulation of filamentous Tau inclusions [1-3, 16]. This particular fact in addition to the lack of other disease-specific neuropathological abnormalities, provided circumstantial evidence that abnormal Tau is implicated in the diseases onset and/or progression [2]. In 1998, multiple mutations were discovered in the Tau gene – *MAPT* – in frontotemporal dementia and parkinsonism linked to chromosome 17 (FTDP-17), which provided unequivocal prove that Tau abnormalities alone are sufficient to cause neurodegenerative diseases [2].

1.1.1 Alzheimer's disease (AD)

AD is the most prevalent form of dementia syndrome accounting for 50% to 80% of the total dementia cases [3, 13, 14, 18] and it is the sixth leading cause of death in the United States [12]. It is a heterogeneous condition that share common clinical symptoms that manifests as progressive memory loss and cognitive impairments [3, 19-24], being age the greatest risk factor followed by family history [25]. This senile form of dementia is genetically complex and heterogeneous and seems to follow an age-related dichotomy with rare and highly penetrant mutations (e.g. amyloid precursor protein gene – APP -, presenilin 1 gene - PSEN1 - and presenilin 2 gene - PSEN2 - mutations) that are transmitted in an autosomal dominant fashion leading to the early onset familial AD; while common polymorphisms with relatively low penetrance, but highly prevalent, lead to increased risk for the late onset AD without Mendelian inheritance (e.g. apolipoprotein gene APOE mutation) [3, 25]. This age-related syndrome results from dysfunction and death of specific neuronal populations, particularly those involved with memory, cognition and self-reflection which finally results in severe brain atrophy [20, 23, 24]. Two or more cognitive domains affected (including memory impairment and at least one of language, visuospatial function, exectutive function and praxis) are required for diagnosis [3]. Unfortunatelly, due to its complex etiology, pharmacological curative treatments have not been identified yet for AD [26].

Two kinds of pathological deposits are hallmarks of this condition: senile plaques and neurofibrillary tangles (NFT) [24]. Senile plaques consist of extracellular deposits of β amyloid protein (Aβ) that are associated with degenerating nerve processes (i.e. dystrophic neurites). It progresses initially from a non-fibrillar diffuse plaque to fibrils, giving rise to the characteristic amyloid plaques [27]. NFT are formed within neuronal cells that usually die during the course of the disease and are made primarily of abnormal paired helical filaments (PHFs) [27]. PHFs are structures builded-up by aberrantly phosphorylated forms of the microtubule-associated protein Tau [27], although other post-translational modifications of such protein in the PHFs have been also documented [10] as it will be discussed further in this communication. Interestingly, senile plaques can be found in large numbers in some cognitively normal individuals, which suggests that not only their presence but also the coexistence of NFTs is required for dementia [28]. Indeed, the number of NFTs in the cerebral cortex and hippocampus positively correlates to the degree of dementia in AD [17, 24] which might be reflecting a final pathway to neuronal cell death and neurodegeneration.

1.1.2 Progressive supranuclear palsy (PSP)

PSP is one of the most common neurodegenerative disorders, with a prevalence of 5 per 100 000 [3] and it is a late-onset atypical parkinsonian disorder [16]. It is characterized by supranuclear vertical gaze paralysis, moderate or severe postural instability, facial, nuchal and troncular dystonia [16]. At late stages, dementia is a common feature [16]. Clinical diagnosis recognizes the importance of the above features and also requires onset of disease over 40 years of age and falls within the first year of the disease [3]. Atrophy of the basal ganglia, subthalamus, and brainstem, with corresponding neuronal loss and gliosis are neuropathological characteristics of PSP [2]. A high densisty of fibrillary Tau pathology is found within this brain regions, that

includes neuropil threads, and NFTs which are typically round or globose [2]. Additionally, glial fibrillary tangles in both astrocytes (tufted astrocytes) and oligodendrocytes (coiled bodies) are also often present [2]. PSP Tau pathology correlates with the biochemical identification of insoluble, hyperphosphorylated Tau in affected brain regions [2, 3, 16], as it will be discussed later on in this communication.

Genetically, *MAPT* polymorphisms may contribute to the risk of developing PSP. Indeed, a polymorphic dinucleotide repeat in the intron between E9 and E10 of the *MAPT* gene has been linked to PSP [29]. In addition, the homozygous Tau allele A0 were found to be overrepresented in PSP patients (84%) compared with controls (53%) [30]. Lastly, two extended *Tau* gene haplotypes – H1 and H2 - consisting of eight common single-nucleotide polymorphisms in addition to the dinucleotide repeat polymorphism have been described and it seems that H1 is significantly overrepresented in Caucasians with PSP [2, 3]. In contranst, H2 haplotype seems to be protective to PSP [2, 3].

1.1.3 Corticobasal degeneration (CBD)

CBD is a rare, sporadic and slowly progressive parkisonian neurodegenerative disorder [2, 3, 16]. This phenotypic heterogenic disorder characterizes clinically by cognitive disturbances such as aphasia and apraxia, and extrapyramidal motor dysfunction, like rigidity, limb dystonia, akinesia and action tremor [3, 16]. Moderate dementia can arise late in the course of the disease [3, 16]. Disease onset is in the sixth or seventh decade and its incidence is estimated as being less than 1 per 100 000 per year [3]. CBD disorder involves the cerebral cortex, deep cerebellar nuclei, and substantia nigra, and neuropathologically it shows depigmentation of the substantia nigra, as well as an asymmetric frontoparietal atrophy that is often most severe in the pre- and postcentral regions [2]. Neuronal loss with sponngiosis, gliosis, and prominent glial and neuronal intracytoplasmic Tau pathology can be observed in the affected regions [2]. Glial pathology is characterized by astrocytic plaques and Tau-immunoreactive inclusions in the white matter in both astrocytes and oligodendrocytes [2, 16]. Extensive accumulation of neropil threads throughout the grey and white matter is observed which includes both PHF-like filaments and straight tubules [2].

Interestingly, similarly to PSP, CBD is also associated with the A0 allele of the *Tau* gene, as well as the H1 haplotype [31]. Considering the current biochemical, genetic, clinical and pathological features, it seems that substantial overlap occurs between PSP and CBD, and it is possible that these two disorders may be different phenotypic manifestations of the same underlying disease process [2].

1.1.4 Pick's disease (PiD)

PiD is a rare form of sporadic Tauopathy that is characterized by a distinct progressive dementing process that includes frontal disinhibition including mood disturbances and progressive language impoverishment leading to mutism [3, 16]. Clinic-based pathological studies suggest a prevalence of less than 1 per 100 000 in those in their sixties and onset is usually between the sixth and seventh decade of life [3].

Neuropathologically, PiD characterizes frontotemporal lobar and limbic atrophy associated with marked neuronal loss, spongiosis, and gliosis, with ballooned neurons and Pick bodies [2, 3, 16]. Pick bodies are composed of a mixture of wide, straight filaments and long-period constricted fibrils [32-34] and are detected by antibodies to hyperphosphorylated Tau [35] being most numerous in layers II and VI of the neocortex and in the dentate granule neurons of the hippocampus [36]. Insoluble Tau accumulation develops mainly in neuronal cells and to a lesser degree in glial cells as thorn-shaped astrocytes and coiled bodies; and the accumulated filamentous material appears as predominantly paired helical filaments on electron microscopy, but in some cases there are only straight filaments [3].

1.1.5 Frontotemporal dementia and parkinsonism linked to chromosome 17 (FTDP-17)

FTDP-17 consists of a group of autosomal-dominantly inherited progressive neurodegenerative syndromes in which behavioral, cognitive and motor disturbances occur in various combinations [2, 3]. Usually symptoms include behavioral changes, loss of frontal executive functions, language deficit and hyperpolarity [2, 3, 16]. Parkinsonism and amyotrophy are not consistent features but are described in some families [3]. Diagnosis of FTDP-17 is suspected when these neurological symptoms develop between the third and fifth decade, particularly if a positive family history suggestive of an autosomal dominant neurodegenerative condition is present [3]. Brains of FTDP-17 patients show the presence of an abundant filamentous Tau pathology in nerve cells, and for some in glial cells [2]. The distribution and type of Tau deposits can overlap with those of AD, PSP, CBD and PiD [3]. Besides they also exhibit an atrophy of frontal and temporal lobes, severe neuronal loss, grey and white matter gliosis and superficial laminar spongiosis as neuropathological features [2, 3, 16].

Genetically, FTDP-17 has been linked to mutations on the Tau gene that is located in the chromosome 17q21–22 [2, 3, 16, 37]. *MAPT* mutations always segregate with the disease and are not found in the control subjects, reason that strongly suggests their pathological role in the onset and/or progression of the disease [16]. Up to 2012, 44 different *MAPT* mutations have been reported [37]. However, there remained a number of FTDP-17 families that were not explained by *MAPT* mutations and recently they were explained by the findings of mutations in progranulin (*GRN*), in the valosin containing protein gene (*VCP*) and charged multivesicular body protein 2B (CHMP2B) genes [37]. Additionally, several families with a combination of FTD and amyotrophic lateral sclerosis (ALS) have been reported with genetic linkage to a locus on chromosome 9p [37].

1.2 Tau Protein

Tau was first described as a microtubule-associated protein from porcine brain that promoted microtubule assembly *in vitro* [1, 38, 39]. Later on, it was demonstrated that Tau is a phosphoprotein and its sequence was elucidated [10, 40]. Human brain samples rendered the discovery of six different Tau isoforms

in the central nervous system (CNS) [27, 38], all of which are derived from a single gene – *MAPT* - by alternative splicing [27].

Tau is a neuronal cytosolic protein which primary function is to stabilize microtubules enabling their role as cytoskeletal element and tracks for the axonal transport [27, 41]. This microtubule-associated protein is natively unfolded, highly soluble and contains very little secondary structure [41]. It has three main domains: the microtubule-binding domain, that comprises the C-terminal half, which is composed of repeats of a highly conserved tubulin-binding motif; the projection domain, an acidic amino-terminal region (N-terminal region) that projects away from the microtubule surface; and the prolin-rich domain that is located in between the C-terminal and N-terminal [27, 41, 42](Figure 2). The number of the tubulin-binding motif in the C-terminus resulting from alternative splicing of the exon 10 of the gene *MAPT* in addition to one or two 29 amino-acid-long inserts (alternative splicing of the exons 2 and 3) at the N-terminus render and differ the six different isoforms mentioned above from each other [1, 27]. Isoforms that include the exon 10 are commonly referred as a four-repeat Tau isoforms – 4R isoforms – while when in absence of the exon 10 the isoforms are named three-repeat Tau isoforms – 3R isoforms [27] (Figure 2). Although in most regions of the adult brain the different isoforms are expressed in a steady ratio, during development and in some Tauophaties disorders a differential expression of them seems to occur [27].

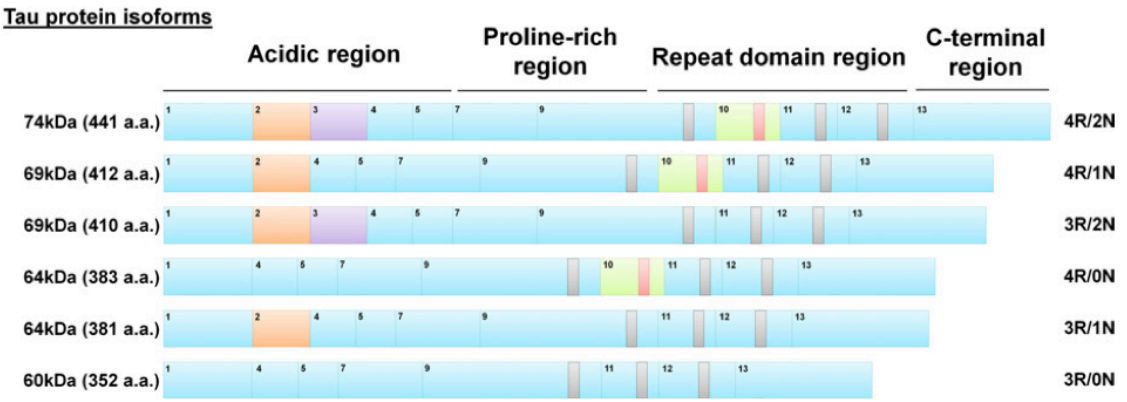

Figure 2: Tau protein isoforms constitution. [42]

As mentioned earlier, Tau is responsible for stabilization and dynamic modulation of the microtublues (MTs), being this canonical function of it central for neuronal homeostasis [27, 43]. It is well documented that Tau action on MT network has great impacts on neurons morphology and as well on axonal transport of signalling molecules, trophic factors and other essential cellular constituents, including organelles (for example mitochondria, lysossome and vesicles) [27]. Therefore, Tau has profound impacts on the viability and function of the neurons and their highly extended processes [27, 43]. The regulation of such function on MT network is achieved primarily by post-translationally phosphorylation of serine/threonine, which can effectively modulate the MT-binding affinity of Tau [10, 27, 44, 45]. Normally, Tau is in a constant dynamic equilibrium, on and off the MTs, cycles which seem to be controlled by kinases and phosphatases and indeed might be crucial for proper axonal cargo transportation [27]. It is important to notice that Tau phosphorylation is most likely developmentally regulated, that is, in adult brain neurons are characterized by

low levels of Tau phosphorylation in contrast to the period of development of the fetal brain in which the levels are substantially higher [27]. Besides, Tau hyperphosphorylation is always observed in Tau-mediated neurodegeneration [10, 27]. Although, this is the most prominent MT-binding regulatory mechanism of Tau, it is important to notice that there are several other post-translational modifications of Tau, such as nitration, glycosylation, glycation, sumoylation and ubiquitination, that might have regulatory impacts on Tau's function and pathology [1, 10, 27]. Unfortunatelly, their significance has been in some extent underestimated in the shadow of the phosphorylation and consequently their roles are yet to be fully characterized.

Another important aspect to mention is that Tau has numerous binding partners besides cytoskeletal elements (which also includes actin in addition to tubulin) [45]. These include signaling molecules[44-46], lipids [45] and DNA [47] suggesting that Tau is a multifunctional protein [44-46]. Indeed, it can act as a scaffolding protein regulating signaling complexes and pathways, and its binding also activates or inhibits several enzymes [45].

1.2.1 Physiological functions and regulation of Tau

1.2.1.1 Cytoskeletal-related functions

As already mentioned, phosphorylation of Tau is the predominant mechanism by which Tau function is regulated [10, 27, 44, 45]. Canonically, Tau is seen by its ability to bind and stabilize MTs [39, 45], and it occurs both *in vivo* and *in vitro* [45]. Phosphorylation of KXGS motifs, that are present in the microtubule-binding domain, has been shown to strongly reduce *in vitro* Tau binding to microtubules [46, 48] and the same seems to happen *in vivo* [46, 49, 50]. *In vitro* studies have shown that the single phosphorylation of Serine 262 (S262) is sufficient to lower Tau affinity to MTs [48], however, *in situ* it seems that at least two KXGS motifs (specifically Ser262 and Ser356) are needed to be phosphorylated in order to Tau disengage from the MTs [50]. Microtubule-associated protein (MAP)-microtubule affinity regulating kinase (MARK) [51], Protein Kinase A (PKA) and calcium/calmodulin-dependent protein kinase II might contribute to the phosphorylation of these sites *in vivo* [46, 49, 52-54]. Phosphorylation of another epitope – Threonine 231 – also appears to play a prominent role in regulating Tau interactions with MTs. Phosphorylation of Thr231 is primed, needing the prior phosphorylation of Ser235 by GSK3β to happen [46]. Thr231 significantly diminishes the binding affinity of Tau to MTs and inhibits the ability of Tau to stabilize this cytoskeleton – as indicated by lowered levels of acetylated tubulin, a marker for MT stability, in this context [46]. Lastly, almost all the Tau that is phosphorylated at the epitope Thr231 is present in the soluble fraction of cell lysates [46].

Of particular interest is that in rat primary neuronal culture and in mouse hippocampus *in vivo* the population of Tau-bound MTs has the highest basal turnover rate of any other MT population [45, 55]. Moreover, siRNA knockdown of Tau does not decrease the number of MTs or their polymerization state and it is not lethal to primary neurons in culture [45, 56, 57]. Hence, MT stabilization might not be a critical function of Tau *in vivo* or at least this Tau function may overlap with another MT-associated protein function that might compensate for the lack of Tau [45, 46].

Tau may also play an important role in the regulation of neurite extension through its binding proprieties to MTs [46, 58]. Experimental data showed that suppression of Tau expression by antisense oligonucleotides in cultured cerebellar neurons significantly suppresses neurite outgrowth [46, 59, 60]. Despite that, Tau knockout mouse again has no overt phenotype with exception for a decrease in the number of MTs of small caliber axons [46, 61]. This result outlines again the possible overlaping function of Tau regarding binding to MTs or yet a possible compensatory mechanism [46]. Interestingly, microtubule-associated protein 1B (MAP1B) seems to play a role in this context. Takei et al., showed by knocking out both Tau and MAP1B in mice that it results in severe dysgenesis of axonal tracts, delayed neuronal migration and disorganization of growth cones [58]. Additionally, the lack of Tau in primary hippocampal neurons leads to defects in the development of axons and dendrites [62] and this defect is even more pronounced in the double knockout of Tau and MAP1B [58]. Although unknown, if these phenotypes correlates to the MT-binding functions of Tau and MAP1B, one might hypothesize that MAP1B might be related to the compensatory mechanisms for the lack of Tau [45]. Although intriguing, it is impossible to come to firm conclusions from the double-knockout phenotype on the functions of Tau and MAP1B in the adult or aging brain due to the early lethality of this model [45, 58].

Of note is that there is a proximo-distal gradient in Tau phosphorylation at Ser199/202 and Thr205 along the nascent axon: Tau in the cell body or its proximity is ~80% phosphorylated, in contrast to the growth cone where only ~20% seems to be phosphorylated [46]. KXGS motifs phosphorylation seems to be required in a specific spatial and temporal way for neurite outgrowth, which is probably achieved through MARK and PKA [46]. In contrast, Glycogen synthase kinase 3β (GSK3β) phosphorylation of Tau might facilitate neurite retraction [46, 63].

Another possible regulation that Tau might exert by binding to MTs is on the axonal transport [45]. Single-molecule studies of motor proteins moving along Tau-decorated microtubule showed that Tau can interfere with the binding and moving proprieties (reversing the direction of the movement) of the motor proteins kinesin and dynein respectively [64]. Additionally, overexpression of Tau in mouse models almost always leads to axonopathy, predominantly in spinal cord neurons [46]. Moreover, the fast axonal transport in ventral root axons is significantly inhibited by the overexpression of the shortest human Tau isoform [46, 65]. Interestingly, in cell culture models kinesin-dependent fast axonal transport can be inhibited by Tau and this might reflect the mechanism in the *in vivo* overexpression models [46]. One explanation might be the fact that Tau affects the binding affinity of kinesin [64] and thus might reduce the attachment frequency of this motor protein when overexpressed [46]. GSK3β seems to play an important role in regulating this function of Tau. In culture models, GSK3β -mediated Tau phosphorylation has been shown to be associated with proper anterograde organelle transport [46, 66]. Furthermore, in mice transgenic for human Tau, the overexpression of GSK3β reduces the pathology in axons when in comparison to mice that overexpresses only human Tau [46]. In this context, one might hypothesize that GSK3β overexpression is probably related to higher levels of Tau phosphorylation compensating for the excess of Tau which leads to a more functional balance between kinesin binding to MTs.

1.2.1.2 Modulation of signaling pathways

When looking further off the canonical functions of Tau (MT binding and stabilization), investigators found out that the microtubule-binding domain may also engage other functions rather than just stabilizing MT as mentioned before. Importantly, it seems that it can interact with other structures and enzymes (including presenilin 1) [67], RNA[68] and DNA [47]. Additionally, the proline-rich region and the projection domain are believed to have several binding partners as well [27].

Indeed, Tau is a polyvalent protein and may act as a scaffold and hence might modulate signaling pathways [45]. In mouse brain tissues, Fyn kinase (Fyn) and postsynaptic density protein 95 (PSD-95) co-immunoprecipitate with Tau; and in its absence, Fyn can no longer traffic to the post-synaptic sites in dendrites [69]. In this context, the authors speculate that, despite Tau's low levels of expression in dendrites, it would target Fyn to PSD-95/NMDA receptor signaling complexes ensuring the correct localization of post-synaptic components [45, 69]. In cell culture, Tau is able to bind to both Fyn and cSrc kinase (cSrc) facilitating actin rearrangements after platelet-derived growth factor stimulus [45].

Although controversial, Tau might act regulating signaling cascades that control neurite extension [45]. In fact, this may be achieved through Tau-mediated facilitation of nerve growth factor (NGF). Indeed, although Tau does not interact directly with growth factor receptors, in PC12 cells NGF or epithelial growth factor (EGF) stimulation appears to cause Tau phosphorylation at Thr231 which is then necessary for the downstream activation of the Ras-MAPK pathway, highlighting the importance of a single epitope phosphorylation in regulating Tau's functions [45, 70].

It has also been shown that in human neuroblastoma cells (SH-SY5Y) Tau can also bind to phospholipase C γ (PLCγ) [71]. It also seems that in cell-free conditions and in the presence of fatty acids it can activate PLCγ independently of the usually required tyrosine phosphorylation, and this was particularly facilitated by arachidonic acid [45, 72].

Besides its functions as activator of enzymes, Tau also appears to be able to bind and direct inhibit enzyme activity as in the case of histone deacetylase, enzyme which can regulate MTs stability by deacetilating tubulin [73]. Thus, Tau might regulate MTs stability by a mechanism independent of its binding to the cystoskeleton [45].

Another important function to mention is the ability of Tau to participate in the response to oxidative stress and heat shock responses [47]. In this study, the authors experimentally demonstrated that upon such insults Tau shuttles to the nucleus and that its presence in such cellular compartment was necessary to protect DNA [47]. This protection was correlated with an increase of Tau bound to DNA [47]. Another interesting finding was, that in order for Tau to be shuttled to the nucleus, it needs to be dephosphorylated, which highlights again the role of phosphorylation in regulating Tau physiological functions [47].

Lastly, Tau might be related to the regulation of gene transcription. Of particular notice, Barreda and Avila recently showed that Tau could alter the sublocalization of calmudolin, a protein that can be located at the nucleous or at the cytoplasm, and thus regulating calmudolin's activity as a co-transcription factor [74]

1.3 Tau-mediated toxicity

It has been more than 25 years since Tau was first discovered as the main component of the NFTs in AD. From then to now, a growing body of evidences suggests that the generation of protein aggregates is a common pathological step on the process of numerous neurodegenerative diseases and, indeed, circumstantial evidence clearly implicates these pathological protein aggregates in the onset and progression of most age-related disorders that clinically manifest as progressive cognitive and/or motor impairments [27]. Regarding AD, despite its characteristics being senile plaques (Aβ pathology) and NFT (Tau pathology), the importance of Tau in the onset of the disease remained in check and was a subject of discussion for several years. However, there are increasing evidences that demonstrate that pathological forms of Tau can compromise neuronal function and that Tau is most likely a central mediator of the Aβ toxicity. Although *MAPT* (Tau gene) has not been genetically linked to AD, cultured hippocampal neurons exposed to Aβ do not undergo degeneration in the absence of Tau [75]. Additionally, it was found that the reduction in endogenous Tau levels in genetically modified mice that express human Aβ prevented its behavioral deficits (without altering their high Aβ levels) [76]. These results provide direct evidence supporting a crucial role for Tau in the Aβ-induced neurodegeneration mechanisms in the central nervous system.

The importance of Tau in neurodegeneration can be corroborated as its pathology is present in several other age-related neurodegenerative diseases such as progressive supranuclear palsy (PSP), corticobasal degeneration (CBD), Pick's disease (PiD), argyrophilic grain disease (AGD), and frontotemporal dementia (FTD) [2, 3, 27]. Moreover, underscoring the pathological relevance of Tau is the discovery of *MAPT* mutations in families with FTD which accounts to up to 30% of the inherited cases of this dementia. Interestingly, oligodendrocytes and astrocytes can also display Tau pathology [1].

1.3.1 Pathological aggregation of Tau

The path that leads from the normal equilibrium of Tau binding to MTs to large aggregates as NFTs is most likely a multi-step mechanism that begins with the de-attachment of Tau from the cytoskeleton [42] (Figure 3). In a pathological background, the binding equilibrium of Tau to MTs is profoundly perturbed as a result of numerous situations, which include increased rates of phosphorylation and/or decreased rates of dephosphorylation. Consequently, the cytosolic concentration of unbound Tau rises likely increasing the chances of pathogenic conformational changes that in turn could lead to aggregation of such protein. Then, small nonfibrillary Tau deposits named 'pretangles', that seem not to contain β-sheets, are formed. Pretangles must then undergo a structural rearrangement that culminates in the β-sheeted PHFs which finally self-assemble to form NFTs [27]. In addition to the disequilibrium in the phosphorylation rates of Tau, it is likely

that other pathological events might trigger disengagement of Tau from the MTs. Examples are Aβ-mediated toxicity, oxidative stress and inflammation [27]. All of them probably have the ability to induce, independently or in combination, such pathological behavior of Tau. [27]. Indeed, oxidative stress might be able to induce the detrimental formation of disulphide bridges and tyrosine nitration and such modifications could lead to Tau misfolding, hyperphosphorylation and aggregation contributing to the abnormal binding equilibrium between Tau and the cytoskeleton [27].

As already mentioned, Tau disengagement from the MTs and the loss of its stabilizing function certainly would lead to neuronal disturbance in high degree, being the structural and regulatory functions of the cytoskeleton the most affected - which would compromise the axonal transport as well as synapses. This hypothesis, indeed, was recently validated in *in vivo* studies by the use of a MT-stabilizing drug (paclitaxel) which showed to lower the neurodegenerative phenotypic burdens of transgenic mouse models of AD-like Tau amyloid pathologies [27]. However, Rapoport et al. showed that depletion of Tau in hippocampal cultured cells did not lead to decreased stable MTs as it was expected, but rather the opposite. Their results suggested that only the subpopulation of stable microtubules containing detyrosinated tubulin was decreased in the absence of Tau, but not the one containing acetylated tubulin [75]. Interestingly they also observed an increase in the highly dynamic subpopulation of acetylated tubulin MTs, which is likely a compensatory mechanism of the neuron that might confer resistance to the Aβ-mediated neurodegeneration [75]. Therefore, it seems that Tau is responsible for stabilizing only one subset of MTs in the CNS, which is in agreement with previous observations [75], and although Tau's loss-of-function might be deleterious in some-extent, this result underscores the importance of Tau's presence for the pathology

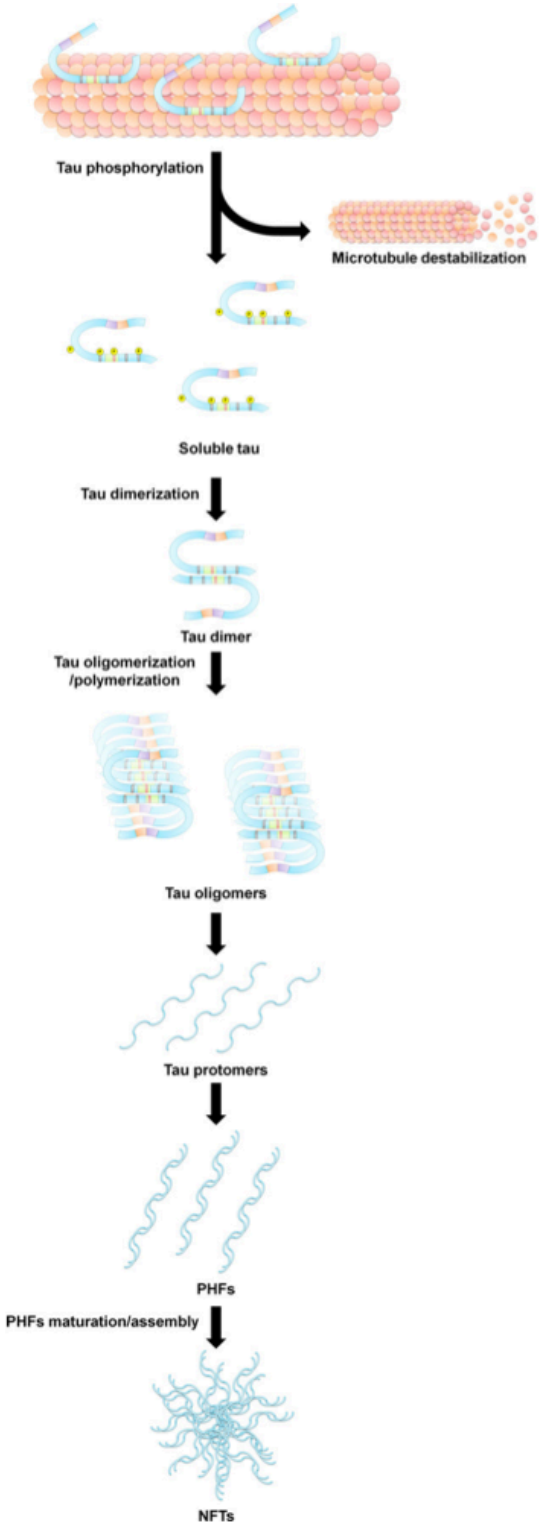

Figure 3: Model for multistep process of Tau aggregation. Initially, impairment of Tau binding to microtubules results in the increase of soluble tau (monomeric form). Monomers, then dimerize leading to oligomers formation. Oligomers organize in protomers which in turn assemble in PHFs. Finally, aggregation of PHFs in NFTs.[42] →

highlighting a possible gain-of-function of the protein.

It has become very clear that Tau plays a central role in the pathogenesis of Tauopathies. However, if this role is due to its loss-of-function or gain-of-function is still a topic of intense debate. Most likely, its role represents the sum of both – gain and loss-of-function - in the deregulation of neuronal homeostasis [1, 2, 16, 27, 44, 77].

Another complex issue that has been addressed is what Tau species is the most toxic one. Indeed, understanding the contribution of NFTs and other putative toxic Tau intermediates shows as a tricky task due the fact that these different Tau species probably coexist and co-localize extensively. Despite that, there are *in vitro* and *in vivo* evidences that give us some good insights on the subject. In an inducible cell model, it was shown that aggregating species of Tau cause toxicity, even at a stage where the aggregates are not yet detected by ThS fluorescence in cells (*e.g.* pre-aggregated oligomers) [78]. Additionally, in a *Drosophila* model expressing a human mutant Tau (an isoform found in early onset AD), transgenic flies showed key features of the human disorders, even though neurodegeneration occurred without the NFT formation [79]. Mice Tauopathy models that parallel better with the human pathology seem to underscore the same trend of results. In a double transgenic model, Tau phosphorylation, cognitive deficits, and dentate gyrus damage are present before the apparition of Tau filaments [80]. In another work, it was found that mice expressing a repressible human Tau variant that developed progressive age-related NFTs, neuronal loss, and behavioral impairments, showed after Tau's suppression memory function recovery, and neuron numbers stabilizement, but NFTs continued to accumulate [81]. Furthermore, treatment of transgenic mice with kinase inhibitors are able to reduce Tau phosphorylation, aggregated Tau, and motor deficits in mutant Tau transgenic mice, but NFT counts or other neuropathological markers are not reduced [82]. Altoghether, these data suggest that the main cytotoxic effects of Tau are not exerted by NFTs but by other species of Tau. In fact, it has been hypothesized that NFTs might exert a protective role in early stages of AD pathology by sequestering toxic species of Tau into a less harmfull state [10, 82]. However, even if this is a true premise, one cannot rule out that although NFTs might not be actively toxic, their continuous accumulation still account for a major cellular disturbance. That is, accumulation of such large aggregates could impose a physical obstacle disrupting cellular functions such as axonal transport. Lastly, NFTs may also contribute to AD progression by also sequestering other proteins (additionally to Tau) and transcription factors [27, 82], and hence reinforcing and amplifying the pathological state.

Despite the doubts regarding which Tau species is more harmfull, altogether this data confirm that Tau aggregation plays a prominent role in the onset of Tauopathies [2, 3, 10, 16, 41]. Hence therapeutic strategies with the final objective to inhibit such pathological aggregation appear as a logical possible solution and were drawn [10, 45]. Indeed, phenothiazine methylene blue seems promising as it slowed AD disease progression in a phase II human clinical trial [83], effect that might be due to the inhibition of Tau-Tau interactions [84, 85] as well as it may reduce soluble Tau levels through other mechanisms as it is known to have many targets [85, 86]. Indeed, in a mouse Tauopathy model (rTg4510) upon methylene blue administration, the levels of the drug in the cerebellum were found to correlate positively with Morris water maze performance and inversely with soluble Tau levels [86]. These results are in agreement with previous findings that show that

NFTs are not associated with functional deficits, but rather the soluble Tau levels are likely to be [86]. Besides, these data suggests that the putative therapeutic effect of this drug might not be completely related to the inhibition of aggregation [10]. The immunosuppressant FK506 is another example of such kind of therapy. This drug may act directly on neurons or yet influence the neuronal environment by modulating microglial activation, and in a transgenic mice overexpressing human P301S under the mouse prion promoter (PS19 model) it has been shown to reduce microgliosis and Tau aggregation [45]. Despite these data above, as it is still not known which Tau entity is responsible for Tau-dependent neuronal dysfunction and degeneration, it remains also unknown if any of the available Tau aggregation blockers are in fact lowering the Tau pathologic specie responsible for the deficits [45]. Indeed, it has been shown that some Tau aggregation inhibitors may enhance the formation of potentially toxic Tau oligomers [45]. Despite that, as the levels of NFTs positively correlates to neuronal deficits and many of the current drugs that block the aggregation of Tau also block the pathological aggregation of other proteins under cell-free conditions, including Aβ and α-synuclein this kind of strategy seems still a reasonable rationale and should be more explored [45].

1.3.2 Pathological modifications of Tau

In order to disengage from MTs and to acquire its pathological features, Tau must pass through post-translational modifications. Up-to-date, many different post-translational modifications have been described for Tau and its aggregates; Phosphorylation, nitration, glycosylation, glycation, sumoylation, ubiquitination, truncation are some of them [10]. Some of these modifications, aside of their possible pathological features, are often employed as cellular mechanisms for regulation of the proteostasis, that is, they often are used to regulate proteins functions as well as their turnover (e.g. phosphorylation and ubiquitination respectively). The most prominent Tau's modification in AD seems to be phosphorylation. As already mentioned, however, truncation and ubiquitination seem also to play a role within the pathogenesis of this and related disorders [10].

1.3.2.1 Tau phosphorylation

Tau was defined as a phosphoprotein in the 1980s [44] and phosphorylation plays a prominent role in regulating its physiological function (Figure 4). Most of the studies focused on the regulation of the ability of Tau to bind to MTs. Besides the disengagement from the cytoskeleton, however, Tau's phosphorylation can lead the protein to other outcomes, such as degradation and translocation to the nucleus [87].

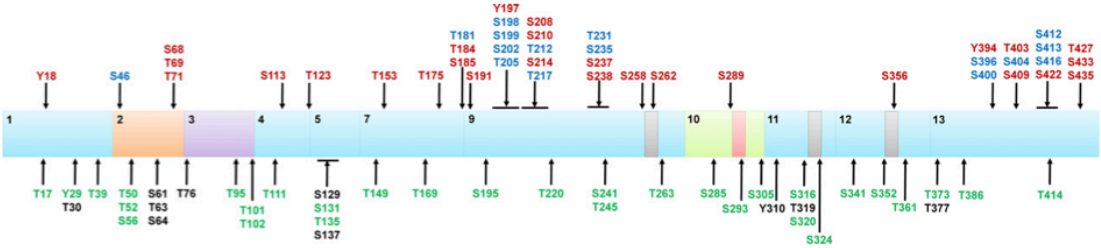

Figure 4: Phosphorylation sites of Tau. In green non-pathogenic phosphorylation sites, in red pathological phosphorylation sites, in blue phosphorylation found in both conditions, in black putative phosphorylation sites of Tau. [42]

Particular attention was given to serine/threonine phosphorylation [10, 44]. 79 potential serine/threonine sites that could be phosphorylated are present in the largest human Tau isoform [38]. It has been clear that Tau phosphorylation occurs in AD and is associated to the pathogenesis of the disease, however it is important to notice that Tau phosphorylation has been detected at many sites that are not normally present in autopsied non-AD material in brain biopsies from non-AD patients, although not in the same extent [10]. This highlights the fact that most phosphorylation epitopes of Tau might be phosphorylated at physiological conditions - hence the differences between Tau's phosphorylation in AD and Tauopathies brains in contrast to a normal brain rely on the extent rather than the sites of phosphorylation [10].

Tau abnormal phosphorylation in AD disease appears to be a progressive event and Threonine 231 (T231) seems to happen at early stages of the disorder [10]. GSK3β is able to perform this specific phosphorylation that reduces significantly Tau's affinity for binding MTs [10]. Besides this epitope, it seems that this enzyme is able to phosphorylate other AD-related epitopes on Tau *in vitro* and in cells, and it is likely deregulated in AD brain [10]. Interestingly, soluble levels of peptidyl prolyl isomerase (Pin1), a protein that specifically binds to pT231 resulting in a conformational change that restores Tau's binding ability to MTs, has been shown to be decreased in AD brain [10]. Furthermore, it was demonstrated that the geneticaly modified mice that lacks Pin1 (Pin1-/-) exhibit progressive age-dependent neuropathy characterized by motor and behavioural deficits, Tau hyperphosphorylation, Tau filament formation and neuronal degeneration [88]. Altogether, these data strongly suggests a role for pT231 in the progression of AD. Of particular notice, GSK3β seems to phosphorylate the substrate in two ways: primed, that needs a prior phosphorylation of the substrate by another kinase, or unprimed. Interestingly, T231 phosphorylation appears to be a primed event [44] and thus this seems to be a limiting event that predisposes to the pT231-mediated pathogenesis. Therefore, identifying the kinase(s) responsible for this prior phosphorylation could give us new insights for new molecular therapeutic targets and a better understanding of this pathogenesis-related pathway.

Another epitope, Serine 262 (S262), has been shown to have its phosphorylation levels increased in pretangle neurons in AD brain suggesting that this is another early event in the progression of this Tau-related disorder [10]. Indeed, this specific phosphorylation significantly decreases Tau binding to MTs and it is mostly performed by the microtubule-associated protein/microtubule affinity-regulating kinase [89]. In a neurodegeneration fly model, studies with alanine mutation of S262 were performed in order to eliminate phosphorylation. Their results suggested a role for Tau toxicity and Aβ-induced Tau-dependent toxicity [10].

Despite all that, one single phosphorylation is probably not enough to convert Tau into its toxic specie. However, it is probably a limiting step that influences the posterior phosphorylation of other epitopes which could lead to the formation pathological species. Indeed, there are evidences that one epitope phosphorylation can influence the phosphorylation of others [10]. In agreement with this cooperative idea of phosphorylation for neurodegeneration, Steinhilb et al, demonstrated that pseudophosphorylation of 14 Ser/Thr-Pro epitopes in Tau significantly enhanced toxicity in a *Drosophila* model for Tauopathy, while eliminating these phosphorylations by alanine mutations counteracted such effect [89]. Although interesting, checking the contribution of each of the phosphorylation sites alone in comparison to the wild-type and to the aforementioned 14 sites mutated would be of particular relevance.

Protein kinases and phosphatases are the main players in this context, thus Tau's phosphorylation level are determined by a balance between these two kinds of enzymes [2]. Although several of these enzymes have been described as acting on this balance, special attention was given to the kinase GS3Kβ and to the protein phosphatase 2A (PP2A) [2, 42]. There are evidences that over-activation of GS3Kβ and inhibition of PP2A could significantly contribute to Tau phosphorylation [42]. These data indicates that imbalances on the phosphorylation and dephosphorylation systems might be implicated in Tau pathology.

As already discussed, the function and aggregation of Tau appear to be regulated by phosphorylation [1-3, 10, 16, 44-47, 66, 77, 90, 91], hence this prominent post-translational modification of Tau led to a logically quest into drugs that could counteract the pathological features of the Tauopathies. In fact, in transgenic mice overexpressing P301L human Tau, lithium, which inhibits GSK3β and is used to treat bipolar disorder, reduced Tau pathology and improved behavior of the animals [92]. However, inhibition of GSK3β activity impairs NMDA-mediated long-term depression [93] and mice heterozygous for GSK3β (GSK3β+/-) as well as intraperitoneal injection of GSK3β inhibitors in wild-type mice resulted in impaired memory reconsolidation [94]. Consequently doubts regarding the potential benefits in comparison to the potential side effects of GSK3β were raised [45]. Additionally to GSK3β, inhibition of other kinases have been also tested as it is the case for CDK5 which inhibition prevents Aβ-induced hyperphosphorylation of Tau and cell death in culture [45]. Kinases, however, are essential for several cell signaling pathways, which limits its appeal as a Tauopathy safe therapy [45].

1.3.2.2 Tau ubiquitination

Canonically, ubiquitination is a reversible covalent binding of one or more ubiquitin protein(s) that tags cytosolic proteins to their degradation by the ubiquitin-proteassome system (UPS) [95]. Despite that, it seems to have other functions being linked to other proteolytic systems (e.g. macroautophagy) and as well as to negative regulation of membrane receptor signaling [8]. In physiological conditions, Tau has been shown to be ubiquitinated and degraded by the proteasome [42]. However, in AD ubiquitin has been mainly found in PHFs [10] which seems to preclude its clearance by this mechanism [96] as it will be discussed further in this review. In this context, this tagging might be an attempt of the cell to signal for the degradation of these pathological aggregates either by UPS or by autophagy. Tau ubiquitination can occur in its C-terminus, and it was proposed that it occurs in PHFs after its hyperphosphorylation and glycosylation [42]. However it is possible that Tau ubiquitination in AD and related Tauopathies could also take place in soluble non-oligomeric fractions of Tau. Indeed, it was demonstrated *in vitro* that when the proteasome is inhibited by treatment with MG-132, the amount of multimeric ubiquitinated Tau increased dramatically within the cells [5]. Although it indicates a role for UPS-mediated degradation of soluble Tau, one cannot rule out that, at least in part, the increase in the aggregated Tau in this model might be happening as well due to less degradation of Tau by the proteasome in a non-ubiquitin dependent manner.

Of particular interest is the fact that it was also found that pathological forms of Tau co-immunoprecipitate with carboxyl terminus of the Hsc70-interacting protein (CHIP) [5]. CHIP is a molecule with dual function: a co-chaperone of Hsp70 and it possesses intrinsic E3 ubiquitin ligase activity [5]; and this interaction with Tau is probably related to Tau's ubiquitination and to the identification of its abnormal state by the chaperone system as well. Tau's relationship with the UPS is becoming undeniable. As a matter of fact, our host laboratory at Janssen, Pharmaceutical Companies of Johnson & Johnson, has recently found that some deubiquitinating enzymes (DUBs) - USP5, USP7, USP9X and OTUB – were also interacting with Tau (data not published). In this context, these DUBs might be stabilizing the pathological species of Tau leading to its accumulation and to the formation of the characteristic tangle lesions in Tauopathies. Lastly, high levels of ubiquitinated Tau proteins were also found in cerebrospinal fluid of AD patients [97, 98]. These data suggest that Tau ubiquitination is most likely involved in Tau pathology.

1.3.2.3 Tau truncation

Sequencial cleavages of Tau appear to take place in the progression of AD [10]. These truncation events (cleavages), enhance the ability of Tau to aggregate [99](Figure 5) and contributes to the neuronal execution of apoptosis [42]. Caspases appear to have its levels elevated in AD brain [10] and are likely to be involved in such events. Caspase-3 is able to cleave Tau on its aspartic acid 421 [42], a truncation that seems to be an early event in AD brain [10]. Interestingly, in a recent work Calignon et al., observed in a mouse Tauopathy model, transient increases in caspase activity, which was followed by NFT formation [100]. Hypothesizing that caspase cleavage of Tau at D421 was on the basis of the formation of the aggregates, they delivered D421 Tau truncated with an adenovirus to wild-type mice brains, resulting in formation of similar aggregates [100]. In addition to these observations, expression of Tau D421-truncated results in mitochondria disfunction, but without massive cell death[10]. However, when cells are subjected to stressors, the presence of this particular truncation sensitizes cells to death [10]. Despite all of that, neurons expressing caspase activation are rare [100], which is logical to think considering that this activation might culminate in apoptosis. Hence, on their work Calignon et al. proposed that the few caspase-positive neurons that further on displayed NFT formation should be the ones that were able to escape somehow the programmed cell death [100]. Within this background, it is possible to imagine that once a neuron escapes death fate and starts displaying Tau pathology it might be the initial step for a pathogenic protein seeding (a prion-like mechanism that will be further elaborated within this work) and for the spreading of the pathology. Thus, although few events of transient caspase activation in a reduced number of neurons might be sufficient to initiate Tauopathy, considering the amount of lesions present in AD brains, it is logical to consider that other enzymes might be related to this phenomenon in order to accelerate the

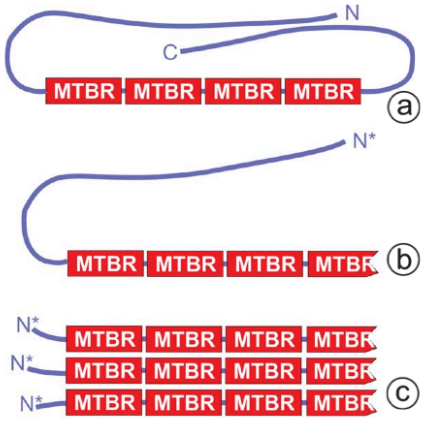

Figure 5: Tau truncation is suggested as a pro-aggregation modification. a) Tau protein can adopt a paper-clip like resting state when idle. b) Truncation prevents the adoption of this state. c) Aggregation is fastly triggered without the interference of the C-terminus (N* = various truncated and non-truncated N-termini) [99]

process. Although this topic remains obscure, a model considering that a defect in chaperone-mediated autophagy of Tau could lead to leakage of lysossomal proteases might help to explain it [41].

Other sites of Tau truncation were also described, such as D13, D402 and glutamic acid 391 (E391) [10] and they also seem to be related do AD pathology. It is important to mention that although truncation of Tau seems to be an early step for aggregation, it is also related to NFTs maturation in later stages. Besides, Tau cleavage can be influenced by its phosphorylation and can later on influence Tau ubiquitination and glycation [42] which highlights the intense cross-talk between these mechanisms and the complexity of Tau disorder etiology.

1.3.3 Amyloid-β in the onset of Tau pathology in Alzheimer's disease

Amyloid-β (Aβ), a peptide with 38-43 kDa of molecular size, is derived from the proteolytic cleavage of the transmembrane amyloid precursor protein (APP) by the sequential enzymatic actions of β-site APP cleaving enzyme 1 (BACE 1), β-secretase, and γ secretase and is the core of the hallmark deposit - senile plaques – observed in AD [37, 101-103]. After the sequential cleavage in the plasma membrane, Aβ is released into the extracellular space where it accumulates and contributes to amyloid plaque formation [102]. Although Aβ is produced by almost all cells in the body, its physiological functions remain elusive [103]. Two main forms of Aβ are found in the human brain, and under normal physiological circumstances the predominant Aβ form is $A\beta_{40}$, a 40 amino acids long peptide [37, 103]. However, in the pathological context a 42 amino acids long peptide ($A\beta_{42}$) that is more toxic and prone to aggregate tends to accumulate, providing the seed for further Aβ deposition [37, 101-103]. Of particular notice is that this peptide has its production increased as a common feature in normal aging [103]. What leads to its accumulation further on the normal range towards AD remains a field of study though.

Importantly, APP can also be internalized by endocytosis and then processed into Aβ along the endoplasmatic reticulum (ER) and Golgi pathway [102]. Moreover, Aβ can be taken up from the extracellular space, which happens through its interaction with cell surface receptors (7 nicotinic acetylcholine receptor, 7nAChR; N-methyl-D-aspartate, NMDA; and receptor for advanced glycation end products, RAGE) and upon its entry it is released into the cytosol [102]. Both, the ER/Golgi pathway Aβ formed and the internalized, are particularly important because they allow a direct interaction and influence of this peptide with intracellular proteins involved in the formation of NFTs [102].

Aβ can influence NFTs formation by upregulation of kinases that can target Tau [102]. Specifically, this peptide can interact with membrane receptors, such as p75 neurotrophin receptor (p75NTR), alpha 7 nicotinic acetylcholine receptor (α7nAChR), formyl-peptide receptor-like-1 (FPRL1), N-Methyl-D-aspartate receptor (NMDA) and RAGE, causing the activation of various signaling pathways that involve the Tau [102]. By binding to p75NTR, α7nAChR, FPRL1 and NMDA receptors, Aβ leads to an increase in the intracellular calcium which then causes activation of p38 MAPkinase pathway through reactive oxygen species (ROS) production or activates CdK5 by involving calpain [102]. Additionally, p75NTR can lead to the

activation of JNK and α7nAChR to GSK3β activation [102]. Another signaling pathways that involves RAGE receptors acts also by inducing the formation of ROS and can lead to the activation of CdK5, p38 and JNK [102]. Interestingly, mitochondria dysfunction induced by Aβ can also culminate in CdK5, JNK and p38 activation due to oxidative stress [102]. Dysfunctioning mitochondria with reduced glucose metabolism can also lead to activation of CdK5, JNK, p38 and GSK3β due to an increase in the extracellular levels of glucose and advanced glycation end products (AGE) production [102]. Besides, Aβ can also activate microglia and astrocytes inducing a neuronal inflammatory response [102]. In this case, there are cytokines release and intracellular ROS stimulation and both culminate in kinases activation (e.g. p38, CdK5 and JNK) [102]. All aforementioned signaling pathways induces Tau hyperphosphorylation and hence Tau disengagement of MTs and NFTs formation, and constitutes major cross-talks between these two neuropathological hallmarks of AD [102].

Pathogenic production of intraneural Aβ can also impair the proteasome function [104] which has been suggested to be by direct physical interaction of the proteasome and Aβ [105]. This data is particularly important considering that phosphorylated Tau in normal physiological circunstances is ubiquitinated and then targeted to proteasome degradation [106]. Consequently in the presence of intracellular Aβ it is possible that Tau would no longer be degraded efficiently and thus promoting hyperphosphorylated Tau accumulation and NFTs formation [102].

Lastly, there are evidences from cell lysates [107] and primary cortical cultures [92] that Aβ presence can elevate caspase-3 activity leading to Tau truncation [102]. Besides, Tau truncation can be further exacerbated due to Aβ-mediated inflammatory response that leads to cytokine receptor binding and consequently stimulation of caspase-3 activity [102]. Tau truncation, as already mentioned, generates Tau species strongly prone to aggregation and NFT formation [10, 102].

1.3.4 Mechanisms of Tau-mediated neurodegeneration

The physiological knowledge of Tau function in addition to its hyperphosphorilation levels and NFT appearance in the onset of Tauopathies has led to the logical hypothesis of loss of function Tau-mediated neurodegeneration [77]. Altogether, it is logical to think that if Tau is under a negative pressure that leads to its improper functioning and aggregation, this would profoundly impact neuronal systems, ranging from energy metabolism, due to defective mitochondria transportation that could lead to oxidative stress, to structural abnormalities that might lead to collapse of neuronal processes [10, 77]. These impacts, and all in between, consist on a strong rationale to the loss-of-function hypothesis which is still strongly defended.

However, when looking deeper on the possible mechanisms of Tau-induced deficts in Tau-related neurodegenerative disorders, there are some rationales. As already discussed, Tau phosphorylation results in reduced affinity of the protein to bind to MTs, and then destabilizes MTs which may lead to cellular damage [10]. Although the rationale for a loss-of-function is logical, recent data strongly suggests that Tau toxicity is probably also linked to gain-of-funtions of modified Tau. Indeed, the inhibition of anterograde axonal

transport is now thought to be associated with the ability of Tau to bind kinesin rather than due to MTs destabilization [91, 108]. Considering that, at least two possibilities are still under investigation: (i) if Tau is inhibiting cargo interaction with kinesin, or (ii) if it disrupts the attachment of kinesin to microtubules [10]. These rationales will be further discussed in the next part of the communication.

Although Tau's influences in axonal transport are prominent and likely key players both in physiological and pathological situations, Tau has been shown to be a protein with a broad range of activities as already discussed [1, 2, 16, 44, 46, 47, 64, 67, 69, 74, 77, 87, 91, 109, 110]. Hence, these non-canonical findings on Tau's functions add another layer of complexity and highlight the fact that when Tau is disengaged from the MTs it might act as an active player in this neuropathology rather than just losing its functions. Indeed, the first circumstantial evidence towards this idea have been made by the observation that the total levels of NFTs directly correlates to the degree of cognitive impairments [27]. This new gain-of-function hypothesis in contrast to the loss-of-function hypothesis will be discussed further in the next part of this communication.

1.3.4.1 Synaptic damage

Synaptic damage occurs early in the progression of AD and congnitive deficits correlates strongly with synapse loss [77, 111, 112]. Furthermore, in other Tauopathies such as PSP and frontemporal lobe dementias (FTD), synaptic loss is also reported [77].

In transgenic mice overexpressing P301S human Tau (PS19 mice), hippocampal synaptic loss is observed even before NFT formation and this was related to a prominent decrease in levels of pre-synaptic proteins (e.g. synaptophysin and β-sinuclein) [113]. In another interesting study, two transgenic mouse lines were created: (i) one expressing full length human Tau with the ΔK280 mutation that strongly promotes Tau aggregation; and (ii) the second containing the same mutation with the addition of other two modifications to disrupt aggregation [114]. In those models, although hyperphosphorylation and somato-dendritic missorting of Tau are observed, just in the pro-aggregation conformational changes occur [114]. Using those, the authors then reported a reduction in the number of spines synapses in the absence of NFT formation, and yet synapse loss was greater in the transgenic animals expressing the pro-aggregation mutant of Tau compared to animals expressing the anti-aggregation mutant [114]. These results highlight that filament formation is not necessary for synaptic dysfunction, but rather that oligomer formation ability seems to play a prominent role in this context [114].

1.3.4.1.1 Synaptic dysfunction through axonal transport dysfunction

There are several possible mechanisms by which non-fibrilar Tau might lead to axonal transport dysfunction and hence leading to synaptic damage. As previously mentioned, Tau is responsible for MTs stabilization and that hyperphosphorylation of this soluble protein can lead ultimately to MTs destabilization and disassembly [77]. It has been shown that soluble hyperphosphorylated Tau isolated from AD brains is able to decrease MT-promoting activity *in vitro* [77, 115, 116]. Besides, it is also able to sequester normal Tau,

MAP1 (A/B) and MAP2, that cause the inhibition of MT assembly and might even cause MT disassembly [77, 117, 118]. Altogether, one possible explanation would be that the abnormal phosphorylation of Tau might lead to destabilization of MT and thus leading to axonal transport dysfunction, and less cargo would reach the synaptic ends [77].

Given that, therapies that compensate for this loss of function and stabilize MTs are being considered. Indeed, a derivate of the MT stabilizing agent taxol showed protection against synaptic loss in response to lysosomal stress in brain slice preparations [10, 119]. Unfortunately, taxol-based derivatives usually show low blood-brain barrier permeability [120]. Despite that, epothilone D, that has better blood-brain barrier permeability, improved MT density and cognition in P301S human Tau mice [121]. Interestingly, MT stabilizing agents might have more than one mechanism of action in Tauopathie. NAP peptide, for instance, that stabilizes MTs [122], can also reduce Tau hyperphosphorylation [123] levels and showed some promise in a phase II clinical trial [124].

It has been previously mentioned within this communication that too much Tau binding to MT could affect the motor cargo proprieties [64]. Particularly it can reverse the direction and/or lead to disengagement of the motor proteins from the MTs [64] and hence it could profoundly impact the axonal transport. Indeed, overexpression of human Tau in mature hippocampal neurons results in improper distribution of Tau (invading dendrites) and inhibition of the mitochondrial transportation [77]. Although it is important to be aware that this was done in an overexpression Tau model in which its levels could be much higher than in disease situations, this model might reflect some aspects of human Tauopathies. That is, in Tauopathies protein turnover systems seem to be dysfunctional [10, 41] and thus this could lead to an increase in Tau soluble levels in the cytosol that could enhance its chances to be hyperphosphorylated [27] or, in the context above, to bind to MTs and inhibit axonal transport [77]. This highlights the possible synergistic effects between wild-type Tau (inhibiting axonal transport [77]) and pathological Tau species (leading to dysfunctional turnover mechanisms [10, 41]) that most likely coexist in the context of the disorders.

However, Tau's ability to impair axonal transport might not be only due to MT dysfunction. It is well known that pathological species of Tau can lead to mislocalization of mitochondria within the neurons [66, 125-127]. Some interesting works provided some insights into what might be behind this mislocalization induced by Tau. It was observed in FTDP-17 Tau mouse model that hyperphosphorylated Tau selectively interacts with c-Jun-N-terminal kinase interacting protein 1 (JIP1) which regulates cargo binding to the kinesin motor complex. JIP1 binding by hyperphosphorylated Tau caused JIP1 to mislocalize to neuronal soma which is likely a contributing factor to the axonal transport deficits observed in these mice [128]. As mitochondria is the main source of energy production and calcium buffering in cells, its sequestration away from high energy and calcium influx areas (e.g. synapses and Ranvier nodes) would certainly have profound impacts on neuronal homeostasis [66, 125, 126], thus this might be a key mechanism in the neurodegenerative process. Moreover, Tau seems to be able to bind to kinesin and by this it could interfere with cargo axonal transportation [77, 91]. Of particular notice is that the phosphorylation state of Tau seems to regulate its affinity to bind kinesin-1: GSK3 phosphorylation of Tau leads to higher affinity of Tau for the kinesin light chain in contrast to dephosphorylated Tau [91]. Thus, hyperphosphorylated Tau that in AD appears first in

distal portions of axons may result from aberrant axonal transport of phosphorylated Tau reported above [91].

Lastly, although soluble pathologic species of Tau appear to play a prominent role within the context of dysfunctional axonal transport, it is important to notice that the disruption of the axonal transport is likely to be achieved as well due to the physical obstruction that large NFTs could impose within the axons [77].

1.3.4.1.2 Receptor-mediated synaptic dysfunction

Although dysfunctional axonal transport seems to have a major role in Tau-induced neurodegeneration, other mechanisms that don't involve this mechanism were also proposed. For instance, expression of a dominant negative form of Tau in mice expressing human mutant APP resulted in the sequestration of Fyn kinase away from synapses, which prevented phosphorylation of the NMDA receptor and coincided with an attenuation of memory deficits [69]. Fyn Phosphorylation of NMDA results in inhibition of NMDA-mediated endocytosis [129] which might lead to sustained activation of such receptors. This is particularly important in AD brain context because Aβ oligomers are present in the extracellular synaptic cleft and recently it was demonstrated that these oligomers bind to or in close proximity to NMDA receptors, triggering neuronal damage through NMDA receptor-dependent calcium flux [130]. Therefore, increased activation of NMDA receptors induced by Tau can facilitate Aβ-induced toxicity. Hence, these evidences highlight again the synergism between these pathological hallmarks of AD.

Although Tau pathology is mainly intracellular, in AD Tau can also be observed in the extracellular space [44] and in both AD and in FTD (although in much less levels) it can be also found in the cerebro-spinal fluid [98, 131]. It has been postulated that extracellular Tau is a result of neuronal cell death [44], although other explanations are possible (as it will be discussed in the next section of this communication). Anyhow, upon interaction of extracellular Tau with muscarinic M1/M3 receptors an increase in intracellular calcium takes place on the surrounding neurons which could lead to toxicity [38]. Interestingly, Tau phosphorylation prevents its interaction with muscarinic receptors, but it was described that extracellular phosphorylated Tau is dephosphorylated by tissue-non-specific alkaline phosphatase (TNAP) [38]. In fact, TNAP levels are increased in the brain of AD patients [38]. Altogether, intracellular Tau, extracellular Tau and Aβ oligomers are likely to be cooperating for the neurodegeneration in neurons co-expressing both receptors (NMDA and M1/M3 receptors). An interesting question that rises up from these results is that at what extent one path influences the other and if there is any interdependence of those paths towards AD toxicity. Altogether these data validate the importance of Tau in Aβ-mediated neurodegeneration, but its mechanisms remain to be fully understood. The same rationale could be hypothesized for other Tauopathies, but in those cases the question would be at what extent intracellular and extracellular Tau might be synergizing towards neurodegeneration.

1.3.4.2 Tau abnormal modulation of signaling pathways

As already mentioned, Tau is a polyvalent protein that have several binding partners [47, 67, 68, 77]. For instance, Fyn can phosphorylate Tau, but most importantly Tau can modulate Fyn activity [77] as well as influence its localization within the cell, functions that for instance can impact NMDA endocytosis [69]. Moreover, Tau has been shown to increase PLCγ activity *in vitro* [45, 77]. Fyn and cSrc can also have their activities increased by Tau both *in vitro* and in COS7 cells [77]. These data suggest a very possible role in Tau modulating signaling through these enzymes. An increase in the activity of tyrosine kinases would impact on synaptic transmission and plasticity [132] and evidences for a role of Fyn in synaptic dysfunction and toxicity has already been shown [69, 133, 134]. Moreover, Tau-mediated Src activation impact on growth-factor-induced actin remodeling and altered actin dynamics have already been reported in AD brain and in Aβ treated neurons [110].

Tau has also been found to associate with plasma membrane [109] which seems to be regulated by its phosphorylation levels [90]. The presence of the PPXXP motif on its proline-rich region might explain, at least in part, Tau's interaction with membrane because that motif could interact with SH3 domains present in some membrane-associated proteins [44]. These interactions are of particular interest considering that there are evidences that link this protein to dysfunctional neuronal terminals [69, 135]. Furthermore, there are evidences of dissemination of Tauopathies from one neuron to another which might happen through pathogenic protein seeding [136] that might be facilitated by those interactions. That is, one can hypothesize that once Tau can bind to membranes it can be easier released to the extracellular space and as well re-taken by their neighboring cells through processes such as exossome release, endocytosis, exocytosis and even through synaptic release.

Importantly, Tau phosphorylation seems to regulate negatively Tau's binding capabilities to SH3 domains and plasma membrane [77]. As so, one might hypothesize that abnormal alterations in the phosphorylation levels of Tau may affect significantly its association with various signaling proteins and with the plasma membrane, possibly having profound impacts on signaling pathways.

Lastly, Barreda and Avila recently showed that Tau could alter the sublocalization of calmudolin, a protein that can be located at the nucleus or at the cytoplasm, and thus regulating calmudolin's activity as a co-transcription factor [74]. It would be interesting to address the question if the pathological forms of Tau could interact with this protein and, if so, until which extent this interaction would impact the overall gene expression.

1.3.4.3 Tau-mediated mitochondrial dysfunction

Additionally to the "classical view" of Tau-mediated disruption of mitochondria axonal transport, it is becoming evident that Tau's gain-of-function may act on several other aspects of mitochondria homeostasis. In fact, in a very interesting study, Rhein et al., used three transgenic mouse models - Tau aggregate forming

P301L Tau mice, Aβ plaque forming $APP^{sw}PS2^{N141I}$ mice, and triple transgenic (3xTg) mice which combine these mutations and pathologies – and assessed the mitochondrial function [137]. Proteomic analysis of 3xTg mice showed vast deregulation of several OXPHOS proteins related to complex I and IV, whereas Tau transgenic mice only showed deregulation of complex I and Aβ plaque forming mice only showed deregulation of complex IV [137]. Besides, the 3xTg mice showed earlier and more severe onset of mitochondria disfunction [137]. These results suggest that Tau may exert an active toxicity through mitochondria and underscore a synergism between Tau and Aβ mechanisms of toxicity. In agreement with these results, another work showed that stable expression of D421 truncated Tau in cortical cell lines leads to fragmentation of mitochondria [10]. These results are of particular importance because they seem to reflect observations from AD patient brains that showed abnormalities in mitochondrial fission/fusion, in respiration protein levels and also in energy metabolism observed by PET scan [10].

Given the physiological importance of the mitochondria and that it seems to be one of the primary targets of pathological forms of Tau [10], therapies that aim to enhance the function of this organelle seem a reasonable strategy. Usually, mitochondrial-targeted strategies aim to reduce ROS production and hence oxidative stress which compromise cell viability [10]. Popular therapeutic candidates are antioxidant molecules, such as vitamins C and E, glutathione, Coenzyme Q_{10} (ubiquinone) and MitoQ (a derivative of ubiquinone) [10]. Interestingly, ubiquinone and MitoQ seem promising due to results of clinical trials for PD, however such molecules have poor translocation across the blood-brain barrier and yield a non-universal response against the cellular oxidative damage, which are main draw-backs regarding its therapeutic use [10].

1.3.4.4 Tau dysfunctional caretaking

Recently it has been shown that Tau protein in its dephosphorylated state can also sub-localize to the nucleus of neuronal cells under stress conditions. In this context, it seems to exert a fundamental role as a DNA caretaker. With this work, Sultan et al. experimentally demonstrated that under acute oxidative stress and mild heat stress, dephosphorylated Tau accumulated in the nucleus and fully protected DNA from damage [47]. Accumulating evidences indicate that oxidative DNA damage probably plays a role in the progression from normal brain to AD brain being one of the earliest events to be noted in the pathogenesis of the human disease [138]. It is interesting to notice that the neurons that show NFT formation in AD seem to be the same that show age-related accumulation of nuclear DNA damage [139]. Neurons are highly susceptible to insults and cannot survive after irreversible damage due to the fact that they are highly differentiated postmitotic cells that are unable to divide [47]. Thus, one might hypothesize that pathological modifications of Tau (e.g. hyperphosphorylation) could impair its ability to translocate to the nucleus and/or might affect its affinity for DNA. As a result, these pathological forms of Tau would fail to protect DNA from insults derived from the pathogenesis of AD and other Tauopathies (e.g. oxidative stress). Regarding the nuclear localization of Tau, it has also been described that Tau phosphorylation could be required for its transport to the nucleus [87], which seems contradictory to the aforementioned work. Despite that, both situations might be happening within the cell but possibly with different goals and outcomes; that is, it is possible that the phosphorylated Tau might have a regulatory function by interacting to other nuclear proteins and enzymes in contrast to the caretaker function of the dephosphorylated Tau. Besides, they

possibly differ on its time and context dependency. Indeed, in the pathological context of Tauopathies there is a shift towards the phosphorylated state of Tau [2, 3, 45], as already mentioned, which would interfere with this balance. It would be interesting to check whether in such situation there is Tau shuttling to the nucleus and if so to check its interactions (e.g. calmudolin). In this hypothetical context, it is attractive to suggest that the pathological Tau could be interfering with DNA repair mechanisms, as well as to gene expression, thus it would be creating a negative pressure culminating in the progression of the pathology.

1.3.4.5 Tau and Amyloid-β synergism towards neurodegeneration

The importance of Tau in the pathogenesis of AD is now evident and this idea gets stronger and stronger as new evidences are continuously being found. Hence, the Aβ-centric hypothesis for AD neurodegenerations is getting renewed for a more up-to-date idea of a synergism between these two major players. Within this context, some studies can be highlighted. Transgenic mice with Tau knowckout (Tau-/-) are very resistant to Aβ-induced neurite degeneration in comparison to wild-type or to mice expressing human Tau [75]. In another mice model, the human mutant APP mouse model that displays Aβ-induced pathology, when it is crossed with Tau-/- mice significant improvements in performance in spatial learning, and reduced premature mortality, hyperactivity and excitotoxicity are found [76]. *In vitro* studies also corroborate such hypothesis, and when comparing primary neuronal cultures from transgenic mice with different Tau levels (Tau+/+, Tau+/- and Tau-/-) it was shown that Tau reduction prevented Aβ-induced defects in axonal transport [140]. These data reflect the previously mentioned cross-talks between Aβ and pathological Tau species formation and vice-versa [102], as well as their pathological mechanisms alone that sum up (as already discussed above).

1.3.5 Tau pathology spreading

Up-to-date, there are two main hypotheses for Tau pathology spreading: (i) in the presence or (ii) absence of neuronal death [38].

1.3.5.1 Tau spreading in the presence of neuronal death

In the case of neuron death, due to Tau toxicity and/or Aβ toxicity, intracellular Tau is released in the extracellular space after to the rupture of the plasma membrane in consequence of neuronal death. As a consequence, extracellular Tau would interact with receptors on the surrounding neurons (as described above) which would trigger signaling pathways that could lead abnormal phosphorylation of intracellular Tau and as well to neuronal death spreading due to the same reasons of the initial event of neuronal death (see above) [38].

1.3.5.2 Tau spreading in the absence of neuronal death

More recently an alternative way of Tau pathology spreading was proposed. In this case, a cell-to-cell transmission would take place without the necessity of cellular death. Similarities between AD and prion diseases induced researchers to speculate that AD might act as a prion-like disorder [136, 141, 142]. In addition, NFTs first appear in the locus coeruleus and entorhinal/limbic brain areas, later spreading to interconnected neocortical regions [136, 143]. This spreading pattern implicates synaptic exchange [143] and neuronal transport in AD pathology within the brain [136]. Indeed, recent evidences strongly suggest that transcellular propagation of protein misfolding occurs for a variety of aggregative proteins including Tau [141, 142]. For instance, intracerebral infusion of brain extract containing pathogenic filaments of Tau can induce NFTs formation in mice bearing human Tau transgene [136]. This is particularly interesting considering that these mice express non-mutant human Tau and do not develop Tau pathology without the infusion. Furthermore, the seeded NFTs are intracellular and although initially they are confined to the injected region, over time they spread to its surrounding cells and as well to axonally connected areas, which strongly suggests a cell-to-cell seeding mechanism [136]. This transcellular propagation includes a mechanism called "template conformational change" or "pathogenic protein seeding", that basically consists on the conversion of a normally folded protein into a new conformation via direct contact with a misfolded protein [136]. Recently, in a very elegant work, Kfoury et al., demonstrated direct evidence for the transcellular propagation of Tau protein misfolding [144]. With a FRET-based approach, this group observed that intracellular Tau is directly released into the media and then it is taken up by co-cultured cells, where, by direct protein-protein contact, induced fibrilization of intracellular Tau of the naïve recipient cells. Interestingly, an anti-Tau monoclonal antibody blocked Tau aggregate propagation by trapping these pathogenic species in the extracellular space [144]. This data suggest that Tau is released by the cell directly to the extracellular media and not within any vesicle (e.g. exossomes) and implicates immunotherapies as good investments for research in Tauopathies [144].

In agreement with this previous work, Pooler et al. also experimentally showed that Tau is physiologically released into the extracellular space not bound to membranes upon stimulation synaptic activity stimulation [143]. Most interesting is that this work that was performed in primary cortical cultures being added another layer of knowledge, demonstrating that endogenous Tau is released upon AMPA receptors activation and that this happened in a calcium-dependent way [143]. This activity was impaired by blocking the pre-synaptic vesicle release by tetanus toxin and by the inhibition of the neuronal activity by tetrodotoxin. Lastly, phosphorylation of extracellular Tau appears reduced in comparison with intracellular Tau [143]. This last data might reflect the release of plasma membrane bound Tau that has been shown to be largely unphosphorylated [145] or yet the dephosphorylation of extracellular Tau by TNAP which is deregulated in AD brains, as already mentioned [38]. This work highlights that this is a physiological and regulatable process and that alterations within this mechanism possible account for trans-synaptic Tau transmission in Tauopathies [143].

Despite the above publications, exosome-mediated release has been identified as a common secretion mechanism for other aggregation-prone, such as α-sinuclein, prion protein and Aβ, that are prominent in

neurodegenerative diseases pathogenesis [146-148]. Hence, Saman et al. hypothesized whether Tau could be secreted by the same mechanism and demonstraded in M1C neuroblastoma cells that Tau secretion can occur via the above mechanism and also that exosome-associated Tau is a major component of the CSF Tau seen in early AD CFS patients samples [149]. Most importantly, is that exosomal Tau was associated both with typical exosomal proteins and with proteins involved in Tau misprocessing and AD pathogenesis, such as Aβ, presenilins, and fyn kinase [149]. Of particular notice is that α-sinuclein, prion protein and Aβ that were found to be released by exosomes [146-148] under neuropathogenic conditions can interact with Tau resulting in the exacerbation of the oligomerization and neurotoxicity of the proteins involved [142] which highlights a very possible cross-talk and/or synergism between different neurodegenerative pathologies.

Although evidences are emerging, the mechanisms by which Tau is released and taken up by the cells remain poorly characterized. They might include endocytosis and exocytosis, but if so, what triggers its endocytosis (interaction with M1 and M3 [38] and other receptors) and how can Tau leave the inner part of the endocytic vesicle and reach the cytosol? Besides, one cannot rule out a possible cooperation between Tau exossomal exchange [149] and Tau synaptic exchange [143] that could be shuttling pathological Tau from one cell to another. Anyhow, it is possible that the SH3 region on Tau might be related to such exchanges. Therefore, it would be interesting to check whether interfering with Tau's plasma membrane-binding capacity could modulate this phenomenon. As a final remark, it is important to highlight that both hypothesis are likely to coexist in an affected Tauopathy brain which once more indicates the complex etiology of this dementia syndromes.

As previously mentioned, Tau aggregates, induce cell death, synaptic and mitochondrial dysfunction and memory impairments [1-3, 10, 16, 45, 46, 77, 150], therefore clearance of pathological species of Tau appears as a good strategy for Tauopathy therapy. However, this is difficult to achieve because most Tau aggregates locate inside neurons [1-3, 10, 16, 45, 46, 77, 150]. In light of this, evidences that Tau can propagate from one cell to another by being released in the extracellular space and then taken up by neighbor cells [136, 141-144, 149] give a new window for targeting this pathological seeds outside the cell by a immunotherapy approach. Indeed, although the mechanisms remain elusive, it has been postulated that Tau immunotherapy might clear extracellular Tau leading to an imbalance between the intra and extracellular Tau that could culminate in more release of Tau and clearance, and hence a good outcome regarding therapy [150]. Anyhow, there are some works that can be highlighted. Asuni et al., in P301L tangle model mice, performed an active immunization with a phosphorylated Tau epitope (residues 379–408 of Tau, with phosphorylation of Ser396 and Ser404, two phosphorine residues commonly associated with NFTs) and this strategy resulted in induction of Tau antibodies that passed the blood-brain barrier reducing Tau aggregates in the brain and slowing the progression of tangle-related behavioral phenotype [151]. In another study, hTau/presenilin 1 transgenic mice, which express human non-mutant Tau and PS1 M146L mutation on Tau knockout mice background, immunization with Tau379–408 peptide (phosphorylated on Ser396 and Ser404) reduced pathological Tau in the brain and prevented cognitive decline [152]. However, immunization of wild-type mice with full-length recombinant Tau protein leads to NFTs structures formation, axonal damage, gliosis and neurological deficits providing a link between Tau autoimmunity and Tauopathy-like abnormalities which highlights potential dangers of using immunotherapy for Tau [153]. Hence, although promising on the light of the evidences of

Tau trans-cellular propagation more knowledge is still required to understand the risks and benefits of this therapeutic strategy.

1.3.5.2.1 Aβ and α-synuclein cross-seeding Tau

Amyloidogenesis is usually a very specific process in which the amyloid form of a protein only converts other copies of the same protein and not proteins with different primary sequences [142]. However, since all amyloidogenic proteins (including Tau) polymerize into fibrils, have similar properties and share similar sheet intemediates, it is very likely that they might interact with these β-pleated sheet domains via a similar fibril formation mechanism which could lead to the catalyzement of the assembly of one or another into amyloid structures – cross-seeding [142, 154]. Indeed, there are evidences that cross-seeding can occur between Aβ and Tau [154, 155] and α-synuclein and Tau [156]. Hence, cross-seeding can have an important role in the initiation of fiber assembly, however it is usually not as effective as self-seeding [142].

Aβ and Tau inclusions are hallmarks of AD [2, 3, 10, 45, 101], however up-to-date there is no reasonable explanation as to why plaques and tangles simultaneously accumulate in AD [155]. Guo et al. and Miller et al. demonstrated that Aβ and Tau can interact and form stable complexes [154, 155]. Furthermore, it seems that Aβ binds to multiple Tau peptides, especially those in exons 7 and 9 and this binding enhances Tau phosphorylation by GSK3β [155]. Interestingly the binding affinity is sharply reduced or abolished by phosphorylation of specific serine and threonine residues [155]. Of particular notice is that Tau and Aβ complexes where also found by ELISA when analyzing soluble extracts of AD brains and control tissue [155]. Therefore, the authors hypothesized that an initial step in the pathogenesis of AD might be the intracellular binding of soluble Aβ to soluble nonphosphorylated Tau and as a consequence this would promote Tau phosphorylation (enhancing the probability of NFTs formation) and Aβ nucleation [155].

Co-occurrence of Tau and α-synuclein inclusions is observed in brains of sporadic neurodegenerative disorders, besides studies in individuals with Parkinson's disease (PD) that share the same rare mutation of α-synuclein – A53T mutation – also revealed widespread Tau and α-synuclein inclusions [156]. Thus, a pathogenic mutation in α-synuclein that is known to increase the propensity of this protein to fibrillize also seems to promote formation of Tau inclusions in humans [156]. Indeed, pure α-synuclein and Tau synergize to promote the fibrilization of each other, and a more deep observation by electron microscopy with immulabeling showed mostly fibers composed of single Tau or α-synuclein (with few exceptions) [156]. In brains of patients with PD Tau co-localize with α-synuclein in portions of Lewis bodies highlighting this possible interplay [142]. Besides, recent studies showed that variation in the *MAPT* gene can confer genetic risk for PD and it seems that the probability of developing concurrent AD and PD is greater than the product of the probabilities of developing each [142].

Although further studies are needed to unequivocally prove these cross-seedings as important players in the pathogenesis of these disorders, the above evidences pinpoint some important mechanistic questions and thus highlights that further studying this subject would probably give major insights to understand the etiology of such neurodegenerative disorders and also to draw new therapeutic strategies.

1.4 Tauopathy models

1.4.1 Transgenic animal models of Tauopathies

The understanding of the complex pathogenic mechanisms by which abnormalities in Tau can lead to systemic neurofibrillary degenerative disease requires the construction and use of experimental model systems in which the behavior of human Tau can be analyzed under controlled conditions. For this purpose, animal models ranging from invertebrate species such as *Caenorhabditis elegans* to *Drosophila melanogaster* and mammalian transgenic mouse models of Tauopathies have been generated [157].

Caenorhabditis elegans are easily genetically manipulated, mature rapidly, and can be utilized to screen pharmacological compounds. This particular animal is well characterized at every level and it is an excellent model for understanding protein function and dysfunction [157]. Consequently, a FTDP-17 *C. elegans* model with V337M and P301L Tau mutations were created and the expression of such in the nerve cells resulted in degenerative phenotype. Of particular notice is that wild-type human Tau expression in this model resulted in some deficits, however in less extent than when the mutant forms were expressed [157].

Drosophila melanogaster, is an intermediate model, between *C. elegans* and vertebrates systems, regarding its complexity. It has a single endogenous Tau gene that is expressed in many neuronal cell types without any up-to-date report of mutation [157]. Additionally, its endogenous Tau protein accumulates in axonal processes, as is the case with mammalian Tau [157]. Besides, up to 70% of human disease genes have *Drosophila* homologs, which makes these animal models, both fly and fly-eye models, powerful tools to elucidate neurodegenerative disorders mechanisms [157]. Importantly, these Tau models replicate several features of human Tauopathies, including adult onset, progressive neurodegeneration, accumulation of abnormal Tau (although not necessarily as NFTs) and early death [157].

Several mouse Tauopathy models have been developed that exhibit some pathological and/or some phenotypic manifestations observed in human Tauopathies. Endogenous mice Tau is spliced only into the 4R isoforms in adult mice in contrast to the six isoforms of the human Tau and is a MT-associated protein that also confers stability for the cytoskeleton [157]. Between the several models, some ablate the mouse gene and thus only human Tau is produced, while others express the human gene without ablating the endogenous Tau, which complicates the interpretation of findings due to different ratios and contribuitions of the mouse and human Tau isoforms [157].

Of note are the transgenic mice harboring the mutations P301L [158] and P301S [159, 160] of FTDP-17 and the triple-transgenic model (3Tg-AD) for AD harboring $PS1_{M146V}$, APP_{Swe}, and Tau P301L transgenes [160]. P301S (1N4R) Tauopathy mouse model closely model human Tau pathology seen in authentic Tauopathies [159]. For instance, they develop synaptic pathology at 3 months of age, filamentous Tau lesions at 6 months of age, and progressive Tau accumulations similar to NFTs in association with neuronal loss as well as hippocampal and entorhinal cortical atrophy by 9–12 months of age [159]. Mice expressing the most common FTDP-17 mutation, P301L, also resemble human Tauopathies [158]. The

expression of this 4R human Tau mutated results in motor and behavioural deficits, with age- and gene-dose-dependent development of NFT [158]. This phenotype occurs as early as 6.5 months in hemizygous and 4.5 months in homozygous animals [158]. NFTs and Pick-body-like neuronal lesions are widespread in the brain and spinal cord [158]. Besides, the most affected areas with NFT have reactive gliosis [158]. The triple-transgenic model for AD is the first model that develops both plaque and tangle formation in AD-relevant brain regions [160]. They develop Aβ deposits prior to tangle formation which is consistent with the amyloid cascade hypothesis [160]. Besides, these mice exhibit deficits in synaptic plasticity (including long-term potentiation) and this occur prior Aβ deposition and tangles but is associated with Aβ intracellular immunoreactivity [160].

In addition to the aforementioned examples there are several other models, such as *Xenopus* [157, 161], zebrafish [161], and several other transgenic mice models [157, 162]. Each of them has pros and cons and should be carefully chosen depending on the work objectives and characteristics [157]. Despite that, each one of them may offer relevant information that can be used as simplified models for Tauopathies [157].

1.4.2 Understanding the propagation of Tau pathology using seeding strategies

Age-related misfolding and progressive aggregation of disease-linked proteins in the brain with regional pattern are amongst the most prominent molecular characteristics of neurodegenerative disorders. Interestingly, these disease-linked proteins share common features and particularities of the propagation mechanisms [163], which supports the idea that nucleation, aggregation and spreading are core mechanisms for toxicity (Figure 6) and that the clearance of these species might halt the progression of the disease.

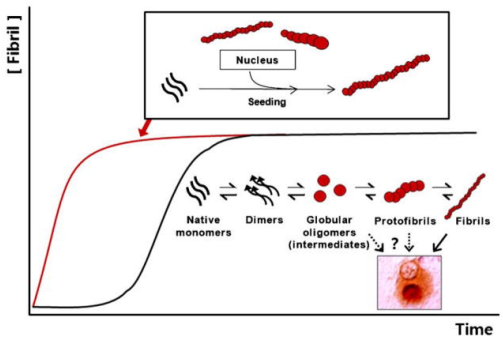

Figure 6 - Scheme of amyloidogenic protein aggregation process. The black line represents the non-induced amyloidogenesis process, whereas the red line represents the induced amyloidogenic process. This process is dependent of nucleation, and after this phenomenon there is a rapid elongation phase [163].

1.4.2.1 Cellular models to study the effect of Tau in Tauopathies

Differently from the mouse models, overexpression of wild-type or mutant Tau turned out to be insufficient to induce Tau aggregation in a wide variety of cell lines under a wide variety of experimental

conditions [164]. Indeed, only recently Tau aggregation could be induced in vitro due to emerging and application of the concept of "pathogenic protein seeding" (Introduction 1.3.2.2.).

Guo et al. established a cellular system that robustly develops NFT-like Tau aggregate, which provides mechanistic insights into NFT pathogenesis [165]. In this study, through the use of in vitro pre-aggregated fibrillized material, it was possible to accelerate the intracellular fibrillization of monomeric Tau, moving the process from the initial lag phase to elongation phase, since the fibrils assembly occurs by a nucleation-dependent mechanism which corresponds to a longer step [165]. In summary, the authors of this paper established a reproducible and robust, cellular model of Tau aggregation in which the key features of Tauopathies are present. Based on such study, a similar model was developed in cortical neurons in our group [166, 167]. To achieve Tau aggregation in rat primary neurons, the full-length Tau with the P301L mutation was overexpressed in such cells followed by the "seeding" with in vitro pre-aggregated fibrils, that in its turn nucleated the Tau aggregation [166, 167]. These models are potential systems for the identification of therapeutic strategies against Tauopathies, and until now they represent the most fitted *in vitro* models to test Tau aggregation.

1.5 Tau clearance in neurodegenerative disorders

AD negatively influences a wide range of cellular processes, including degradative mechanisms that are responsible for the "protein quality control" of the cell. In fact, proteasome activity in AD brain is lower than in controls and this happens independently of the expression of proteasome subunits [10]. Furthermore, it seems that autophagy-lysossomal pathways are also compromised in AD brains [10]. In this case, it is possible that decreased levels of Beclin-1, a macroautophagy regulatory protein, might be playing a role and/or there seems to be an impaired clearance of the autophagic vacuoles by lysosomes as well [10]. Tau, like most of the aggregative proteins involved in neurodegeneration, has been described as substrate for both UPS and autophagy [10]. The UPS and autophagy–lysosome systems are thought to be the two main routes of protein and organelle clearance in eukaryotic cells [96].

1.5.1 UPS and Tau clearance

Proteasomes, the end point of the UPS pathway, are barrel-shaped multiprotein complexes that predominantly degrade short-lived nuclear and cytosolic proteins [96]. An important fact to be mentioned is that proteasomal substrates must be unfolded to pass through the narrow pore of the proreasome barrel, which precludes the clearance of oligomeric and aggregated proteins [96]. Proteins are usually targeted to the proteasome by being tagged with ubiquitin. This happens by the covalent attachment of a polyubiquitin chain(s), which is recognized by the 26S proteasome [96, 168]. This conjugation is a multi-step process that typically involves three types of enzyme: E1 (ubiquitin-activating enzyme) hydrolyses ATP and forms a thioester-linked conjugate between itself and ubiquitin; E2 (ubiquitin-conjugating enzyme) receives ubiquitin from E1 and forms a similar thioester intermediate with ubiquitin; and E3 (ubiquitin ligase) binds both E2

and the substrate, and transfers the ubiquitin to the substrate (Figure 7). Because ubiquitin itself contains seven lysine (K) residues (K6, K11, K27, K29, K33, K48 and K63) that can serve as acceptor sites for chain elongation, chains that contain multiple ubiquitin moieties can be formed [8]. Diverse types of ubiquitin modifications can be displayed in cellular proteins: (i) monoubiquitination, the attachment of a single ubiquitin, (ii) multiple monoubiquitination, the attachment of multiple single ubiquitin molecules to several lysine residues in the target protein, and (iii) polyubiquitination, a modification with ubiquitin chains of diverse lengths and linkages [8]. These diverse types of modifications are recognized by an array of effector proteins that then influence numerous cellular processes [8]. The most known ubiquitin modification is K48-linked polyubiquitination that labels proteins for proteassomal degradation, however other ubiquitin chains can control from receptor endocytosis and protein sub-localization to NF-kβ signaling and autophagy [8].

Ubiquitination is a highly versatile and reversible modification. Indeed, nearly a hundred (the deubiquitinating enzymes or DUBs) reverse this modification by hydrolyzing the (iso)peptide bond tethering ubiquitin to itself or the target protein [169] recycling ubuiquitin to the cytoplasm and regulating several processes mediated by ubiquitin tagging [8]. Deubiquitination is achieved because the DUBs are cysteine proteases (excluding JAMM which are metalloproteases) that catalyse the removal of Ub from Ub-modified proteins [170]. DUBs are divided into five subclasses based on their catalytic mechanism and their active site conformation, these subclasses include: UCHs (Ub C-terminal hydrolases), USPs (Ub-specific proteases), MJDs (Machado-Joseph disease protein domain proteases), OTUBs (ovarian tumor proteases), and JAMMs (JAB1/MPN/MOV34 metalloenzyme) [170, 171]. These DUBs regulate proteolysis by several means: directly interacting with and co-regulating E3 ligases; altering the level of substrate ubiquitination; hydrolyzing or remodeling ubiquitinated and poly-ubiquitinated substrates; acting in specific locations in the cell and altering the localization of the target protein; and acting on proteasome bound substrates to facilitate or inhibit proteolysis [169]. Therefore, the ubiquitin pathway displays a scope and regulation similar to that of phosphorylation, with the DUBs serving the same functions as the phosphatase. Interestingly, in a previous work form our group the DUBs USP5, USP7 and OTUB1 have been shown to interact with Tau in mouse brain [11]. Hence, in this project we focused on the aforementioned DUBs that will be further characterized in the next sessions of this communication (Introduction 5.1.2.; 5.1.3. and 5.1.4.) and evaluated whether their knockdown could alter Tau levels in primary neurons.

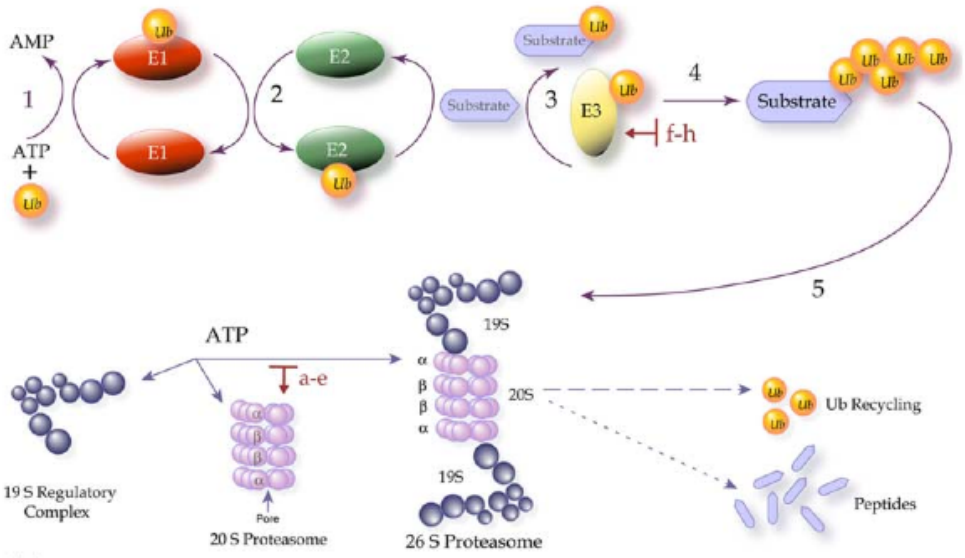

Figure 7: Overview of the ubiquitin-proteasome pathway

As already mentioned, Tau can interact with CHIP which can ubiquitinate it [5] and thus probably regulating its turnover. Contraditory results were found when considering the influence of Tau phosphorylation levels on CHIP-mediated ubiquitination of Tau [10]. Despite that, *in vitro* studies showed that CHIP is able to catalyze K11, K48 and K63 ubiquitination of Tau [10]. It is important to notice that these *in vitro* assessments do not correspond to a physiological context were there will most likely be present co-factors which could influence these results. Besides, it would be interesting to understand if in a particular context CHIP would preferable catalyze one or another chain as they would have different outcomes. However, Petrucelli et al. found out in a cell model using HEK-293 and COS-7 that CHIP interacts, ubiquitinates (both K48 and K63 chains) and induces aggregation of Tau [5]. Indeed, growing evidences support the view that Tau ubiquitination end up in aggregation. In this context, knockout of CHIP results in accumulation of hyperphosphorylated Tau, but not Tau aggregation in transgenic mice [172]. Besides, promoting Tau ubiquitination by overexpressing K63 or K48 ubiquitin, that are ubiquitin mutants containing arginine substitutions on all lysine residues except the one at position 63 or 48 respectively, leads to the appearance of inclusions positive for Tau in SH-SY5Y cells overexpressing Tau mutant, data that suggests that ubiquitination might enhance Tau aggregation [173]. Although one should expect more proteasomal degradation in this context, these results could be explained by the fact that ubiquitination can also signalize to autophagy that is able to degrade protein aggregates [8, 174]. Therefore, in this context, CHIP might be inducing Tau aggregation in an attempt to lead to its degradation by autophagy. A complementary assay for this work would be to check the levels of autophagic markers and/or autophagossomal accumulation. That is, although Tau is aggregating and not being degraded by the UPS, the autophagic pathway might be activated, even if it is dysfunctional and not able to cope with the aggregates (hence the autophagossomal accumulation assay). However, CHIP up-regulation has been shown to attenuate Tau aggregation *in vivo* and its levels seems to be increased in human AD brain samples [175]. Hence, whether Tau ubiquitination enhances or not Tau aggregation is still a topic of intense debate and needs further investigation to clarify its role in Tau clearance regulation.

Tau degradation by the proteasome is still a controversial, and although it has been demonstrated in *in vitro* assays it can be degraded by the proteasome [176], its degradation in cellular models is still a controversial issue in which there are evidences favoring both views (Tau being degraded and not) [6]. This might be reflecting the fact that these studies have been performed in different conditions and that Tau degradation can be influenced by several conditions or factors, for instance the cell type, post-translational modifications and as well Tau's conformational state [6] and hence a better characterization is still needed. Of particular notice is that, although the great majority of the proteasome substrates are ubiquitinated, there are evidences that this degradative complex can degrade proteins in an ubiquitin-independent way [10, 176]. As a matter of fact, Tau degradation by the proteasome seems to be able to occur in the absence of such conjugation [10, 176]. Interestingly, as already mentioned, our host laboratory has found out that Tau interacts with some DUBs, namely USP5, USP7 and OTUB1 [11]. Considering all that (ubiquitin-independent Tau clearance, CHIP-induced Tau aggregation and interaction of Tau with DUBs), it is possible that pathological soluble species of Tau might be preferable cleared by the proteasome in an ubiquitin-independent way and thus DUBs interaction might be an attempt of the cell to target Tau to the proteasome. However, it is also plausible that this interaction might be a reflection of the toxic effects of pathological Tau and/or Aβ that further enhances AD pathology by stabilizing Tau not leading to its delivery to the UPS. Indeed, the deubiquitinating enzyme USP14 has been shown to stabilize Tau by inhibiting its turnover in a cellular model [177]. Additionally, the DUB USP9X has been shown to stabilize survival motor neuron protein (SMN) [178] and seems to be related to the regulation of the degradation of α-synuclein in PD [179]. Anyhow, it would be interesting to address such questions by modulating the DUBs and checking its influences on these pathways.

Another important class of molecules that should be mentioned when talking about the UPS in the context of proteinopathies are the molecular chaperons [168]. These proteins are responsible for the surveillance of non-native misfolded proteins and selectively bind to them in an attempt to re-fold such proteins into a functional native state [168]. However, when the target protein cannot be re-folded, this protein is targeted to the UPS with the assistance of the chaperon [168]. Hence, aggregation-based diseases ultimately reflect a failure of the quality control system, either on surveillance or in degradation of the pathological protein species. In this context, it is important to mention that Tau is targeted to degradation by the complex formed by CHIP and the Heat shock protein 70 (Hsp70) (a molecular chaperone) [5, 176]. Interestingly, up-regulation of Hsp70 both *in vivo* and *in vitro* with P301L Tau background has shown to reduce Tau levels (including detergent insoluble Tau) [5]. Despite that, CHIP can also interact with other chaperons, particularly Hsp90 [174]. Interestingly, Hsp90 is able to increase the stability of the Tau mutant P301L as well as that of p35 (an activator of CdK5 Tau kinase) and cellular treatment with the Hsp90 inhibitor 17-AAG leads to both reduced levels of p35 and Tau mutant and this appeared to be mediated by proteasomal activity [180]. Lastly, Hsp90 seems to regulate the autoactivation of GSK3β kinase and Hsp90 inhibitors appear to be able to trigger the degradation of this well-known Tau kinase [174].

Together these data demonstrate that the UPS and its components play an important role in the regulation of Tau turnover and the selective elimination of abnormal Tau species [5, 6, 10, 175, 176]. Besides,

it most likely plays an important role in the pathogenesis of Tauopathies [5, 10, 176] and thus it represents a potential therapeutic target.

1.5.1.1 USP5

USP5, more commonly known as isopeptidase T, is involved in disassembly of free polyubiquitin chains. Conjugation of Ub to a target protein involves formation of a peptide bond between the C-terminal glycine of Ub and the ε-amino group of a lysine on the target protein. Subsequent addition of Ubs is achieved by the formation of a peptide bond between the C-terminal glycine of the next Ub, and an ε-amino group of a lysine on the first ubiquitin. Therefore, the proximal end of the ubiquitin chain is the C-terminal of the initial ubiquitin, and the distal ends are the N-terminals of ubiquitin branches. One role of USP5 is to sequentially remove ubiquitin from the proximal end of unanchored polyubiquitin chains. In order to USP5 do that, a free carboxyl terminus is required at the proximal end of the polyubiquitin chains as this moiety is required to the activation of USP5[181-183]. Hence, when a polyubiquitin chain is still attached to a peptide or lacking the C-terminal glycine on the proximal ubiquitin it is not efficiently hydrolyzed by USP5. Due to such reason, USP5 is able to disassembly the polyubiquitin end products of proteasomal degradation but is thought as not being able to prematurely deubiquitinate a polyubiquitinated protein [182].

Fan et al. evaluated the impact of USP5 knockout in *Drosophila* model and observed that the ablation of this DUB leads to severe defects in the specification and differentiation of photoreceptors and loss of USP5 activates apoptosis and the JNK MAPK pathway [184]. There are also evidences that links USP5 to DNA double-strand breaks repair [185] and that such DUB is a key molecule for the production of TNF-α [186].

1.5.1.2 USP7

Ubiquitin specific peptidase 7 (USP7) or herpesvirus-associated ubiquitin-specific protease (HAUSP) is a cysteine protease [187]. It was was originally identified as a binding partner for the Herpes simplex viral (HSV) protein infected cell protein 0 (ICP0/Vmw110) and later on, numerous proteins have been identified as potential substrates/binding partners of USP7, including Tau [11, 187]. Of particular notice is that some of the better characterized substrates of USP7 play crucial roles in tumor suppression, DNA repair, immune responses, viral replication, and epigenetic control and hence such DUB has emerged as a potential target on oncological and anti-viral studies [187]. Amongst the many substrates and binding partners of USP7, p53, a well-known tumor suppressor protein, had its interaction with this DUB well established. Indeed, it has been shown that USP7 deubiquitynates autoubiquitylated human double minute 2 (HDM2) and its binding partner human double minute 4 (HDMX/HDM4; human ortholog of MDMX/MDM4) with net result of these actions being the stabilization of HDM2 and HDMX and the destabilization of p53 [187]. Therefore, inhibition or knockdown of USP7 is predicted to lead to activation of p53. USP7 has also been linked to the stabilization of repressor element 1- silencing transcription factor (REST) consequently promoting the maintenance of neuronal stem/progenitor cells [188] as well as the regulation of cell cycle or mitotic check

points through Claspin and Chfr respectively [187]. Interestingly, UPS7 has been shown to also regulate the sub-localization of some important cellular effectors. Indeed, under oxidative stress conditions USP7 inhibits nuclear localization and transcriptional activity of FOXO4 (forkdhead box O transcription factor) by deubiquitinating FOXO4 [189]. PTEN is another example of a similar situation. In another words, USP7 also interacts with this protein deubiquitinating it and hence regulates its nuclear exclusion [189]. Of particular notice is that, both FOXO transcription factors and PTEN, have been linked to autophagy regulation[190, 191], which underscores a possible cross-talk between the ubiquitin proteasome system and autophagy. Lastly, USP7 might be involved in epigenetic regulation, by deubiquitinating the histones H2B and H2A [187].

1.5.1.3 OTUB1

Ovarian tumor domain-containing ubiquitin aldehyde-binding protein 1 (OTUB1) is a deubiquitinating enzyme that has been shown via its *in vitro* deubiquitinating activity to be highly specific for cleaving K48-linked polyubiquitin chains [170, 192]. This DUB enzyme has been implicated in regulating diverse processes including T cell anergy, virus-triggered interferon 1 induction and stabilization of p53, estrogen receptor α and cIAP [192]. Interestingly, despite its preference for K48-linked polyubiquitin chains, OTUB1 has bee shown to regulate the synthesis of K63-linked chains in a non-canonical manner. In fact, unexpectedly, it was found that this enzyme is able to inhibit the accumulation of K63-linked polyubiquitin in the DNA double strand break response in a non-catalytic fashion [170, 192]. Indeed, OTUB1 inhibits K63 polyubiquitin chain synthesis by its interaction with the E2 enzymes by binding itself directly to the E2~Ub thioester and holding the donor ubiquitin in its proximal ubiquitin binding site, which includes the OTUB1 N-terminal residues that has been shown to be critical for such inhibition [170, 192]. Interestingly, OTUB1 binding to the charged E2~Ub is allosterically regulated by an additional free ubiquitin monomer and such observation raised the interesting possibility that changes in cellular ubiquitin concentrations might regulate the ability of OTUB1 to inhibit E2 enzymes [170, 192]. Interestingly, a second role of OTUB1-E2 interactions was recently suggested. It seems that those interactions are responsible for the stimulation of OTUB1 cleavage of K48 polyubiquitin, and that this stimulation is regulated by the ratio of charged to uncharged E2 and by the concentration of K48-linked polyubiquitin and free ubiquitin [192]. Altogether, these observations underscore the vast complexity of regulatory possibilities that the DUB enzymes are related to. Hence, further studies to better characterize and discriminate the biological relevance of these non-canonical roles of the DUB enzymes are still needed.

1.5.2 Tau clearance by autophagy

Autophagy, from the Greek "auto" oneself, and "phagos" to eat, is every cellular degradative pathway that involves the delivery of citoplasmic constituents to the lysosome. There are at least three forms of autophagy: chaperone-mediated autophagy (CMA), microautophagy and macroautophagy. Chaperone-mediated autophagy was yet only described in mammals and involves a selectively deliver of proteins from

the cytoplasm to the lysosome in a process that depends of a recognition by receptors from the lysosome of a motif present in cytosolic proteins. Microautophagy refers to a process in which portions of cytoplasm are sequestered by invagination of the lysosomal or vacuole membrane to be degraded. Macroautophagy is the major regulated catabolic mechanism in eukaryotic cells that is responsible for the removal of long-lived proteins and damage organelles by the lysosome or vacuole [191, 193]. This dynamic self-digesting process will hereafter be referred as Autophagy. Autophagy was discovered in mammalian cells and is present in a wide range of eukaryotic cells. Over the last years, many genes involved in fundamental steps of the autophagy were identified and studied – the AuTophaGy-related genes (*ATG*) - in *S. cerevisiae*, *Hansenula polymorfa* and *Pichia pastoris*, which raised again the interest at this topic. Many of these genes are present in higher eukaryotes therefore indicating that this is an evolutionary conserved process [191].

In virtually all cells, Autophagy is active at a basal level performing homeostatic functions such as protein and organelle turnover and it is upregulated in response to both extracellular and intracellular stress conditions such as nutrient starvation, growth factor withdrawal, and hypoxia, aggregation of proteins and accumulation of damaged mitochondria, oxidative stress, or high bioenergetics demands. It is also stimulated when cells prepare themselves to undergo structural remodeling, for example during developmental transitions. Other cues like temperature and cell density are also important in the control of the autophagy [193]. Although autophagy protects cell during caloric restriction, pathogen invasion and growth factor starvation, it can also lead to a programmed cell death type II (Autophagic cell death) [194].

In response to the stimulus, autophagy begins in the cytoplasm with a "C" shaped double membrane structure – phagophore. In yeast, the preautophagosomal structure – PAS – which is localized in the perivacuolar region, where almost all Atg proteins assemble has been assumed to be the origin of the phagophore. Such structure has not been observed in mammalian cells. The initial steps of autophagy include the vesicle nucleation (formation) and vesicle elongation (expansion) of the phagophore. After the expansion of the phagophore its edges fuse themselves engulfing citoplasmatic cargo and forming the autophagossome (vesicle completition) [193] (Figure 8). Then the autophagosome may fuse with an endosome originating an acidic vesicle – amphisome. The formation of the autophagosome or amphisome is then followed by a fusion with a lysosome or vacuole – autolysosome – where the captured material is degraded together with the inner membrane (Figure 8). The recycled products can be reused after leave the autophagolysosome through permeases. The dynamic of membrane is highly conserved among the organism, from yeast and plants to animals [4, 193, 195]. Until recently autophagy was considered to be a non-selective degradation process in which cytosolic materials were randomly engulfed, however recent evidences support that, in most cases, cargo is specifically recognized by a growing number of cargo-recognition molecules or autophagy receptors that physically interact with the material tagged for degradation and with effectors of the autophagy process [7]. Depending on the cargo to be degraded, new terms to describe this selective nature of autophagy have been proposed, such as reticulophagy, for the degradation of ER, mitophagy for mitochondrial degradation, ribophagy for ribosomes, xenophagy for pathogens, pexophagy for peroxisomes, lipophagy for lipid droplets, and aggrephagy for aggregates [7]. This selectivity is ensured by a family of cargo-recognition proteins, such as p62 and NBR1 that are able to interact with LC3 and as well with specific tags in the cargo to be cleared

[7]. Of particular notice, is that ubiquitination is one of the tags recognized by these proteins which render a mechanistic molecular link between autophagy and UPS [7].

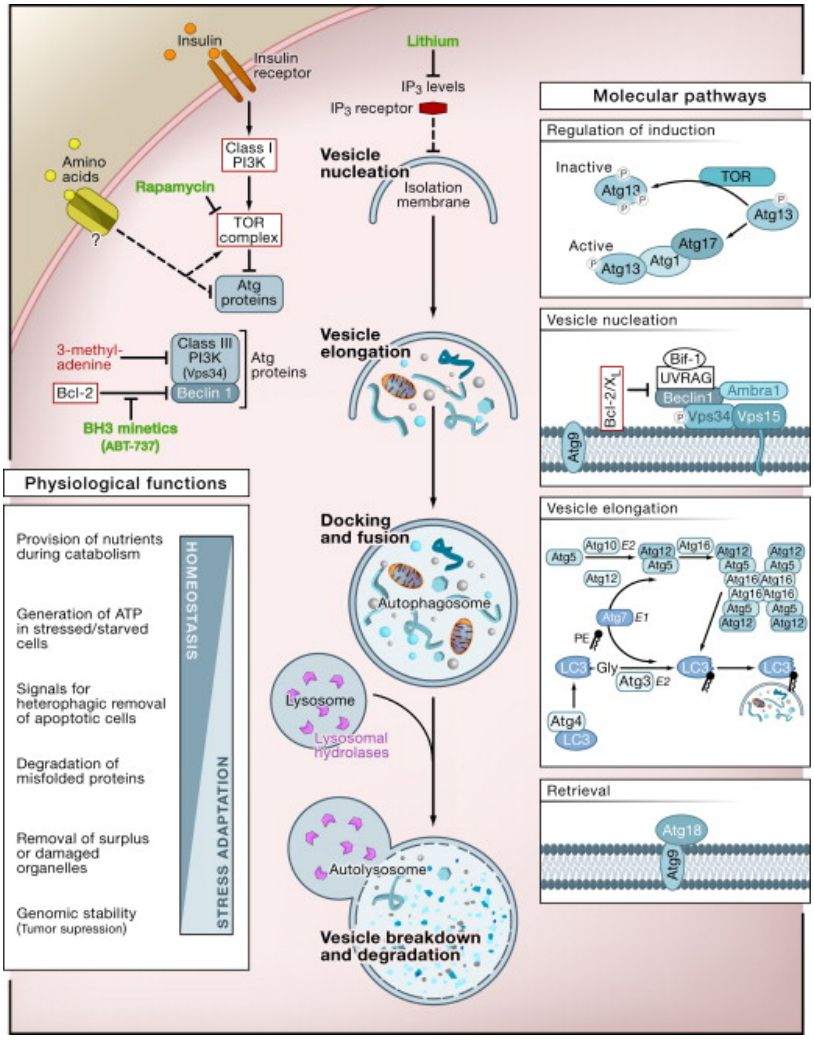

Figure 8: Overview of the autophagy-lysosomal pathway [193]

In the brain of an AD patient as well as the AD model (APP+PS1 double transgenic mice), the autophagic pathway is significantly compromised [196]. In the transgenic AD APP/PS1 mutant mouse model, LC3-II levels, a molecular marker of autophagy, is significantly elevated and it is correlated to large amounts of autophagic vacuoles [196]. Furthermore, electronic microcopy shows that these vacuoles are accumulated in the cell bodies and neurites of APP/PS1 mice indicating that there is induction of autophagy but somehow there is a defect in the maturation of these vacuoles leading to its accumulation [196]. In addition, the accumulation of the autophagic vacuoles starts even before the Aβ-positive plaque and NFTs formations [196]. Indeed, it was proposed that the Aβ toxic species might be formed within the autophagic vacuoles where there are proteolytic enzymes that are capable of such processing [196]. Thus, although autophagy can be greatly beneficial and therapeutic to eliminate toxic proteins and aggregates, it can also enhance the pathology; hence better understanding this complex mechanism is crucial to develop new strategies to deal with these diseases.

Tau, additionally to be cleared by the proteasome, can also be processed by autophagy. Of note is that both soluble and insoluble Tau (regardless its phosphorylation levels) can be processed by this pathway in contrast to the UPS [41]. Besides, there are evidences that indicates autophagy as the primary degradative pathway for endogenous Tau in primary neurons [197]. In agreement with this finding, Hamano et al. using a neuroblastoma cell model that inducible overexpress wild-type human Tau found out that upon inhibition of autophagy enhanced Tau aggregation [198]. Additionally to the wild-type Tau, D421 truncated Tau produced in SK-N-SH neuroblastoma cells due to inflammation seem to be degraded in a cathepsin-dependent manner [10]. Moreover, stable cell lines expressing human Tau when treated with chloroquine, 3-methyladenine (3-MA), or cathepsin inhibitors resulted in delayed degradation of Tau and promoted aggregates [10]. Interestingly, it has been demonstrated that Tau D421-cleaved is more prone to autophagy degradation in comparison to full-length Tau, which tends to undergo non-ubiquitin dependent degradation by the proteasome [10]. Moreover, when cathepsin D (a lysosomal protease involved in autophagy) is deleted in flies, accumulation of Tau truncated D421 is observed [10]. This Tau specie is thought to be more prone to aggregation than full-length Tau [10] which might explain the preference by the autophagic pathway. Recently, Tan et al, described a K63-linked ubiquitynation of both Tau and superoxide dismutase 1 (SOD1) leading to their autophagic clearance [10]. Interestingly, a mechanism for K63-linked ubiquitynation by the E3 ligase TRAF6 has been proposed [10]. In the same work, K63-ubiquitynated Tau was described to bind to p62, which has been linked to both the proteasome and autophagy [10]. Therefore, it remains likely that Tau might be degraded by either the proteasome or autophagy and it would be interesting to address the question whether different Tau conformations and/or aggregative states are differentially ubiquitinated (K11, K48 and K63) and/or phosphorylated. By characterizing such molecules with its specific post-translational modifications, it is possible that a mechanistic link between those and the degradative end-points could be traced.

Autophagy, indeed, due to the aforementioned characteristics appears as a polyvalent degradative pathway and hence reducing aggregated proteins and its possible toxics intermediates burdens through up-regulation of this pathway is logical and was proposed as a potential therapeutic approach for various neurodegenerative disorders [10, 45]. Thus, several studies have focused in the well characterized and clinically approved drug rapamycin that up-regulates autophagy by inhibiting the central regulatory protein mammalian target of rapamycin (mTOR) [10]. Although it showed promising results as an autophagic-inducing agent to clear insoluble and soluble Tau forms both *in vitro* and *in vivo*, major concerns regarding its safety have been raised due to the fact that mTOR is a major regulator of a wide range of cellular homeostatic processes, from stress responses to protein transcription and translation [10]. Hence, new molecular targets that could modulate this degradative pathway are being researched. Thus, better understanding autophagy in the context of the central nervous system as well as the interplay and cross-talks between UPS and autophagy are of particular interest, particularly considering that ubiquitin can lead to a certain level of specificity for autophagy [7].

Chaperone-mediated autophagy (CMA) is a selective degradative pathway that is solely dedicated to the degradation of soluble proteins [199]. The presence of a pentapeptide motif biochemically related to KFERQ in its amino acid sequence, is necessary for a protein to be degraded by CMA. This motif is recognized by a

cytosolic chaperone, the heat shock cognate protein of 70 kDa (Hsc70) that in cooperation with its modulatory co-chaperones (Bag1, Hip, Hop and Hsp40) target the substrate protein to the surface of the lysosomes [199]. Then, the substrate protein–chaperone complex docks at the lysosomal membrane through interaction with the cytosolic tail of the lysosome associated membrane protein type 2A (LAMP-2A), which acts as a receptor for this autophagic pathway [199]. Unfolding is needed and preceded the internalization of the substrate. In addition for the protein translocation the presence of the luminal form of Hsc70 (lys-Hsc-70) is needed [199]. After the translocation the degradative process takes place [199]. Of particular interest, chaperons are also related to the UPS and can target proteins to this pathway as well [168]. Defects in CMA activity have also been described in some neurodegenerative disorders, such as Parkinson's disease and certain Tauopathies [199]. Interestingly, in a recent work Wang et al., using an inducible neuroblastoma cell model of Tauopathy expressing the repeat domain of Tau with a FTDP-17 mutation ($Tau_{RD}\Delta K280$) to test whether the autophagy-lysosomal pathways play a role in the degradation of the protein and its aggragates, observed that macroautophagy can efficiently degrade both soluble mutant Tau and its aggregates, whereas proteasomal degradation plays only a minor role in this system [41]. Furthermore, upon inhibition of macroautophagy enhanced aggregation and cytotoxicity of Tau mutant taked place. They further demonstrated that macroautophagy can also degrade full-length Tau and that phosphorylation in its repeat domain, which regulates the affinity of Tau for microtubules and possibly inhibits its proteasomal clearance, does not alter its sensitivity to autophagy–lysosomal degradation. As a surprise, they also found that the lysosomal protease cathepsin L was involved in the cleavage of mutant Tau, and that this was giving rise to fragments which strongly promotes aggregation to PHFs [41]. To determine the mechanism involved in the targeting of Tau to lysosomes for this partial cleavage, it was tested whether full-length Tau or Tau fragments were substrates for CMA in addition to macroautophagy. Indeed, $Tau_{RD}\Delta K280$ and its F1 fragment (result of a cytosolic cleavage) interact with the cytosolic hsc70 chaperone and this facilitates its binding to lysosomes in a manner depending on the CMA receptor LAMP-2A [41]. However, these Tau isoforms failed in translocate into the lysosomes. Instead, their association with the lysosomes through the CMA machinery seems to have further contributed to the cleavage of this mutant form of Tau and the organization of the protein into oligomeric complexes that may interfere with normal lysosomal function [41]. As a consequence, they proposed a very interesting model: when mutant Tau is expressed in N2a cells, it would first be cleaved by a "thrombin-like" activity in the cytosol to generate fragment F1. Then this fragment would be delivered to lysosomes via CMA, where it would be only partially translocated but still expose its C-terminus allowing cathepsin L-mediated cleavage to generate F2 and F3. Consequently, part of the truncated products would remain initially associated with the lysosomal membrane that could favor oligomerization at or near the surface of the organelle and eventually resulting in membrane disruption, lysosomal leakage and release of other F2 and F3 fragments into the cytosol where they would induce the aggregation of $Tau_{RD}\Delta K280$, together with other aggregation-competent forms of Tau. Altogether, this work suggests that dysfunctional CMA might be a central player concerning the origin of PHFs and NFTs in early stages of the disorder [41]. This work provides mechanistic evidences and molecular targets that might be useful for development of early therapeutic interventions for Tauopathies.

Another interesting and very recent work, showed the first evidence that ubiquitin might be also involved in CMA. Ferreira et al., experimentally demonstrated that CHIP is required for the transcription

factor HIF1A degradation by CMA. Within this context and considering that Tau can be ubiquitinated by CHIP, it is possible that this "tagging system" might be playing a role in targeting toxic Tau species to CMA as well [200]. As already mentioned, soluble misfolded Tau can be degraded by the UPS but it seems that it is not its main route [197]. Altogether, this is a strong rationale to consider a possible ubiquitin role in mediating CMA targeting of Tau. Indeed, it would be interesting to check whether CMA-mediated Tau clearance might be dependent on the activity of CHIP and/or TRAF6 (or even other E3 ligases). If true, characterizing its ubiquitin chains conjugation would be particularly important to better understand the mechanism; besides, it would possibly be used to molecularly target these specific Tau isoforms (Tau could lead to CMA dysfunction and aggregation) for an antibody-mediated intervention that might be used in very early stages of the disease. Moreover, in this context, checking the influences of the expression of the aforementioned DUBs [177, 179] would also be relevant as they most likely could have a prominent role in regulating any ubiquitin-mediated Tau turnover regulation.

1.6 Project goals

Data accumulated from over the years led to a better understanding of the role of Tau in the pathogenesis of many neurodegenerative disorders [1, 2, 16, 44, 45]. These data highlighted the complex biology of this protein and showed that Tau contributes to toxicity by multiple mechanisms and at different stages of the diseases [1, 2, 16, 44, 45]. Unfortunately, despite the growing body of evidence that strongly supports the involvement of pathologically modified Tau (from soluble to insoluble aggregates) in neurodegeneration, the neurotoxic Tau species have not been identified yet [1, 2, 16, 44, 45]. Besides, toxic gains and losses of function are believed to play a role in inducing neurodegeneration, but the exact mechanisms by which this occurs remain to be further elucidated [1, 2, 16, 44, 45]. However, despite this complexity, this knowledge has opened new and encouraging avenues for future Tau research. Indeed, the better understanding of Tau's turnover mechanisms seems to open new and exciting possibilities towards finding new molecular targets that could reduce the burdens associated to the aggregative pathological behavior of toxic Tau [6, 10, 41, 176, 197]. In light of these data, the identification of ubiquitin in NFTs and UPS-related proteins interacting with Tau, such as E3 ligases, DUBs and heat-shock proteins that can modulate both the UPS and autophagic lysosomal pathways give a new range of possibilities to study [5, 6, 41, 172, 174, 177, 180]. Hence, identifying the roles of such proteins in the context of Tau degradation might give major insights into Tau's turnover, and succeeding in creating a successful therapeutic approach passes through the understanding of such mechanisms.

In light of such observations, the main goals of this project are:

- To evaluate the effect of Tau aggregation on the UPS and autophagy activity in primary neurons over time;
- To evaluate the effect of UPS inhibition and autophagy induction on clearance of soluble and aggregated Tau *in vitro*
- To evaluate the effect of knockdown of USP5, USP7 and OTUB1 on soluble aggregated Tau levels *in vitro*.

2 MATERIAL AND METHODS

2.1 Culture of primary neurons

Cortical neurons were isolated from brains of embryos of Wistar rat (WT rat) and B6;C3-Tg(Prnp-MAPT*P301S)PS19Vle/J mice (PS19hTauP301S mice) from The Jackson Laboratory that expresses the P301S clinical mutant of human microtubule-associated protein Tau. Cortical neurons were dissected on embryonic day E16-19. Brains were placed in pre-warmed HBSS/Hepes solution (7mM Hepes in HBSS and Penicilin-Streptomycin) until all cortices were collected. Neurons were dissociated via trypsinization in 1% trypsin in HBSS/Hepes, 10-15 min, 37°C) followed by mechanical trituration with Pasteur pipettes in MEM-Horse medium (10%Horse serum and 0.6%, MEM medium). Neurons were centrifuged for five minutes at 1000rpm and ressuspended in the fresh MEM-Horse medium. Number of neurons plated depended on the format of dishes used for the experiment: 1,5 x10^5 cells/well in 12 well plate, 2-3 x10^4 cells/well in 96 well plates and 1x10^4 cells/well in 384 well plates. 4-18 hours later MEM-Horse medium was replaced by Neurobasal medium containing B27 suplement (2% B27 and 10 mM L-glutamine in Neurobasal medium). Neurons were maintained in Neurobasal / B27 medium during the whole experiment

2.2 Overexpression of human full length Tau containing the P301L mutation (hTauP301L) and enhanced green fluorescent protein (eGFP) in primary neurons

Adeno-associated viral vectors were used to mediate neuronal expression of genes of interest. AAV6 serotype was shown before to efficiently deliver genes to neurons of central nervous system. AAV6 Synapsin-1 promoter (SYN1) was used to control transcription of both genes: hTauP301L and eGFP. This strategy warranties that the gene of interest will be expressed specifically in neurons.

Transduction of the rat primary cortical neurons with AAV6 for hTauP301L overexpressin was done on day 3 *in vitro* (3DIV) for the "long model" and on day one *in vitro* (1DIV) for the "short model" at a multiplicity of infection 100 (MOI 100). Transduction with AAV6 for eGFP overexpression was done on day 1 day *in vitro* (1DIV) at a multiplicity of infection 100 (MOI100). The "long" and "short" models will be further elaborated in the section Results.

Adeno-associated viruses were diluted in Neurobasal/ B27 immediately before the treatment.

2.3 Knockdown of genes in primary neurons

Lentiviruses encoding the appropriate targeting short hairpins RNAs (shRNAs) were used to knockdown the genes of interest. (Table 1).

The transduction of the PS19hTauP301S primary neurons with lentiviruses in order to down-regulatate hTauP301S was performed on day 2 in vitro (2DIV) at a multiplicity of infection 200 (MOI 200). To downregulate the expression of the deubiquitinating enzmes (DUBs) OTUB1, USP5 and USP7 neurons were transduced with lentiviruses at MOI 100 (see Table 1 for lentiviruses information).

Lentiviruses were diluted in Neurobasal/B27 immediately before the treatment. Table 1 shows nucleotide sequences used to target the given genes

Table 1: Target gene, oligonucleotide sequence and vector of shRNAs used to downregulate hTau and DUBs.

shRNA reference	Target Gene	Vector	Oligonucleotide sequence	Company
shRNA hTau 974	Human Tau	pLKO_TRC005	5' CCGGCCAGTCCAAGTGTGGCTCAAACTCGAGTTT GAGCCACACTTGGACTGGTTTTTG 3'	Sigma-Aldrich
shRNA hTau 976	Human Tau	pLKO_TRC005	5' CCGGGCAGTGTGCAAATAGTCTACACTCGAGTG TAGACTATTTGCACACTGCTTTTTG 3'	Sigma-Aldrich
shRNA OTUB1 #1	Mice Otub1	pLKO_TRC005	5' CCGGGCAAGAGATTGCTGTGCAGAACTCGAGTT CTGCACAGCAATCTCTTGCTTTTTG 3'	Sigma-Aldrich
shRNA OTUB1 #2	Mice Otub1	pLKO_TRC005	5' CCGGGAGCAAGTTCTTCGAGCACTTCTCGAGAA GTGCTCGAAGAACTTGCTCTTTTTG 3'	Sigma-Aldrich
shRNA OTUB1 #3	Mice Otub1	pLKO_TRC005	5´ CCGGTGGTTGTAAATGGTCATATTTCTCGAGAAA TATGACCATTTACAACCATTTTTG 3	Sigma-Aldrich
shRNA OTUB1 #4	Mice Otub1	pLKO_TRC005	5' CCGGGTCCATCCAAGTGGAGTACATCTCGAGAT GTACTCCACTTGGATGGACTTTTTG 3'	Sigma-Aldrich
shRNA OTUB1 #5	Mice Otub1	pLKO_TRC005	5' CCGGAGCGACTCCGAAGGTGTTAACCTCGAGGT TAACACCTTCGGAGTCGCTTTTTTG 3'	Sigma-Aldrich
shRNA USP5 #1	Mice USP5	pLKO_TRC005	5' CGAATGTTCAAGGCCCTCATT 3'	Sigma-Aldrich
shRNA USP5 #2	Mice USP5	pLKO_TRC005	5' CCTGGGCTACATCTACTTCTA 3'	Sigma-Aldrich
shRNA USP5 #3	Mice USP5	pLKO_TRC005	5' CGAGGATGTGAAGATTGTCAT 3'	Sigma-Aldrich
shRNA USP7 #1	Mice USP7	pLKO_TRC005	5' CCGGCAACAAGATGAAGAGCACCAACTCGAGTT GGTGCTCTTCATCTTGTTGTTTTTGAATTC 3'	Sigma-Aldrich
shRNA USP7 #2	Mice USP7	pLKO_TRC005	5' CCTACAGCAAGCTGAAGAGCACCTACTCGAGTTG GTGCTCTTCATCTTGTTGGGTTTGAATTC 3'	Sigma-Aldrich

2.4 Aggregation of recombinant Tau *in vitro*.

Truncated form of human Tau containing four repeats microtubule-binding domain (K18) with the clinical point mutation at Proline 301 (P301L) and fused to Myc tag at C- or N- terminal (K18P301L; Figure 9) was expressed in bacteria and purified to obtain pre-fibrilized Tau seeds. The fibrilization of K18P301L proceded as follows: 40 µM of K18P301L seeds was mixed with 40 µM low molecular weight heparin and 2 mM DTT in 100 mM sodium acetate buffer (pH 7.0) [165]. The fibrilization mixture was incubated at 37°C for 48 to 72 hours followed by ultracentrifugation at 100 000g during 30 minutes at 4°C. The supernatant was

discarded and the pellet was re-suspended in 100mM sodium acetate buffer to the final concentration of 40uM. The K18P301L fibrils were stored at -80°C.

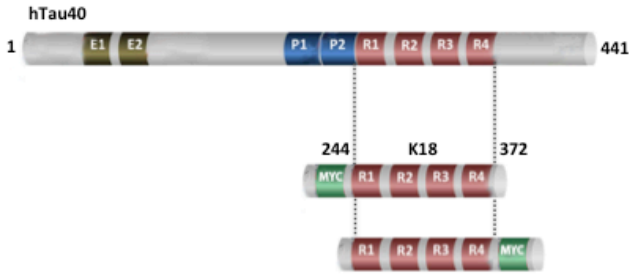

Figure 9: The isoform htau40 is the longest isoform in the human Central Nervous System. Construct K18 comprises the sequence of four repeats, the point mutation P301L (not shown in the image) and the Myc tag.

2.5 K18P301L fibrils delivery into primary cortical neuronal cultures

K18P301L fibrils were diluted on sodium acetate to the final concentration of 10uM and mental tip sonicated with 25 pulses of 2 seconds with 30 seconds of pause between each pulse on ice. After sonication, K18P301L fibrils were diluted in Neurobasal/B27 and added to the cultures to the final concentration of 25nM for the "long model" on day 10 *in vitro* (10DIV) and 12.5nM for the "short model" on day 3 *in vitro* (3DIV). For the knockdown experiments 12.5nM of K18P301L were added on the day 4 *in vitro* (4DIV).

2.6 Sarkosyl extraction

Cells (12 well plate with 200 000 cells/well) were washed with PBS and extracted in 200µl of H buffer: 10 mM Tris HCl (pH 7.6), 0.8 M NaCl, 10% sucrose, with proteases & phosphatases inhibitors on ice followed by homogenization and sonication (6 pulses of 2 seconds with 30 seconds of pause between each pulse on ice). Samples were then centrifuged for 30 min, 20 000g and the supernatant was collected (total extract) and mixed with sodium lauroyl sarcosinate (sarkosyl) (final concentration 1%) followed by a 1 hour room temperature incubation under agitation. Subsequently, a 1 hour ultracentrifugation at 150 000g was performed and the supernatant was removed and kept as "soluble fraction". The pellet (insoluble fraction) was dissolved in an equal volume of H buffer as the sarcosyl soluble fraction. Total extract was used to quantify the sample protein content by the Bicinchoninic Acid method (BCA method, Thermo Scientific) and samples were run on Bis-Tris 4-12% gel as described bellow in the Western blotting technique.

2.7 Western Blotting

After extraction of total protein with RIPA buffer with protease and phosphatase inhibitors, or extraction of soluble and insoluble protein fractions as described above (Material and Methods 2.6.) from 12-well plates cultures, protein quantification by the BCA method was performed according to manufacturer's instructions (Thermo Scientific). 4.5ug protein samples were used for hTauP301L overexpressed protein detection and 6ug to endogenous proteins. Samples were diluted in sample buffer (2.5 parts of LDS with 1 part of sample reducing agent (Life Technologies), heated 10 minutes at 75ºC and then put on ice and centrifuged in a benchtop centrifuge (Eppendorf) for 5 minutes at 10 000rpm. Finally, samples were loaded

on a NuPage Novex Bis-Tris 4-12% gel and ran in MOPS SDS running buffer with exception of gels intending LC3 detection, in which case MES SDS running buffer was used. Protein transfer was performed onto a 0.2um nitrocellulose membrane by Trans-Blot® Turbo™ Transfer System (BioRad). Membrane was subsequently washed in TBS-T (1M Tris, 150nM NaCl and 0.05% (v/v) Tween-20, pH 8.5) and blocked with 5% non-fat dry milk (NFDM) diluted in TBS-T or 5% BSA diluted in TBS-T for 1 hour at room temperature with gentle agitation. After blocking, membranes were incubated with primary antibody diluted in 1% NFDM in TBS-T overnight at 4°C. Table 2 shows the final dilutions which were applied to the given antibodies. In the following day membranes were washed four times for five minutes with TBS-T and incubated with the appropriate secondary antibody labeled with horsedish peroxidase (HRP; 1:10000 in TBS-T) for one hour at room temperature. Afterwards, membranes were washed in TBS-T four times for five minutes. Signals were detected with ECL reagent (West Dura or Femto; Thermo Scientific) and captured on a luminescence imager (G-Box, Syngene). Internal controls are essential for accurate, quantitative measurement of target protein expression on Western blots. These controls are used to correct for errors introduced by sampling irregularities, unequal loading, and uneven protein transfer across a membrane. The protein products of housekeeping genes (HKGs) are often used as loading controls, because they are generally thought to be expressed at consistent levels across nearly all tissue types and experimental conditions. To correct for loading the membranes were stripped of the secondary antibody with RestoreTM Western Blot Stripping Buffer for 15min at room temperature under gentle agitation. Subsequently, membranes were washed in TBS-T, blocked and re-probed with another set of primary and secondary antibodies as described above. Western blot images were quantified using ImageJ version 1.47 software (NIH, Bethesda, Maryland).

2.8 AlphaLISA assay

The AlphaLISA technology allows the detection of molecules of interest in cell lysates. It bases itself on an antibody sandwich strategy being a highly sensitive, quantitative and reproducible assay. The principle of the assay is based on the following settings: an anti-analyte antibody which is biotinylated binds the streptavidin donor bead while another anti-analyte antibody is conjugated to AlphaLISA acceptor beads. In the presence of the analyte, the beads come into close proximity. The excitation of the donor beads provokes the release of singlet oxygen molecules that results in the energy transfer onto the acceptor beads and emission of light (Figure 10). Here we used two specific alphaLISAs: HT7/hTau10 alphaLISA to detect total human Tau (i.e.: that does not discriminate between postranslational modifications neither between different hTauP301L protein conformations) and hTau10/hTau10 alphaLISA to detect the aggregated human Tau. For total Tau the sandwich was optimized with two antibodies (HT7 biotinylated and hTau10 conjugated to acceptor beads, see Table 2), which recognize two different epitopes within one Tau molecule (Figure 10). In consequence, this assay measures intra and inter-molecular interactions of Tau and detects soluble and insoluble Tau levels. hTau10/hTau10 Alpha LISA, which detects the aggregated Tau, engages a single antibody which recognizes one epitope within Tau molecule (Figure 10). In this assay one fraction of hTau10 antibody (Table 2) is biotinylated and other fraction of hTau10 antibody is conjugated to acceptor beads. In consequence, the light will be emitted exclusively if at least, two Tau molecules happen to be in close vicinity to close the sandwich. The eptitope that is recognized by hTau10 (Table 2) is phosphrynation independent.

This assay was performed as follows: B27 medium was removed and 96-well plates rat primary cortical neuronal cultures were washed with PBS and lysed in 40ul of 1% Triton X-100 with protease and phosphatase inhibitors. 5ul of the cellular extract were used for the analysis and added to white OptiPlate-384 microplate. In the first step the sample was incubated with the mix of biotinylated and acceptor conjugated beads for two hours at room temperature in the alphaLISA immunoassay buffer (25 mM HEPES, pH 7.4, 0.1% Casein, 1 mg/mL Dextran-500, 0.5% Triton X-100 and 0.05% Proclin-300). Table 2 specifies the concentrations of biotinylated antibodies and antibodies conjugated to acceptor beads used for the given assays. In the second step, the streptavidin coated donor beads (0.015mg/mL for total Tau levels detection and 0.01mg/mL for aggregated Tau levels detection) were added for 30 minutes incubation. AlphaLISA assay was read on a Perkin Elmer EnVision® 2102 Multilabel Reader and EnVision® 2102 software.

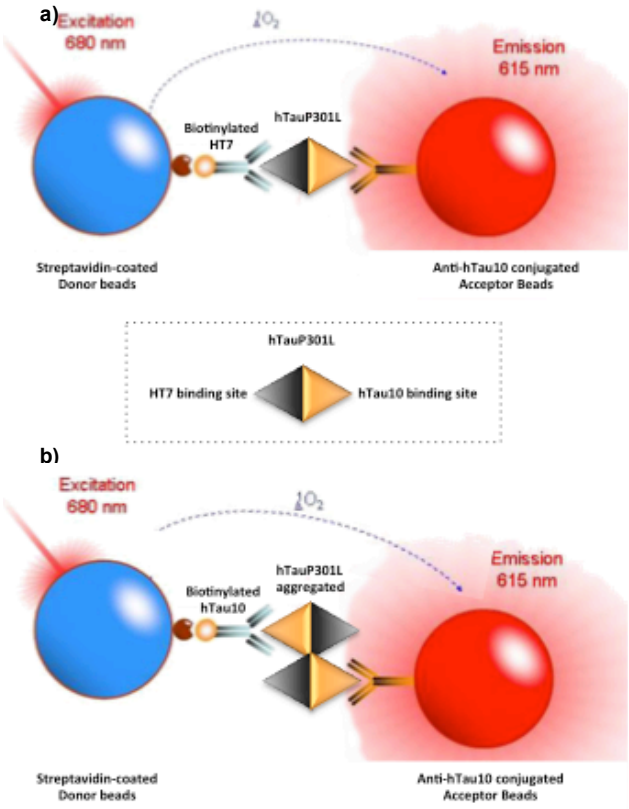

Figure 10: Principle of the alphaLISA technology and antibody sandwich configurations. a) Sandwich design for detection of total hTauP301L. Two antibodies were used (HT7 biotinylated and hTau10 conjugated to acceptor beads – HT7/hTau10 -, see Table 2), which recognize two different epitopes within one Tau molecule. b) Sandwich design for detection of aggregated hTauP301L. A single antibody was used which recognizes one epitope within hTauP301L molecule (hTau10 biotinylated and conjugated to aceptor beads – hTau10/hTau10 – Table 2.)

2.9 Sandwich Enzyme-Linked Immunosorbent Assay (ELISA)

The sandwich ELISA technology allows the detection of molecules of interest in solutions (e.g.: cell lysates) by quantifying antigens between two layers of antibodies (i.e. capture and detection antibody). To detect antigen, the wells of multiwell plates are coated with specific capturing antibody followed by incubation with sample to be analysed. Unbound antigen is washed out and an antigen-specific antibody conjugated to enzyme (i.e., detection antibody) is added, followed by another incubation. Unbound conjugate is washed out and substrate is added. After a last incubation the degree of substrate hydrolysis is measured which is proportional to the amount of antigen in the test solution. Here we used one set of antibodies (mTau5 as a capturing antibody and hTau24 conugated to a horseradish peroxidase – HRP – as the detection antibody) to detect rodent Tau (see Table 2 for information on antibodies). For such purpose, Costar 96 well Half-Area Plates and Nunc Maxisorp 96 well plate were coated with a solution of capturing antibody mTau5 (table2) at 1µg/mL in a coating buffer (10mM Tris, 10mM NaCl pH 8.5; 50µL per well) overnight at 4ºC. After that, plates were washed in the microplate washer AquaMax 4000 form Molecular Devices for 5 times

with PBS-T (10 mM phosphate buffer pH 7.4, 150 mM NaCl, 0.05% Tween 20), and overblocked with 75µL (for Costar plates) and with 120ul (for Nunc Maxisorp plates) of 0.1% Casein in PBS per well for one to four hours at room temperature. The plates were then washed again and 50uL of samples from the 96-well plates where the cellular cultures were kept, previously diluted in blocking solution in a ratio of 1:20, were added to the assay plate and incubated overnight at 4°C. After that, plates were washed and 50µL per well of the detection antibody hTau24-HRP (Table 2) diluted 1:1000 in blocking buffer was added. Finally, another wash was made and 50µL of fluorogenic peroxidase substrate QuantaBlu (ThermoScientific) (Costar plate) or TMB Peroxidase EIA (Nunc Maxisorp plate) substrate was added. Incubation with substrate was made for 15 minutes with QuantaBlu and in the case of using TMB Peroxidase EIA Substrate the incubation time was based on visual inspection of the colorimetric intensity of the samples and positive controls. TMB Peroxidase EIA substrate reaction was stopped by adding 50µL of 2N (1M) H_2SO_4. Readings were performed in Perkin Elmer EnVision® 2102 Multilabel Reader and EnVision® 2102 software.

2.10 Proteasome Activity assessments

Chymotrypsin-like protease activity associated with the proteasome complex in cultured cells (96well plate format and 384-well plate format) was assayed by using the Proteasome-Glo™ Chymotrypsin-Like Cell-Based Assays (Promega) according to manufacturer's instructions.

This assay involves the addition of a previously mixed reaction buffer directly to cultured cells. The reaction buffer used in this work is optimized for cell permeabilization, proteasome activity and luciferase activity and contains Suc-LLVY- aminoluciferin (Succinyl-leucine-leucine-valine-tyrosine-aminoluciferin) substrate and the thermostable luciferase, Ultra-Glo™ Recombinant Luciferase. The Suc-LLVY-aminoluciferin substrate is recognized by the proteasome and cleaved by its chymotrypsin-like activity (one of the three major proteolytic activities associated to the 20S catalytic core of the proteasome). Following cleavage by the proteasome, the substrate for luciferase (aminoluciferin) is released, allowing the luciferase reaction to proceed and produce a luminescent signal proportional to the amount of chymotrypsin-like associated proteasome activity in the cultured cells (Figure 11).

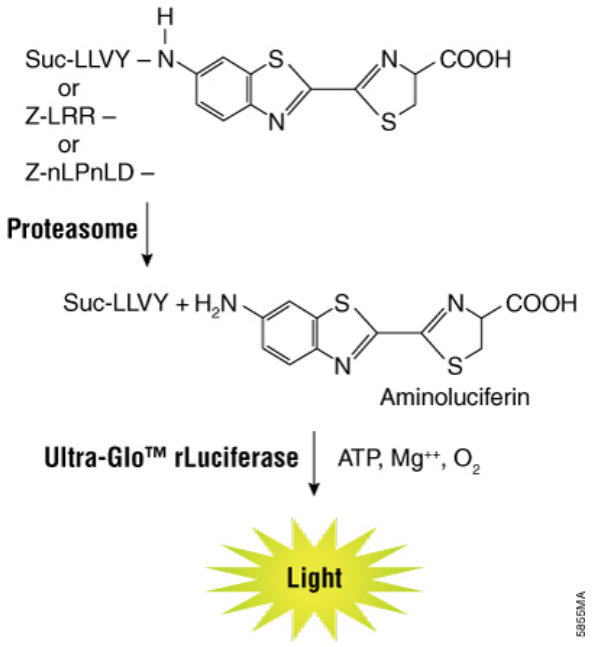

Figure 11: Principle of the Proteasome-Glo™ technology. The luminogenic substrate containing the Suc-LLVY sequence is recognized by the 20S proteasome.

2.11 Autophagy Activity assessments

To measure activity of autophagy in living cells the Cyto-ID® Autophagy Detection Kit (Enzo Life Sciences) was used according to manufacturer's instructions. Cyto-ID® Autophagy Detection probe becomes brightly fluorescent in vesicles produced during autophagy and reacts weekly with lysosomes. The probe is a cationic amphiphilic tracer (CAT) dye that rapidly partitions into cells in a similar manner as drugs that induce phospholipidosis that was developed by a careful selection of titratable functional moieties on the dye preventing its accumulation within lysosomes, but enabling labeling of vacuoles associated with the autophagy pathway. To assess the autophagy-related fluorescence and activity plates (384-well plate format) were scanned on Digilab MIAS-2™ Microscopy System (Ex: 482nm and Em: 536nm for Cyto-ID and Ex: 387 nm and Em: 447 for Hoechst 33342). Images were taken with Digilab MIAS-2™ Microscopy System and quantified by the software Grain Detection Assay (DCILabs).

2.12 Immucytochemistry

To allow for insoluble Tau detection and visualization, the insoluble Tau fraction has to be enriched, hence soluble proteins present in the cells need to be extracted. As this extraction occurs automatically during methanol fixation this methodology was chosen to probe insoluble Tau aggregates. For this purpose, primary neurons plated both on 96-well or 384 well format were washed with PBS and subsequently fixed with Methanol (MetOH). MetOH fixation was performed with ice cold 100% MetOH for 10 minutes in -20ºC followed by rehydration in PBS. Samples were subsequently blocked with 5% goat serum diluted in PBS for 45 min at room temperature. Finally samples were incubated with primary antibody diluted in bloking solution overnight at 4ºC. Such incubation was followed by three washes in PBS and incubation with appropriate secondary antibody conjugated to the fluorescent dies: Alexa Fluor® 555 or Alexa Fluor® 488. Secondary antibody incubations lasted 30 min at room temperature. Table 2 shows the final concentration of the antibodies used for this assay. Cells were then analyzed by fluorescent microscopy on the Digilab MIAS-2™ Microscopy System.

Table 2: List of antibodies, their applications and concentrations/dilutions used in this project.

Antibody	Target	Host specie	Clonality	Company and Catalog number	Application	Dilution or final concentration
JRD/hTau/10 (hTau10)	Human Tau (N-terminal)	Mouse	Monoclonal	Produced in house	AlphaLISA	Biotynilated hTau10 0.3nM or 0.08; hTau10 conjugated with acceptor beads 0.01nM
HT7	Human Tau	Mouse	Monoclonal	Pierce MN1000	AlphaLISA; Western blot;	1.2nM for alphaLISA (Biotynilated HT7); 1:1000 for western blot
Anti-Actin clone C4	Actin	Mouse	Monoclonal	Milipore MAB1501	Western blot	1:5000

↵**Table 2 (continuation)**: List of antibodies, their applications and concentrations/dilutions used in this project.

Anti-LC3B	LC3B-I and LC3B-II	Rabbit	Polyclonal	Sigma-Aldrich L7543	Western blot	1:500
Neuronal Class III β-Tubulin	neuron specific Class III β-tubulin	Rabbit	Polyclonal	Covance PRB-435P	Western blot	1:1000
ECL Mouse IgG, HRP-linked whole Ab	IgG	Mouse	Polyclonal	GE Healthcare Life Sciences	Western blot	1:10 000
ECL Rabbit IgG, HRP-linked whole Ab	IgG	Rabbit	Polyclonal	GE Healthcare Life Sciences	Western blot	1:10 000
Ubiquitin Antibody	Ubiquitin Antibody detects ubiquitin, polyubiquitin and ubiquitinated proteins	Rabbit	Polyclonal	Cell Signaling Technology #3933	Western blot	1:1000
AT8	Phosphorylated Tau on ser202/thr205	Mouse	Monoclonal	Produced in house	Western Blot; Immunocytochemistry	1:1000 for both applications (2ug/mL)
Alexa Fluor® 555 Goat Anti-Mouse IgG (H+L)	IgG	Mouse	Polyclonal	Life Technologies A-21424	Immunocytochemistry	1:500
Alexa Fluor® 488 Goat Anti-Rabbit IgG (H+L)	IgG	Rabbit	Polyclonal	Life Technologies A-11008	Immunocytochemistry	1:500
MAP-2	Human, mouse and rat MAP-2	Rabbit	Polyclonal	Santa Cruz Biotechnology H-300	Immunocytochemistry	1:1000
JRD/hTau/24 (hTau24)	Human and rodent Tau	Mouse	Monoclonal	Produced in house	ELISA	1:1000
JRD/mTau/5 (mTau5)	Rodent Tau	Mouse	Monoclonal	Produced in house	ELISA	1ug/mL

2.13 Pharmacological treatments of neuronal primary cultures

Lactacystin, MG132 and rapamycin (Table 3) were prepared in dimethyl sulfoxide (DMSO), diluted in Neurobasal/B27 and added to the cultures to the wanted final concentrations (as depicted in the Results 3.3.1. and 3.3.2.). For all treatments DMSO concentration was controlled to 1µL/mL. Negative controls were performed by only treating primary neurons with 1µL/mL of DMSO.

Table 3: List of compounds used in this project

Compound	Molecular formula	Activity	Company and Catalog number
Lactacystin	$C_{15}H_{24}N_2O_7S$	Irreversible 20S proteasome inhibitor	Calbiochem (426100)
MG132	$C_{26}H_{41}N_3O_5$	Reversible proteasome inhibitor / autophagy inducer	Sigma-Aldrich (C2211)
Rapamycin	$C_{51}H_{79}NO_{13}$	Autophagy inducer (mTOR inhibitor)	Sigma-Aldrich (R0395)

2.14 Statistical analysis

All quantitative results are expressed as means ± SEM. Statistical analysis were performed using one-way ANOVA followed by Tukey *post-hoc* multicomparisons with an alpha = 0.05, two-way ANOVA followed by Tukey's and Sidak's *post-hoc* multicomparisons with an alpha = 0.05, as discriminated in the results section for each case. When *post-hoc* multicomparisons were used, multiplicity adjusted P values (adjusted p values) [201, 202] were computed for each comparison. The definition of the adjusted P value is the answer to the following question: "what is the smallest significance level, when applied to the entire family of comparisons, at which this particular comparison will be deemed statistically significant?" One-tailed Student's *t*-test was used to analyze the assay controls on the UPS and autophagy time-course assessments with a confidence interval of 95% (statistically different $p < 0.05$). All statistical analysis was performed with GraphPad Prism 6 (GraphPad Software, La Jolla California USA, www.graphpad.com).

3 RESULTS

3.1 Characterization of Tau aggregation in rat cortical neurons – "long" model

An *in vitro* Tau aggregation model was initially developed in HEK293 cell line [165]. To mimic as closely as possible Tau pathology, this model was transferred to rat primary cortical neurons. Neurons were dissected on embryonic day 19 (E19) (Material and Methods 2.1.). On day 3 in vitro (3DIV), neurons were transduced with adenoassociated virus encoding for hTauP301L under the control of the neuron specific promoter SYN1 (Material and Methods 2.2.). However, hTauP301L aggregation is not a spontaneous process just by the overexpression of hTauP301L. In order to induce aggregation of hTauP301L neurons were seeded with K18P301L fibrils (Material and Methods 2.5.) on day 10 in vitro (10DIV). To confirm hTauP301L aggregation, on the 17DIV samples were collected followed by a sarkosyl extraction (Material and Methods 2.6.) and western blotting (Material and Methods 2.7.). Additionally, to determine the kinetics of hTauP301L aggregation in this model the samples were collected on the 6DIV and daily between 10-20DIV for biochemistry (alphaLISA; Material and Methods 2.8.) and daily between 10-18DIV for immunocytochemistry (Material and Methods 2.12.) assessments.

3.1.1 Aggregation of hTauP301L in rat primary neurons

It was reported that direct membrane penetration of α-synuclein occurred in cell cultures [203]. More importantly and similarly to such observation is that spontaneous uptake of in vitro pre-aggregated K18P301L in rat cortical primary cultures was observed and previously described in our laboratory [166]. Hence to confirm such finding in our model, AAV6hTauP301L MOI 100 transduction was performed on 3DIV and K18P301L 25nM seeding on 10DIV (Material and Methods 2.2. and 2.5.), followed by sample collection, sarkosyl extraction (Material and Methods 2.6.) and western blotting (Material and Methods 2.7.) on 17DIV (Figure 12).

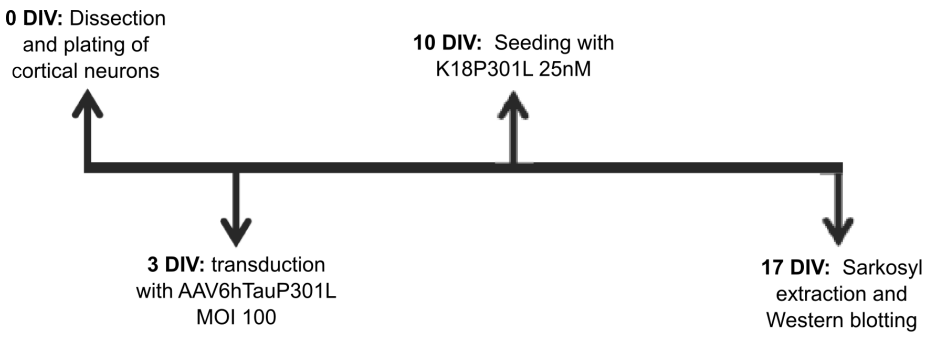

Figure 12: Graphic overview of the experiment

Analyzing the sample by western blotting using the anti-Tau antibody HT7, which detects human Tau in the residues between 159-163 [204] (absent in the in vitro synthetic K18P301L), hTauP301L was detected in the total fractions for both conditions – neurons overexpressing hTauP301L not seeded and seeded with K18P301L (non-aggregative and aggregative conditions, respectively) – and only in the insoluble fraction after seeding with pre-aggregated K18P301L fibrils (Figure 13). In the total fraction a shift in the apparent molecular weight of the hTauP301L band was observed after seeding with the fibrils (Figure 13).

This may be due to an increase in phosphorylation of aggregated Tau causing the protein to migrate significantly slower in the SDS-PAGE gel compared with non-phosphorylated Tau. However, after separating soluble and insoluble proteins we found that the slower migrating form of hTauP301L was insoluble and the faster migration was soluble (Figure 13).

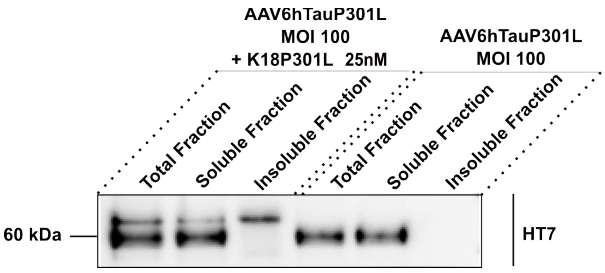

Figure 13: Western blotting analysis of Total, Soluble and Insoluble fractions of rat primary neurons overexpressing hTauP301L seeded or not with K18P301L. WT rat primary neurons were transduced with AAV6hTauP301L MOI100 on the 3DIV and seeded with 25nM of K18P301L on 10DIV. Cellular lysis was done on the 17DIV with posterior Western blotting. Based on the Total fraction quantification, equal portions of extracted protein were loaded on SDS-polyacrylamide gels. Monoclonal antibody HT7 against human Tau was used for hTauP301L detections.

In summary, the pattern observed in the cell line seeding models [166, 167] was reproduced in rat cortical primary cultures and the detection of a slower migrating band in the insoluble fraction in neurons overexpressing hTauP301L and seeded with K18P301L seeds (aggregative conditions) confirms that nucleation of hTauP301L aggregation occurred in our model.

3.1.2 Kinetics of hTauP301L aggregation in rat primary neurons assessed by immunocytochemistry

In addition to a biochemical approach to inspect the kinetics of hTauP301L expression and aggregation (Results 3.1.3. and 3.1.4.), we hypothesized whether such model would indeed lead to the formation of Tau aggregates and which features would be presented and associated with hTauP301L aggregation in an imaging inspection along time. For this purpose, the same strategy described earlier with AAV6hTauP301L MOI 100 transduction on 3DIV and K18P301L 25nM seeding on 10DIV (Material and Methods 2.2. and 2.5.) was adopted and one culture plate per day for nine days, beginning on 10DIV (day of K18P301L seeding – 0DAS), was fixed with methanol (Material and Methods 2.12.) in order to remain only with the insoluble fraction of the aggregates consequently allowing us to isolate and confirm the presence of such entities (Figure 14).

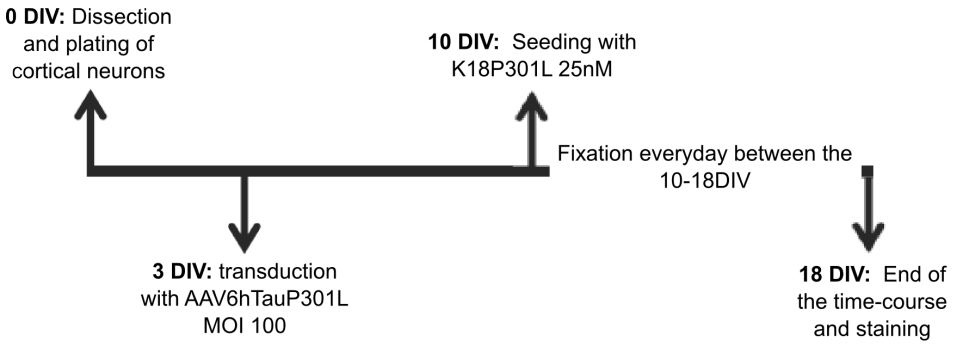

Figure 14: Graphic overview of the experiment

The capacity of *in vitro* pre-fibrilized K18P301L to induce intracellular aggregation of hTauP301L was thus visualized by immunocytochemistry as seen in the Figure 15 by means of the use of AT8 and MAP-2 antibodies. Microtubule-associated protein 2 (MAP-2) is an abundant neuronal specific cytoskeletal protein that co-localizes to dendrites [205]. MAP-2 detecting antibody were used to discriminate between neurons and non-neuronal cell types – astrocytes and microglia – as primary cultures are not homogeneous. Augustinack et al. have previously shown that the immunoreactivity of AT8 is associated with different stages of NFT formation in AD brains [206], therefore such antibody was used to identify hTauP301L aggregates.

No insoluble hTauP301L was detected either in wild-type primary neurons or in neurons overexpressing hTauP301L cultured in the absence of the seeds (Figure 15). When neurons, which overexpress hTauP301L, were cultured in the presence of K18P301L seeds (25nM), insoluble AT8 hyperphosphorylated hTauP301L was detected. AT8 specific signal can be seen, at very low levels, on the day 12DIV (day 2 after seeding – DAS - with K18P301L) as a ring-like pattern restricted to the neuronal somas. This pattern also evolves to the dendrites on the day 13DIV resembling strings (Figure 15). On the same day, a doted pattern can be observed in the neuronal somas (Figure 15) in addition to the ring-like pattern. Different levels of hTauP301L expression, which results from unequal AAV viral transduction efficiency, may cause the difference between the dotted and the ring-like patterns. The dotted AT8 pattern might be related to initial stages of hTauP301L aggregation that could be only spotted in neurons expressing lower levels of hTauP301L from the 13DIV onwards. On the 14DIV, a comet-like pattern that goes from the cell body in direction to the neurites (including at least the proximal part of those) is observed (Figure 15). Additionally, in the neurites the AT8 fluorescence starts showing itself in its majority as doted pattern rather than a continuous string (Figure 15). For the next days, the aggregation staining continues to increase and shows itself more spread along the microscopical field of view, although with the same features already described that continued until the end of the experiment. Importantly, these ring-like pattern and comet-like pattern resemble pathological NFT structures present in AD patients' brains that have been previously described [207]. These observations show that in this neuronal model hTauP301L aggregates upon seeding with K18P301L fibrils and closely resemble microscopically features of aggregated Tau in the brain.

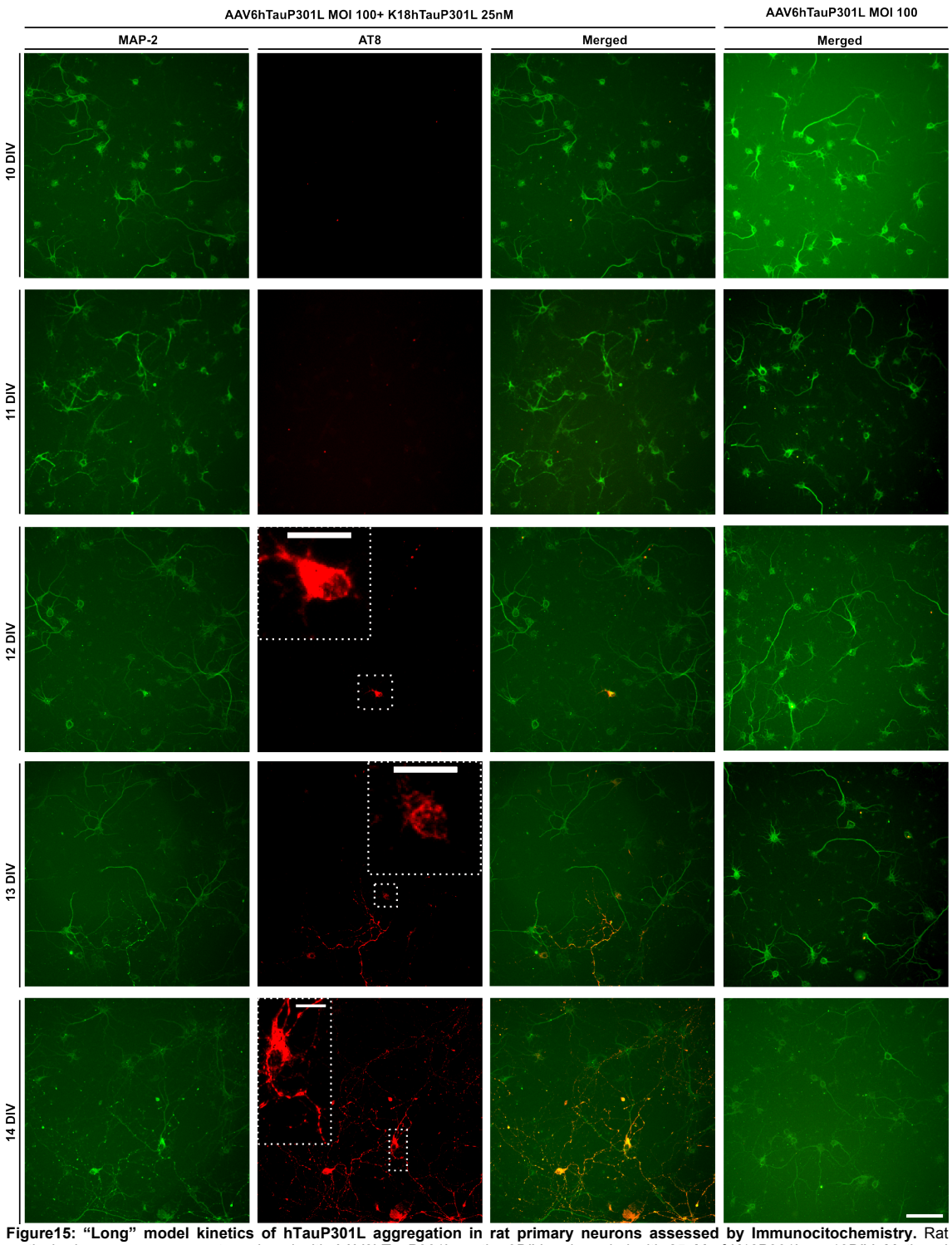

Figure15: "Long" model kinetics of hTauP301L aggregation in rat primary neurons assessed by Immunocitochemistry. Rat cortical primary neurons were transduced with AAV6hTauP301L on the 3DIV and seeded with 25nM of K18P301L on 10DIV. Methanol fixation was performed daily from the 10DIV to the 18DIV. AT8 antibody was used to detect aggregated hTauP301L phosphorylated on Ser202 and on Thr205 and corresponds to the red staining. MAP-2 antibody was used to discriminate between neurons and non-neuronal cells and corresponds to the green staining. Images were acquired by Digilab MIAS-2™ Microscopy System with a 20x magnification. Scale bar: 100µM. Close-up scale bar: 10µM. Wild-type rat cortical neurons not transduced with the AAV6hTauP301L and not seeded with K18P301L displayed the same phenotype as seen in the neurons overexpressing hTauP301L but not seeded with K18P301L (no AT8 signal) and hence are represented in this image by the neurons transduced with AAV6hTauP301L MOI100 in non-aggregative conditions. Rat cortical neurons overexpressing hTauP301L and seeded with 25nM of K18P301L display temporal-dependent hTauP301L aggregation.

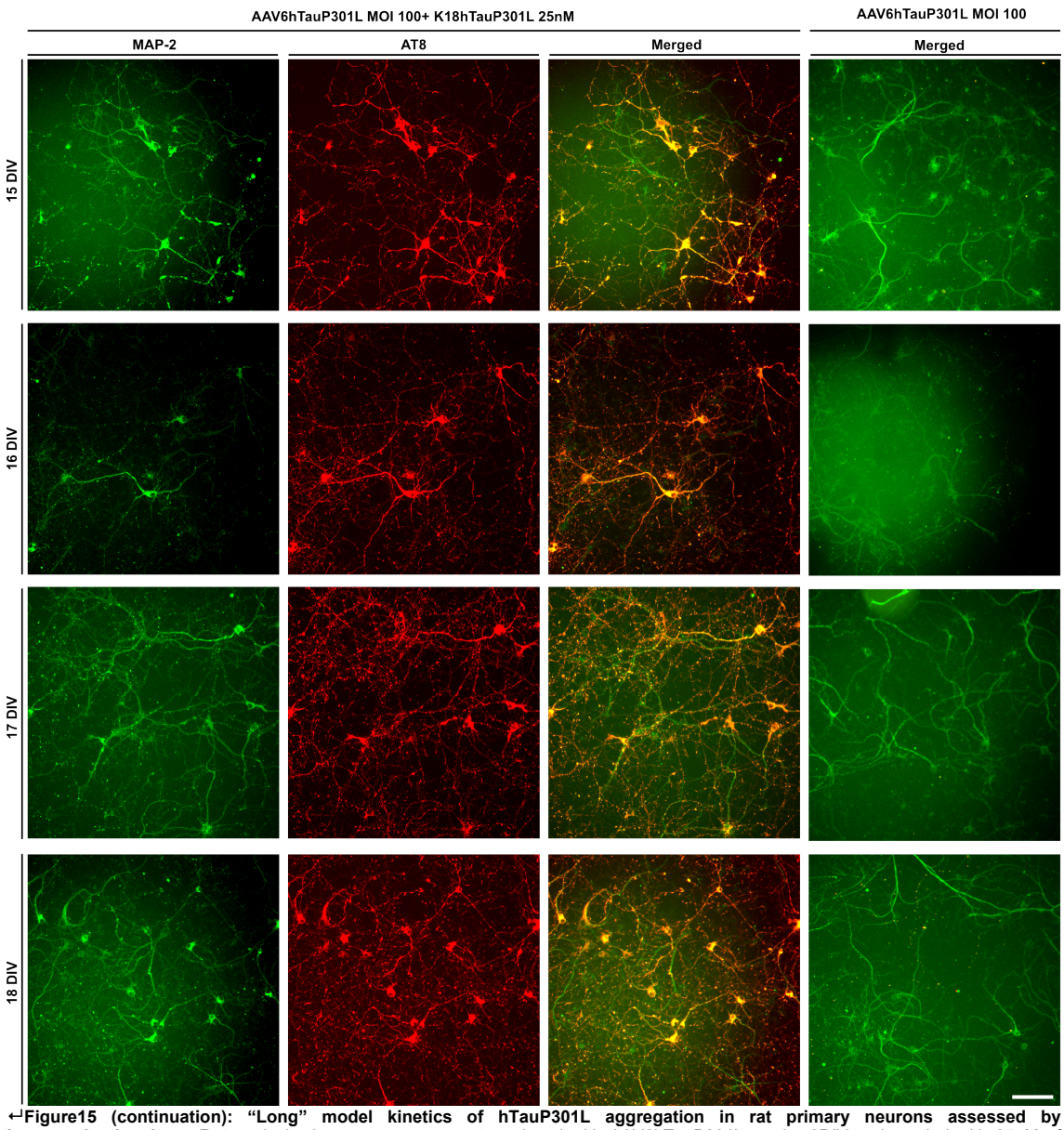

↵**Figure15 (continuation): "Long" model kinetics of hTauP301L aggregation in rat primary neurons assessed by Immunocitochemistry.** Rat cortical primary neurons were transduced with AAV6hTauP301L on the 3DIV and seeded with 25nM of K18P301L on 10DIV. Methanol fixation was performed daily from the 10DIV to the 18DIV. AT8 antibody was used to detect aggregated hTauP301L phosphorylated on Ser202 and on Thr205 and corresponds to the red staining. MAP-2 antibody was used to discriminate between neurons and non-neuronal cell types and corresponds to the green staining. Images were acquired by Digilab MIAS-2™ Microscopy System with a 20x magnification. Scale bar: 100µM. Wild-type rat cortical neurons not transduced with the AAV6hTauP301L and not seeded with K18P301L displayed the same phenotype as seen in the neurons overexpressing hTauP301L but not seeded with K18P301L (no AT8 signal) and hence are represented in this image by the neurons transduced with AAV6hTauP301L MOI100 in non-aggregative conditions. Rat cortical neurons overexpressing hTauP301L and seeded with 25nM of K18P301L display temporal-dependent hTauP301L aggregation.

3.1.3 hTauP301L MOI and K18P301L concentration influences hTauP301L initial slope of expression and hTauP301L slope of aggregation

In order to determine the optimal conditions in which hTauP301L aggregates we needed to determine the influences of MOI of AAV6hTauP301L virus and concentration of K18P301L seeds which were used to induce the aggregation. We transduced neurons with AAV6hTauP301L in MOI 50 and 100 combined with 2.5nM and 25nM of K18P301L seeds (Material and Methods 2.2. and 2.5.). To this end, the same experimental description above with AAV6hTauP301L MOI 100 or 50 transductions on 3DIV and K18P301L 25nM or 2.5nM seedings on 10DIV (Material and Methods 2.2. and 2.5.) was employed and on 6DIV and daily between the 10-20DIV neurons were lysed for biochemical analysis (Figure 16). Statistical analyses of the results were performed by a two-way ANOVA followed by Tukey *post-hoc* comparisons with an alpha set to 0.05.

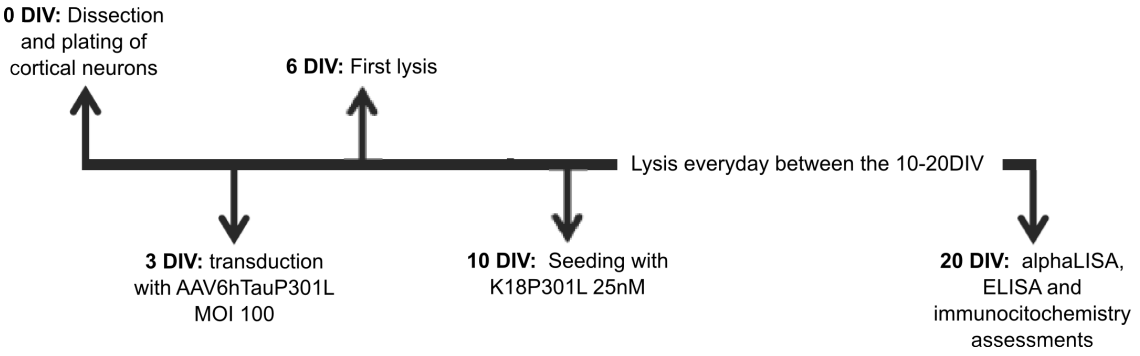

Figure 16: Graphic overview of the experiment

AAV6hTauP301L MOI does not influence the final overall alphaLISA signal either in soluble and total hTauP301L (HT7/hTau10 alphaLISA; Material and Methods 2.8.) expression values (neurons overexpressing hTauP301L not seeded and seeded with K18P301L, respectively) or hTauP301L aggregation signal (hTau10/hTau10 alphaLISA; Material and Methods 2.8.) for any of the treatments – AAV6hTauP301L MOI100, AAV6hTauP301L MOI50, AAV6hTauP301L MOI100 in the presence of K18P301L 25nM; AAV6hTauP301L MOI100 in the presence of K18P301L 2.5nM; AAV6hTauP301L MOI50 in the presence of K18P301L 25nM; and AAV6hTauP301L MOI50 in the presence of K18P301L 2.5nM, as it can be seen in the Figure 17. However, MOI 50 treated culture shows a reduced initial slope of soluble hTauP301L signal increase in comparison to neurons transduced with AAV6hTauP301L MOI 100 (HT7/hTau10 alphaLISA; Material and Methods 2.8.) as highlighted by a two-way ANOVA interaction p value highly significant ($p<0.0001$; alpha=0.05) and by statistical differences on the on the days 11, 12, 13, 14 and 15 *in vitro* – with an average of -34% difference in hTauP301L signal - when comparing neurons transduced with MOI 50 to MOI 100 and not seeded with the fibrils (Figure 17a; Tukey *post-hoc* adjusted p values of <0.0001; <0.0001; 0.0267 and <0.0001, respectively; alpha=0.05; Material and Methods 2.14.). From the 16DIV to the 20DIV MOI 50 and MOI 100 treatments that were not seeded with the fibrils display signal oscillations with statistical difference between the treatments on 17DIV (Tukey *post-hoc* adjusted p value <0.0001, alpha=0.05) and

19DIV (Tukey *post-hoc* adjusted p value =0.039; alpha=0.05; Material and Methods 2.14.) ending the experiment with equal signal levels (Figure 17a). When comparing the MOI 50 and MOI 100 treatments that were seeded with 25nM K18P301L fibrils (aggregative conditions), again a reduced initial slope of hTauP301L signal (total levels, i.e. soluble and aggregated hTauP301L present) is observed and underscored by a two-way ANOVA interaction p value highly significant ($p<0.0001$; alpha=0.05) and statistical differences on the 11DIV, 12 DIV, 14DIV and 15DIV (Tukey *post-hoc* adjusted p values of <0.0001; <0.0001; 0.001 and <0.0001, respectively; alpha=0.05; Material and Methods 2.14.) – with an average of difference in MOI 50 hTauP301L signal of -47% between the 11-12DIV and an average of -18% between the 14-15DIV when comparing to the MOI 100 (Figure 17b). Neurons treated with MOI 50 and MOI 100 in the presence of 25nM K18P301L also display oscillations on their hTauP301L signals between the 16-20DIV with statistical differences on the 17DIV and 19DIV (Figure 17b; Tukey *post-hoc* adjusted p values of 0.0092 and <0.0001, respectively; alpha=0.05; Material and Methods 2.14.). When comparing the MOI100 and MOI50 treated cultures in the presence of 2.5nM K18P301L (aggregative conditions) similar results to the previously described data are observed with a two-way ANOVA interaction p value highly significant ($p<0.0001$; alpha=0.05) in which an average of 43% reduction in the hTauP301L signal for the MOI50 treated cultures in comparison to the MOI100 treatment can be observed between the 11-12DIV (Figure 17c; Tukey *post-hoc* adjusted p values of <0.0001 for both days; alpha=0.05; Material and Methods 2.14.). Between the 16-20DIV the hTauP301L levels of the different MOIs (50 and 100) within the 2.5nM concentration of K18hTauP310L oscillate with statistical significance on the 16DIV, 17DIV and 19DIV (Figure 17c; Tukey *post-hoc* adjusted p values of 0.0219; 0.0012 and <0.0001, respectively; alpha=0.05; Material and Methods 2.14.). These reductions on the hTauP301L overexpression levels can be highlighted by a delay in reaching plateau levels of one day *in vitro* in the total hTauP301L levels when comparing both MOIs in the absence and in the presence of K18P301L in both concentrations – MOI 100 transduced neurons display plateau levels at 12DIV and MOI 50 at 13DIV when seeded with 25nM and 2.5nM of K18P301L concentrations or not seeded (Figures 17 a; b and c). Regarding the aggregation signals (hTau10/hTau10 alphaLISA; Material and Methods 2.8.), as expected, there were negligible hTauP301L aggregated signals in the treatments in absence of K18P301L (non-aggregative conditions; Figure 17d). On the other hand, there are statistical differences on the 17DIV, 18DIV, 19DIV and 20DIV (Tukey *post-hoc* adjusted p values of 0.0432; 0.0002; <0.0001 and <0.0001, respectively; alpha=0.05; Material and Methods 2.14.) between the different MOIs – 100 and 50 - when the neurons were cultured with 25nM of K18P301L, with lower hTauP301L aggregated signals of MOI 50 on 18DIV and 19DIV in comparison to the MOI 100 treated neurons and higher in the 17DIV and 20DIV when in comparison to the MOI 100 (Figure 17f). 2.5nM K18P301L treated neurons only display statistical differences between the two MOIs – 50 and 100 – on the 19DIV (Tukey *post-hoc* adjusted p value <0.0001; alpha=0.05; Material and Methods 2.14.) with lower detected levels of hTauP301L aggregation in neurons transduced with MOI 50 (Figure 17e).

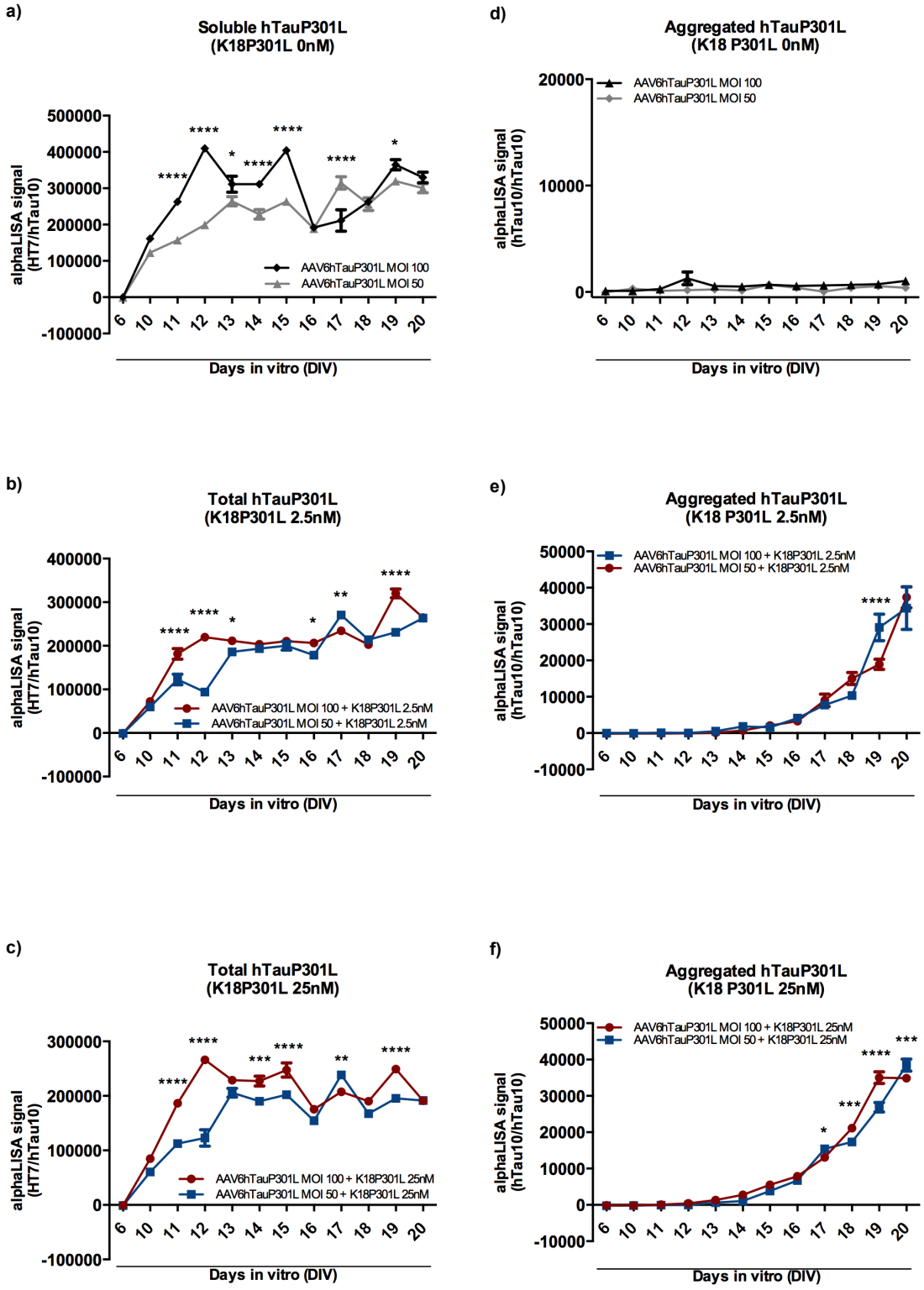

Figure 17: Comparison between hTauP301L levels of AAV6hTauP301L MOI100 and AAV6hTauP301L MOI50 transduced rat primary neurons within a single K18P301L concentration. Rat cortical primary neurons were transduced with AAV6hTauP301L MOI100 or MOI50 on the 3DIV, seeded with K18P301L 2.5nM, 25nM or not seeded – 0nM – on the 10DIV. Lyses were done on the 6DIV and daily between 10-20DIV. Soluble hTauP301L: HT7/hTau10 alphaLISA quantification of primary neurons overexpressing hTauP301L and not seeded with K18P301L. Total hTauP301L: HT7/hTau10 alphaLISA quantification of primary neurons overexpressing hTauP301L and seeded with K18P301L (both soluble and aggregated hTauP301L are present on the sample). Aggregated hTauP301L: hTau10/hTau10 alphaLISA quantification (see Material and Methods 2.8. for alphaLISA description). a) Comparison between soluble hTauP301L levels of primary neurons transduced with AAV6hTauP301L MOI100 and MOI50 and not seeded; b) Comparison between total hTauP301L levels of primary neurons transduced with AAV6hTauP301L MOI100 and MOI50 and seeded with 2.5nM

↵**Figure 17 (continuation):** of K18P301L; c) Comparison between total hTauP301L levels of primary neurons transduced with AAV6hTauP301L MOI100 and MOI50 and seeded with 25nM of K18P301L; d) Comparison between aggregated hTauP301L levels of primary neurons transduced with AAV6hTauP301L MOI100 and MOI50 and not seeded; e) Comparison between aggregated hTauP301L levels of primary neurons transduced with AAV6hTauP301L MOI100 and MOI50 and seeded with 2.5nM of K18P301L; and f) Comparison between total hTauP301L levels of primary neurons transduced with AAV6hTauP301L MOI100 and MOI50 and seeded with 25nM of K18P301L. Data is presented as ± SEM and are representative of a N=1 and n=6. Statistical analyses of the results were performed by a two-way ANOVA followed by Tukey *post-hoc* comparisons with an alpha set to 0.05.

When focusing on the differences between the K18P301L different treatments (2.5nM and 25nM) within one transduction MOI, the signal of total hTauP301L that is detected in HT7/hTau10 alphaLISA (Material and Methods 2.8.) show very similar profiles. Total HT7/hTau10 alphaLISA (Material and Methods 2.8.) signal differs mainly after plateau levels as highlighted by the statistical significance on 12DIV, 16DIV 17DIV, 18DIV, 19DIV and 20DIV (Tukey *post-hoc* adjusted p values of 0.0225; 0.0354; 0.0033; <0.0001; 0.0009 and <0.0001, respectively; alpha=0.05; Material and Methods 2.14.) for MOI 50 treatment and on 12DIV, 14DIV, 15DIV, 16DIV, 17 DIV, 19DIV and 20DIV (Tukey *post-hoc* adjusted p values of <0.0001; 0.0379; 0.0005; 0.0046; 0.0169; <0.0001 and <0.0001, respectively; alpha0.05; Material and Methods 2.14.) for MOI 100 cultured cells (Figures 18 a and b). For both MOIs treatments, 50 and 100, between the 6-15DIV neurons treated with 2.5nM usually display comparable or lower signal levels than neurons seeded with 25nM K18P301L fibrils (Figures 18 a and b). Interestingly, for both MOI cases, from the 16DIV onwards such profile changes and 2.5nM K18P301L seeded neurons show higher hTauP301L signal levels when in comparison to the 25nM treatment with K18P301L differences that are reflected in significant two-way ANOVA interaction p values (Figures 18 a and b; interaction p values <0.0001 for both cases; alpha=0.05; for Tukey *post-hoc* adjusted p values see description above). Of note is that HT7/hTau10 alphaLISA (Material and Methods 2.8.) signal on neurons cultured without K18P301L seeds was significantly different (higher levels) when comparing with the signal of the seeded neurons as underscored by a two-way ANOVA highly significant interaction p value for any of the cases (interaction p values <0.0001; alpha=0.05; Figures 19 a; b; c and d). In such case, when comparing the MOI 50 neurons in the presence and absence of 25nM K18P301L, neurons not treated with the fibrils display significant higher detected levels of hTauP301L everyday with the exception of the 6DIV – with an average of 1.49-fold higher signal levels of MOI 50 in absence of K18P301L in comparison to MOI 50 transduced neurons and seeded with the fibrils when comparing the days with statistical significance (Figure 19 a; Tukey *post-hoc* adjusted p values: 10DIV <0.0001; 11DIV =0.0039; 12DIV <0.0001; 13DIV = 0.0001; 14DIV =0.0172; 15DIV <0.0001; 16DIV =0.0343; 17DIV <0.0001; 18DIV <0.0001; 19DIV <0.0001 and 20DIV <0.0001; alpha=0.05; Material and Methods 2.14.). Similarly, the same MOI 50 neuronal transduction treatment in the absence of the fibrils show higher hTauP301L signal levels when compared to neurons treated with 2.5nM K18P301L on the 10DIV, 12DIV, 13DIV, 14DIV, 15DIV, 17DIV, 18DIV, 19DIV and 20DIV (Tukey *post-hoc* adjusted p values of <0.0001; <0.0001; <0.0001; 0.033; <0.0001; 0.0043; 0.0066; <0.0001 and 0.0214, respectively; alpha=0.05; Material and Methods 2.14.) – with an average of 1.47-fold higher hTauP301L signal levels of MOI 50 in absence of the fibrils in comparison to neurons transduced with MOI 50 and seeded with 2.5nM of K18P301L (Figure 19 b). When observing the results for neurons transduced with AAV6hTauP301L MOI 100 in the absence and presence of K18P301L (non-aggregative conditions and aggregative conditions, respectively), there are statistical significant higher levels of hTauP301L when neurons were not seeded with K18P301L on the 10DIV, 11DIV, 12DIV, 13DIV, 14DIV, 15DIV, 18DIV, 19DIV and 20DIV when comparing to both treatments with 25nM and 2.5nM concentrations of the fibrils (Figures 19 c and d; Tukey *post-hoc* adjusted p

values when comparing not seeded neurons to seeded with 25nM of K18P301L: for all cases <0.0001; and when comparing not seeded neurons to seeded with 2.5nM of K18P301L: for 10-15DIV, 18DIV and 20DIV <0.0001 and for 19DIV =0.0036; alpha=0.05; Material and Methods 2.14.). These statistical differences reflect in an average of 1.5-fold higher signals when comparing neurons transduced with MOI 100 and not seeded with the fibrils in comparison to 25nM K18P301L treated neurons when comparing the days with statistical significance (Figure 19c). For neurons transduced with AAV6hTauP301L MOI 100 and seeded with 2.5nM of K18P301L in comparison to the not seeded condition, the same average difference of 1.5-fold higher levels in non-aggregative condition applies between the 10-15DIV, and between the 18-20DIV this difference is reduced to 1.2-fold increase (Figure 19d). Such differences when comparing hTauP301L levels in neurons in aggregative conditions (i.e. K18P301L seeded neurons) and non-aggregative conditions (not seeded with K18P301L) are likely to be due to the aggregation of hTauP301L that could lead to decreased accessibility of the epitope for interaction with the detection antibodies (i.e.: shielding of epitopes) – phenomenon that has already been observed with other protein aggregates [208]. Regarding hTauP301L aggregation signal, as expected, neurons not seeded with K18P301L (0nM) display negligible hTauP301L levels (Figure 20 a and b). Comparing seeded neurons, although similar profiles can be seen in both K18P301L 2.5nM and 25nM concentrations treatments within the same MOI, when performing a two-way ANOVA, significant interaction p values are observed for both cases (interaction p values of 0.0002 when comparing neurons seeded with K18P301L 2.5nM and 25nM within MOI 50 and 0.0068 when comparing neurons seeded with K18P301L 2.5nM and 25nM within MOI 100; alpha=0.05) and they significantly differ on 16DIV, 17DIV and 19DIV (Tukey *post-hoc* adjusted p values of 0.0263; <0.0001 and <0.0001, respectively; alpha=0.05; Material and Methods 2.14.) for the MOI 50 cultured neurons and on 17DIV, 18DIV and 19DIV (Tukey *post-hoc* adjusted p values of 0.0273; <0.0001 and 00117, respectively; alpha=0.05; Material and Methods 2.14.) within MOI 100 transduced neurons (Figures 20 a and b). These differences underscore a reduction in hTauP301L aggregation rate in the neurons that were treated with 2.5nM K18P301L seeds when compared to 25nM - treatments which are needed to induce hTauP301L aggregation *in vitro*.

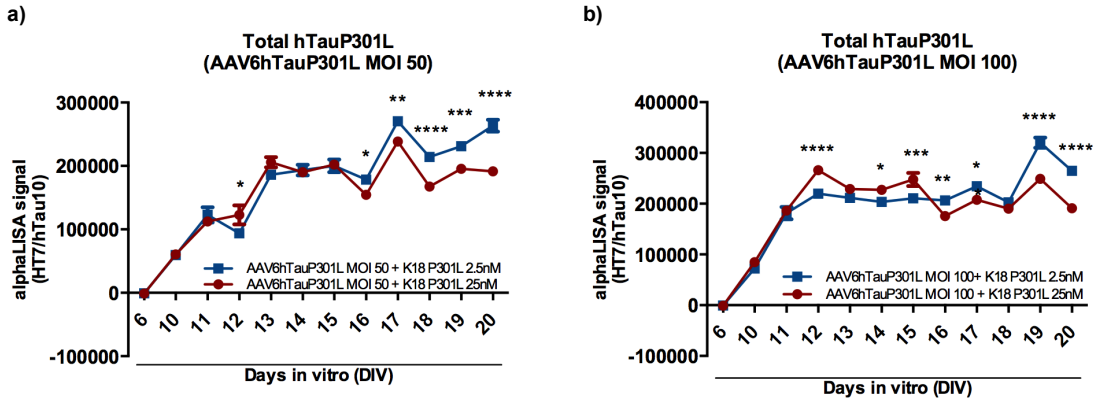

Figure 18: Comparison between total hTauP301L levels of K18P301L seeded rat primary neurons within a single AAV6hTauP301L MOI transduction. Rat cortical primary neurons were transduced with AAV6hTauP301L MOI100 or MOI50 on the 3DIV, seeded with K18P301L 2.5nM or 25nM on the 10DIV. Lyses were done on the 6DIV and daily between 10-20DIV. Total hTauP301L: HT7/hTau10 alphaLISA quantification of primary neurons overexpressing hTauP301L and seeded with K18P301L (both soluble and aggregated hTauP301L are present on the sample; see Material and Methods 2.8. for alphaLISA description). a) Comparison between total hTauP301L levels of primary neurons transduced with AAV6hTauP301L MOI50 and seeded with 2.5nM or 25nM of K18P301L; b) Comparison between total hTauP301L levels of primary neurons transduced with AAV6hTauP301L MOI50 and seeded with 2.5nM or 25nM of K18P301L. Data is presented as ± SEM and are representative of a N=1 and n=6. Statistical analyses of the results were performed by a two-way ANOVA followed by Tukey *post-hoc* comparisons with an alpha set to 0.05.

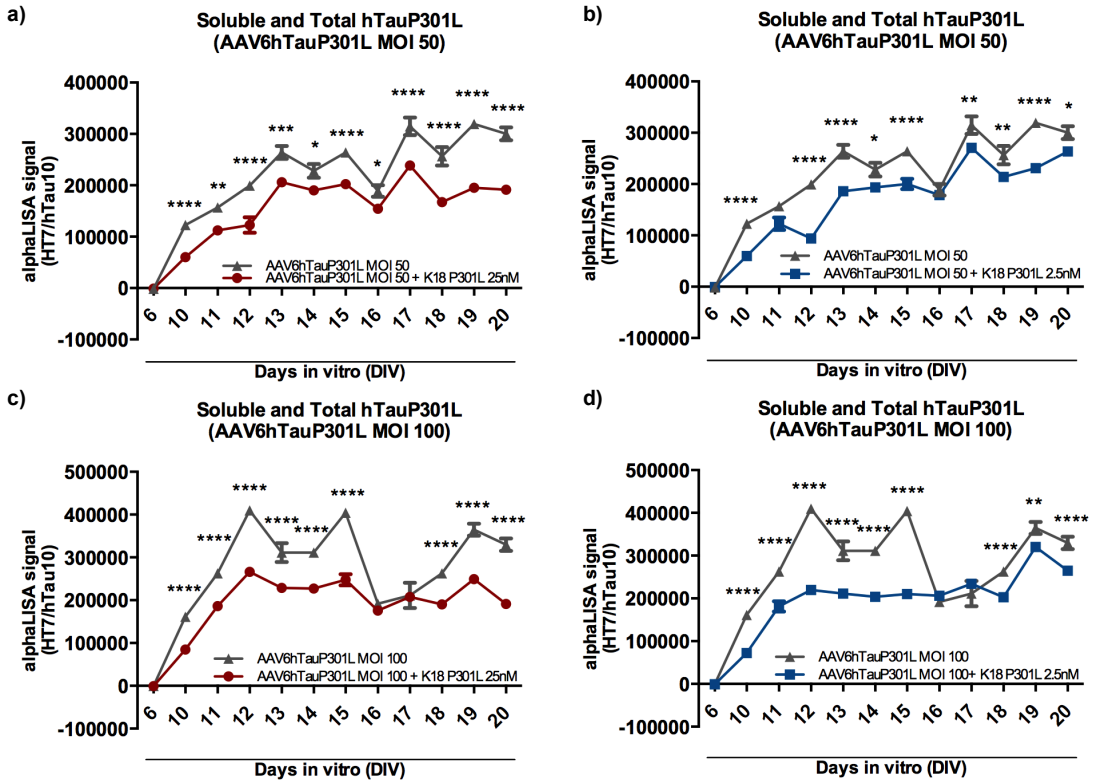

Figure 19: Comparison between soluble and total hTauP301L levels of K18P301L seeded rat primary neurons or not within a single AAV6hTauP301L MOI transduction. Rat cortical primary neurons were transduced with AAV6hTauP301L MOI100 or MOI50 on the 3DIV, seeded with K18P301L 2.5nM or 25nM or not – 0nM - on the 10DIV. Lyses were done on the 6DIV and daily between 10-20DIV. Soluble hTauP301L: HT77hTau10 alphaLISA quantification of primary neurons overexpressing hTauP301L and not seeded with K18P301L. Total hTauP301L: HT7/hTau10 alphaLISA quantification of primary neurons overexpressing hTauP301L and seeded with K18P301L (both soluble and aggregated hTauP301L are present on the sample; see Material and Methods 2.8. for alphaLISA description). a) Comparison between soluble and total hTauP301L levels of primary neurons transduced with AAV6hTauP301L MOI100 and seeded with 2.5nM of K18P301L; b) Comparison between soluble and total hTauP301L levels of primary neurons transduced with AAV6hTauP301L MOI100 and seeded with 25nM of K18P301L. c) Comparison between soluble and total hTauP301L levels of primary neurons transduced with AAV6hTauP301L MOI50 and seeded with 2.5nM of K18P301L; d) Comparison between soluble and total hTauP301L levels of primary neurons transduced with AAV6hTauP301L MOI50 and seeded with 25nM of K18P301L. Data is presented as ± SEM and are representative of a N=1 and n=6. Statistical analyses of the results were performed by a two-way ANOVA followed by Tukey *post-hoc* comparisons with an alpha set to 0.05.

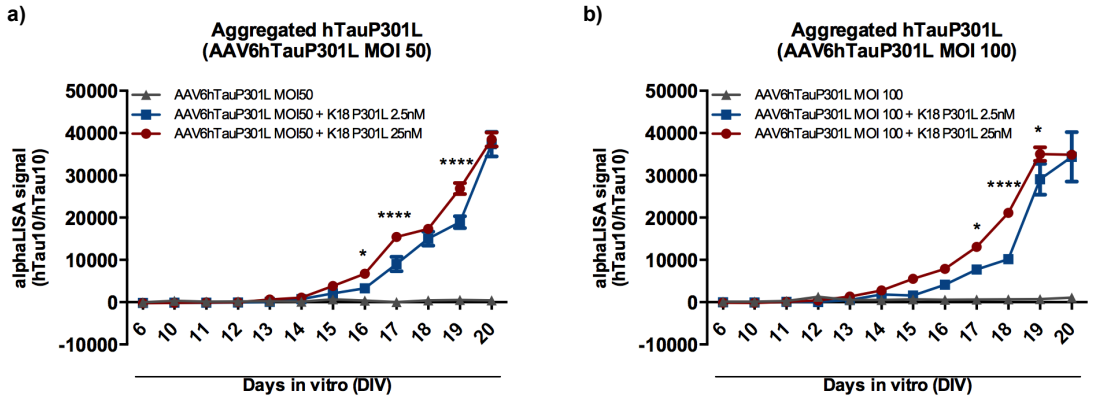

Figure 20: Comparison between aggregated hTauP301L levels of K18P301L seeded rat primary neurons within a single AAV6hTauP301L MOI transduction. Rat cortical primary neurons were transduced with AAV6hTauP301L MOI100 or MOI50 on the 3DIV, seeded with K18P301L 2.5nM, 25nM or not – 0nM - on the 10DIV. Lyses were done on the 6DIV and daily between 10-20DIV. Aggregated hTauP301L: HT7/hTau10 alphaLISA quantification of primary neurons overexpressing hTauP301L and seeded or not with K18P301L (see Material and Methods 2.8. for alphaLISA description). a) Comparison between aggregated hTauP301L levels of primary neurons transduced with AAV6hTauP301L MOI50 and seeded with 0nM, 2.5nM or 25nM of K18P301L; b) Comparison between aggregated hTauP301L levels of primary neurons transduced with AAV6hTauP301L MOI50 and seeded with 0nM, 2.5nM or 25nM of K18P301L. Data is presented as ± SEM and are representative of a N=1 and n=6. Statistical analyses of the results were performed by a two-way ANOVA followed by Tukey *post-hoc* comparisons with an alpha set to 0.05.

In summary, AAV6hTauP301L MOI transduction influences hTauP301L initial slope of soluble and total (aggregated and soluble present) hTauP301L build-up, and K18P301L concentration influences the initial slope of hTauP301L aggregation. Additionally, when comparing hTauP301L levels in neurons in aggregative conditions to non-aggregative conditions, higher levels are observed in neurons in absence of the aggregates, which is likely due to the epitope shielding phenomenon [208].

3.1.4 Kinetics of hTauP301L expression and aggregation in rat primary neurons – "long" model, validated by biochemical means

As an outcome of the described results above, AAV6hTauP301L MOI 100 and K18P301L 25nM were chosen as optimal conditions within this model towards our objectives showing a faster increase in hTauP301L expression and aggregation signal, but still with a good temporal window to be analyzed. Hence, these conditions were further characterized. For such purpose, AAV6hTauP301L MOI 100 transduction took place on 3DIV and K18P301L 25nM seeding on 10DIV (Material and Methods 2.2. and 2.5.; Figure 16). On 6DIV and daily between the 10-20DIV plates were lysed for biochemical analysis. Statistical analyses of the results were performed by a two-way ANOVA followed by Sidak's *post-hoc* comparisons with an alpha set to 0.05.

Observing the kinetics of hTauP301L total protein signal (HT7/hTau10 alphaLISA; Material and Methods 2.8.; Figure 21a), it can be seen that there is an initial high rate of increase signals going from 0 (zero) to 400 000 counts in the AAV6hTauP301L treatment in the absence of the K18P301L seeds (soluble hTauP301L) from the 6DIV to the 12DIV. Similar profile can be observed when the neurons are transduced with the virus and seeded with K18P301L (aggregative conditions), although in comparison to the control (AAV6hTauP301L MOI 100 treatment not seeded with K18P301L – non-aggregative conditions) it shows itself lower than the latter (Figure 21a; two-way ANOVA interaction p value <0.0001; alpha=0.05). This difference can be highlighted by the signal levels difference (statistically significant) in this initial phase (between 6-12DIV) that is in average 1.5-fold higher in the AAV6hTauP301L treatment when comparing with K18P301L seeded neurons (Figure 21a; Sidak's *post-hoc* adjusted p values of <0.0001 for the 10DIV, 11DIV and 12DIV; alpha=0.05; Material and Methods 2.14.). On the 12DIV both treatments reach a plateau phase that continues until the end of the experiment. During this plateau phase, with exception of the 16DIV and 17DIV, the same average of 1.5-fold difference also applies to the data being statistically significant when comparing the control condition (AAV6hTauP301L MOI 100 in absence of K18P301L) and AAV6hTauP301L MOI 100 seeded with 25nM of K18P301L fibrils (Figure 21a; Sidak's *post-hoc* adjusted p values of <0.0001 for all days with exception of 16DIV and 17DIV; alpha=0.05; Material and Methods 2.14.). Such difference is likely to account for the epitope shielding [208] mentioned in the Results 3.1.3. Despite that, the AAV6hTauP301L treatment in absence of K18P301L shows a fall in its signal in the days *in vitro* 16 and 17 with a posterior recovery. As this data is not normalized, such fall is likely due to biological variations related to the fact that the neuronal cultures are not homogeneous (i.e., with non-neuronal cells present) and that they are higly dynamic in regard of the neuronal processes development over time.

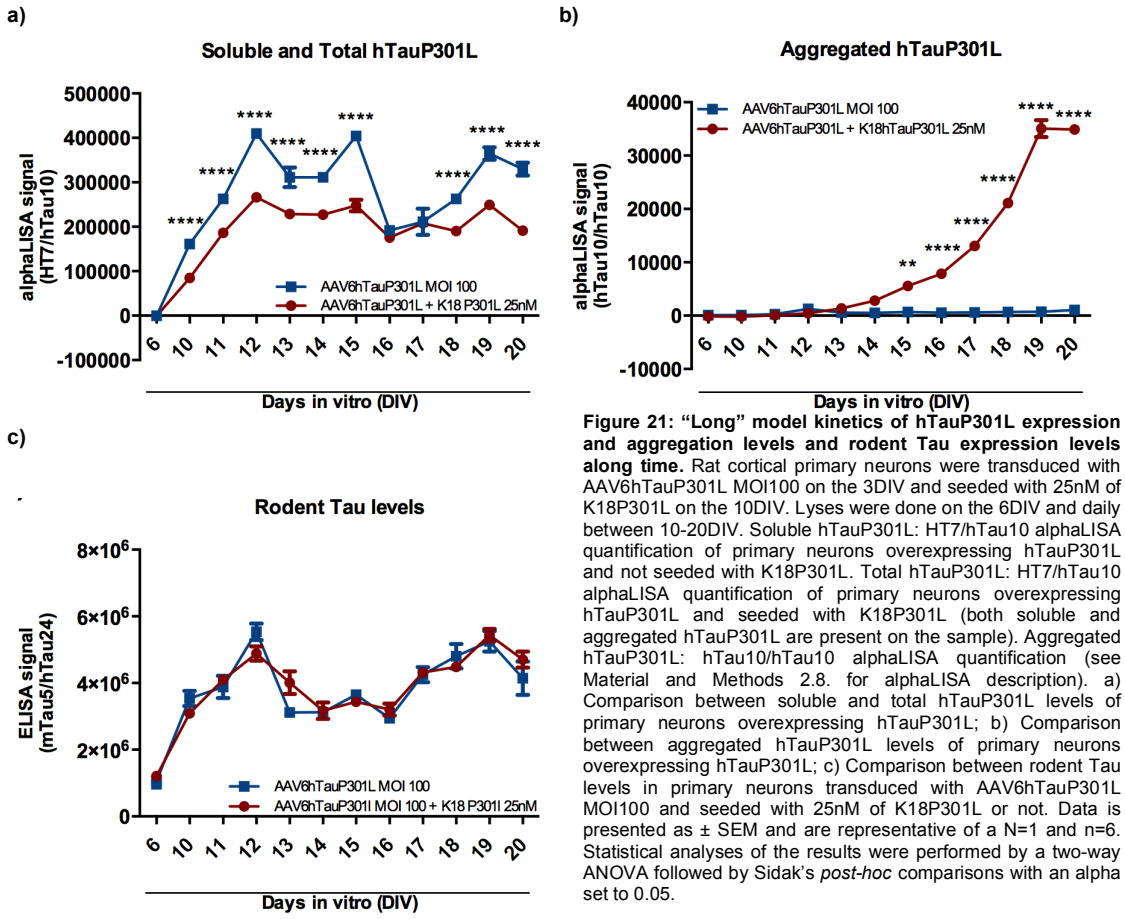

Figure 21: "Long" model kinetics of hTauP301L expression and aggregation levels and rodent Tau expression levels along time. Rat cortical primary neurons were transduced with AAV6hTauP301L MOI100 on the 3DIV and seeded with 25nM of K18P301L on the 10DIV. Lyses were done on the 6DIV and daily between 10-20DIV. Soluble hTauP301L: HT7/hTau10 alphaLISA quantification of primary neurons overexpressing hTauP301L and not seeded with K18P301L. Total hTauP301L: HT7/hTau10 alphaLISA quantification of primary neurons overexpressing hTauP301L and seeded with K18P301L (both soluble and aggregated hTauP301L are present on the sample). Aggregated hTauP301L: hTau10/hTau10 alphaLISA quantification (see Material and Methods 2.8. for alphaLISA description). a) Comparison between soluble and total hTauP301L levels of primary neurons overexpressing hTauP301L; b) Comparison between aggregated hTauP301L levels of primary neurons overexpressing hTauP301L; c) Comparison between rodent Tau levels in primary neurons transduced with AAV6hTauP301L MOI100 and seeded with 25nM of K18P301L or not. Data is presented as ± SEM and are representative of a N=1 and n=6. Statistical analyses of the results were performed by a two-way ANOVA followed by Sidak's *post-hoc* comparisons with an alpha set to 0.05.

By inspecting the hTau10/hTau10 alphaLISA (aggregated hTauP301L; Material and Methods 2.8.) kinetics, as expected, there are negligible signals from the AAV6hTauP301L treatment in absence of K18P301L, as it does not aggregate spontaneously (Figure 21b). When hTau301L is seeded there is an increase in signal from the 14DIV, beginning to be significant on the 15DIV (Figure 21b; Sidak's *post-hoc* adjusted p value = 0.0027; alpha=0.05; Material and Methods 2.14.) and continuing until the end of the experiment (Figure 21b; Sidak's *post-hoc* adjusted p values between 16-20DIV of <0.0001; alpha=0.05; Material and Methods 2.14.). This increase in signal shows itself with a high slope in the graph (Figure 21b) reaching 35 000 counts by the 19DIV and maintaining this level on the 20DIV.

Additionally we assessed the levels of rodent Tau to confirm whether we could use it as an endogenous control to normalize data against possible technical variation and eventual neuronal loss. Choice of rodent Tau was based on the following factors: specific neuronal expression of Tau [209, 210] and the fact that rodent Tau does not aggregate by itself when exposed to K18P301L seeds (data not shown). Consequently, the level of rodent Tau should be comparable between treatments when measured at a single time-point (the different treatments should not account for an overall statistical difference). To determine the level of rodent Tau, we used a sandwich ELISA (Material and Methods 2.9.) that applies mTau5 as a capturing antibody and hTau24 conjugated to horseradish peroxidase (HRP) as a secondary antibody. Indeed, rodent Tau levels do not differ significantly due to the treatment factor, as it can be seen in the Figure 21c and is underscored by a not significant interaction p value (two-way ANOVA interaction p value =0.2094;

alpha=0.05) and overall treatment factor p value (two-way ANOVA treatment factor p value =0.5565; alpha=0.05). Neurons overexpressing hTauP301L in absence and in the presence of K18P301L fibrils show similar and overlapping profiles with no statistical differences within a single time-point (Figure 21c). Rodent Tau levels increase between the days 6 and 12 *in vitro* when likely a plateau is reached (although with some fluctuations) and that continues until the end of the experiment (Figure 21c). Consequently, mTau5/hTau24 ELISA assay can be used to normalize the alphaLISA data if only used within a single time-point.

3.2 Development of a "short" model for hTauP301L aggregation in primary neurons

In light of the results obtained studying the "long" hTauP301L aggregation model, in wich there was already a statistically significant hTauP301L aggregation signal on the 15DIV (5 days after seeding – 5DAS), we asked ourselves whether we could shorten the assay making it more suitable for future high throughput screen (HTS) campaigns. A shorter model would indeed have the advantages of leading to a more homogeneous culture (i.e.: limiting the time for proliferation of non-neuronal cell lines) and also it would reduce the overall time expended for experiments and costs. Additionally, a reduced duration of the experiments would likely reduce toxicity problems that are commonly associated to drug treatments and screens in *in vitro* cellular models. With this purpose we transduced neurons on day 1 *in vitro* (1DIV) with AAV6hTAUP301L MOI100 followed by 12.5nM K18P301L seeding on day 3 *in vitro* (3DIV / 0DAS; Material and Methods 2.2. and 2.5.) and observed a significant hTauP301L aggregation on day 10 *in vitro* (10DIV / 7DAS) upon neuronal transduction. To characterize the kinetics of hTauP301L expression and aggregation in this "short" model, we lysed the neurons every day from the 5th day *in vitro* (5DIV / 2DAS) up to the 14th day *in vitro* (14DIV / 11DAS). hTauP301L aggregation in this model was assessed biochemically by alphaLISA and western blotting (daily between the 5-14DIV – 2-11DAS - for both alphaLISA and western blot) - as well as by immunocytochemistry (daily between the 8-14DIV – 5-11DAS).

3.2.1 Kinetics of hTauP301L expression and aggregation in rat primary neurons – "short" model, validated with immunocytochemistry

In addition to a biochemical approach to inspect the kinetics of hTauP301L expression and aggregation (Results 3.1.2. and 3.1.3.) we hypothesized whether the alterations in the model strategy would not influence hTauP301L aggregation and if the same features would be presented and associated with hTauP301L aggregation in an imaging inspection in comparison to the "long" model along time. For this purpose, neurons were transduced with AAV6hTauP301L MOI 100 on the 1DIV and seeded with 12.5nM of K18P301L on the 3DIV (0DAS; Material and Methods 2.2. and 2.5.). Hence, we performed a time course, collecting the samples every day beginning in the day 8 *in vitro* (8DIV / 5DAS) until the day 14 *in vitro* (14DIV / 11DAS). Neurons were fixed with methanol (Material and Methods 2.12.) to enrich for insoluble hTauP301L. See Figure 22 for a graphic overview of the experiment.

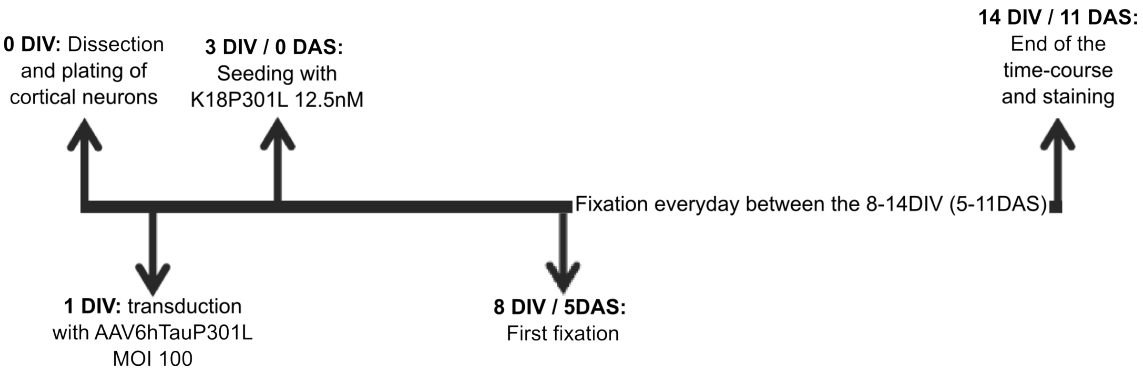

Figure 22: Graphic overview of the experiment. DIV=day *in vitro*; DAS=day after seeding.

With the objectives described above, the intracellular aggregation of hTauP301L was inspected by means of use of AT8 and MAP-2 antibodies. MAP-2 antibody (Table 2), as mentioned in the section Results 3.1.2., was used to discriminate between neurons and non-neuronal cell types – astrocytes and microglia – as neuronal primary cultures are not homogeneous [205]; and AT8 (Table 2), which immunoreactivity has been associated with different stages of NFT formation in AD brains [206], was used to stain the insoluble phosphorylated hTauP301L present in the neurons. As expected, no insoluble hTauP301L was detected either in wild-type neurons or in neurons expressing hTauP301L and not seeded with K18P301L (Figure 23). On the other hand, when neurons expressing hTauP301L were cultured in the presence of K18P301L 12.5nM, insoluble immunoreactivity with AT8 could be observed. On the 8DIV (5DAS), it was already possible to observe the presence of a comet-like pattern that characterizes itself by a ring-like immunoreactivity in the soma elongating to the proximal parts of the dendrites in a doted configuration (Figure 23). The same immunoreactivity can be observed for the next days, evolving to a complete spreading of the doted immunoreactivity associated to the neurites along the microscopical view on the 11DIV (8DAS; Figure 23). On the 12DIV (9DAS), the same spreading and previous described features were observed and this panorama continues until the end of the experiment (Figure 23). Importantly, these ring-like pattern and comet-like pattern resembles the ones displayed in the "long" model previously described. Additionally, as already mentioned, similar features have been described in NFT structures present in AD patients' brains [207]. With all these observations, it can be concluded that this "short" version of the neuronal hTauP301L aggregative *in vitro* model is able to induce the pathological aggregation of soluble hTauP301L in the presence of K18P301L with microscopical features resembling the previously described "long" model and AD patients' brains, which makes it a valuable mean to study such pathological process.

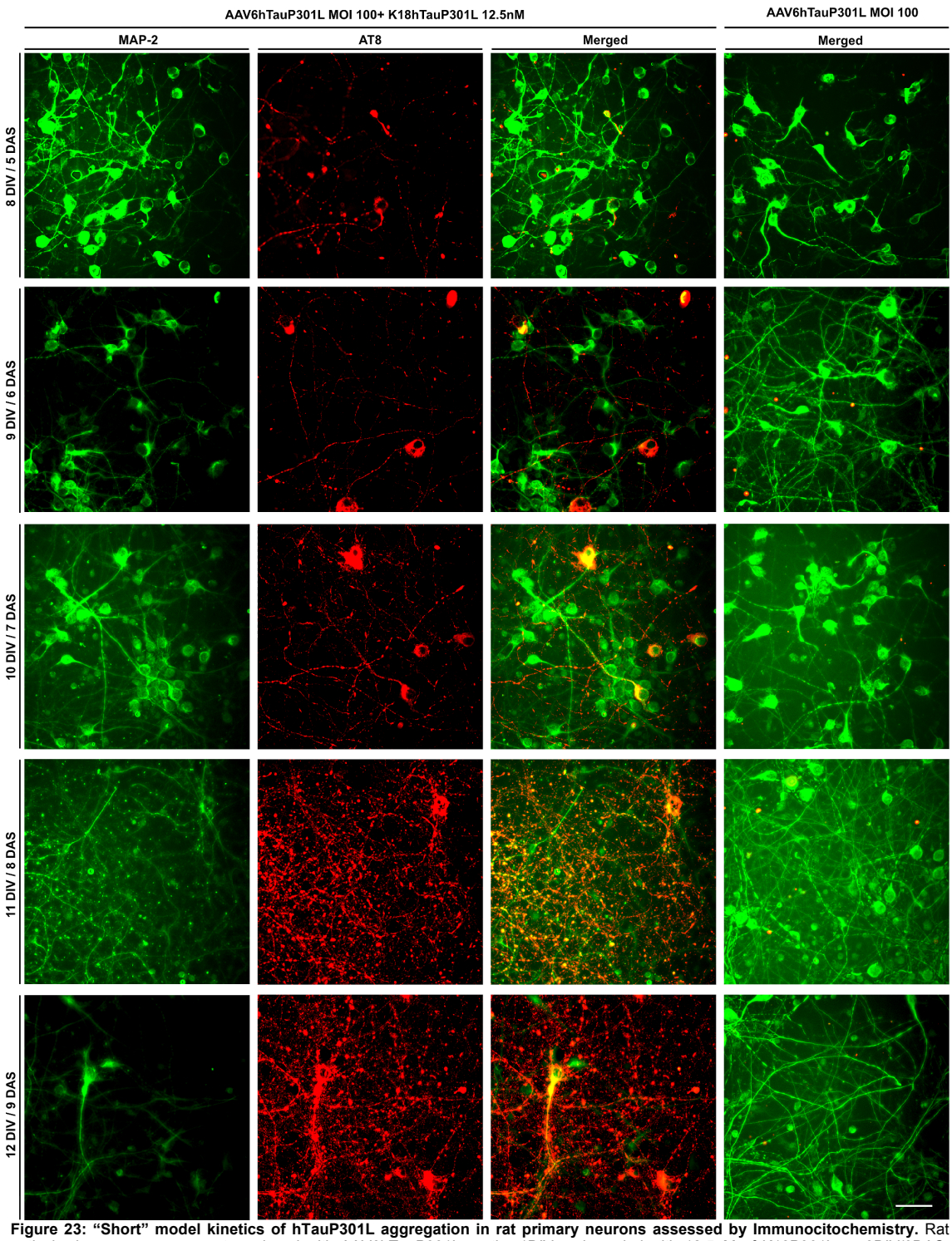

Figure 23: "Short" model kinetics of hTauP301L aggregation in rat primary neurons assessed by Immunocitochemistry. Rat cortical primary neurons were transduced with AAV6hTauP301L on the 1DIV and seeded with 12.5nM of K18P301L on 3DIV/0DAS. Methanol fixation was performed daily from the 8DIV/5DAS to the 14DIV/11DAS. AT8 antibody was used to detect aggregated hTauP301L phosphorylated on Ser202 and on Thr205 and corresponds to the red staining. MAP-2 antibody was used to discriminate between neurons and non-neuronal cell types and corresponds to the green staining. Images were acquired by Digilab MIAS-2™ Microscopy System with a 40x magnification. Scale bar: 50µM. Wild-type rat cortical neurons not transduced with the AAV6hTauP301L and not seeded with K18P301L displayed the same phenotype as seen in the neurons overexpressing hTauP301L but not seeded with K18P301L (no AT8 signal) and hence are represented in this image by the neurons transduced with AAV6hTauP301L MOI100 in non-aggregative conditions. Rat cortical neurons overexpressing hTauP301L and seeded with 12.5nM of K18P301L display temporal-dependent hTauP301L aggregation. DIV= day *in vitro;* DAS= day after seeding.

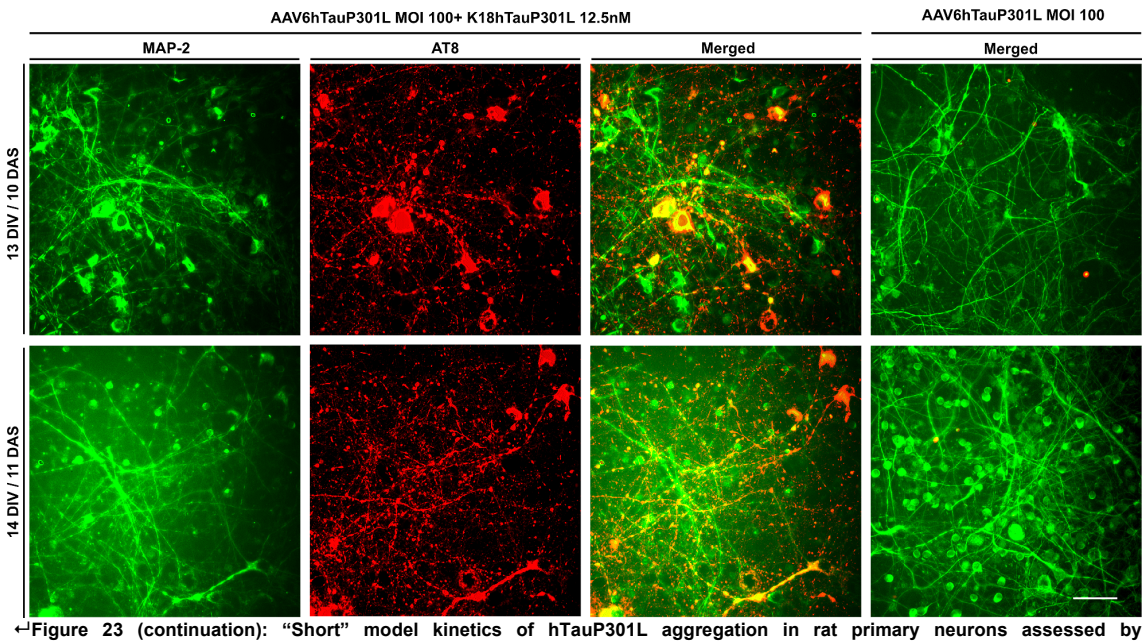

↵**Figure 23 (continuation): "Short" model kinetics of hTauP301L aggregation in rat primary neurons assessed by Immunocitochemistry.** Rat cortical primary neurons were transduced with AAV6hTauP301L on the 1DIV and seeded with 12.5nM of K18P301L on 3DIV/0DAS. Methanol fixation was performed daily from the 8DIV/5DAS to the 14DIV/11DAS. AT8 antibody was used to detect aggregated hTauP301L phosphorylated on Ser202 and on Thr205 and corresponds to the red staining. MAP-2 antibody was used to discriminate between neurons and non-neuronal cell types and corresponds to the green staining. Images were acquired by Digilab MIAS-2™ Microscopy System with a 40x magnification. Scale bar: 50μM. Wild-type rat cortical neurons not transduced with the AAV6hTauP301L and not seeded with K18P301L displayed the same phenotype as seen in the neurons overexpressing hTauP301L but not seeded with K18P301L (no AT8 signal) and hence are represented in this image by the neurons transduced with AAV6hTauP301L MOI100 in non-aggregative conditions. Rat cortical neurons overexpressing hTauP301L and seeded with 12.5nM of K18P301L display temporal-dependent hTauP301L aggregation. DIV= day *in vitro;* DAS= day after seeding.

3.2.2 Kinetics of hTauP301L expression and aggregation in rat primary neurons – "short" model, validated by biochemical means

3.2.2.1 Human Tau detecting AlphaLISA assessments

In order to kinetically characterize hTauP301L expression and aggregation in rat primary neurons by alphaLISA (Material and Methods 2.8.), neurons were transduced with AAV6hTauP301L MOI 100 on the 1DIV and seeded with 12.5nM K18P301L on the 3DIV (0DAS; Material and Methods 2.2. and 2.5.). Time course was performed, collecting the samples every day beginning in the day 5 *in vitro* (5DIV / 2DAS) until the day 14 *in vitro* (14DIV / 11DAS). Statistical analyses of the results were performed by a two-way ANOVA followed by Sidak's *post-hoc* comparisons with an alpha set to 0.05. See Figure 24 for a graphic overview of the experiment.

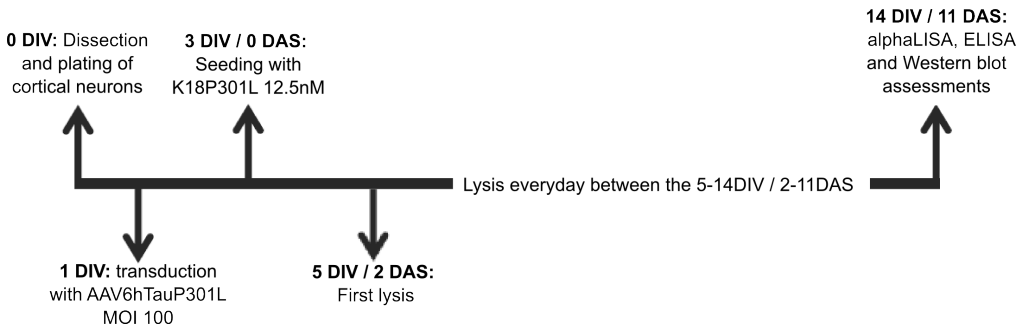

Figure 24: Graphic overview of the experiment. DIV= day *in vitro;* DAS= day after seeding.

The total hTauP301L signals and soluble hTauP301L signals (treated and not treated with K18P301L, respectively) share similar profiles, as it can be seen by the HT7/hTau10 alphaLISA results (Figure 25a; Material and Methods 2.8.). Their signal display high initial rates of increase with a 8.2-fold increase and 7.3-fold increase from the 6DIV (3DAS) to the 7DIV (4DAS) for neurons in non-aggregative conditions (overexpressing hTauP301L) and neurons in aggregative conditions (overexpressing hTauP301L and seeded with K18P301L), respectively. From the 7DIV (4DAS) to the 10DIV (7DAS), reductions in the slope of those curves are seen, and for neurons overexpressing hTauP301L in non-aggregative conditions a 1.6-fold increase is observed, and for neurons overexpressing hTauP301L and seeded with K18P301L a 1.4-fold increase is displayed between such days (7-10DIV / 4-7DAS). Of note is that on the 10DIV (7DAS), both conditions reach plateau levels. Such levels are statistically significant lower for neurons in aggregative conditions when comparing to neurons in non-aggregative conditions. In such plateau phase - 10-14DIV / 7-11DAS -, an average of 1.4-fold higher levels could be observed for neurons overexpressing hTauP301L not seeded with K18P301L when comparing to neurons in aggregative conditions (Figure 25a; two-way ANOVA interaction p value <0.0001 and Sidak's *post-hoc* adjusted p values: 10DIV <0.0001; 11DIV = 0.0049; 12DIV <0.0001; 13DIV <0.0001 and 14DIV <0.0001; alpha=0.05; Material and Methods 2.14.). These differences are likely related to the epitope shielding [208] mentioned in the previous sections (Results 3.1.3. and 3.1.4.).

Observing the aggregation levels by hTau10/hTau10 alphaLISA (Material and Methods 2.8.) it can be seen that the AAV6hTauP301L treated neurons not seeded with K18P301L (non-aggregative conditions) show negligible hTau10/hTau10 signal levels, in contrast to the fibril treated ones that start to show statistical significant difference from the 10DIV (7DAS) until the 14DIV (11DAS; two-way ANOVA interaction p value <0.0001 and Sidak's *post-hoc* adjusted p values: 10DIV=0.0003 and every day between the 11-14DIV <0.0001; alpha=0.05; Material and Methods 2.14.) when comparing to the neurons not seeded with K18P301L (Figure 25b). This signal relevance shows itself with an initial highly accentuated slope in the graph reaching a 4.2-fold increase in the signal from the 10DIV (7DAS) to the 11DIV (8DAS), followed by a drop-down in aggregated hTauP301L levels on 12 -13DIV (9-10DAS) and recovery on 14DIV (11DAS; Figure 25b). As this data is not normalized, such drop-down is likely due to biological variations related to the fact that the neuronal cultures are not homogeneous (i.e., with non-neuronal cells present) and that they are higly dynamic in regard of the neuronal processes development over time.

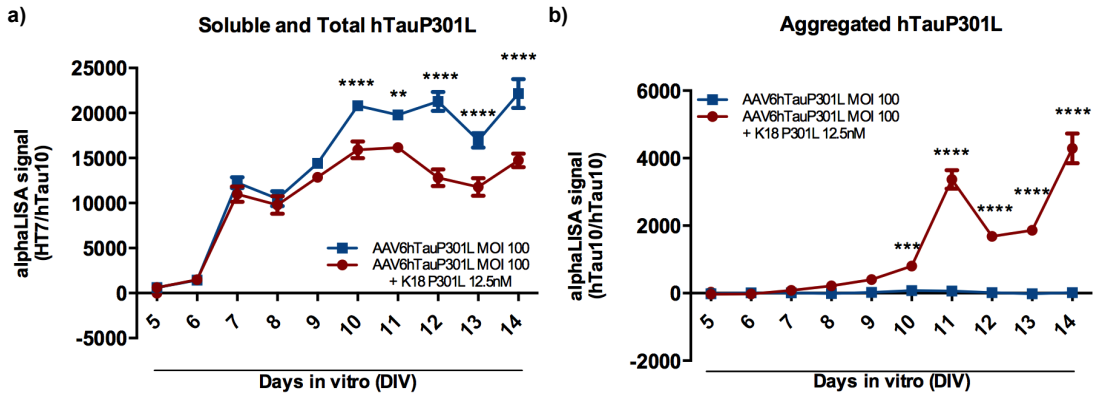

Figure 25: "Short" model kinetics of hTauP301L expression and aggregation levels. Rat cortical primary neurons were transduced with AAV6hTauP301L MOI100 on the 1DIV and seeded with 12.5nM of K18P301L on the 3DIV/0DAS. Lyses were done daily between 5-14DIV / 2-11DAS. Soluble hTauP301L: HT7/hTau10 alphaLISA quantification of primary neurons overexpressing hTauP301L and not seeded with K18P301L. Total hTauP301L: HT7/hTau10 alphaLISA quantification of primary neurons overexpressing hTauP301L and seeded with K18P301L (both soluble and aggregated hTauP301L are present on the sample). Aggregated hTauP301L: hTau10/hTau10 alphaLISA quantification (see Material and Methods 2.8. for alphaLISA description). a) Comparison between soluble and total hTauP301L levels of primary neurons overexpressing hTauP301L; b) Comparison between aggregated hTauP301L levels of primary neurons overexpressing hTauP301L. Data is presented as ± SEM and are representative of a three independent experiments (N=3) with an average of 15 replicates per experiment per condition (n=15). Statistical analyses of the results were performed by a two-way ANOVA followed by Sidak's *post-hoc* comparisons with an alpha set to 0.05.

3.2.2.2 Rodent Tau detecting ELISA assessments

Additionally to the alphaLISA (Material and Methods 2.8.) data above (Results 3.2.2.1), we assessed the levels of rodent Tau by mTau5/hTau24 ELISA (Material and Methods 2.9.) to confirm whether we could use it as an endogenous control to normalize data against possible technical variation and eventual neuronal loss, just as done for the "long" model. For such purpose, rat cortical primary neurons were transduced with AAV6hTauP301L MOI 100 on the 1DIV (Material and Methods 2.2.) and seeded with 12.5nM of K18P301L on the 3DIV (0DAS; Material and Methods 2.5.). Hence, we performed a time course, collecting the samples every day beginning in the day 5 *in vitro* (5DIV / 2DAS) until the day 14 *in vitro* (14DIV / 11DAS). Statistical analyses of the results were performed by an ordinary two-way ANOVA with an alpha set to 0.05. See Figure 24 for a graphic overview of the experiment.

Comparing the rodent Tau levels (via rodent mTau5/hTau24 ELISA; Material and Methods 2.9.) of neurons in aggregative conditions to neurons overexpressing hTauP301L in non-aggregative conditions (seeded and not seeded with K18P301L respectively), it can be highlighted that the K18P301L treatment does not account for an overall significant effect on the experiment (treatment factor p value=0,3192; alpha=0,05), which is reflected in overlapping profiles between both conditions (Figure 26). Such profiles show themselves with few signal level changes between the 5DIV (2DAS) and 9DIV (6DAS), moment in which accentuated signals increase takes place and leads to plateau levels on the 11DIV (8DAS). Such signal increase likely accounts to the development of the neuronal processes over time. Such development is higley dynamic and should reflect on the rodent Tau levels as this is a microtubule-associated protein.

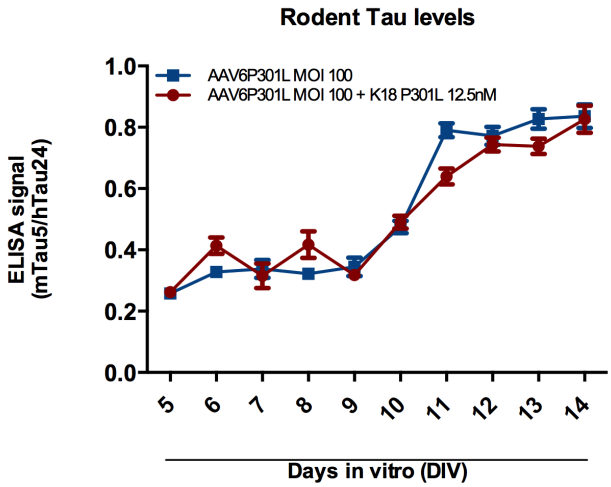

Figure 26: Rodent Tau expression levels along time in the "short" model. Rat cortical primary neurons were transduced with AAV6hTauP301L MOI100 on the 1DIV and seeded with 12.5nM of K18P301L on the 3DIV. Lyses were done on5-14DIV / 2-11DAS. The graphic shows the comparison between rodent Tau levels in primary neurons transduced with AAV6hTauP301L MOI100 and seeded with 25nM of K18P301L or not. Data is presented as ± SEM and are representative of a N=1 and n=14. Statistical analyses of the results were performed by an ordinary two-way ANOVA an alpha set to 0.05

Therefore, as such profiles show increasing signals along time, which was also observed in the "long" model, such neuronal marker is only suitable for alphaLISA (Material and Methods 2.8.) data normalization if used within a single time-point.

3.2.2.3 HT7 and AT8 hTauP301L Western Blot assessments

In order to further characterize the kinetics of hTauP301L expression in rat primary neurons and so complementing our data assessed by the alphaLISA technique (Material and Methods 2.8.) we decided to assess such levels by an alternative approach – by the western blotting technique. Hence we made use of a strategy based in two different antibodies – HT7 (Table 2) that detects human Tau independently of its phosphorylation levels and AT8 (Table 2) that recognizes human Tau which is phosphorylated on Ser-202 and Thr-205 [204, 211]. Normal adult neurons exhibit low levels of Tau phosphorylation; however neurons of AD brain and other Tau-related neurodegenerative diseases show high levels of Tau phosphorylation at both physiological and pathological disease-specific residues [211]. Additionally, hyperphosphorylated Tau has been correlated to the formation of the filamentous intracellular inclusions of several neurodegenerative disorders, including AD, and the extent of such aggregates correlates to cognitive decline and disease progression [207, 212]. Additionally, AT8 antibody renders two bands in the *in vitro* aggregation model used here, being an upper band that is related to an insoluble hyperphosphorylated hTauP301L and a lower band that is related to soluble phosphorylated hTauP301L [166]. Hence, assessing the phosphorylated and hyperphosphorylated human Tau levels would give us important insights in the kinetics of such process (Tau phosphorylation) that is strongly correlated to Tau aggregation. HT7 was used as a tool to detect total hTauP301L protein levels due to its phospho-independent hTau detection [204]. Such levels are pivotal in hTauP301L aggregation in our *in vitro* model, as their soluble fraction constitutes the substrate for aggregation. Thus, only by assessing these levels any conclusion can be drawn in our model regarding hTauP301L aggregation and/or phosphorylation. In other words, only by understanding the hTauP301L

aggregation and/or phosphorylation substrate levels one can determine what is happening to the hTauP301L aggregation and/or phosphorylation levels as the levels of these latter entities are directly related to its substrate levels. Intending such characterization, rat primary neurons were transduced on day 1 *in vitro* (1DIV) with AAV6hTauP301L MOI 100 (Material and Methods 2.2.) and seeded on day 3 *in vitro* (3DIV / 0DAS; Material and Methods 2.5.). Neurons were then lysed daily between the day 5 *in vitro* (5DIV; corresponding to the 2nd day after seeding - 2DAS) until the day 14 *in vitro* (14DIV; 11DAS) and human Tau (hTau) detecting western blot was performed (Material and Methods 2.7.). Neuron specific Class III β-tubulin was used as a loding control for AT8 and HT7 probing western blot as hTauP301L expression is neuronal specific. Statistical analyses of the results were performed by a two-way ANOVA followed by Sidak's *post-hoc* comparisons with an alpha set to 0.05. See Figure 24 for a graphic overview of the experiment time-points.

Overexpression of hTauP301L in the presence and absence of the fibrils induces an average 5-fold initial increase in the relative total HT7 hTauP301L levels from the 5DIV to the 7DIV, (2-4DAS) as seen in the Figure 27 a and c. Overexpression of hTauP301L in non-aggregative conditions (i.e.: not seeded with K18P301L) from the day 7 *in vitro* (7DIV / 4DAS) to the day 8 *in vitro* (8DIV / 5DAS) induces an accentuated slope with a 3-fold increase of total soluble hTauP301L relative protein levels (HT7 human Tau probing western blot; Material and Methods 2.7.; Table 2; Figure 27a and c). A slight decrease in signal, probably related to a technical variation, can be observed in the 9DIV (6DAS) in comparison to the 8DIV (5DAS) followed by a recovery and increasing signal until the end of the experiment, reaching a 2.7-fold increase when comparing the HT7 hTauP301L levels of the 9DIV to the 14DIV (6DAS to the 11DAS) in such non-aggregative conditions (AAV6hTauP301L transduced neurons in absence of K18P301L; Figure 27 a and c). When inspecting neurons in aggregative conditions (transduced with AAV6hTauP301L and seeded with K18P301L), from the 7DIV (4DAS) to the 9DIV (6DAS) there is a 3.3-fold increase in signal followed by a plateau phase. It is important to note that such time-course renders a highly significant interaction p value (two-way ANOVA interaction p value <0.0001; alpha=0.05) which is reflected in the statistical differences on the 9DIV and on the 10DIV (6DAS and 7DAS) between the two different conditions (i.e., neurons in aggregative conditions and neurons in non-aggregative conditions) in which it is highlighted higher levels of hTauP301L HT7 immunoreactive relative signal in the K18P301L seeded neurons (Figure 27a, b and c; Sidak's *post-hoc* adjusted p values of <0,0001 for the 9DIV and 0,0291 for the 10 DIV; alpha=0,05; Material and Methods 2.14.). As the same amount of protein was for each lane in the gels and the quantifications were corrected to a standard sample, it is likely that this difference accounts for the presence of aggregated hTauP301L in the sample. In other words, as the protein sample is denatured to run in a SDS-PAGE, no shielding of epitopes should occur and, hence, such result could be expected as the turnover rates of soluble and aggregated hTauP301L are likely to be different. On the other hand, on the last day of the experiment (14DIV; 11DAS) the situation inverts and there is a statistical relevant difference between the treatments - but in this case the signal is higher for the non-aggregative condition culture (Sidak's *post-hoc* adjusted p value of <0,0001; alpha=0,05; Material and Methods 2.14.). Such difference might account for a technical artifact or a random biological variation as such final increase is not recapitulated in the alphaLISA results (Resullts 3.2.2.1.; Material and Methods 2.8.) and it does not seem to be comparable to the profile seen in the same HT7 western blot for neurons in aggregative conditions (overexpressing hTauP301L and seeded with K18P301L).

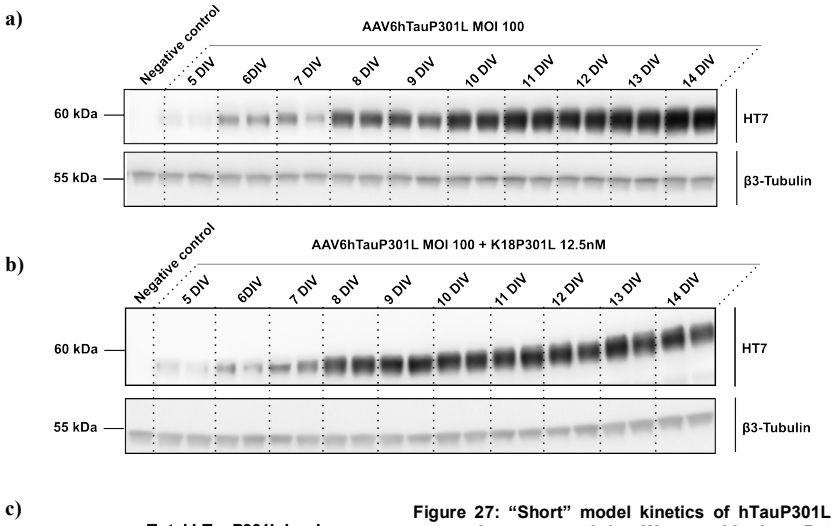

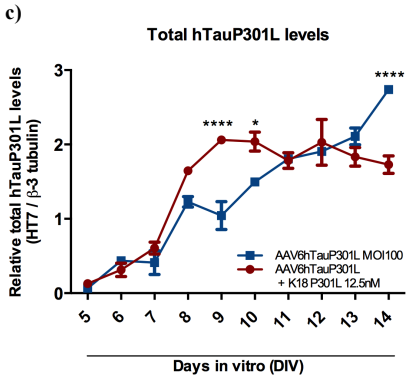

Figure 27: "Short" model kinetics of hTauP301L expression assessed by Western blotting. Rat cortical primary neurons were transduced with AAV6hTauP301L MOI100 on the 1DIV and seeded with 12.5nM of K18P301L on the 3DIV. Lyses were done on 5-14DIV / 2-11DAS. HT7 antinody was used for the hTauP301L detection and Class III β-tubulin was used as a loding control a) Western blotting analysis of hTauP301L expression in rat primary neurons transduced with AAV6hTauP301L MOI100; b) Western blotting analysis of hTauP301L expression in rat primary neurons transduced with AAV6hTauP301L MOI100 and seeded with 12.5nM of K18P301L; c) Quantification of the hTauP301L relative expression levels based on the images "a" and "b" Data is presented as ± SEM and are representative of a N=1 and n=2. Statistical analyses of the results were performed by a two-way ANOVA followed by Sidak's *post-hoc* comparisons; alpha=0.05.

As mentioned in the beginning of this section, AT8 antibody (Table 2) differently from HT7 antibody (Table 2) recognizes Tau phosphorylated on Ser-202 and Thr-205 [204, 211]. In Tauopahies, hTau is highly phosphorylated at several sites, including those recognized by AT8 [206]. Importantly, such phosphorylation has been associated to the formation of hTau-related aggregates in Tauopathies, including AD patient's brains [206, 207, 211, 212], and such aggregates seem to have a correlation with cognitive decline in such disorders [211]. Hence, assessing AT8 immunoreactivity in our model would give us complementary insights to the hTauP301L aggregation kinetics *in vitro*. By observing our data, non-aggregative neurons (transduced with AAV6hTauP301L and not seeded with the K18P301L fibrils) displayed a fast increase in hTauP301L AT8 immunoreactive relative protein levels from the 9DIV (6DAS) to the 11DIV (8DAS), having a small decrease in its levels in the 12DIV (9DAS) followed by a recover and a 3-fold increase until the 14DIV (11DAS; Figure 28 a and c). For neurons in aggregative conditions (i.e.: overexpressing hTauP301L and K18P301L seeded neurons), the profile is very similar to the one seen in the hTau10/hTau10 alphaLISA (Results 2.3.1. and Material and Methods 2.8.), showing a 30-fold increase from the 9DIV (6DAS) until the end of the time-course (Figure 28 b and c). When comparing AT8 hTauP301L relative levels in neurons in aggregative conditions to non-aggregative conditions along time, a highly significant interaction p value is observed (Figure 28 a, b and c; two-way ANOVA interaction p value <0.0001; alpha=0.05). Indeed, hTauP301L phosphorylation levels significantly differ on the 12DIV (9DAS), 13DIV (10DAS) and 14DIV (11DAS) with Sidak's *post-hoc* adjusted p values of <0,0001 for all the days mentioned; alpha=0,05 (Material and Methods 2.14.; Figure 28 a, b and c). Such differences are probably

related to the presence of hyperphosphorylated hTauP301L, which is known to be present in hTau aggregates [206, 207]. Of note is that, when inspecting the AT8 western blot image for the neuronal aggregative condition (AAV6hTauP301L transduced and K18P301L seeded neurons), from the 11DIV (8DAS) until the end of the experiment (14DIV / 11DAS), a hTauP301L upper band can be visualized with increasing levels towards the end of the time-course (Figure 28b). As mentioned in the beginning of this section, such upper band was correlated to hTauP301L insoluble fraction in our *in vitro* model [166], therefore such data further corroborate our hypothesis that between the 12-14DIV (9-11DAS) the statistical differences may account for the presence of hTauP301L aggregates.

Taken together the immunocytochemistry, alphaLISA and western blots data, one can conclude that such "short" *in vitro* model of hTauP301L aggregation in primary neurons provide valuable model for future HTS campaigns in primary neurons as it resembles features of AD patients' brains and leads to a fast hTauP301L aggregation. Additionally, in this "short" model the stability of compound used for treatment will be increased and therefore, the chance to observe its effect on Tau aggregation will be possibly higher than using the "long" model. Moreover such experimental settings lead to more homogeneous culture (i.e.: limiting the time for proliferation of non-neuronal cells) and reduce the overall time and costs

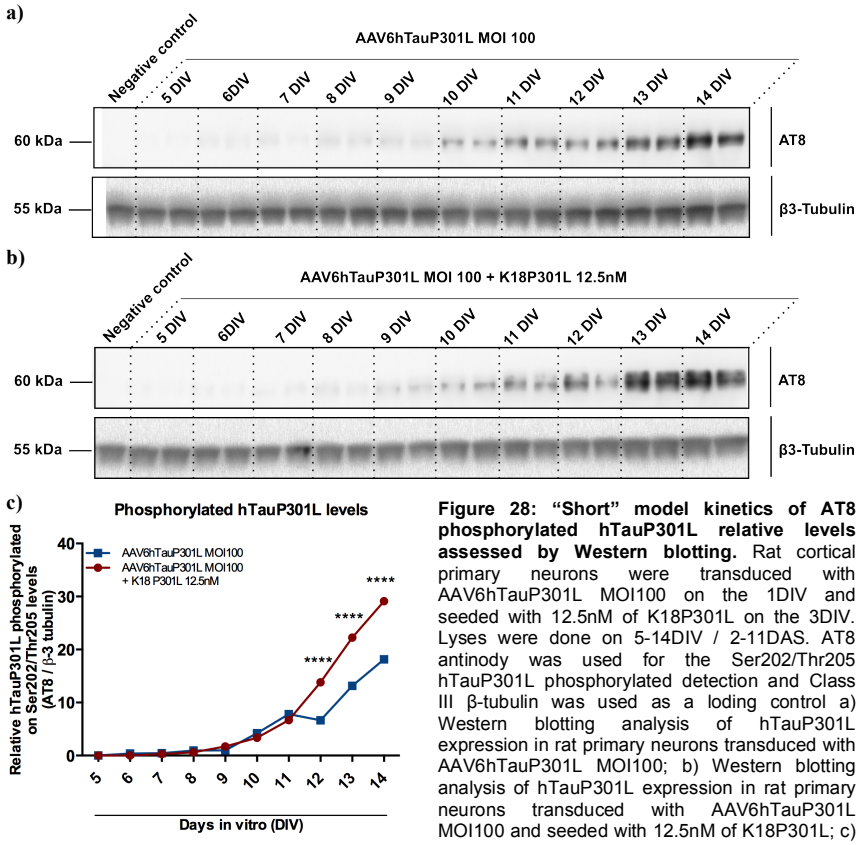

Figure 28: "Short" model kinetics of AT8 phosphorylated hTauP301L relative levels assessed by Western blotting. Rat cortical primary neurons were transduced with AAV6hTauP301L MOI100 on the 1DIV and seeded with 12.5nM of K18P301L on the 3DIV. Lyses were done on 5-14DIV / 2-11DAS. AT8 antinody was used for the Ser202/Thr205 hTauP301L phosphorylated detection and Class III β-tubulin was used as a loding control a) Western blotting analysis of hTauP301L expression in rat primary neurons transduced with AAV6hTauP301L MOI100; b) Western blotting analysis of hTauP301L expression in rat primary neurons transduced with AAV6hTauP301L MOI100 and seeded with 12.5nM of K18P301L; c) Quantification of the hTauP301L relative expression levels based on the images "a" and "b" Data is presented as ± SEM and are representative of a N=1 and n=2. Statistical analyses of the results were performed by a two-way ANOVA followed by Sidak's *post-hoc* comparisons; alpha=0.05.

3.2.3 Proteasome activity in neurons with hTauP301L aggregates- time course

Proteins aggregation, which is often observed in brains of patients with neurodegenerative diseases such as amyloidosis, Tauopathies and synucleopathies, caused a strong interest in the clearing of those entities [6, 213, 214]. Interestingly, Tau has been shown to be physically associated with the proteasome in AD brains [214]. Indeed, immunoprecipitation of Tau leads to the pull-down both the 26S and 20S proteasomes, while 20S catalytic core immunoprecipitation pulled-down Tau [214]. Although this strongly suggests that Tau is being targeted to the proteasome, it may also indicate impaired ability to complete its degradation. Additionally, an inverse correlation between proteasome activity and high molecular weight forms of Tau was described in AD patients' brains [215], indicating that abnormal proteins themselves may interfere with proteasomal degradation processes. Therefore, we questioned ourselves, would Tau aggregation influence the proteasome activity in primary neurons? To answer this question AAV6hTauP301L MOI100 transduction took place on the day 1 *in vitro* (1DIV) (Material and Methods 2.2.), K18P301L 12.5nM seeding (Material and Methods 2.5.) was performed on the day 3 *in vitro* (3DIV /0DAS), and cortical neurons were lysed for the Proteasome-Glo assay (Material and Methods 2.10.) every day from the day of K18P301L seeding (3DIV; 0DAS) for 12 days (Figure 29). To assure the role of hTauP301L expression and aggregation additional controls to wild-type neurons not treated with either AAV6hTauP301L or K18P301L (proteasome activity of which was set as the baseline of proteasome activity) and rat cortical neurons transduced with AAV6hTauP301L in the absence of the fibrils were performed as follows: transduction of primary neurons with AAV6eGFP MOI100 (Material and Methods 2.2.) alone or in the presence of K18P301L (12.5nM) seeds (Material and Methods 2.5.) instead of the adeno-associated virus containing hTauP301L transgene was used to confirm the specificity of the effect to hTauP301L overexpression and/or aggregation. Additionally to such controls, an assay control was performed to assure that the assay was working. As an assay control we used wild type neurons treated with 50nM MG132 for 24 hours before measuring the UPS activity. The statistical analyses were based on a two-way ANOVA followed by Tukey *post-hoc* comparisons for the time-course and on Student's *t*-test for the assay control. P values were considered statistically significant when <0.05.

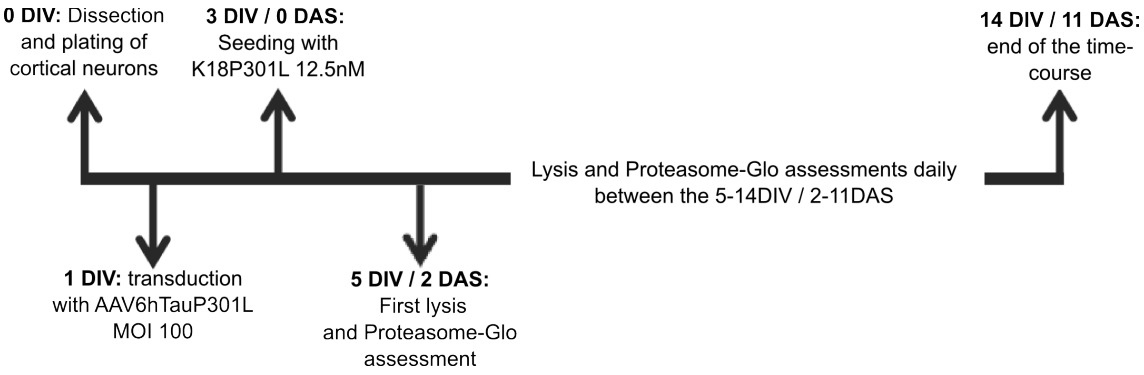

Figure 29: Graphic overview of the experiment. DIV= day *in vitro;* DAS= day after seeding

3.2.3.1 Chymotrypsin-like protease activity associated with the proteasome complex is increased in a time-dependent manner upon treatment with K18P301L in primary neurons

In this experiment, highly statistical significant main effects – treatment factor and time factor – and interaction can be observed (two-way ANOVA p values <0.0001 for the three factors, alpha=0.05). Indeed, it can be observed in our model that, upon K18P301L seeding treatment of neurons transduced with AAV6hTauP301L, there is an average of 10% trend of increase in the proteasome chymotrypsin-like activity signal, from the day of the seeding (0DAS) until the 4DAS – not statistically significant (Figure 30a). However, from the 5DAS seeding until the 7DAS the signal increasing rate accentuates, and by the 6DAS there is a statistically significant increase in the proteasome activity of 40% (Tukey *post-hoc* adjusted p value=0,0358; alpha=0,05; Material and Methods 2.14.) followed by an 80% increase by the 7DAS (Tukey *post-hoc* adjusted p value=<0,0001; alpha=0,05; Material and Methods 2.14.) in comparison to the negative control (not treated wild-type WT primary neurons; Figure 30a). Despite that, it is followed by an oscillation with a fast decrease to 120% of the negative control's activity (negative control = 100%), an increase reaching 150% of the control's activity (statistically significant; Tukey *post-hoc* adjusted p value=0,0016; alpha=0,05; Material and Methods 2.14.), another decrease to the baseline - 100% - and finally ending with a proteasome activity bellow the baseline with -85% of the negative control's UPS activity (Figure 30a). The 8DAS drop in signal is likely due to biological variations related to the fact that these results are the reflection of five (5) independent experiments. When observing the neurons overexpressing hTauP301L in the absence of K18P301L, there are no statistical differences between this treatment and the wild-type WT neurons (negative control – baseline; Figure 30). On the 7DAS and in the 10DAS there is non-statistically significant increase on its proteasome activity (Figure 30a). It is important to notice that, despite this increase in the 7DAS that approximates the levels of such treatment (neurons transduced with AAV6hTauP301L not seeded with K18P301L) to the levels of neurons in aggregative state (overexpressing hTauP301L seeded with K18P301L), there is a significant difference between those two treatments in such time-point – Tukey *post-hoc* adjusted p value=0,0118; alpha=0,05; Material and Methods 2.14.). Considering neurons overexpressing eGFP, in the presence and absence of K18P301L seeds, their proteasome activities are lower when comparing with wild-type WT cortical neurons. It was statistically significant on the 3DAS, 8DAS and 9DAS (Tukey *post-hoc* adjusted p values of 0,0029; 0,0297 and 0,0373, respectively; alpha=0,05; Material and Methods 2.14.) for the AAV6eGFP in the absence of the fibrils and on the 2DAS and 9DAS (Tukey *post-hoc* p values of 0,0283 and 0,0061, respectively; alpha=0,05; Material and Methods 2.14.) in the presence of K18P301L (Figure 30a). These data highlights an effect related to the overexpression of a non-related protein to hTauP301L aggregation with a different profile that the one seen for primary neurons in hTauP301L aggregative conditions and such comparison suggests that altered proteasome activity is specifically related to the hTauP301L aggregative conditions. Lastly, it is important to notice that the assay was working properly as an average of 42% of reduction in the proteasome activity can be observed when wild-type WT primary neurons were treated for 24 hours with MG132 at a 50nM concentration (Student's *t*-test p values: 2DAS = 0.0011; 3DAS = 0.0009; 4DAS = 0.0072; 5DAS = 0.0099; 6DAS = 0.0061; 7DAS = 0.0057; 8DAS = 0.0278; 9DAS = 0.01; 10DAS = 0.0006 and 11DAS = 0.0024; significant different p <0.05; Figure 30b).

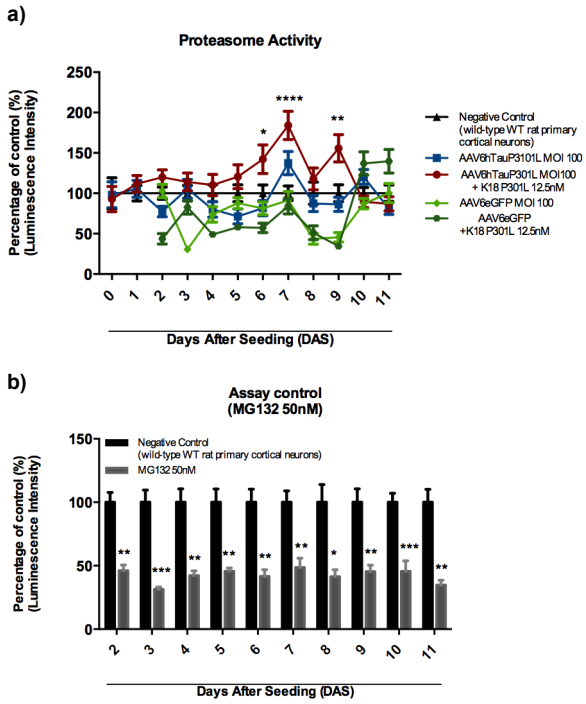

Figure 30: Chymotrypsin-like protease activity associated with the proteasome complex in primary neurons along time. Rat cortical primary neurons were transduced with AAV6hTauP301L MOI100 on the 1DIV and seeded with 12.5nM of K18P301L on the 3DIV. Assessments were done daily between 3-14DIV / 0-11DAS. UPS activity of wild-type rat primary cortical neurons was used as the baseline (negative control) a) Comparison between the UPS activity in wild-type primary neurons, primary neurons overexpressing hTauP301L, primary neurons overexpressing hTauP301L and seeded with K18P301L (aggregative conditions), primary neurons overexpressing eGFP and primary neurons overexpressing eGFP and seeded with K18P301L. Statistics displayed in the graphic are the comparison between the baseline and the neurons in aggregative conditions. For detailed description see Results 3.2.3.1..b) Student's t-test comparison between the negative control UPS activity and primary neurons treated with MG132 50nM – assay control. Data is presented as ± SEM and are representative of a N=5 and n=7 per condition/per experiment, except for the AAV6eGFP treatments in which N=2 and n=8 per experiment and the Assay control in which the n=2. Statistical analyses of the results were performed by a two-way ANOVA followed by Tukey's *post-hoc* comparisons; alpha=0.05 for the time-course and Student's t-test for the assay control (statistically significant $p<0.05$).

3.2.4 Activity of autophagy in neurons with hTauP301L aggregates- time course

As Tau is a long-lived protein, it is expected that it would be degraded through the autophagy-lysosomal pathway [216]. Indeed, in the AD brain, modified forms of Tau (Alz-50 immunoreactive) co-localizes with lysosomes [6]. Additionally, there is evidence that pharmacological enhancement and blocking of autophagy can lead to clearance and aggregates formation respectively [198, 217]. Considering the current data, we asked whether autophagy would get upregulated and/or downregulated upon K18P301L seeding of primary neurons expressing hTauP301L. To address this question, cortical neurons were transduced with AAV6hTauP301L MOI100 on the day 1 *in vitro* (1DIV; Material and Methods 2.2.), seeded with K18P301L 12.5nM on day 3 *in vitro* (3DIV; 0DAS; Material and Methods 2.5.) and everyday from the day 2 after seeding (2DAS) until the day 11 after seeding (11DAS) cells were treated with Cyto-ID® Green Detection Reagent (Material and Methods 2.11.). Subsequently readings of each plate were done in the Digilab MIAS-2™ Microscopy System (Material and Methods 2.11.) with pictures taken for posterior quantification (Figure 31). Wild-type WT cortical neurons were used as a negative control to determine the baseline autophagy levels to compare with WT cortical neurons overexpressing hTauP301L seeded or not with K18P301L fibrils. As an assay control we used wild-type neurons treated with 50 nM MG132 for 24 hours prior each reading. The statistical analyses were based on a two-way ANOVA followed by Tukey *post-hoc* comparisons for the time-course, and on Student's *t*-test for the assay control. P values were considered statistically significant when<0.05.

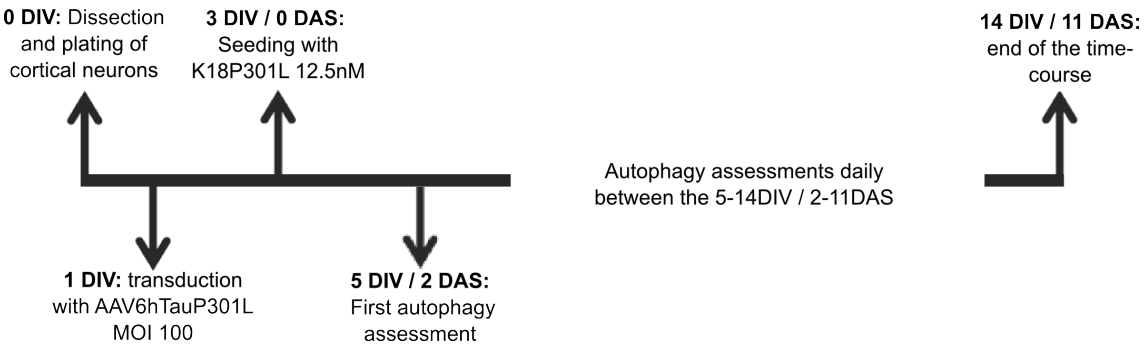

Figure 31: Graphic overview of the experiment. DIV= day *in vitro;* DAS= day after seeding

3.2.4.1 Autophagy activity is increased in a time-dependent manner in neurons with hTauP301L aggregates

As mentioned above (Results 3.2.4.) WT rat cortical primary neurons were transduced with AAV6hTauP301L MOI100 on the day 1 *in vitro* (1DIV; Material and Methods 2.2.), seeded with K18P301L 12.5nM on day 3 *in vitro* (3DIV; 0DAS; Material and Methods 2.5.) and everyday from the day 2 after seeding (2DAS) until the day 11 after seeding (11DAS) cells were treated with Cyto-ID® Green Detection Reagent (Material and Methods 2.11.) with subsequently reading of each plate in the Digilab MIAS-2™ Microscopy System (Material and Methods 2.11.; Figure 31). The images – Figure 32 - taken allowed us to make two independent assessments in those cultures – a fluorescence intensity-based quantification and quantification of the number of autophagolysosomes. For both quantifications – Figure 33 a and b - a highly statistical significance interaction p value can be observed (two-way ANOVA interaction p values <0.0001 for both quantification methods). Indeed, neurons overexpressing hTauP301L and not seeded with K18P301L (non-aggregative conditions) show statistical differences on the 9DAS and 10DAS for both the number of autophagolysosomes quantification (Tukey *post-hoc* adjusted p values of <0,0001 for the 9DAS and 0,0203 for the 10 DAS; alpha=0,05; Material and Methods 2.14.) and the intensity of fluorescence (Tukey *post-hoc* adjusted p values of <0,0001 for 9 DAS and 0,0305 for the 10DAS; alpha=0,05; Material and Methods 2.14.), in comparison to the negative control (wild-type WT cortical neurons) – reaching over 200% counts in the 9DAS in both cases (Figures 33 a and b). Autophagy activity of neurons overexpressing hTauP301L in non-aggregative conditions does not differ from the autophagy activity of wild-type WT primary neurons in the remaining days. On the other hand, when the cultures overexpressing hTauP301L were treated with K18P301L seeds (hTauP301L aggregative conditions), there is a statistically significant increase in the autophagy activity already in the 3DAS for both evaluations (intensity and number-based) – signal counts 50% higher than the baseline (Figures 33 a and b; Tukey *post-hoc* adjusted p values of 0,001 for number-based quantification and 0,0003 for intensity-based quantification; alpha=0,05; Material and Methods 2.14.). This increase is followed as assessed by both quantifications – number and intensity-based - by a decrease to the control levels (wild-type WT neurons) and by a slight higher decrease in the 6DAS, reaching 85% counts (15% lower than the control signal levels; Figures 33 a and b). 7DAS and 8DAS in this aggregative condition remain in the baseline signal levels with a statistical significant increase in the autophagy activity in the 9DAS for both quantifications (Figures 33 a and b; Tukey *post-hoc* adjusted p values of 0,0009 for number-based quantification and 0,0013 for intensity-based quantification; alpha=0,05 Material and Methods 2.14.). It is

important to notice that, despite this increase in the 9DAS that approximates the levels of such treatment to the levels of neurons in non-aggregative state, there is still a significant difference between those two treatments (overexpressing hTauP301L neurons in non-aggregative conditions and in aggregative conditions) in such time-point (Tukey *post-hoc* adjusted p values of 0,0278 when considering the autophagolysosomes quantification and 0,0239 for the intensity-based quantification; alpha=0,05; Material and Methods 2.14.). This increase is followed by a return to control levels towards the last day of the studied temporal window (Figures 33 a and b). Lastly, it is important to notice that the assay was working properly which is displayed by higher autophagy activities when treating the rat cortical neurons with 50nM MG132 concentration (Figures 33 c and d). However, an oscillation of such levels can be observed, and, indeed, on the 2DAS, 6DAS and 11DAS for the quantification based on the number of autophagolysosomes and on the 2DAS and 11DAS for the fluorescence intensity-based quantification, no statistical differences between the 50nM treatment with MG132 and the negative control could be seen (Figures 33 c and d; Student's *t*-test p values for the number of autophagolysosomes-based quantification: 2DAS = 0.2988; 3DAS = 0.0006; 4DAS = 0.0305; 5DAS = 0.0094; 6DAS = 0.1002; 7DAS <0.0001; 9DAS = 0.001; 11DAS = 0.0595; and for the fluorescence intensity-based quantification: 2DAS = 0.3659; 3DAS = 0.0014; 4DAS = 0.03; 5DAS = 0.0042; 6DAS = 0.0462; 7DAS <0.0001; 9DAS = 0.0365 and 11DAS = 0.0581; significant different p <0.05). Such data highlights the extremely temporal-dependent autophagic scenario, indicating that depending on the moment of the treatment, autophagy seems to have different levels of induction when treated with the same compound and concentration settings. Lastly, on the 8DAS and 10DAS, due to technical problems of the imaging system, only one image could be used for the quantification of the assay control and consequently it was not possible to calculate any statistics for such time-point. However, for the 10DAS there is a trend towards increase on the levels of autophagy when treated with MG132 suggesting that in such time-point there was autophagy induction.

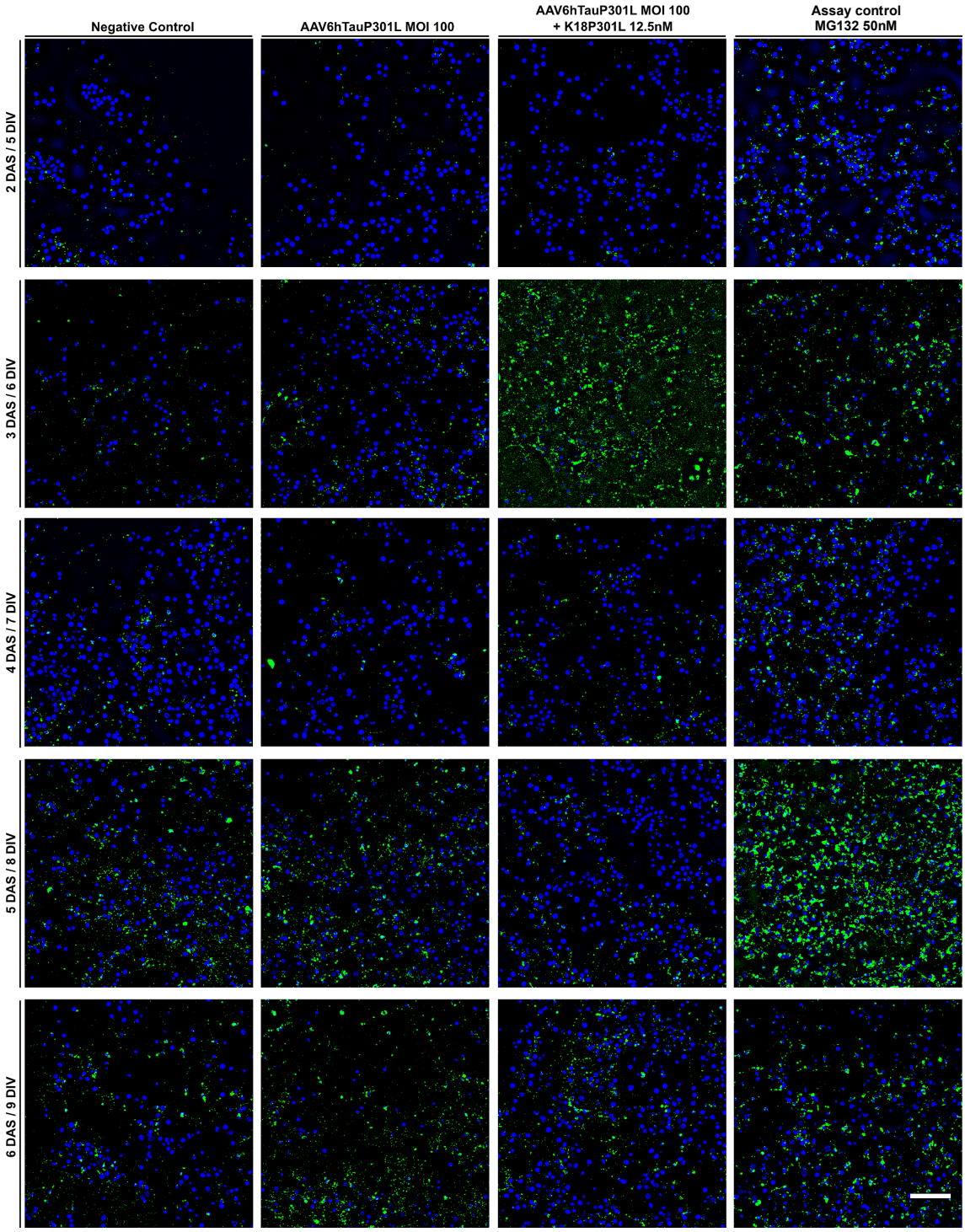

Figure 32: Representative images acquired after Cito-ID staining of autophagolysosomes in primary neurons along time. Rat cortical primary neurons were transduced with AAV6hTauP301L MOI100 on the 1DIV and seeded with 12.5nM of K18P301L on the 3DIV. Assessments were done daily between 5-14DIV / 2-11DAS. Cito-ID staining is the green channel and Hoechst 33342 is the blue channel. Images were acquired by Digilab MIAS-2™ Microscopy System with a 20x magnification. Scale bar: 100µM. Two independent quantifications were performed based on the images taken: (1) based on the number of autophagolysosomes and (2) based on the fluorescence intensity of the autophagolysosomes – see Figure 33 a and b for the quantification results. The images above represent two independent experiments (N=2) with an average of 28 images acquired per well (n=28) with exception of the assay control that were an average of two 16 images per well (n=16).

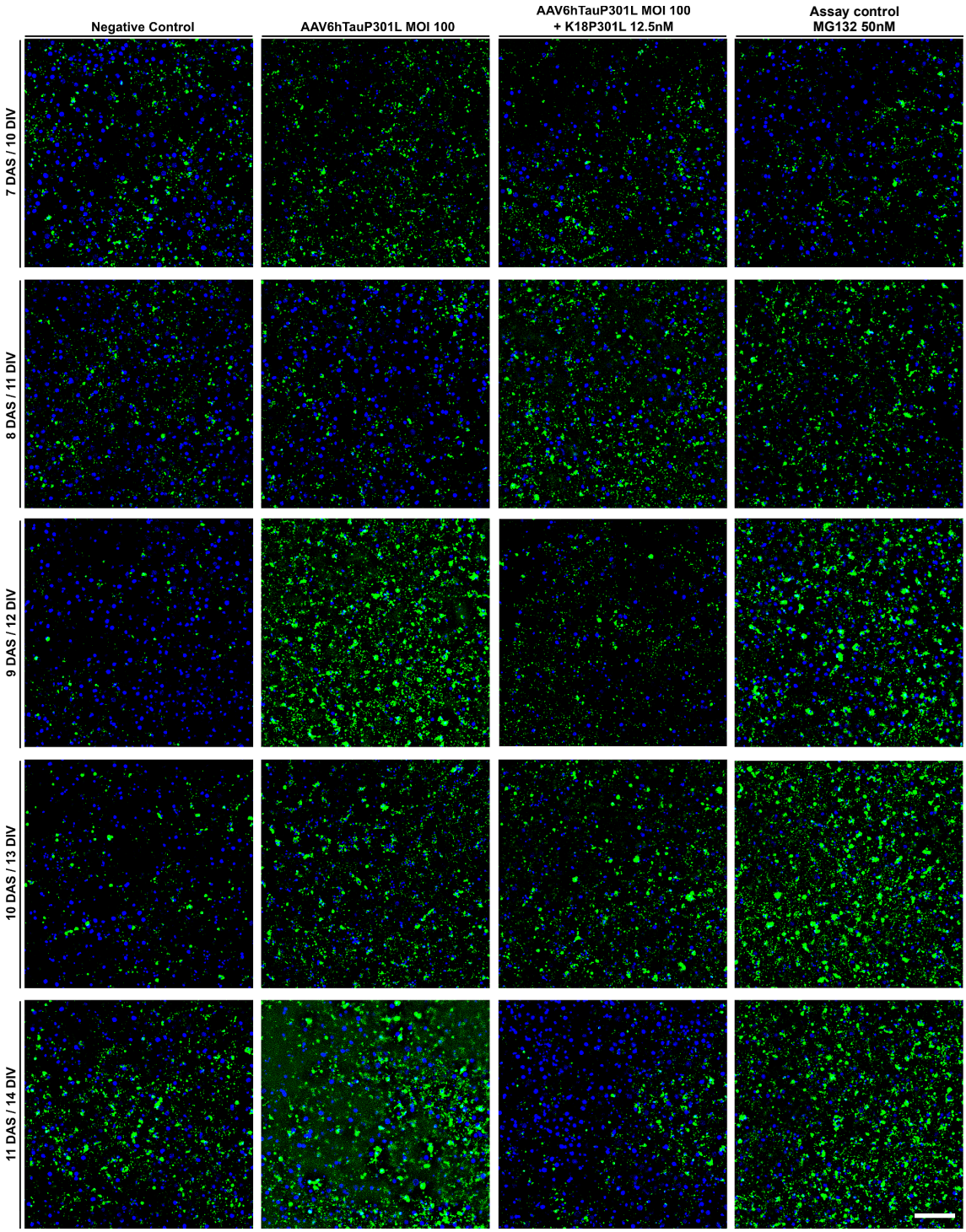

↵**Figure 32 (continuation): Representative images acquired after Cito-ID staining of autophagolysosomes in primary neurons along time.** Rat cortical primary neurons were transduced with AAV6hTauP301L MOI100 on the 1DIV and seeded with 12.5nM of K18P301L on the 3DIV. Assessments were done daily between 5-14DIV / 2-11DAS. Cito-ID staining is the green channel and Hoechst 33342 is the blue channel. Images were acquired by Digilab MIAS-2™ Microscopy System with a 20x magnification. Scale bar: 100µM. Two independent quantifications were performed based on the images taken: (1) based on the number of autophagolysosomes and (2) based on the fluorescence intensity of the autophagolysosomes – see Figure 33 a and b for the quantification results. The images above represent two independent experiments (N=2) with an average of 28 images acquired per well (n=28) with exception of the assay control that were an average of two 16 images per well (n=16).

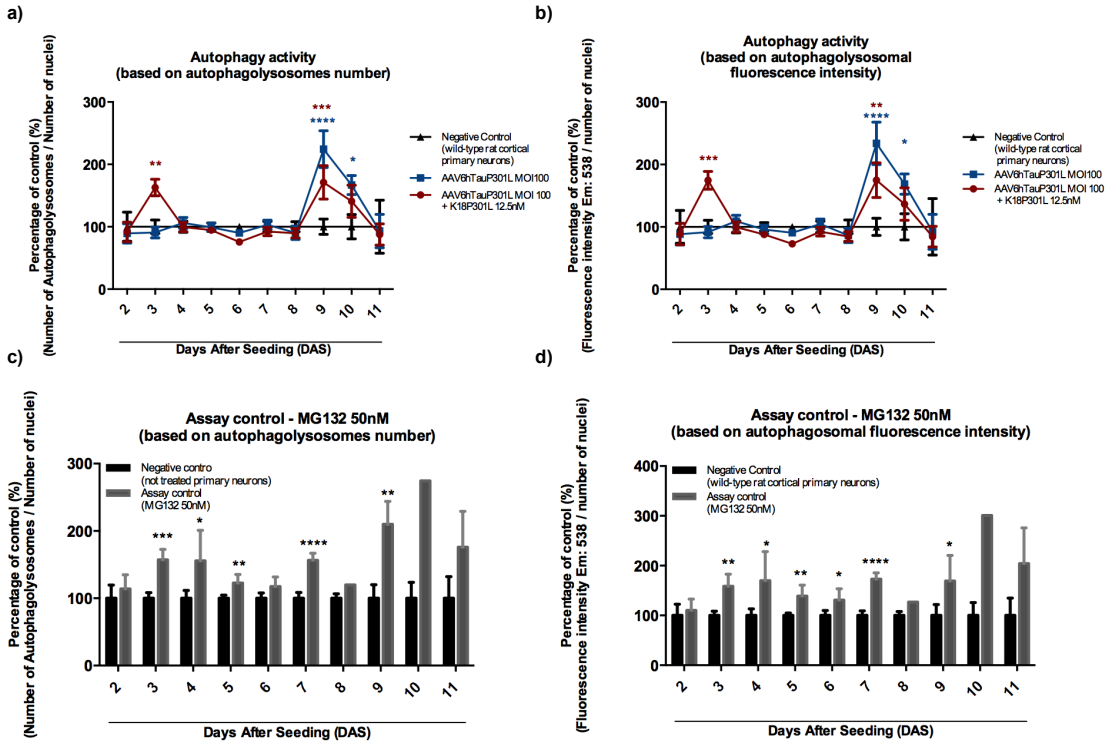

Figure 33: Autophagy activity in rat primary neurons with or without hTauP301L aggregates along time. Rat cortical primary neurons were transduced with AAV6hTauP301L MOI100 on the 1DIV and seeded with 12.5nM of K18P301L on the 3DIV. Assessments were done daily between 5-14DIV / 2-11DAS with image acquisition by Digilab MIAS-2™ Microscopy System with a 20x magnification (see Figure 32 for representative images). Autophagy activity of wild-type rat primary cortical neurons was used as the baseline (negative control) a) Comparison between the Autophagy activity with a quantification based on the number of autophagolysosomes of wild-type primary neurons, primary neurons overexpressing hTauP301L and primary neurons overexpressing hTauP301L and seeded with K18P301L (aggregative conditions); b) Comparison between the Autophagy activity with a quantification based on the fluorescence intensity of autophagolysosomes of wild-type primary neurons, primary neurons overexpressing hTauP301L and primary neurons overexpressing hTauP301L and seeded with K18P301L (aggregative conditions).c) Student's t-test comparison between the negative control Autophagy activity and Autophgy activity of primary neurons treated with MG132 50nM – assay control – with a quantification base on the number of autophagolysosomes and d). Student's t-test comparison between the negative control Autophagy activity and Autophagy activity of primary neurons treated with MG132 50nM – assay control – with a quantification base on the fluorescence intensity of autophagolysosomes. Data is presented as ± SEM and are representative of two independent experiments (N=2) with an average of 28 images acquired per well (n=28) with exception of the assay control that were an average of two 16 images per well (n=16). During the assay control images acquisition technical problems with the Microscopy system was encountered and hence on the 8DAS and 10DAS only one frame could be acquired reason of which no statistics could be calculated for such days. Statistical analyses of the results were performed by a two-way ANOVA followed by Tukey's *post-hoc* comparisons with an alpha=0.05 for the time-course and Student's t-test for the assay control (statistically significant $p<0.05$). *'s represents the comparison between the baseline and the neurons overexpressing hTauP301L in aggregative conditions: *'s represents the comparison between the baseline and the neurons overexpressing hTauP301L in non-aggregative conditions.

3.3 Autophagy and Ubiquitin Proteasome systems validation as pivotal players in Tau build-up and/or clearance – a pharmacological approach

The two major routes for protein degradation in cells, the autophagy-lysosome and ubiquitin-proteasome pathways, have long been associated with the clearance of misfolded proteins [6, 218, 219]. Indeed, there are evidences that autophagical dysfunction contributes to the formation of Tau oligomers and insoluble aggregates [6, 198, 218]. Adding to these data, inhibitors of various autophagy processes, such as NH_4Cl, chloroquine, 3-methyladenine (3-MA), and cathepsin inhibitors, have been shown to delay Tau degradation and enhance the formation of high molecular weight species of Tau [198, 220, 221]; and autophagy inducers have been shown to facilitate the degradation of insoluble forms of Tau [221]. On the other hand, recent accumulating data closely relates the UPS with Tau degradation/aggregation and neurodegeneration in AD [221]. Related to this information are the observations that reversible and irreversible proteasome inhibitors including lactacystin, leupeptin, and epoxomicin are able to delay the degradation of endogenous and/or transiently overexpressed Tau [176, 221-223], and that blocking proteasomes using Aβ oligomers also effectively facilitates Tau accumulation in AD mice [104]. Despite all of that, the relative contributions of these two major processes to normal and pathological Tau clearance are still poorly understood. Hence, we developed pharmacological strategies (described bellow; Results 3.3.1. and 3.3.2.) to try to understand the contributions of autophagy and ubiquitin proteasome systems (UPS) in hTauP301L aggregation in rat cortical neurons *in vitro*. The reference compounds MG132, a potent reversible proteasome inhibitor [224] that is also known to induce autophagy [225]; Lactacystin, an specific and irreversible proteasome inhibitor [224]; and Rapamycin, a canonical allosteric inhibitor of the mammalian target of rapamycin (mTOR) kinase that strongly induce autophagy *in vitro* [226] were chosen to manipulate UPS and autophagy in primary neurons. By choosing such compounds, we could isolate the specific contribution of an inhibition of the proteasome alone (lactacystin treatment) and the specific contribution of an activation of autophagy alone (rapamycin treatment) in the hTauP301L aggregation, as well as, these two factors acting together in the hTauP301L aggregation *in vitro* (MG132 treatment). Consequently, we could, at least partially, discriminate between the contributions of autophagy and UPS in hTauP301L aggregation levels when analysing the results.

3.3.1 Determination of the concentration of the compounds – Lactacystin, MG132 and Rapamycin

Lactacystin concentrations used in this project were chosen based on previous studies in primary neurons [227, 228] and based on the information provided in the datasheet of the Proteasome-Glo™ Chymotrypsin-Like Cell-Based Assay (Promega). MG132 and rapamycin concentrations were also set based on recent literature [226, 229-231]. For MG132 and rapamycin, we further assessed the inhibition of the UPS by total ubiquitin probing western blot (MG132 treatment) and autophagy induction by LC3-II probing western blot (MG132 and rapamycin treatments). Ubiquitin is a conserved polypeptide unit that plays an important role in the ubiquitin-proteasome pathway. Ubiquitin can be covalently linked to many cellular proteins by the ubiquitination process, which targets proteins for degradation by the 26S proteasome [232]. Hence, free ubiquitin, polyubiquitin and ubiquitinated proteins levels are directly related to the UPS activity

and treatment with proteasome inhibitors, such as MG132, leads to increased reactivity of such molecules in western blotting [233, 234]. As a consequence, an increase in the levels of polyubiquitinated proteins suggests that the UPS is inhibited. Upon induction of autophagy, the exposed glycine of LC3-I is conjugated to the highly lipophilic phosphatidylethanolamine (PE) moiety to generate LC3-II [235]. The PE group promotes integration of LC3-II into lipid membranes at the phagophore and autophagosomes and, to date, LC3-II is the only well-characterized protein that is specifically localized to autophagic structures throughout the process from phagophore to lysosomal degradation [235]. As a consequence, LC3B-II detection by western blot has been one of the mainstays for autophagy detection. Hence, in case of MG132, LC3-II and total ubiquitin levels were assessed to check for the autophagy and UPS activity by western blotting (Material and Methods 2.7.) and LC3-II to check for autophagy induction upon rapamycin treatment by the same methodology. For the western blotting loading controls (Material and Methods 2.7.), actin was used as those processes are not neuronal specific and the cultures are not homogeneous. To this end, rat cortical primary neurons were transduced with AAV6hTauP301L MOI100 on the day 1 *in vitro* (1DIV; Material and Methods 2.2.) and treated with MG132 (50nM, 25nM, 10nM, 5nM and 1nM) and rapamycin (1µM, 0.1µM, 0.01µM, 0.001µM and 0.0001µM) on day 3 *in vitro* (3DIV; 0DAS; Material and Methods 2.13.). Cells were lysed on 10DIV followed by protein quantification and western blotting (Material and Methods 2.7.; Figure 34).

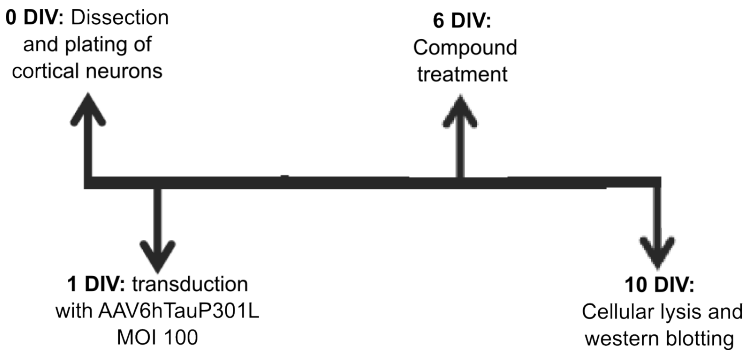

Figure 34: Graphic overview of the experiment

Inspecting the total ubiquitin probing western blot upon MG132 treatment, a dose response trend is observed, in which primary neurons treated with 50nM and 25nM of MG132 display a 1.3-fold and 1.18-fold higher total ubiquitin levels, respectively, when in comparison to the DMSO treated neurons (negative control; Figure 35 a and b). Neurons treated with 10nM, 5nM and 1nM of MG132 seem to display slighter lower levels than the DMSO treated neurons (negative control; Figure 35 a and b). Such dose response trend suggests that UPS inhibition might be taking place within the 50nM-10nM range of the compound.

When observing the LC3-II levels upon the same compound treatment, again a dose response trend can be observed. In this case, 50nM, 25nM and 10nM of MG132 seem to induce a 2.98-fold, 1.78-fold and 1.3-fold increase in LC3-II levels, respectively, when compared to the negative control (DMSO treated neurons; Figure 35 a and c). 5nM and 1nM treatments with MG132 seem to display comparable levels with the negative control (Figure 35 a and c). These data suggests that autophagy might be induced within the 50-10nM compound range of concentrations.

When observing the LC3-II levels upon neuronal treatment with rapamycin, again a dose response tendency takes place (Figure 35 d and e). In such treatment, LC3-II levels seem to have 2.9-fold, 2.69-fold and 1.8-fold increased levels respectively to the 1μM, 0.1μM and 0.01μM concentrations of rapamycin. 0.001μM and 0.0001μM rapamycin treatments seem to display control levels of LC3-II (Figure 35 d and e). Therefore, such tendency also suggests an autophagy induction within the 1-0.01μM used range of the compound.

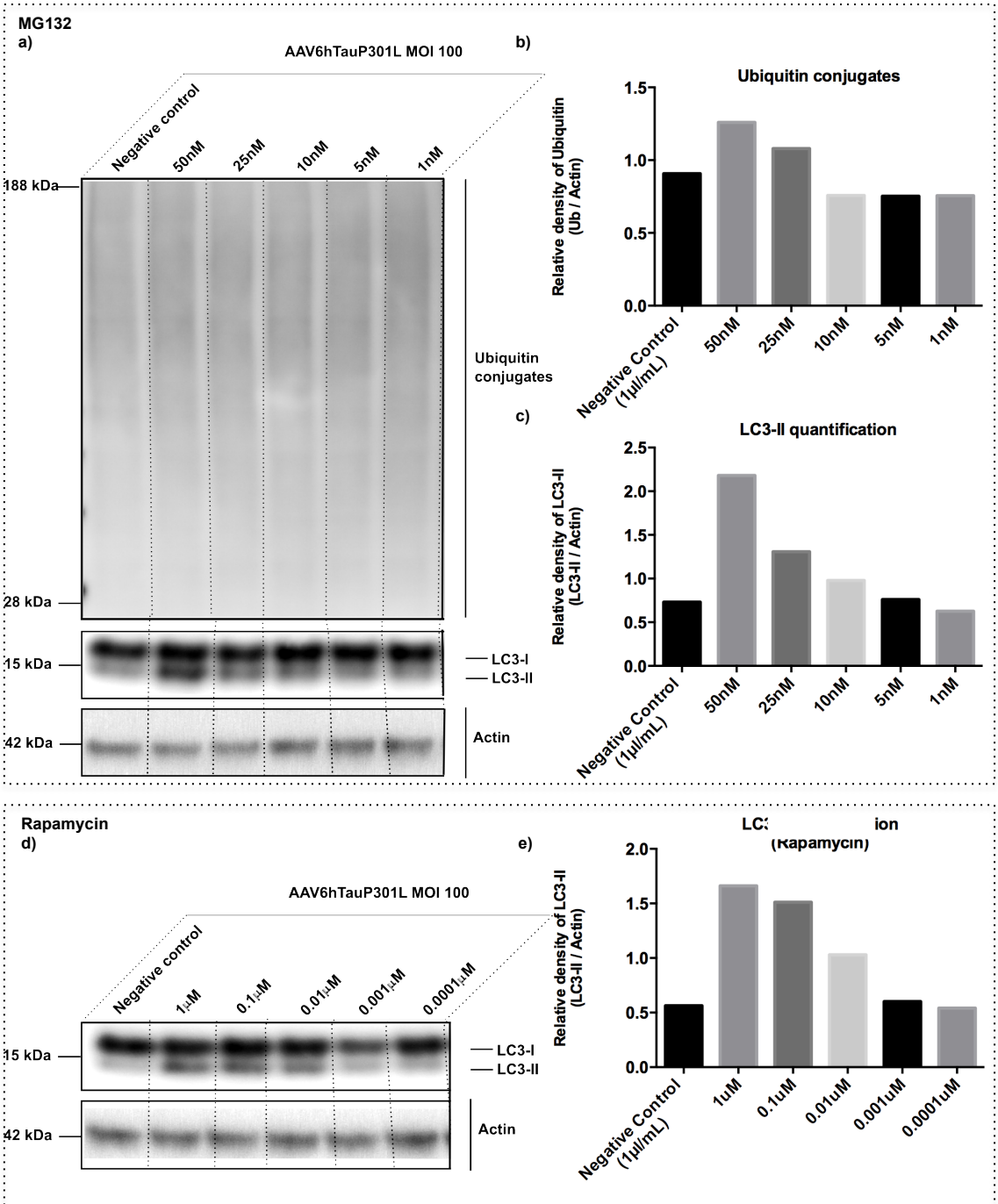

Figure 35: Total ubiquitin and LC3-II probing western blot analyses of MG132 and rapamycin treatments of rat primary neurons overexpressing hTauP301L. Rat cortical primary neurons were transduced with AAV6hTauP301L MOI100 on the 1DIV and treated with MG132 (concentrations 50nM; 25nM; 10nM; 5nM and 1nM); rapamycin (1μM; 0.1μM; 0.01μM; 0.001μM and 0.0001μM) or DMSO (1μL/mL) on the 6DIV. Cellular lyses were done on the 10DIV. Total Ubiquitin probing antibody was used to check for total ubiquitin levels and LC3B antibody was used to detect LC3-II. Anti-Actin Clone C4 was used to detect Actin that was used as a loading control (see Table 2 for antibody information) a) MG132 treatment Western blotting images acquired;.b) MG132 treatment quantification of the total ubiquitin relative protein levels probed by the total Ubiquitin antibody; c) MG132 treatment quantification of the LC3-II relative protein levels probed by the anti-LC3B antibody; d) Rapamycin treatment western blotting images acquired and e) rapamycin treatment quantification of LC3-II relative levels protein levels probed by LC3B (see Table 2 for antibody information). N=1 and n=1.

3.3.2 Effect of Lactacystin and MG132 treatments on hTauP301L soluble and aggregated levels when treated with the compounds on 4 and 7 days after seeding with K18P301L in rat cortical neurons

Based on the previously described characterization data (Results 3.2.) of the hTauP301L expression/aggregation, proteasome activity and autophagy activity along time in our "short" model, initially two treatment time-points were chosen: 4DAS (7DIV) and 7DAS (10DIV). They had the main goal of manipulating hTauP301L soluble and aggregation levels, and hence identifying the contribution on soluble, total and aggregate hTauP301L signals of an earlier inhibition of the proteasome (considering its highest peak of activity on 7DAS in our model, Results 3.2.3.; Figure 30a) when treating the cells with both inhibitors at 4DAS, and identifying the effect on the soluble, total and aggregated hTauP301L levels of an UPS inhibition on the time-point of the highest proteasome activity peak – 7DAS (Figure 30a). The MG132 treatment also intended to assess the contribution of an early rescue of the autophagical levels when treated at 4DAS or a late induction of this system on hTauP301L signals (considering its peaks of activity on 3DAS and on 9DAS, Figures 32; 33a and 33b). In order to do that, neurons were transduced with AAV6hTauP301L (MOI100) on 1DIV (Material and Methods 2.2.) and K18P301L (12.5nM) seeded on the 3DIV (0DAS; Material and Methods 2.5.). Treatments with MG132, Lactacystin and DMSO (vehicle for the negative controls) took place on the 7DIV and 10 DIV for neurons not seeded with K18P301L and on the corresponding day 4 after seeding – 4DAS and day 7 after seeding - 7DAS for neurons treated with K18P301L. Cellular lyses were performed on the 14DIV (11DAS) with posterior alphaLISA quantification (Material and Methods 2.8.) and ELISA measurements (Material and Methods 2.9.; Figure 36). ELISA was performed to normalize the alphaLISA data against possible technical variations or neuronal loss.

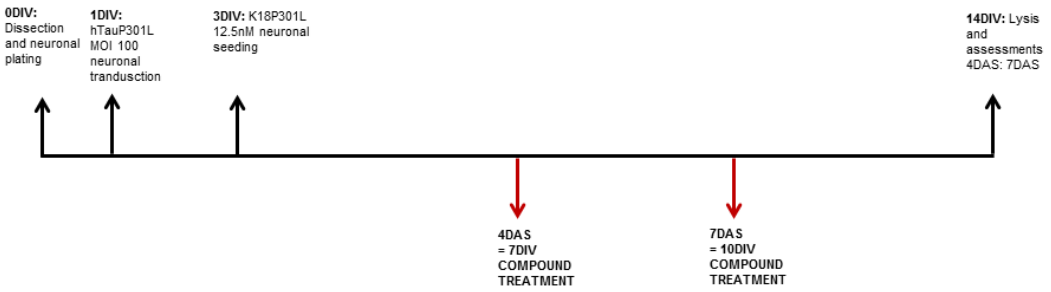

Figure 36: Graphic overview of the experiments. DIV= day *in vitro;* DAS= day after seeding

3.3.2.1 Treatment with lactacystin on the 4th day after seeding reduces the level of soluble hTauP301L in primary neurons and treatment on the 7th day after seeding do not affect hTauP301L levels

Primary neurons were transduced with AAV6hTauP301L MOI 100 on 1DIV (Material and Methods 2.2.) and K18P301L 12.5nM seeded on the 3DIV (Material and Methods 2.5.). Treatment with lactacystin with final concentrations of 500nM, 100nM and 10nM took place on the 4DAS (on the corresponding 7DIV for neurons overexpressing hTauP301L but not K18P301L seeded). Cellular lyses were performed on the 11DAS (14DIV) with posterior alphaLISA (Material and Methods 2.8.) and ELISA measurements (Material and Methods 2.9.). ELISA was performed to normalize the alphaLISA data against possible technical

variations or neuronal loss - see Figure 36 for a graphic overview of the experiment. The statistical analyses were performed using a one-way ANOVA followed by Dunnett's *post-hoc* multi-comparisons. P values were considered statistically significant when<0.05.

When treating primary neurons with lactacystin on the 4DAS, a drop in the soluble HT7/hTau10 alphaLISA (Material and Methods 2.8.) signal can be highlighted for both treatments concentrations – 500nM and 100nM – in comparison to the negative control (DMSO treated neurons), as observed by the quantification of the soluble levels of hTauP301L (Figure 37a). This reduction in signal is statistically significant accounting for 35% and 46% of reduction in comparison to the DMSO treated neurons (Dunnett's *post-hoc* adjusted p values of 0,0025 and 0,0005 respectively; alpha=0,05; Material and Methods 2.14.). However, this data is not translated to the total hTauP301L and aggregated hTauP301L quantification in which there are no statistical differences between the treatments and the control condition (DMSO treated neurons) with the exception of the 10nM concentration of lactacystin condition for the total HT7/hTau10 alphaLISA (Material and Methods 2.8.) levels measurements (i.e.: 10nM of lactacystin treatment of primary neurons overexpressing hTauP301L in the presence of K18hTaP301L) that shows a reduction of 48% in comparison to the negative control (Figures 37 b and c; Dunnett's *post-hoc* adjusted p value=0,0012; alpha=0,05; Material and Methods 2.14.).

As can be seen in the Figures 37 "d", "e" and "f", lactacystin treatment on the 7DAS fail to induce any response at the hTauP301L signal levels in the soluble, total and aggregates quantification for any of the tested conditions.

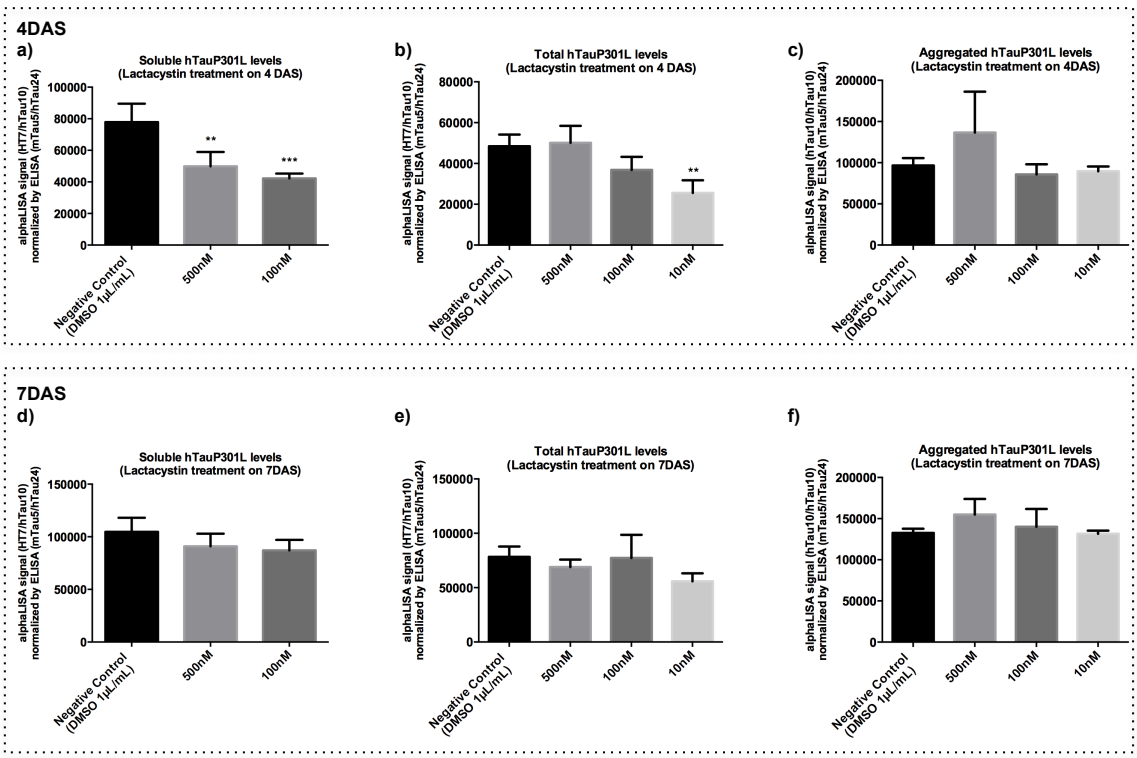

Figure 37: Effect of lactacystin treatment on 4DAS and 7DAS in soluble, total and aggregated hTauP301L levels in primary neurons. Rat cortical primary neurons were transduced with AAV6hTauP301L MOI100 on the 1DIV and seeded with 12.5nM of K18P301L on the 3DIV/0DAS. Lactacystin treatment (500nM; 100nM and 10nM) took place on the 4DAS (7DIV) and on 7DAS (10DIV). Cellular lyses were done on the 11DAS (14DIV) with posterior alphaLISA and ELISA quantifications (Material and Methods 2.8. and 2.9.). ELISA data was used to normalize the alphaLISA data against possible technical and/or biological variation. Soluble hTauP301L:

↵**Figure 37 (continuation):** HT7/hTau10 alphaLISA quantification of primary neurons overexpressing hTauP301L and not seeded with K18P301L. Total hTauP301L: HT7/hTau10 alphaLISA quantification of primary neurons overexpressing hTauP301L and seeded with K18P301L (both soluble and aggregated hTauP301L are present on the sample). Aggregated hTauP301L: hTau10/hTau10 alphaLISA quantification (see Material and Methods 2.8. for alphaLISA description). a) Comparison between soluble hTauP301L levels of primary neurons overexpressing hTauP301L treated or not with the compound on the 4DAS; b) Comparison between total hTauP301L levels of primary neurons seeded with K18P301L and treated or not with the compound on the 4DAS c) Comparison between aggregated hTauP301L levels of primary neurons overexpressing hTauP301L and seeded with K18P301L, treated or not with the compound on the 4DAS d) Comparison between soluble hTauP301L levels of primary neurons overexpressing hTauP301L treated or not with the compound on the 7DAS; e) Comparison between total hTauP301L levels of primary neurons seeded with K18P301L and treated or not with the compound on the 7DAS f) Comparison between aggregated hTauP301L levels of primary neurons overexpressing hTauP301L and seeded with K18P301L, treated or not with the compound on the 7DAS. Data is presented as ± SEM. N=1 and n=4. Statistical analyses of the results were performed by a two-way ANOVA followed by Dunnett's *post-hoc* comparisons with an alpha set to 0.05.

3.3.2.2 MG132 treatment on the day 4 after seeding reduces soluble levels of hTauP301L in primary neurons

Primary neurons were transduced with AAV6hTauP301L MOI 100 on 1DIV (Material and Methods 2.2.) and K18P301L 12.5nM seeded on the 3DIV (Material and Methods 2.5.). Treatment with MG132 with final concentrations of 100nM, 50nM and 10nM took place on the 4DAS (on the corresponding 7DIV for neurons overexpressing hTauP301L but not K18P301L seeded). Cellular lyses were performed on the 11DAS (14DIV) with posterior alphaLISA (Material and Methods 2.8.) and ELISA measurements (Material and Methods 2.9.). ELISA was performed to normalize the alphaLISA data against possible technical variations or neuronal loss. See Figure 36 for a graphic overview of the experiment. The statistical analyses were performed using a one-way ANOVA with Dunnett's *post-hoc* multi-comparisons. P values were considered statistically significant when<0.05.

Upon treatment with MG132, it can be seen that the treatment with 100nM and 50nM of this compound results in - 25% and - 37% of reduction of soluble hTauP301L levels (i.e. neurons overexpressing hTauP301L and not seeded with K18P301L) respectively, in comparison the DMSO treated negative control (Dunnett's *post-hoc* adjusted p values of 0,0483 and 0,0059, respectively; alpha=0,05; Material and Methods 2.14.) as assessed by the HT7/hTau10 alphaLISA (Figure 38a; Material and Methods 2.8.). Emphasizing the relation between soluble and total hTauP301L levels, similar results are also seen in the alphaLISA for total hTauP301L levels (HT7/hTau10 quantification of neurons overexpressing hTauP301L and seeded with the fibrils; Material and Methods 2.8.). In this case the treatments with the compound in the concentrations of 100nM, 50nM and 10nM show statistical differences when compared to the control conditions – 35%, 32% and 47% of reduction respectively to the negative control (Figure 38b; Dunnett's *post-hoc* adjusted p values of 0,0006; 0,0014 and <0,0001 respectively; alpha=0,05; Material and Methods 2.14.). Nevertheless, when inspecting the aggregation hTauP301L signal (hTau10/hTau10 alphaLISA; Material and Methods 2.8.) no statistical significant differences between the treatments with 50nM and 10nM of MG132 and the control conditions are observed (Figure 38c). Despite that, the treatment with 100nM of MG132 displays an increase of 33% in aggregated hTauP301L signal comparing to the negative control – primary neurons overexpressing hTauP301L in aggregative conditions treated with DMSO (Figure 38c; Dunnett's *post-hoc* adjusted p value = 0,0037; alpha=0,05), which likely accounts for a technical artefact as only reductions in both soluble and total levels were observed.

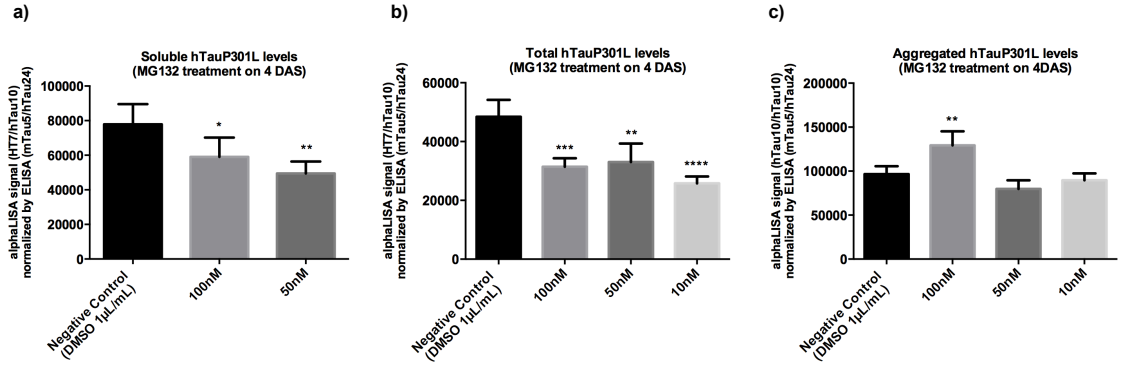

Figure 37: Effect of MG132 treatment on 4DAS in soluble, total and aggregated hTauP301L levels in primary neurons. Rat cortical primary neurons were transduced with AAV6hTauP301L MOI100 on the 1DIV and seeded with 12.5nM of K18P301L on the 3DIV/0DAS. MG132 treatment (100nM; 50nM and 10nM) took place on the 4DAS (7DIV). Cellular lyses were done on the 11DAS (14DIV) with posterior alphaLISA and ELISA quantifications (Material and Methods 2.8. and 2.9.). ELISA data was used to normalize the alphaLISA data against possible technical and/or biological variation. Soluble hTauP301L: HT7/hTau10 alphaLISA quantification of primary neurons overexpressing hTauP301L and not seeded with K18P301L. Total hTauP301L: HT7/hTau10 alphaLISA quantification of primary neurons overexpressing hTauP301L and seeded with K18P301L (both soluble and aggregated hTauP301L are present on the sample). Aggregated hTauP301L: hTau10/hTau10 alphaLISA quantification (see Material and Methods 2.8. for alphaLISA description). a) Comparison between soluble hTauP301L levels of primary neurons overexpressing hTauP301L treated or not with the compound on the 4DAS; b) Comparison between total hTauP301L levels of primary neurons seeded with K18P301L and treated or not with the compound on the 4DAS c) Comparison between aggregated hTauP301L levels of primary neurons overexpressing hTauP301L and seeded with K18P301L, treated or not with the compound on the 4DAS Data is presented as ± SEM. N=1 and n=4. Statistical analyses of the results were performed by a two-way ANOVA followed by Dunnett's *post-hoc* comparisons with an alpha set to 0.05.

3.3.2.3 MG132 treatment on the day 7 after seeding results in reduction of soluble hTauP301L levels

Primary neurons were transduced with AAV6hTauP301L MOI 100 on 1DIV (Material and Methods 2.2.) and K18P301L 12.5nM seeded on the 3DIV (Material and Methods 2.5.). Treatment with MG132 with final concentrations of 100nM, 50nM and 10nM took place on the 7DAS (on the corresponding 10DIV for neurons overexpressing hTauP301L but not K18P301L seeded). Cellular lyses were performed on the 11DAS (14DIV) with posterior alphaLISA (Material and Methods 2.8.) and ELISA measurements (Material and Methods 2.9.). ELISA was performed to normalize the alphaLISA data against possible technical variations of neuronal loss - see Figure 36 for a graphic overview of the experiment. The statistical analyses were performed using a one-way ANOVA with Dunnett's *post-hoc* multi-comparisons. P values were considered statistically significant when<0.05.

Late treatment (on the 7DAS) with MG132 also shows efect on the soluble hTauP301L (HT7/hTau10 alphaLISA of neurons overexpressing hTauP301L and not seeded with K18P301L; Material and Methods 2.8.) signal levels as can be seen in the Figure 38a. Both treatments – 100nM and 50nM of MG132 - show 33% and -32% of reduction of soluble hTauP301L signals, respectively, when compared to DMSO treated neurons (Dunnett's *post-hoc* adjusted p values of 0,0005 and 0,0007, respectively; alpha=0,05; Material and Methods 2.14.). Reductions can also be observed in the total hTauP301L levels (neurons overexpressing hTauP3011 in the presence of K18P301L; Figure 38b). In this case both 100nM and 10nM treatments with MG132 resulted in statistically significant reduced levels of total hTauP301L with similar signals – 21% and 19% of reduction when compared to the DMSO control (Dunnett's *post-hoc* adjusted p values of 0,0053 and 0,0075 respectively; alpha=0,05; Material and Methods 2.14.). 50nM, although not statistically significant shows lower signal mean than the control (DMSO treatment; -11%). These total hTauP301L levels reductions are likely to be a reflection of the soluble hTauP301L signal reduction described

above. Regarding hTauP301L aggregated levels, there are significant differences when comparing the compound treatments with 50nM and 10nM final concentrations to neurons treated with the vehicle – 24% and 25% of reduction, respectively (Figure 38c; Dunnett's *post-hoc* adjusted p values of 0,0064 and 0,0046 respectively; alpha=0,05; Material and Methods 2.14.). However, as 100nM of MG132 treatment of neurons showed no statistical difference in comparison to the DMSO treated neurons and as there is a higher reduction in the treatment with the lowest MG132 concentration, such results are likely to account for a random biological variation or a technical artefact.

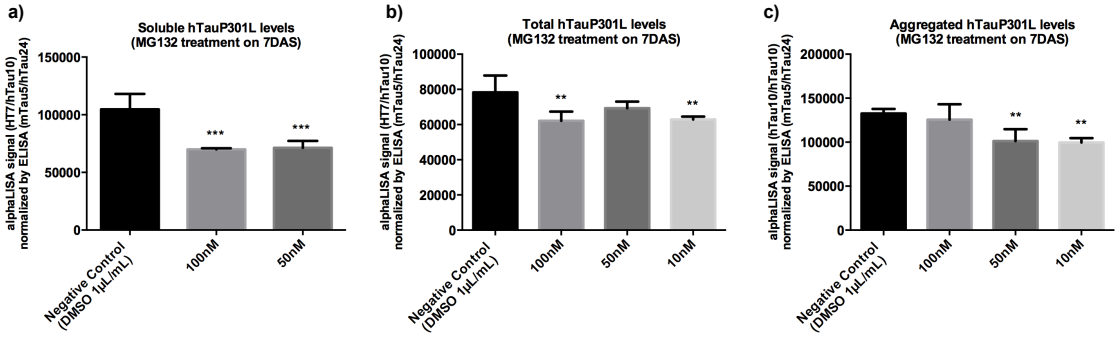

Figure 38: Effect of MG132 treatment on 7DAS in soluble, total and aggregated hTauP301L levels in primary neurons. Rat cortical primary neurons were transduced with AAV6hTauP301L MOI100 on the 1DIV and seeded with 12.5nM of K18P301L on the 3DIV/0DAS. MG132 treatment (100nM; 50nM and 10nM) took place on the 7DAS (10DIV). Cellular lyses were done on the 11DAS (14DIV) with posterior alphaLISA and ELISA quantifications (Material and Methods 2.8. and 2.9.). ELISA data was used to normalize the alphaLISA data against possible technical and/or biological variation. Soluble hTauP301L: HT7/hTau10 alphaLISA quantification of primary neurons overexpressing hTauP301L and not seeded with K18P301L. Total hTauP301L: HT7/hTau10 alphaLISA quantification of primary neurons overexpressing hTauP301L and seeded with K18P301L (both soluble and aggregated hTauP301L are present on the sample). Aggregated hTauP301L: hTau10/hTau10 alphaLISA quantification (see Material and Methods 2.8. for alphaLISA description). a) Comparison between soluble hTauP301L levels of primary neurons overexpressing hTauP301L treated or not with the compound on the 7DAS; b) Comparison between total hTauP301L levels of primary neurons seeded with K18P301L and treated or not with the compound on the 7DAS c) Comparison between aggregated hTauP301L levels of primary neurons overexpressing hTauP301L and seeded with K18P301L, treated or not with the compound on the 7DAS Data is presented as ± SEM. N=1 and n=4. Statistical analyses of the results were performed by a two-way ANOVA followed by Dunnett's *post-hoc* comparisons with an alpha set to 0.05.

3.3.3 Effect of Lactacystin, MG132 and Rapamycin on hTauP301L soluble and aggregation levels when treated with the compounds on -1, 0 and 3 days after seeding with K18P301L in rat cortical neurons

Based on the previous described pharmacological manipulation (Results 3.3.2.) and characterization data of the Tau expression/aggregation (Results 3.2.1.), proteasome and autophagy activity (Results 3.2.3. and 3.2.4.), we asked ourselves whether earlier manipulations of these systems in comparison to the pharmacological approach above would be more effective in reducing hTauP301L soluble, total and aggregated levels. The rationale comes from the observation that MG132 and Lactacystin treatments were able to effectively reduce soluble hTauP301L signal levels in early time-point treatments (Results 3.3.2.2. and 3.3.2.3.). Additionally, as it has already been shown that upon K18P301L seeding autophagy induction is seen early on the 3DAS (Results 3.2.4.; Figures 32, 33a and 33b), therefore it would be plausible that earlier treatments leading to early or sustained boost of autophagy induction, when hTauP301L expression levels are lower, could render more efficient reductions on this entity, either by reducing its substrate or because the aggregation burden is still in controllable levels – or both. Additionally, as lactacystin and MG132 induce inhibition of the proteasome and upon MG132 treatment autophagy seems to be activated (Results 3.3.1.), it

is likely that the autophagy-lysosome pathway would be the main responsible for such effects. With this purpose, rapamycin was added to the list of compounds, as it is a known inducer of autophagy [226], and the time-points of one day before (-1DAS), the day of the seeding (0DAS) and three days after seeding (3DAS) were chosen intending to early activate autophagy (-1DAS and 0DAS) and to sustain and/or further enhance autophagy activation (3DAS) considering that in our model autophagy's highest activation levels were seen in the day 3 after seeding (Results 3.2.4.; Figures 32; 33a and 33b). To this end, neurons were transduced with AAV6hTauP301L MOI 100 on 1DIV (Material and Methods 2.2.) and K18P301L 12.5nM seeded on the 3DIV (Material and Methods 2.5.). Treatments with rapamycin, MG132, lactacystin and DMSO (negative control) took place on the -1DAS, 0DAS and 3DAS or in the same corresponding days *in vitro* (2DIV, 3DIV and 6DIV) in neurons not seeded to assess soluble hTauP301L levels (Material and Methods 2.13.). Cellular lyses were performed on the 7DAS (10DIV) with posterior alphaLISA (Material and Methods 2.8.) quantification and ELISA measurements (Material and Methods 2.9.). ELISA was performed to normalize the alphaLISA data against possible technical variations and/or neuronal loss. See figure 39 for a graphic overview of the experiment.

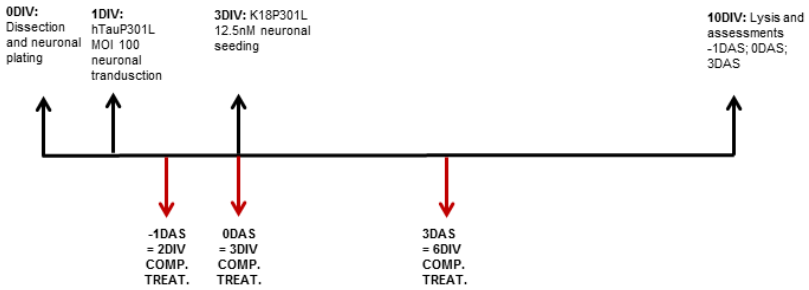

Figure 39: Graphic overview of the experiments. DIV= day *in vitro;* DAS= day after seeding

3.3.3.1 Lactacystin treatments on the day before seeding (-1DAS) and on the day of seeding (0DAS) and on the day 3 after seeding (3DAS) do not affect hTauP301L levels in primary neurons

Primary neurons were transduced with AAV6hTauP301L MOI 100 on 1DIV (Material and Methods 2.2.) and K18P301L 12.5nM seeded on the 3DIV (Material and Methods 2.5.). Treatment with lactacystin with the final concentrations of 1µM, 0,1µM, 0,01µM, 0,001µM and 0,0001µM and DMSO at 1µL/mL (negative control) took place on the 0DAS (on the corresponding 3DIV for neurons overexpressing hTauP301L but not K18P301L seeded; Material and Methods 2.13.). Cellular lyses were performed on the 7DAS (10DIV) with posterior alphaLISA (Material and Methods 2.8.), and ELISA measurements (Material and Methods 2.9.). ELISA was performed to normalize the alphaLISA data against possible technical variations and/or neuronal loss - see Figure 39 for a graphic overview of the experiment. The statistical analyses were performed using a one-way ANOVA followed by Dunnett's *post-hoc* multi-comparisons. P values were considered statistically significant when <0.05

Observing the results of the lactacystin neuronal treatment on the -1DAS and on the 0DAS, no statistical differences can be seen between the neurons treated with the drug and the DMSO treatment for any of the lactacystin's contcentrations tested. Despite that, soluble HT7/hTau10 alphaLISA (Material and

Methods 2.8.) quantification for the treatments with lactacystin on the 3DAS in the concentrations of 0,1µM and 0,01µM display an average of 25% statistically significant reductions in hTauP301L soluble signals (neurons overexpressing hTauP301L and not seeded with K18P301L) when compared to the negative control (DMSO treatment; Dunnett's *post-hoc* adjusted p values of 0,0302 for both treatment concentration; alpha=0,05; Material and Methods 2.14.; Figure 40g). Additionally, when observing the quantification of hTauP301L aggregates from the same time-point treatment, lactacystin samples of 0,01 and 0,0001uM display statistical reduced levels with Dunnett's *post-hoc* adjusted p values of 0,0201 and 0,0158 respectively; alpha=0,05 (Material and Methods 2.14.; Figure 40i). However, such signal reductions are not translated to the total hTauP301L levels, they are not highly statistically significant, they do not display any dose response and they are seen in medium to low molar concentrations of the compound (not the highest). Therefore, it is very likely that such reductions are mere assay and/or random biological variations.

Therefore, lactacystin neuronal treatments fail to induce any effect on soluble, total and aggregated hTauP301L signal levels when in comparison to the negative DMSO treated control for any of the treatment time-points when quantified by alphaLISA (Figure 40 a, b, c, d, e, f, g, h and i: Material and Methods 2.8.).

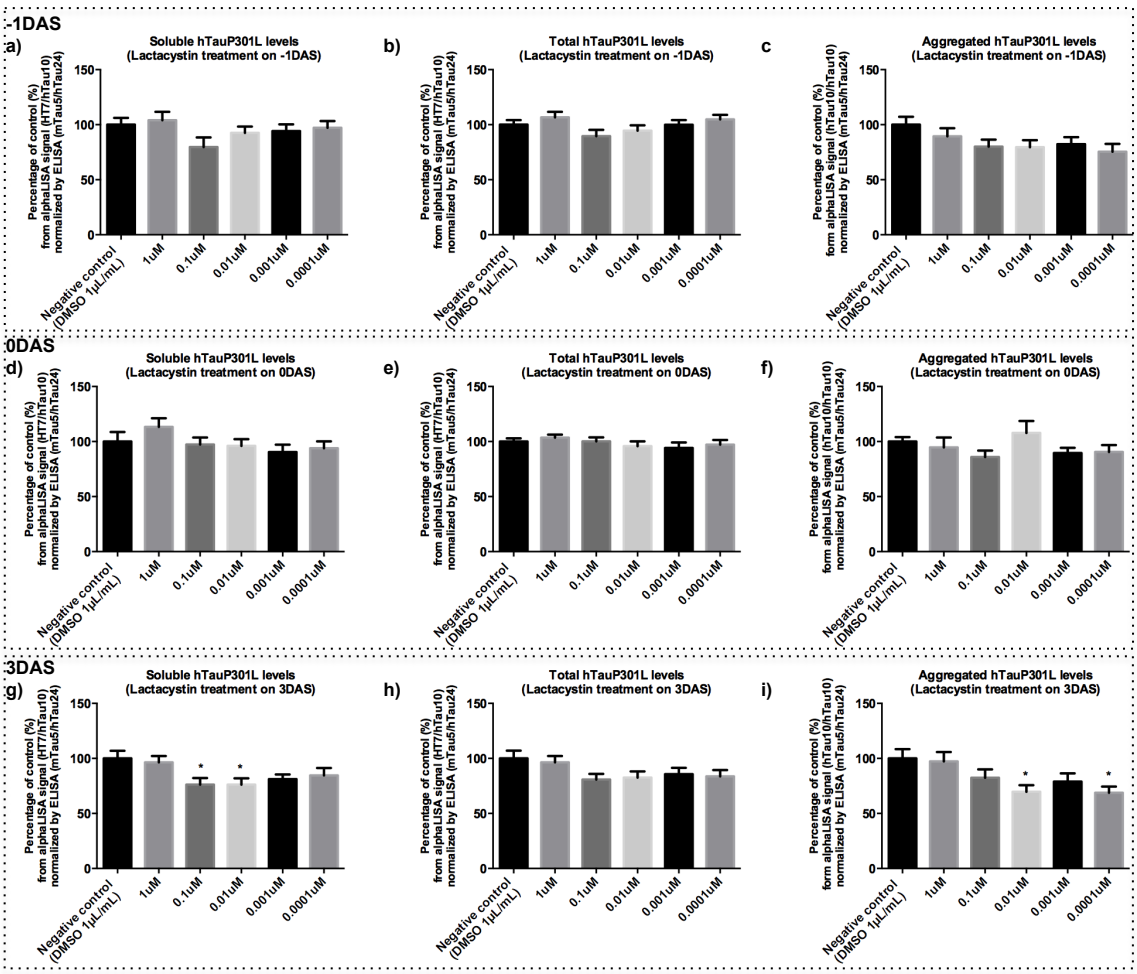

Figure 40: Effect of lactacystin treatment on -1DAS, 0DAS and 3DAS in soluble, total and aggregated hTauP301L levels in primary neurons. Rat cortical primary neurons were transduced with AAV6hTauP301L MOI100 on the 1DIV and seeded with 12.5nM of

↵**Figure 40 (continuation):** K18P301L on the 3DIV/0DAS. Lactacystin treatment (1μM; 0.1μM; 0.01μM; 0.001μM; 0.0001μM) took place on the -1DAS (2DIV), on 0DAS (3DIV) and on the 3DAS (6DIV). Cellular lyses were done on the 7DAS (10DIV) with posterior alphaLISA and ELISA quantifications (Material and Methods 2.8. and 2.9.). ELISA data was used to normalize the alphaLISA data against possible technical and/or biological variation. Soluble hTauP301L: HT7/hTau10 alphaLISA quantification of primary neurons overexpressing hTauP301L and not seeded with K18P301L. Total hTauP301L: HT7/hTau10 alphaLISA quantification of primary neurons overexpressing hTauP301L and seeded with K18P301L (both soluble and aggregated hTauP301L are present on the sample). Aggregated hTauP301L: hTau10/hTau10 alphaLISA quantification (see Material and Methods 2.8. for alphaLISA description). a) Comparison between soluble hTauP301L levels of primary neurons overexpressing hTauP301L treated or not with the compound on the -1DAS; b) Comparison between total hTauP301L levels of primary neurons seeded with K18P301L and treated or not with the compound on the -1DAS c) Comparison between aggregated hTauP301L levels of primary neurons overexpressing hTauP301L and seeded with K18P301L, treated or not with the compound on the -1DAS d) Comparison between soluble hTauP301L levels of primary neurons overexpressing hTauP301L treated or not with the compound on the 0DAS; e) Comparison between total hTauP301L levels of primary neurons seeded with K18P301L and treated or not with the compound on the 0DAS f) Comparison between aggregated hTauP301L levels of primary neurons overexpressing hTauP301L and seeded with K18P301L, treated or not with the compound on the 0DAS; g) Comparison between soluble hTauP301L levels of primary neurons overexpressing hTauP301L treated or not with the compound on the 3DAS; h) Comparison between total hTauP301L levels of primary neurons seeded with K18P301L and treated or not with the compound on the 3DAS i) Comparison between aggregated hTauP301L levels of primary neurons overexpressing hTauP301L and seeded with K18P301L, treated or not with the compound on the 3DAS Data is presented as ± SEM. N=2 and n=8 per condition/per experiment. Statistical analyses of the results were performed by a two-way ANOVA followed by Dunnett's *post-hoc* comparisons with an alpha set to 0.05.

3.3.3.2 MG132 treatment on the day before seeding (-1DAS), on the day of the seeding (0DAS) and on the day 3 after seeding (3DAS) do not affect hTauP301L levels in primary neurons

Primary neurons were transduced with AAV6hTauP301L MOI 100 on 1DIV (Material and Methods 2.2.) and K18P301L 12.5nM seeded on the 3DIV (Material and Methods 2.5.). Treatment with MG132 with the final concentrations of 50nM, 25nM and DMSO at 1μL/mL (negative control) took place on the 0DAS (on the corresponding 3DIV for neurons overexpressing hTauP301L but not K18P301L seeded; Material and Methods 2.13.). Cellular lyses were performed on the 7DAS (10DIV) with posterior alphaLISA (Material and Methods 2.8.) and ELISA measurements (Material and Methods 2.9.). ELISA was performed to normalize the alphaLISA data against possible technical variations and/or neuronal loss - see Figure 39 for a graphic overview of the experiment. The statistical analyses were performed using a one-way ANOVA followed by Dunnett's *post-hoc* multi-comparisons. P values were considered statistically significant when <0.05

Observing the results of the MG132 neuronal treatment on the -1DAS, 0DAS and 3DAS, statistical differences could only be seen in the total hTauP301L levels on the -1DAS MG132 treatment for the concentrations 50nM; 25nM; 10nM and 1nM and for the 25nM MG132 concentration treatment on the aggregation levels of the MG132 0DAS treatment. Hence, when examining the HT7/hTau10 alphaLISA (Material and Methods 2.8.) signals that were quantified when neurons overexpressing hTauP301L were treated with MG132 on the -1DAS in aggregative conditions – i.e.: neurons overexpressing hTauP301L and seeded with K18P301L - (total hTauP301L HT7/hTau10 alphaLISA; Material and Methods 2.8.) the means of the treatments with 50nM, 25nM, 10nM and 1nM of MG132 show statistical significance as it can be seen in the Figure 41b. In such conditions, total hTauP301L signal levels were similar and showed an average of 40% less signal than the vehicle treated neurons - negative control (Dunnett's *post-hoc* adjusted p values of 0,0032; 0,0071; 0,0038 and 0,0149 respectively for 50nM, 25nM, 10nM and 1nM; alpha=0,05; Material and Methods 2.14.). Despite that, as already mentioned, the same results are not shared by the soluble HT7/hTau10 and aggregated hTau10/hTau10 alphaLISA (Material and Methods 2.8.) quantifications. Importantly, one could expect that soluble and/or aggregated hTauP301L reductions could be translated in reductions in total HT7/hTau10 alphaLISA (Material and Methods 2.8.); however, total hTauP301L reductions alone strongly suggests that such panorama is a technical variation and not a real effect. On the aggregated hTau10/hTau10 alphaLISA (Material and Methods 2.8.) performed with samples of the 0DAS, the 25nM MG132 treatment sample display increased hTauP301L signal levels (Figure 40f; Dunnett's

adjusted p value =0.0438; alpha=0.05; Material and Methods 2.14.). Nonetheless, as this result is only seen in a single concentration that is not the highest and is not shared on the total hTauP301L levels it strongly suggests that such discrepancy is a technical artefact.

Therefore, MG132 neuronal treatments fail to induce any effect on soluble, total and aggregated hTauP301L signal levels when in comparison to the negative DMSO treated control for any of the treatment time-points (Figure 41 a, b, c, d, e, f, g, h and i).

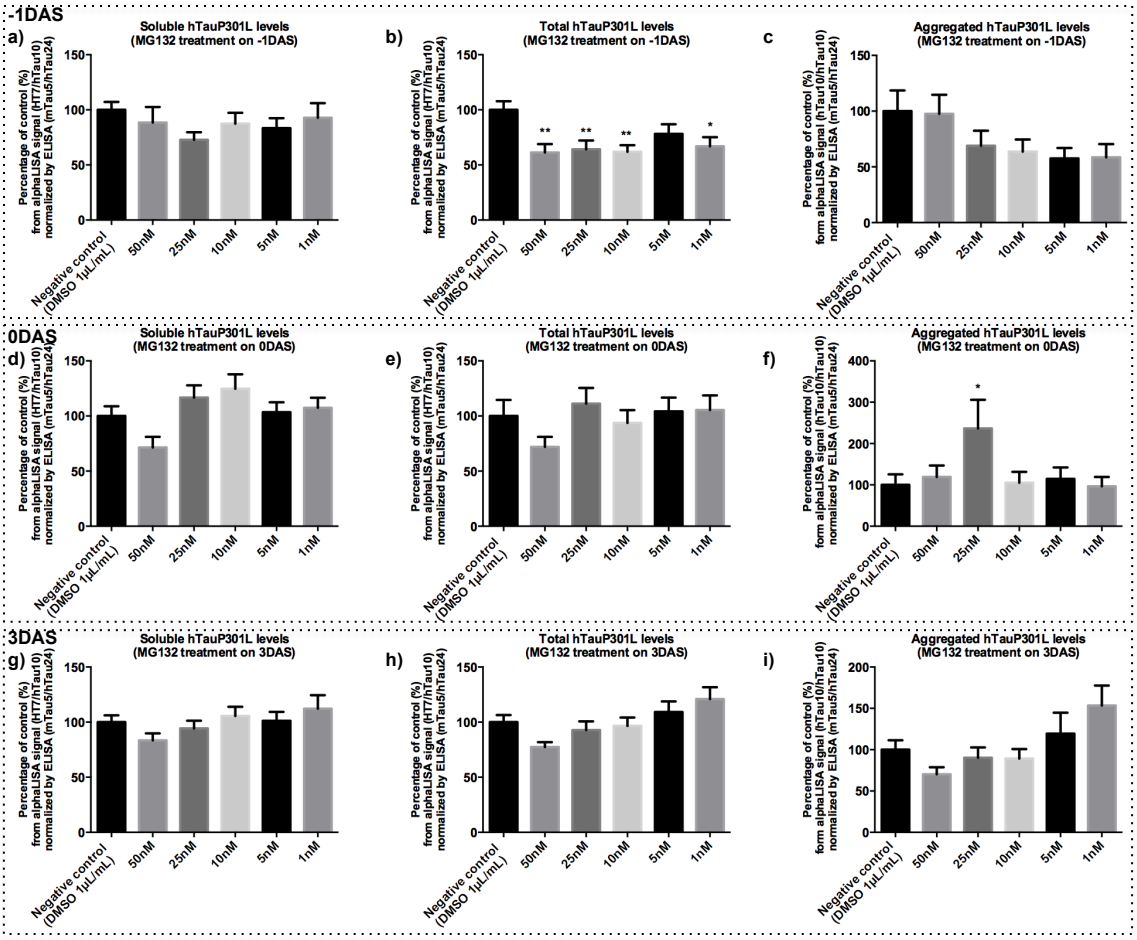

Figure 41: Effect of MG132 treatment on -1DAS, 0DAS and 3DAS in soluble, total and aggregated hTauP301L levels in primary neurons. Rat cortical primary neurons were transduced with AAV6hTauP301L MOI100 on the 1DIV and seeded with 12.5nM of K18P301L on the 3DIV/0DAS. MG132 treatment (50nM; 25nM; 10nM; 5nMM; 1nM) took place on the -1DAS (2DIV), on 0DAS (3DIV) and on the 3DAS (6DIV). Cellular lyses were done on the 7DAS (10DIV) with posterior alphaLISA and ELISA quantifications (Material and Methods 2.8. and 2.9.). ELISA data was used to normalize the alphaLISA data against possible technical and/or biological variation. Soluble hTauP301L: HT7/hTau10 alphaLISA quantification of primary neurons overexpressing hTauP301L and not seeded with K18P301L. Total hTauP301L: HT7/hTau10 alphaLISA quantification of primary neurons overexpressing hTauP301L and seeded with K18P301L (both soluble and aggregated hTauP301L are present on the sample). Aggregated hTauP301L: hTau10/hTau10 alphaLISA quantification (see Material and Methods 2.8. for alphaLISA description). a) Comparison between soluble hTauP301L levels of primary neurons overexpressing hTauP301L treated or not with the compound on the -1DAS; b) Comparison between total hTauP301L levels of primary neurons seeded with K18P301L and treated or not with the compound on the -1DAS c) Comparison between aggregated hTauP301L levels of primary neurons overexpressing hTauP301L and seeded with K18P301L, treated or not with the compound on the -1DAS d) Comparison between soluble hTauP301L levels of primary neurons overexpressing hTauP301L treated or not with the compound on the 0DAS; e) Comparison between total hTauP301L levels of primary neurons seeded with K18P301L and treated or not with the compound on the 0DAS f) Comparison between aggregated hTauP301L levels of primary neurons overexpressing hTauP301L and seeded with K18P301L, treated or not with the compound on the 0DAS; g) Comparison between soluble hTauP301L levels of primary neurons overexpressing hTauP301L treated or not with the compound on the 3DAS; h) Comparison between total hTauP301L levels of primary neurons seeded with K18P301L and treated or not with the compound on the 3DAS i) Comparison between aggregated hTauP301L levels of primary neurons overexpressing hTauP301L and seeded with K18P301L, treated or not with the compound on the 3DAS Data is presented as ± SEM. N=2 and n=8 per condition/per experiment. Statistical analyses of the results were performed by a two-way ANOVA followed by Dunnett's *post-hoc* comparisons with an alpha set to 0.05.

3.3.3.3 Rapamycin treatment on the day 1 before seeding (-1DAS) reduces the levels of soluble, total and aggregated hTauP301L. Drug treatment on the day of the seeding (0DAS) and on the day 3 after seeding (3DAS) do not affect hTauP301L levels in primary neurons

Primary neurons were transduced with AAV6hTauP301L MOI 100 on 1DIV (Material and Methods 2.2.) and K18P301L 12.5nM seeded on the 3DIV (Material and Methods 2.5.). Treatment with rapamycin with the final concentrations of 1μM, 0,1μM, 0,01μM, 0,001μM and 0,0001μM and DMSO at 1μL/mL (negative control) took place on the -1DAS (on the 2DIV for neurons overexpressing hTauP301L but not K18P301L seeded; Material and Methods 2.13.). Cellular lyses were performed on the 7DAS (10DIV) with posterior alphaLISA (Material and Methods 2.8.), and ELISA measurements (Material and Methods 2.9.). ELISA was performed to normalize the alphaLISA data against possible technical variations and/or neuronal loss - see Figure 39 for a graphic overview of the experiment. The statistical analyses were performed using a one-way ANOVA followed by Dunnett's *post-hoc* multi-comparisons. P values were considered statistically significant when <0.05.

Strikingly, treatment of rat cortical primary neurons with rapamycin on the -1DAS rendered significant reductions in soluble, total and aggregates hTauP301L levels measured by alphaLISA (Material and Methods 2.8.). As it can be observed in the Figure 42a, soluble hTauP301L levels (HT7/hTau10 alphaLISA in neurons overexpressing hTauP301L and not seeded with K18P301L; Material and Methods 2.8.) are significantly reduced upon treatment with rapamycin (1μM to 0.001μM) in comparison to the vehicle treated cultures. 1μM, 0.1μM, 0,01μM and 0,001μM of rapamycin neuronal treatment resulted in similar levels of reduction of the signal – in average 25% less than the control – with Dunnett's *post-hoc* adjusted p values of 0,0431; 0,0360; 0,0046 and 0,0196 respectively for an alpha of 0.05 (Material and Methods 2.14.).

When quantifying total hTauP301L levels (HT7/hTau10 alphaLISA; Material and Methods 2.8.) in neurons treated with rapamycin on the -1DAS, in accordance to the soluble data described above and emphasizing the link between soluble and total hTauP301L levels there were significant signal reductions, although with stronger adjusted p values (Figure 42b). 1uM, 0.1uM and 0,01uM showed similar levels of reduction of the signal – in average 30% less than the control – with Dunnett's *post-hoc* adjusted p values of 0,0003; 0,0011 and 0,0001 respectively for an alpha of 0,05 (Material and Methods 2.14.). Rapamycin treatment with 0,001uM rendered less but still significant reduction reaching 79% of the control signal levels – Dunnett's *post-hoc* adjusted p value of 0,0207, alpha=0,05 (Figure 42b; Material and Methods 2.14.).

Importantly, the aforementioned results are translated to the hTau10/hTau10 alphaLISA (Material and Methods 2.8.) signal levels from the -1DAS rapamycin neuronal treatment. In such case there are similar reduction signal levels for the treatments with the concentrations 1uM, 0,1uM, 0,001uM and 0,0001uM – in average 50% less than the control culture (DMSO treated) – with Dunnett's *post-hoc* adjusted p values <0.0001 for the three first mentioned conditions and 0,0004 for the 0,0001uM condition (alpha=0,05; Material and Methods 2.14.; Figure 42c). For the rapamycin treatment with 0,01uM there is a slightly higher reduction in the aggregates signals observed – reaching 35% of the control levels with a Dunnett's *post-hoc* adjusted p value <0,0001 for an alpha of 0,05 (Materiala and Methods 2.14.; Figure 42c). Reduction in aggregated hTauP301L

levels could be expected as the aggregative substrate soluble hTauP301L is substantially reduced (Figure 42 a and b), which then would render in less aggregates build-up. However, one cannot exclude the possibility that aggregates are also being cleared and hence summing up to the effect of less soluble substrate could in turn result in significant reductions on the hTauP301L aggregates levels.

Remarkably, when comparing to the above described data, rapamycin treatment executed on the day of the seeding (0DAS) do not result in any effect on hTauP301L levels when compared to neurons treated with DMSO. (Figure 42 d, e, and f).

Treatment of neurons with rapamycin (1uM, 0,1uM and 0,01uM) on 3DAS display reductions in hTauP301L total levels (HT7/hTau10 alphaLISA of neurons overexpressing hTauP301L and seeded with K18P301L; Material and Methods 2.8.) when comparing to the negative control (DMSO treated neurons) – Dunnett's *post-hoc* adjusted p values of 0,0064; 0,0025 and 0,0081 respectively; alpha=0,05 (Figure 42h; Material and Methods 2.14.). These reductions were in average -30% when comparing to the vehicle treated neurons (Figure 42h). Soluble and aggregated Tau measured by HT7/hTau10 and hTau10/hTau10 alphaLISAs (Material and Methods 2.8.), respectively, were not reduced (Figures 42 g and i). Importantly, one could expect that soluble and/or aggregated hTauP301L reductions could be translated in reductions in total HT7/hTau10 alphaLISA (Material and Methods 2.8.), however total hTauP301L reductions alone strongly suggests that such panorama is not a real effect, but likely a random biological variation.

Summarizing the pharmacological data described above, one can conclude that lactacystin treatment on the 4DAS and MG132 treatment on 4DAS and 7DAS results in reduction of soluble hTauP301L levels. Additionally, treatment of neurons with rapamycin on -1DAS results in reduction of soluble and aggregated hTauP301L levels. Thus, such data strongly suggests a role of autophagy in clearing soluble hTauP301L in primary neurons *in vitro* and indicates that UPS is not the main degradative pathway of hTauP301L in this model (as no hTauP301L accumulation was seen upon UPS inhibition for any of the conditions and time-points).

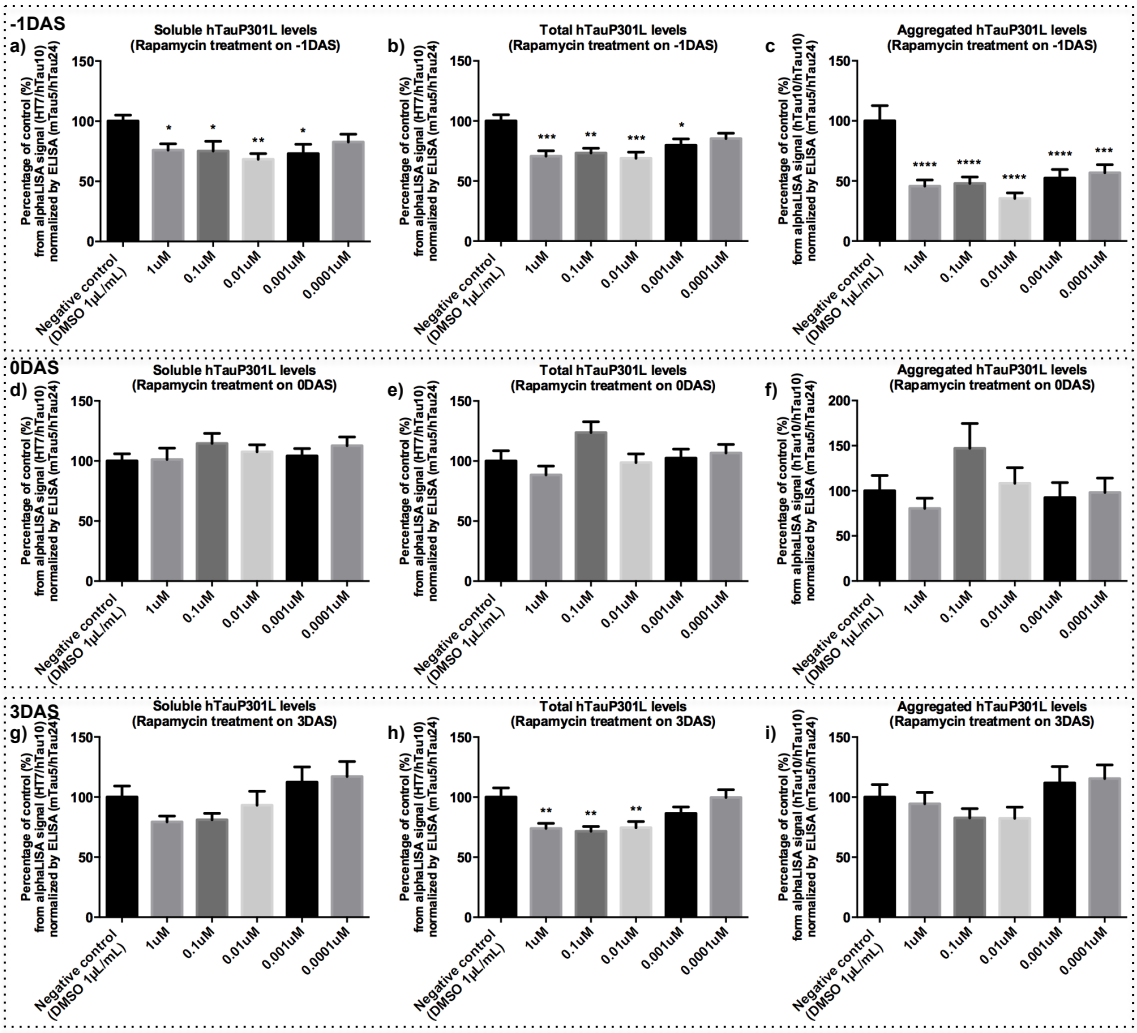

Figure 42: Effect of Rapamycin treatment on -1DAS, 0DAS and 3DAS in soluble, total and aggregated hTauP301L levels in primary neurons. Rat cortical primary neurons were transduced with AAV6hTauP301L MOI100 on the 1DIV and seeded with 12.5nM of K18P301L on the 3DIV/0DAS. Rapamycin treatment (1µM; 0.1µM; 0.01µM; 0.001µM; 0.0001µM) took place on the -1DAS (2DIV), on 0DAS (3DIV) and on the 3DAS (6DIV). Cellular lyses were done on the 7DAS (10DIV) with posterior alphaLISA and ELISA quantifications (Material and Methods 2.8. and 2.9.). ELISA data was used to normalize the alphaLISA data against possible technical and/or biological variation. Soluble hTauP301L: HT7/hTau10 alphaLISA quantification of primary neurons overexpressing hTauP301L and not seeded with K18P301L. Total hTauP301L: HT7/hTau10 alphaLISA quantification of primary neurons overexpressing hTauP301L and seeded with K18P301L (both soluble and aggregated hTauP301L are present on the sample). Aggregated hTauP301L: hTau10/hTau10 alphaLISA quantification (see Material and Methods 2.8. for alphaLISA description). a) Comparison between soluble hTauP301L levels of primary neurons overexpressing hTauP301L treated or not with the compound on the -1DAS; b) Comparison between total hTauP301L levels of primary neurons seeded with K18P301L and treated or not with the compound on the -1DAS c) Comparison between aggregated hTauP301L levels of primary neurons overexpressing hTauP301L and seeded with K18P301L, treated or not with the compound on the -1DAS d) Comparison between soluble hTauP301L levels of primary neurons overexpressing hTauP301L treated or not with the compound on the 0DAS; e) Comparison between total hTauP301L levels of primary neurons seeded with K18P301L and treated or not with the compound on the 0DAS f) Comparison between aggregated hTauP301L levels of primary neurons overexpressing hTauP301L and seeded with K18P301L, treated or not with the compound on the 0DAS; g) Comparison between soluble hTauP301L levels of primary neurons overexpressing hTauP301L treated or not with the compound on the 3DAS; h) Comparison between total hTauP301L levels of primary neurons seeded with K18P301L and treated or not with the compound on the 3DAS i) Comparison between aggregated hTauP301L levels of primary neurons overexpressing hTauP301L and seeded with K18P301L, treated or not with the compound on the 3DAS Data is presented as ± SEM. N=2 and n=8 per condition/per experiment. Statistical analyses of the results were performed by a two-way ANOVA followed by Dunnett's *post-hoc* comparisons with an alpha set to 0.05.

3.4 Validation of the deubiquitinating enzymes OTUB1, USP5 and USP7 as targets to manipulate hTauP301L levels in primary neurons

A microarray exercise in which primary neurons overexpressing hTauP301L were compared to neurons overexpressing and aggregating hTauP301L identified genes which expression was altered due to Tau seeding. Genes related to the ubiquitin proteasome system (UPS) and autophagy, the mechanisms known to be involved in clearance of misfolded proteins were affected (data not shown). Moreover, previous experiments from the host laboratory identified that deubiquitinating enzymes (DUBs) interact with Tau in mouse brain [11]. Within those, the DUBs: OTUB1, USP5 and USP7 stood out as possible targets to manipulate and in this way affect levels of aggregated Tau. In light of such data, a strategy to downregulate such protein levels by the delivery of lentiviral shRNAs against each of the targets was developed. A set of lentiviruses that encode shRNAs for each of the target, with different but target-specific sequences, was used (Table 1) in order to certain the role of these DUBs in human Tau aggregating *in vitro*. Primary neurons were isolated from brains of PS19hTauP301S mice embryos [113] (Material and Methods 2.1.) rendering in 50 % of the neurons overexpressing hTauP301S. The expression level of hTauP301S is equal in all neurons carrying the transgene. Transductions of neurons with lentiviruses (MOI 100 for shRNAs targeting OTUB1, USP5 and USP7 and MOI 200 for shRNA targeting hTau) were performed on day 2 *in vitro* (2DIV; Material and Methods 2.3.) and K18P301L seeding (12.5nM) on day 4 *in vitro* (4DIV/0DAS; Material and Methods 2.5.). The time of exposure to shRNAs was decided in this way to allow the efficient integration of the shRNA to the genome resulting in the knockdown of the gene of interest while the level of aggregated hTauP301S was still low making its clearance more feasible if occurring. Cellular lyses were performed 7 days after seeding (7DAS/11DIV). Besides the negative control (not transduced with lentiviruses and not K18P301L seeded neurons) and the positive control (neurons transduced with lentiviruses delivering shRNAs against hTau and seeded with K18P301L), non-targeting shRNAs controls were used to exclude a possible non-specific effects on hTauP301S expression and aggregation (Table 1). Indeed, as it can be seen in the quantifications (Figure 44), the non-targeting hTau shRNAs controls affected levels of hTauP301S. Consequently, statistical comparisons were made considering the non-targeting shRNAs as the negative controls. In cases where two non-targeting sequences were used, an average of those was used as the reference.

3.4.1 Two out of five OTUB1-targeting shRNAs are able to induce reduction of hTauP301S soluble levels

Transduction of primary neurons of PS19hTauP301S mice with lentiviruses (MOI 100 for shRNAs targeting OTUB1 and non-targeting sequences; and MOI 200 for shRNA targeting hTau) was performed on day 2 in vitro (2DIV; Material and Methods 2.3.) and K18P301L seeding (12.5nM) on day 4 in vitro (4DIV/0DAS; Material and Methods 2.5.). Cellular lysis was performed 7 days after seeding (7DAS/11DIV) with posterior alphaLISA and ELISA measurements (Material and Methods 2.8. and 2.9.). ELISA was performed to normalize the alphaLISA data against possible technical variations and/or neuronal loss - see Figure 43 for a graphic overview of the experiment. The statistical analyses were performed using a one-way

ANOVA followed by Dunnett's *pos-hoc* comparisons. P values were considered statistically significant when<0.05.

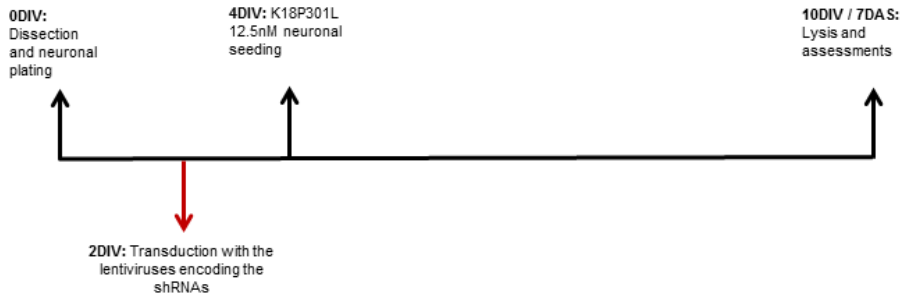

Figure 43: Graphic overview of the experiments from Results 3.4.

Two out of five OTUB1-targeting shRNAs were able to induce statistical relevant differences in hTauP301S levels (Figure 44). Precisely OTUB1 shRNA #2 (Table 1) rendered 28% of reduction in the soluble hTauP301S signal and 27% of reduction in the total hTauP301S signal (primary neurons seeded with K18P301L fibrils) – Dunnett's *post-hoc* adjusted p values of 0,0002 and <0,0001, respectively; alpha=0,05 (Figure 44 a and b; Material and Methods 2.14.). Such results were reflected to the hTauP301S aggregates levels (hTau10/hTau10 alphaLISA; Material and Methods 2.8.), where a 50% signal reduction could be observed – Dunnett's *post-hoc* adjusted p value of 0,0002; alpha=0,05 (Figure 44c; Material and Methods 2.14.). These data again emphasize the link between soluble and aggregated hTau levels. OTUB1 shRNA #4 also showed a 30% reduction in the HT7/hTau10 soluble alphaLISA (Material and Methods 2.8.) signals which was reflected to a 40% decrease in the total quantification (Figures 44 d and e; Dunnett's *post-hoc* adjusted p values of <0,0001 for the two quantifications; alpha=0,05; Material and Methods 2.14.), however, such panorama was not transposed to the hTau10/hTau10 alphaLISA (Material and Methods 2.8.) signals that showed no statistical differences to the averaged aggregated hTauP30S levels measured upon treatment with non-targeting shRNAs (Figure 44f). OTUB1 shRNAs #1, #3 and #5 (Table 1), failed to induce any statistical relevant effect on hTauP301S soluble, total and aggregated levels when compared to the averaged hTauP301S levels measured upon treatment with non-targeting shRNAs (Figures 44 a, b, c, d, e and f). Importantly, it can be also observed that the assay was working properly as the transduction of the primary neurons with the lentivirus delivering the shRNA targeting hTau (shRNA #976; Table1) resulted in highly significant soluble, total and aggregated hTauP301S levels reductions as follows: Figure44a (soluble hTauP301S) – -90%; Figure44b (total hTauP301S) - -94%; Figure 44c (aggregated hTauP301S) - -84.5%; Figure 44d (soluble hTauP301S) - -91.3%; Figure 44e (total hTauP301S) - -93.25% and Figure44f (aggregated hTauP301S)- -81.45% (Dunnett's adjusted p values <0.0001 for all cases; alpha=0.05; Material and Methods 2.14.; Figures 44 a, b, c, d, e and f).

In summary, considering that the overall phenotype displayed by treatments with different shRNAs targeting OTUB1 pointed-out to no significant reductions on hTauP301S levels, it is likely that the positive results displayed are shRNA off-target effects on hTauP301S. As a consequence one cannot conclude that the downregulation of OTUB1 has any specific effects on hTauP301S levels.

3.4.2 One out of three USP5-targeting shRNA is able to induce reduction of hTauP301S soluble, total and aggregates signal levels

Transductions of primary neurons of PS19hTauP301S mice with lentiviruses (MOI 100 for shRNAs targeting USP5 and non-targeting sequences; and MOI 200 for shRNA targeting hTau) were performed on day 2 in vitro (2DIV; Material and Methods 2.3.) and seeding with K18P301L (12.5nM) on day 4 in vitro (4DIV/0DAS; Material and Methods 2.5.). Cellular lysis was performed 7 days after seeding (7DAS/11DIV) with posterior alphaLISA and ELISA measurements (Material and Methods 2.8. and 2.9.). ELISA was performed to normalize the alphaLISA data against possible technical variations and/or neuronal loss - see Figure 43 for a graphic overview of the experiment. The statistical analyses were performed using a one-way ANOVA followed by Dunnett's *pos-hoc* comparisons. P values were considered statistically significant when<0.05.

USP5 shRNA #2 neuronal delivery to PS19hTauP301S primary neurons resulted in significant reductions of hTauP301S levels – Figure 44 g, h and i. In such condition, soluble and total hTauP301S signal levels were reduced in 25%, results that were translated into a 55% reduction in the aggregation signal levels for the studied protein – Dunntt's *post-hoc* adjusted p values <0,0001 for all cases; alpha=0,05 (Material and Methods 2.14.; Figures 44 g, h and i). When analysing the other two USP5-targeting shRNA conditions, only USP5 shRNA #3 affected the level of total hTauP301S and an increase of 15% was observed (Figure 44h; Dunntt's *post-hoc* adjusted p value of 0,0229; alpha=0,05; Material and Methods 2.14.). However, such data was not reflected either on levels of soluble or on aggregate hTauP301L. Possible reasons for such discrepancy is that the p value of such analysis is only borderline significant and hence a variation within this sample could have rendered a random significant status for it. Additionally, when comparing the HT7/hTau10 and hTau10/hTau10 alphaLISAs (Material and Methods 2.8.) due to the different antibody configuration to close the sandwich this might result in differential resolution of hTau detection, which is likely accounting for such differences. When looking at the results for the treatment with USP5 shRNA #1, no statistical significance were observed regarding hTauP301S soluble, total and aggregated signals when comparing to the averaged levels of hTauP301S in neurons treated with non-targeting shRNAs controls (Figures 44 g, h and i). Of note is that the assay was working properly as the transduction of the primary neurons with the lentivirus delivering the shRNA targeting hTau (shRNA #976) resulted in highly significant soluble, total and aggregated hTauP301S levels reductions as follows: Figure 44d (soluble hTauP301S) - -91.3%; Figure 44e (total hTauP301S) - -93.25%; Figure 44f (aggregated hTauP301S)- -81.45%; Figure 44g (soluble hTauP301S) - -89.9%; Figure 44h (total hTauP301S) - -91% and Figure 44i (aggregated hTauP301S) - -81% (Dunnett's adjusted p values <0.0001 for all cases; alpha=0.05; Material and Methods 2.14.; Figures 44 d, e, f, g, h and i).

3.4.3 Two out of two USP7-targeting shRNA are able to induce an increase in hTauP301S aggregated hTauP301S levels

Transductions of primary neurons of PS19hTauP301S mice with lentiviruses (MOI 100 for shRNAs targeting USP7 and non-targeting sequences, and MOI 200 for shRNA targeting hTau) were performed on

day 2 in vitro (2DIV; Material and Methods 2.3.) and seeding with K18P301L (12.5nM) on day 4 in vitro (4DIV/0DAS; Material and Methods 2.5.). Cellular lysis was performed 7 days after seeding (7DAS/11DIV) with posterior alphaLISA and ELISA measurements (Material and Methods 2.8. and 2.9.). ELISA was performed to normalize the alphaLISA data against possible technical variations and/or neuronal loss - see Figure 43 for a graphic overview of the experiment. The statistical analyses were performed using a one-way ANOVA followed by Dunnett's *pos-hoc* comparisons. P values were considered statistically significant when<0.05.

In contrast to the above results, transduction with lentivirus encoding shRNAs targeting USP7 resulted in increased levels of aggregated hTauP301S measured by hTau10/hTAU10 Alpha LISA (Material and Methods 2.8.). USP7 shRNA #1 treated neurons, although not displaying any significant differences in the soluble and total signal levels of hTauP301S, show statistical significant difference when considering the aggregation signals. Indeed, it shows a 50% increase when compared to the non-targeting control (Figure 44l) – Dunnett's *post-hoc* adjusted p value of <0,0001; alpha=0,05 (Material and Methods 2.14.). Similar results were displayed when inspecting the effects of USP7 shRNA #2. In such condition, again there is no significant differences when quantifying the soluble hTauP301S signal levels, however signals for total and aggregated alphaLISAs (Material and Methods 2.8.) are significantly increased (Figure 44k and l) – 35% (Dunnett's *post-hoc* adjusted p value= <0,0001; alpha=0,05; Material and Methods 2.14.) and 32% (Dunnett's *post-hoc* adjusted p value= 0,0004; alpha=0,05; Material and Methods 2.14.) respectively. Such result again highlights the link between hTauP301S aggregated levels and total levels when assayed in such paradigm. Of note is that the assay was working properly as the transduction of the primary neurons with the lentivirus delivering the shRNA targeting hTau (shRNA #976) resulted in significant soluble, total and aggregated hTauP301S levels reductions as follows: Figure 44j (soluble hTauP301S) - -90.35%; Figure 44k (total hTauP301S) - -81.9% and Figure 44l (aggregated hTauP301S) - -59.6% (Dunnett's adjusted p values <0.0001 for soluble and total levels and p =0.031 for aggregated levels; alpha=0.05; Material and Methods 2.14.; Figures 44 j, k and l).

It is important to highlight that USP5 and USP7 shRNAs downregulation potency were previously verified in mouse neuronal cell line N2a (data not shown). Additionally, although shRNAs are engineered targeting specific sequences of the chosen genes, such shRNAs may still target an average other 5 genes (information based on BLAST searches). This way, considering that the overall phenotype displayed by treatments with different shRNAs targeting OTUB1 and USP5 pointed-out to no significant reductions on hTauP301S levels, it is likely that the positive results displayed are shRNA off-target effects on hTauP301S. As a consequence one cannot conclude that the downregulation of OTUB1 and USP5 has any specific effects on hTauP301S levels. When considering USP7 downregulation, although only two shRNA were used, their treatment displayed similar hTauP301S phenotypes, which suggests a possible involvement of this DUB in Tau aggregation. However, it is important to highlight that such downregulations were only performed once and hence they should be repeated to confirm the aforementioned results. It would be important then to include more shRNAs against each of the targets to assure the validity and specificity of results.

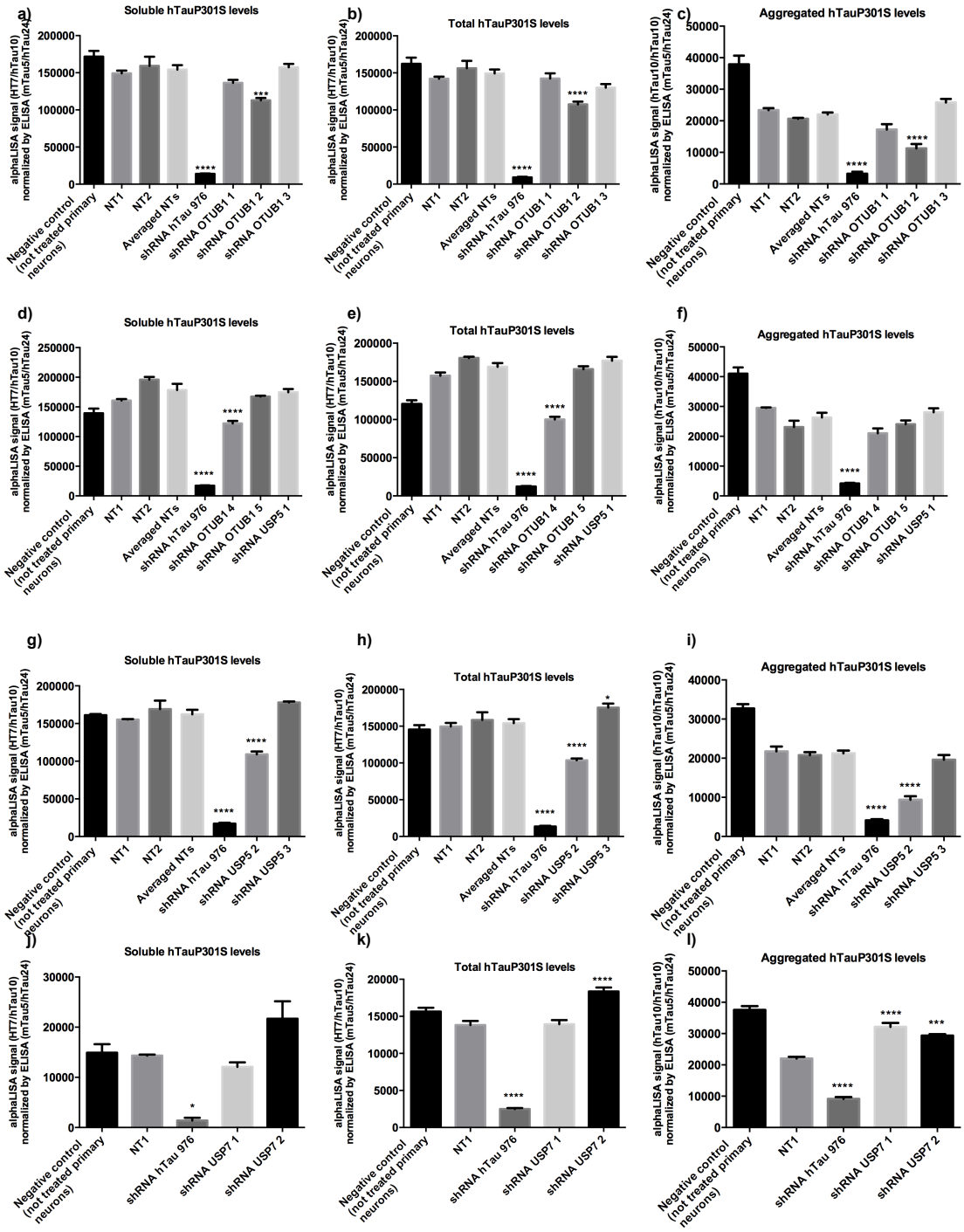

Figure 44: Effect of the knockdown of OTUB1, USP5 and USP7 on soluble, total and aggregated hTauP301S levels in primary neurons. PS19hTauP301S mice cortical primary neurons were transduced with the lentiviruses encoding the shRNAs against OTUB1, USP5 and USP7 on the 2DIV and seeded with 12.5nM of K18P301L on the 4DIV/0DAS. Cellular lyses were done on the 7DAS (10DIV) with posterior alphaLISA and ELISA quantifications (Material and Methods 2.8. and 2.9.). ELISA data was used to normalize the alphaLISA data against possible technical and/or biological variation. Soluble hTauP301S: HT7/hTau10 alphaLISA quantification of primary neurons overexpressing hTauP301S and not seeded with K18P301L. Total hTauP301S: HT7/hTau10 alphaLISA quantification of primary neurons overexpressing hTauP301S and seeded with K18P301L (both soluble and aggregated hTauP301L are present on the sample). Aggregated hTauP301L: hTau10/hTau10 alphaLISA quantification (see Material and Methods 2.8. for alphaLISA description). a) Comparison between soluble hTauP301S levels of primary neurons overexpressing hTauP301S treated with the shRNAs to knockdown OTUB1 or hTau, treated with non-targeting sequences or not treated with any shRNA b) Comparison between total hTauP301S levels of primary neurons overexpressing hTauP301S treated with the shRNAs to knockdown OTUB1 or hTau, treated with non-targeting

↵**Figure 44 (continuation):** sequences or not treated with any shRNA c) Comparison between aggregated hTauP301S levels of primary neurons overexpressing hTauP301S treated with the shRNAs to knockdown OTUB1 or hTau, treated with non-targeting sequences or not treated with any shRNA d) Comparison between soluble hTauP301S levels of primary neurons overexpressing hTauP301S treated with the shRNAs to knockdown OTUB1, USP5 or hTau, treated with non-targeting sequences or not treated with any shRNA e) Comparison between total hTauP301S levels of primary neurons overexpressing hTauP301S treated with the shRNAs to knockdown OTUB1, USP5 or hTau, treated with non-targeting sequences or not treated with any shRNA f) Comparison between aggregated hTauP301S levels of primary neurons overexpressing hTauP301S treated with the shRNAs to knockdown OTUB1, USP5 or hTau, treated with non-targeting sequences or not treated with any shRNA g) Comparison between soluble hTauP301S levels of primary neurons overexpressing hTauP301S treated with the shRNAs to knockdown USP5 or hTau, treated with non-targeting sequences or not treated with any shRNA h) Comparison between total hTauP301S levels of primary neurons overexpressing hTauP301S treated with the shRNAs to knockdown USP5 or hTau, treated with non-targeting sequences or not treated with any shRNA; i) Comparison between soluble hTauP301S levels of primary neurons overexpressing hTauP301S treated with the shRNAs to knockdown USP5 or hTau; j) Comparison between soluble hTauP301S levels of primary neurons overexpressing hTauP301S treated with the shRNAs to knockdown USP7 or hTau, treated with non-targeting sequences or not treated with any shRNA, treated with non-targeting sequences or not treated with any shRNA; k) Comparison between total hTauP301S levels of primary neurons overexpressing hTauP301S treated with the shRNAs to knockdown USP7 or hTau and l) Comparison between aggregated hTauP301S levels of primary neurons overexpressing hTauP301S treated with the shRNAs to knockdown USP7 or hTau, treated with non-targeting sequences or not treated with any shRNA, treated with non-targeting sequences or not treated with any shRNA. Data is presented as ± SEM. N=1 and n=8 per condition/per experiment. Statistical comparisons were made considering the non-targeting treatments as the negative controls. In cases where two non-targeting sequences were used, an average of those was used as the reference Statistical analyses of the results were performed by a two-way ANOVA followed by Dunnett's *post-hoc* comparisons with an alpha set to 0.05.

4 DISCUSSION

The specific mechanisms underlying the onset and progression of AD have not been fully elucidated yet; however, the two diagnostic neuropathologies in the AD brain (i.e., amyloid plaques and neurofibrillary lesions) [16, 236] have been implicated mechanistically in the degeneration of the AD brains, and yet, they are considered to be plausible targets for the discovery of potential therapeutic agents to treat this prevalent dementing disorder. Of particular notice is that neurofibrillary lesions are not restricted to AD. Indeed, thioflavin-S, silver stains, and anti-Tau positive structures, which proves the presence of aggregated Tau, are observed as the predominant markers in a group of neurodegenerative disorders other than AD – the Tauopathies [16]. In some of these disorders, abundant coexistence between Tau and amyloid plaques (e.g., Aβ and prion protein amyloid deposits)[16] suggest an interaction between them in neurodegeneration mechanisms. However, Tau lesions are also seen in the absence of amyloid deposits in several Tauopathies (e.g., argyrophilic grain dementia, Pick disease, corticobasal degeneration, progressive supranuclear palsy, multiple system atrophy, Niemann-Pick disease type C, diffuse neurofibrillary tangles with calcification, Hallervorden-Spatz disease, subacute sclerosing panencephalitis, and frontotemporal dementia and parkinsonism linked to chromosome 17) [16, 237] strongly indicating that these neurofibrillary lesions are not mere consequences of neurotoxicity owing to amyloid deposits, but are direct causes of neurodegeneration. Additionally, although there is still an intense debate whether soluble or insoluble Tau aggregates are the most toxic species for the neurons, it is well known that the accumulation of hyperphosphorylated and ubiquitinated Tau aggregates and the extent of their presence correlates with cognitive decline and disease progression [211], hence the strong interest in the clearing of those entities [6, 213, 214]. The two major routes for protein degradation in cells, the autophagy-lysosome and ubiquitin-proteasome pathways, have long been associated with the clearance of misfolded proteins [218] [6, 218, 219], and most importantly to both clearance of physiological and pathological Tau and Tau aggregation [6, 104, 176, 198, 218, 220-223]. However, the relative contributions of these two major processes to normal and pathological Tau clearances are still poorly understood, and yet the effect of Tau aggregation in modulating such endogenous processes was barely studied. In an attempt to make advances in understanding such panorama, it is necessary to have a fast, flexible and robust model.

During the years, a lot of effort was made to produce cell-based models to mimic Tau aggregation, in a similar way to what is observed in Tauopathies, but without much success. Only recently this was achieved, by the use of pre-fibrillized material [165-167], which acts as a "seed" which overcomes the nucleation-dependent lag-phase moving the process into the rapid elongation phase [163]. In this way, the formation of NFTs is strongly enhanced and allows *in vitro* aggregation of Tau. Our study clearly demonstrates that the intracellular delivery of exogenous pre-formed seeds can nucleate overexpressed hTauP301L and trigger its aggregation in an *in vitro* neuronal model, as it can be seen by the detection of HT7 immunoreactivity in the insoluble fraction of a sarkosyl extraction by the western blotting technique (Results 3.1.1.; Figure 13). Indeed, the idea that exogenously supplied fibrils can recruit endogenous hTauP301L into insoluble fibrillar material is also supported by the immunofluorescence data where we observed AT8 positive NFTs-like structures along time (Result 3.1.2.; Figure 15). In such immunocytochemistry experiment we adopted a strategy in which we performed a methanol extraction, which resulted in a stringent extraction of soluble proteins and, consequently, to the enrichment of the insoluble hTauP301L fraction. Therefore we could specifically isolate and detect insoluble hTauP301L aggregates. Importantly, along the whole experimental

window in our study this material was found predominantly in the perinuclear space showing a ring-like morphology that is similar to previously the described in immunohistochemistry of AD's brains [207]. Interestingly, such morphology evolved also to a string-like structures localized in the dendrites from the 13DIV (only the day 3 after seeding – 3DAS) until the 18DIV (end of the experiment). Such Tau mislocalization is well known described in AD brains and AD models [238, 239]. Additionally, more diffuse morphologies could be observed, with a special attention to a dotted pattern diffusely distributed along the cell body in the 13DIV. Although such diffused pattern may appear later in time it likely represents the earlier stages of hTauP301L aggregation. Difference between the dotted and ring-like patterns may be caused by different expression level of hTauP301L, which results from unequal adenoassociated viral transduction efficiency in all neurons. The dotted AT8 pattern, which was detected in singular neurons on 13DIV, might be related to initial stages of hTauP301L aggregation that could be only spotted in neurons expressing lower levels of hTauP301L. It is important to point out that diffused Tau aggregative patterns were also observed in other cellular-based models, such as described by Guo et al. and Santa-Maria et al. [165, 240]. In contrast to the dotted pattern, from the 14DIV onwards a comet-like pattern in the soma of some neurons as well as a dotted morphology along the neurites can be observed. Such patterns likely account for more advanced stages of hTauP301L aggregation. Considering the neurites, the doted pattern shows itself more pronounced in neurons with hTauP301L aggregates present, but it is also displayed in neurons in non-aggregative conditions, highlighting a possible burden of hTauP301L overexpression that seems to be leading to the "blebbing" of the plasmatic membrane. It would be of interest to measure which structures are thioflavin-S positives as done by Guo and colleagues, where large inclusions were positive for this staining [165], to detect hTauP301L aggregates by making use of other phospho-dependent antibodies that detect different Tau phosphorylation epitopes (e.g., 12E8 and PHF1 antibodies, that detects hTau phosphorylated, Ser262/Ser356 and Ser396/Ser404, respectively [241]), as well as to detect hTauP301L aggregates by using a non-phosphrylation dependente antibody, such as HT7 [204]. Consequently, a more broad view of the subject would be provided.

In order to be able to draw conclusions about UPS and autophagy involvement in Tau clearance and/or build-up, as well as the effect of pharmacological and genetic approaches in regard of Tau aggregation, optimization and kinetic characterization of the model in use is important. With this purpose, we performed a time-course experiment comparing levels of soluble, total (soluble and aggregates present) and aggregated Tau in our "long" neuronal model of hTauP301L aggregation *in vitro*. To understand the effect of expression level of hTauP301L as well as the effect of the concentration of K18P301L seeds on hTauP301L aggregation, we used different MOIs of AAV6hTauP301L with a given K18P301L fibril concentration and different K18P301L fibril concentrations together with a given MOI of AAV6hTauP301L (alphaLISA –Material and Methods 2.8.; Results 3.1.3.). When focusing on soluble and total hTauP301L levels (hTauP301L measured in neurons overexpressing hTauP301L and not seeded with K18P301L –non-aggregative conditions - and neurons overexpressing hTauP301L and seeded with K18P301L – aggregative conditions -, respectively) in neurons transduced with AAV6hTauP301L MOI 100 or 50 within one K18P301L fibril concentration (for 25nM or 2.5nM and in the absence of fibrils – 0nM), a 50% reduction in the MOI of the virus results in slowing-down the initial slope of soluble and total hTauP301L levels when comparing the MOI 50 to the MOI 100 transduced neurons leading to one day delay on reaching plateau levels (12DIV for MOI 100 and

13DIV for MOI 50; Figures 17 a, b and c). By the end of the experiment – 20DIV –, when comparing the two viral MOIs, soluble and total hTauP301L levels are comparable (again similar results in the three conditions, within 25nM, within 2.5nM and 0nM). Lower levels of AAV6hTauP301L infection, in the case of MOI 50, leading to lower hTauP301L DNA integration/expression and consequently delaying the plateau phase, can explain these data. Of note is that when comparing MOI 100 transduced neurons in the presence of K18P301L (both 25nM and 2.5nM) to MOI 100 transduced neurons in the absence of the fibrils (0nM), hTauP301L levels are higher in the condition in the absence of K18P301L (Figures 19 c and d). Similar results are observed when comparing neurons transduced with MOI50 and cultured in the presence of the fibrils (both 25nM and 2.5nM) to the absence (0nM), where also higher hTauP301L levels are observed for the non-aggregative condition (neurons overexpressing hTauP301L and not seeded with K18P301L; Figures 19 a and b). Such difference is likely due to the aggregation of hTauP301L that could lead to decreased accessibility of the epitope for interaction with the detection antibodies (i.e.: shielding of epitopes [208]), hence reflecting in reduced biochemical signals – phenomenon that has already been described for other aggregated proteins [208]. AAV6hTauP301L MOI 100 transfected neurons show higher hTauP301L neuronal levels early in the time-course, which as a result should increase the pool of hTauP301L and, consequently, the amount of hTauP301L available for aggregation. This increase in the aggregation "substrate" should accelerate the nucleation-dependent lag-phase moving the process into an accelerated elongation phase [163]. However, when comparing the MOI factor within a single K18P301L fibril concentration (for both cases, within 25nM and within 2.5nM), no difference on the rate of hTauP301L aggregation was seen (Figures 17 e and f). Interestingly, such result underscores that a certain threshold of hTauP301L expression was reached and hence a 50 % decrease in the MOI no longer makes difference in the elongation rate of hTauP301L aggregation. Considering the K18P301L concentration factor – 25nM in comparison to 2.5nM of K18P301L – on total hTauP301L levels, very similar hTauP301L levels can be seen within a single viral MOI neuronal treatment (for both, within MOI 100 and within MOI 50, similar results are shared) until the 18DIV for neurons transduced with MOI 100 and 16DIV for the MOI 50 (Figures 18 a and b). Interestingly, in the final days of the experiment, for MOI 100 from 18-20DIV and for MOI 50 form 16-20DIV, higher hTauP301L levels can be observed in neurons treated with K18P301L 2.5nM when compared to 25nM for both transduction conditions (Figures 18 a and b). These final differences highlight a possible difference in the hTauP301L aggregates kinetics build-up when in the presence of a 10 times less K18P301L seeds content, in which when considering the epitope shielding [208] factor it is possible that there are more soluble hTauP301L aggregates when compared to insoluble hTauP301L aggregates (i.e., due to a higher fraction of soluble hTauP301L aggregates, more epitopes would be available, consequently leading to a shift towards higher signal levels in this case when in comparison to a situation where more insoluble hTauP301L aggregates would be present and less epitopes available for detection). To address this question it would be important to perform a hTauP301L sarkosyl extraction and compare the levels of both soluble and insoluble levels of hTauP301L in neurons treated with different 2.5nM and 25nM within a given MOI in between the 18-20DIV. If this hypothesis is confirmed, a setting based on such data could render a good paradigm to try to understand effects and consequences related to an enriched soluble hTauP301L aggregates environment on neuronal physiology. This is particularly interesting considering that recent findings in *Drosophila* and rodent models of Tauopathy suggested that large insoluble aggregates such as Tau filaments and tangles may not be the key toxic species in these disease, but rather pre-filament Tau species - e.g., hyperphosphorylated

monomers and oligomers [242, 243]. Lastly on these set of results is the observation that seeding neurons with 10 times less K18P301L leads to a slower aggregation of hTauP301L (results based on the comparison hTauP301L aggregation levels of K18P301L 25nM and 2.5nM fibril concentrations within a single MOI – similar results are shared within MOI 100 and MOI 50; Figures 20 a and b). Eisenberg and Jucker suggested that the exposure of the amyloid backbone is essential for amyloid formation but not sufficient [244]. The concentration of this segment must be sufficient to overcome the entropy that prevents ordered fibrils formation, and higher concentration of the fibrils leads to an increase in aggregation if the transition of the nucleation phase limiting step is exceeded [244, 245]. Additionally, it was previously observed in the hTauP301L neuronal model that the amount of hTauP301L aggregation is dependent on the amount of K18P301L mutant fibrils added to the system [166, 167]. This strongly suggests that an increase in uptake of *in vitro* pre-aggregated fibrils will trigger a higher level of intracellular hTauP301L aggregation. Intriguingly, live immunostaining followed by immunofluorescence after fixation and permeabilization (two-stage staining) revealed that a great amount of K18P301L fibrils that are added to the system were membrane-associated [165]. Therefore, it is likely that increasing the amount of fibrils added to the system could also render in a constant uptake of the fibrils by the neurons, which in turn could also result in higher hTauP301L aggregation levels. However, our time-course characterization underscores that this is only partially true and dependable on the time-point of the sample collection. That means that, with higher amounts of K18P301L fibrils, the limiting nucleation phase is exceeded faster; however, by the end of the time-course – 20DIV – hTauP301L aggregation levels are comparable regardless the fibril concentration. Therefore, if one collects a sample between the 15-19DIV, higher hTauP301L aggregates levels would be seen in neurons treated with 25nM K18P301L concentration when comparing to the 2.5nM concentration, but sampling on the 20DIV would render similar results for both concentrations. These data are in accordance to Friedhoff et al. observations in a non-cellular *in vitro* modelling of PHFs assembly. In their study they show that in the presence of added seeds the NFTs assembly curves can be fitted by a simple exponential approach to equilibrium, and that the slope of the curve is dependable on the "seeds" concentration [245].

Due to the aforementioned results, transduction of the primary neurons with AAV6hTauP301L MOI 100 and seeding with K18P301L 25nM (Material and Methods 2.2. and 2.5.) were chosen as optimal conditions within this model towards our objectives (pharmacological validation of autophagy and UPS as central players in hTauP301L and for genetic manipulation and target validation), showing a faster increase in hTauP301L expression and aggregation signal, but still with a good temporal window to be analysed. Hence, these conditions were further characterized – Results 3.1.4.. Soluble and total (soluble and aggregates present in the sample) hTauP301L levels in this model are characterized by an increase from the beginning of the experiment reaching their maximum signals on 12 DIV, moment in which plateau levels seems to be reached (Figure 21a). Of note is that the epitope shielding [208] seems to be accounting for an average of 1.5-fold higher levels when comparing the soluble hTauP301L with the sample where soluble and aggregated hTauP301L are present (total hTauP301L levels). In accordance to previously described modelling of Tau aggregation, hTauP301L aggregates shows themselves dependable on the exposure of β-sheeted seeds [163, 245] as can be highlighted by the observation that neurons overexpressing hTauP301L in the absence K18P301L fibrils are not able to overcome the entropy that prevents ordered fibrils formation (Figure 21b). Additionally, hTauP301L aggregation seems to fit to a simple exponential profile towards equilibrium [245] in

which, by the time the nucleation phase seems to be overcame, a fast elongation phase takes place [163, 245] between the 13-19DIV (3-10DAS) with equilibrium being reached on the 19DIV (10DAS; Figure 21b). Altogether, the data presented here are supported by the amyloid fibrillation process [163]. As we intended to use the hTauP301L aggregation model for pharmacological and genetic approaches to manipulate hTau levels, an endogenous control to normalize data against possible technical variation and eventual neuronal loss is indispensable. Rodent Tau was then chosen due to its specific neuronal expression of Tau [209, 210] and the fact that rodent Tau does not aggregate by itself when exposed to K18P301L seeds (data not shown). Our data shows that rodent Tau levels do not differ significantly due to the overall treatment factor, as it can be seen in the Figure 21c. Neurons overexpressing hTauP301L in absence and in the presence of K18P301L fibrils show a similar profile with no statistical differences within a single time-point. However, a temporal variation on rodent Tau levels can be seen (comparable between the treatments within single-time points; Figure 21c). Such data underscores a limitation in the use of this protein as an endogenous control – rodent Tau levels can only be used to normalize the alphaLISA (Material and Methods 2.8.) data within a single time-point. Hence, for our genetic and pharmacological approaches such control is still valid as we measure a single time-point (day of the lysis) and compare the different treatments. However, if one wants to make temporal conclusions upon Tau manipulation, a more adequate endogenous control should be developed as in mTau5/hTau24 ELISA quantification (rodent Tau; Material and Methods 2.9.) situation false negatives would be created when comparing different time-points. MAP-2 or neuron specific Class III β-tubulin could be used as they are neuronal specific, but even those impose a possible complication when considering normalization in Tau manipulation models (which is also present in the rodent Tau case). That is, all these proteins are related to microtubules and, as Tau deeply influences microtubules stability, it would be better to use a non-microtubule related neuronal-specific protein to exclude any possibility of an influence on the endogenous control levels. Therefore, a possible optimization of our model that could solve such endogenous control issue would be the overexpression of hTauP301L simultaneously to eGFP using a bicistronic construct – AAV6SYN1-eGFP-SYN1hTauP301L. With such optimization, eGFP would be specifically expressed in neurons and consequently would render a good candidate for a normalization control, as it is not related to microtubules.

A stereotypical spatial and temporal spreading of Tau protein inclusions within affected brains has been shown [212, 246]. We observed that the hTauP301L aggregation increased also over time both by immunocytochemistry and alphaLISA (Material and Methods 2.8. and 2.12.; Results 3.1.2.; 3.1.3.; 3.1.4.). The increase of insoluble hTauP301L can be explained by the continuous expression of hTauP301L within the neuron that bears the seed. If the soluble and insoluble pools of hTauP301L are dynamic, the newly expressed soluble hTauP301L will aggregate contributing to an increase in insoluble protein. On the other hand, the increase in hTauP301L levels in both alphaLISA, but particularly in immunocytochemistry (where it shows more spread on the microscopical view), suggests cell-to-cell transmission of oligomeric Tau proteins may also occur that in our neuronal model. We hypothesize that insoluble hTauP301L levels increased over-time because templating species are inducing aggregation in neighbouring neurons, due to their spreading, possibly by trans-synaptic transmission and/or non conventional secretory pathways [247]. However, it is not possible to determine the existence of spreading in these experimental procedures. This is because it is not noticeable in these kinds of neuronal cultures whether the aggregated Tau spreading is from one cell to

another or each neuron only uptakes the pre-aggregated fibrils by the time of seeding. In order to overcome this problem and investigate if there is a spreading mechanism associated with the hTauP301L aggregation, microfluidic polydimethylsiloxane chambers could be used, since this kind of technique can allow separating two chambers with different conditions while keeping dendrites and axons across both chambers, so the uptake and movement inside cells could be studied [248]. Additionally, the manipulation of events at the synapse level could point out some answers. The inhibition of proteins involved in endocytic-vesicle fission like amphiphysin and dynamin [249] would be a possible strategy to test the hypothesis that these seeds spread via endocytosis [250].

As mentioned above, the "long" hTauP301L neuronal aggregation model described here shows a fast elongation phase that begins on the 13DIV, and on the 15DIV (only 5DAS and 5 days prior the end of the experiment) statistical significant difference can already be observed when comparing neurons overexpressing hTauP301L and treated with K18P301L (Material and Methods 2.2. and 2.5.). The 20DIV (the final day of the time-course) was commonly used by our laboratory as the standard moment to lyse the cells and compare hTauP301L levels. Such model is very time and cost-consuming model that is not well suited for HTS campaigns. In light of such data and in the need of a faster and better-suited neuronal Tau aggregating model for HTS screens (up-to-now only available in non-neuronal cell models), we hypothesized whether we could shorten the "long" model. With this purpose, upon neuronal transduction on day 1 *in vitro* (AAV6 hTAUP301L, MOI100) followed by 12.5nM K18P301L seeding on day 3 *in vitro* (Material and Methods 2.2. and 2.5.) we observed by HT7/hTau10 alphaLISA measurements (Material and Methods 2.8.) an increase in the soluble and total (soluble and aggregates present in the sample) hTauP301L levels in which they seem to reach an equilibrium phase on the 10DIV which is two days *in vitro* before to the "long" model where such phase was reached on the 12DIV (Results 3.2.2.; Figure 25a). When comparing soluble and total levels by the HT7/hTau10 alphaLISA (Material and Methods 2.8.), just as in the "long" model, soluble values are higher than total levels possibly due to epitope shielding [208]. In accordance to previously described models of Tau aggregation from other groups and from our "long" model results, the "short" model hTauP301L aggregates shows themselves dependent on the exposure of β-sheeted seeds [163, 245] as can be highlighted by the observation that neurons overexpressing hTauP301L in the absence K18P301L fibrils are not able to overcome the entropy that prevents ordered fibrils formation (Figure 25b). Most importantly, by seeding hTauP301L with K18P301L earlier than the "long" model (7 days earlier than in the "long" model; "long" model seeding on 10DIV and "short" model seeding on 3DIV; Material and Methods 2.5.), it can be observed a significant hTauP301L aggregation on the 10DIV, as measured by the hTau10/hTau10 alphaLISA (Results 3.2.2.; Figure 25b; Material and Methods 2.8.). Similar results were only observed in the "long" model on the 15DIV. Hence, hTauP301L aggregation signal (hTau10/hTau10 alphaLISA; Material and Methods 2.8.) in this model looks similar to the displayed in the long aggregation model although with a shift to its left side (i.e.: aggregation signal displayed earlier in time when comparing to the "long" model). This was possible due to simultaneous aggregation and synthesis of hTauP301L achieved by transducing the neurons with the AAV6hTauP301L and seeding with K18P301L earlier (1DIV and 3DIV, respectively) in comparison to the "long" model. HTauP301L aggregation again seems to fit to a exponential profile [245] in which a fast elongation phase takes place by the time the nucleation phase seems to be overcame [163, 245], data that are supported by the amyloid fibrillation process [163]. Additionally, when inspecting rodent Tau levels, again,

neurons overexpressing hTauP301L in non-aggregative conditions and in aggregative conditions (seeded with K18P301L fibrils) display very similar profiles and, by analysing the data by an ordinary two-way ANOVA, neurons overexpressing hTauP301L and seeded with K18P301L do not differ significantly when compared to neurons overexpressing hTauP301L in non-aggregative conditions (i.e., the overall treatment factor do not induce an overall statistical significant difference; Results 3.2.2.2.; Figure 26).

Altogether, this new hTauP301L aggregation model is better suited for HTS campaigns aiming Tau manipulation, as it is less time and money consuming and, hence, more straightforward. Additionally, due to its shorter duration when in comparison to the "long" model, this "short" model of hTauP301L aggregation in primary neurons should results in cleaner neuronal cultures since the shorter experimental time will limit number of cellular divisions of non-neuronal cells. Another advantage linked to the "short" model is that in pharmacological approaches, compound incubation time would be shorter which brings at least two major advantages: (i) less toxicity should be expected by the end of the experiments due to reduced exposure time of the neurons to the compounds; and (ii) less variation related to compound instability and degradation along time. However, since an equilibrium phase was not observed within the studied temporal window, a limitation was imposed for this "short" model when comparing to the "long" model – one could not draw conclusions about the effect of compound treatment on Tau clearance, but rather it should be used to focus on the influences on hTauP301L build-up kinetics. In other words, as one is not comparing plateau levels, effective clearing cannot be observed as a shift in the plateau levels earlier in time or towards lower numbers. The only exceptions would be if a very strong clearing mechanism took place and an early plateau is reached, or if the curve had a clear inverted slope towards reduction - but such phenomenon is not likely to happen as the clearance mechanisms have been often shown to be dysfunctional in such pathological situations [214]. Therefore, if one wants to address such question, either the use of the "long" model is indicated or a further optimization of the "short" model is needed. In such case, increasing the K18P301L fibril concentration from 12.5nM to 25nM or even higher might render in an earlier equilibrium phase as a higher concentration of the fibrils leads to a faster rate of aggregation [244, 245](Results 3.1.3.). Another alternative would be increasing the transduction MOI. In such case higher hTauP301L overexpression would take place increasing the aggregation substrate available which could in turn increase hTauP301L aggregation rates [163]. However, such possibility might impose toxicity issues that have to be controlled.

The observation that the intracellular delivery of exogenous pre-formed seeds – K18P301L - can nucleate overexpressed hTauP301L and trigger its aggregation in this newly developed "short" hTauP301L aggregative model is corroborated by the immunofluorescence data (Material and Methods 2.12.) where we observed AT8 positive NFTs like structures along time (Results 3.2.1.; Figure 23). Importantly, along the whole experimental window in our study, this material was found predominantly with a comet-like morphology, that is, a densely located inclusion with preinuclear localization (ring-like pattern), morphology that is similar to previously the described in immunohistochemistry of AD's brains [207] that is also associated to the proximal parts of the dendrites in a doted configuration. Such doted configuration is similar to the observed in the "long" model, which as already discussed might highlight a possible burden related to the overexpression of hTauP301L. It can also be observed that the doted pattern appears well spread across the microscopical view along the days towards the end of the experiment. Of note is that many of the dots

seen do not co-localize with the MAP-2 staining (Table2). These AT8 positive dots suggests that hTauP301L aggregates might have been secreted by the neurons and got glued in the plate surface or were internalized by non-neuronal cells present in the culture. Indeed, Tau secretion through non-conventional secretory pathways has been described in several different cellular models [247] and NFTs presence in non-neuronal cell are observed in some Tauopathies brains (e.g. MSA, CBD, PSP, and FTDP- 17 contain abundant Tau deposits in astrocytes as well as oligodendrocytes [237]). Despite that, one cannot exclude a third explanation in which neuronal cell death might have occurred and hence hTauP301L aggregates are being released to the extracellular space getting glued to the plate. However, before fixing the cells with methanol (Material and Methods 2.12.), visual inspections were performed and no apparent cell loss was observed. Also, no differences were seen between the neurons in aggregative conditions and non-aggregative conditions (both overexpressing hTauP301L and wild-type neurons). Just as for the long model, it would be of interest to measure in this immunocytochemistry approach which structures are thioflavin-S positives as done by Guo and colleagues, where large inclusions were positive for this staining [165], to detect hTauP301L aggregates by making use of other phospho-dependent antibodies that detect different Tau phosphorylation epitopes (e.g., 12E8 and PHF1 antibodies, that detects hTau phosphorylated, Ser262/Ser356 and Ser396/Ser404, respectively [241]), as well as to detect hTauP301L aggregates by using a non-phosphrylation dependent antibody, such as HT7 [204]. Consequently, a more broad view of the subject would be provided.

Normal adult neurons exhibit low levels of Tau phosphorylation. On the other hand, neurons of AD brain and other Tau-related neurodegenerative diseases show high levels of Tau phosphorylation at both physiological and pathological disease-specific residues [211]. Additionally, a correlation between hyperphosphorylated Tau and the formation of the filamentous intracellular inclusions of several neurodegenerative disorders, including AD, has been done, with the extent of such aggregates being related to cognitive decline and disease progression [207, 212]. When used in western blotting to detect hTauP301L, AT8 antibody (Table 2) that recognizes human Tau which is phosphorylated on Ser-202 and Thr-205 [211], renders two bands in the *in vitro* aggregation model used in this work, being a higher migrating band that seems to be related to an insoluble fraction of hyperphosphorylated hTauP301L and a lower migrating band that is related to the soluble fraction of phosphorylated hTauP301L [166]. Hence, AT8 antibody was used to assess the phosphorylated and hyperphosphorylated human Tau levels giving us insights in the kinetics of such process (Tau phosphorylation) that is strongly correlated to Tau aggregation. HT7 antibody (Table2), on the other hand, was used as a tool to detect total hTauP301L protein levels due to its phospho-independent hTau detection [204]. Interestingly, HT7-based western blot shows profiles that resemble the HT7/hTau10 alphaLISA (Material and Methods 2.8.) data, with the samples from neurons overexpressing hTauP301L and seeded with K18P301L apparently reaching an equilibrium phase on the 8DIV, and in neurons overexpressing hTauP301L in non-aggregating conditions such plateau phase is not displayed, which is likely happening due to biological and/or technical variations related to the limited n number of the experiment (Results 3.2.2.3.; Figure 27 a; b and c). When focusing on the phosphorylated and hyperphosphorylated hTauP301L levels probed by AT8, again the data seem to fit to a simple exponential profile [245] in which a fast elongation phase takes place by the time the nucleation phase is overcame [163, 245] between the 9-14DIV, data that are supported by the amyloid fibrillation process [163] (Figure 28 a; b and c). As AT8 probes for total phosphorylated hTau, similar profiles are seen for samples from both neurons

overexpressing hTauP301L not treated with the K18P301L fibrils and neurons overexpressing hTauP301L and seeded with K18P301L. Importantly, when inspecting the western blot of samples that were treated in aggregative conditions (neurons overexpressing hTauP301L and seeded with K18P301L fibrils), from the 8DIV onwards a higher migrating band can be observed (Results 3.2.2.3.; Figure 28b). This band likely corresponds to the statistical differences seen from the 9DIV to the 14DIV between the two conditions (aggregative and non-aggregative) in which neurons overexpressing hTauP301L and treated with K18P301L display higher signals (reflected in a highly significant two-way ANOVA interaction p value; Figure 28c). As mentioned above, such higher molecular weight band seems to be related to an insoluble fraction in our *in vitro* model when a sequential protein extraction takes place [166]. Altogether strongly suggests the presence of hTauP301L hyperphosphorylated aggregates in neurons transduced with AAV6hTauP301L and seeded with K18P301L. Of particular note is that in the western blot analysis from the samples collected from neurons in non-aggregative conditions, the higher migrating band is not seen – it is only displayed the lower migrating band that seems to be related to the soluble fraction when a sequential protein extraction takes place [166](Figure 28a). Therefore, it suggests that there are increasing hTauP301L phosphorylation levels, but aggregates are absent in such condition. This data is in accordance with previously described models of Tau aggregation from other groups and from our "long" and "short" models results, in which hTauP301L aggregates shows themselves dependent on the exposure of β-sheeted fibrils [163, 245]. It and also indicates that phosphorylation is not enough to drive hTauP301L aggregation process further on from the lag phase. Despite all that, two additional experiments could be done to confirm the presence of hTauP301L aggregates on such samples and conditions - a native gel probing for hTau with HT7 and AT8 and/or a sarkosyl extraction with posterior SDS-PAGE probing hTau with HT7 and AT8 for the total, insoluble and soluble fractions.

Altogether these data show that, similarly to what was observed in the "long" hTauP301L aggregative neuronal model, it was observed that *in vitro* pre-aggregated fibrils induced hTauP301L aggregation in a time dependent manner in the "short" model as assessed by alphaLISA, western blotting and immunocytochemistry (Material and Methods 2.7.; 2.8. and 2.12). As mentioned before, NFTs spreading in affected brains in a temporal and spatial fashion has been associated with Tau pathology [212, 246]. As a consequence, although one cannot exclude that hTauP301L increasing in aggregation might be only due to the continuous expression of hTauP301L in neurons bearing the "seeds", the same hypothesis discussed above for the "long" hTauP301L aggregative model about Tau oligomers spreading applies (e.g., non-conventional secretory pathways and/or trans-synaptic transmission)[247]. Of particular note is that AT8 staining spreading within the microscopical field starts to be more evident between the 8-9DIV as seen by immunocytochemistry (Figure 23; Material and Methods 2.12.), and that in the alphaLISA data hTauP301L aggregation reaches its elongation phase with a rapid increase in its levels from the 10DIV onwards (Figure 25b). Taking together these results and the observation that rat cortical neurons *in vitro* start to have functional synapses on average around the 7-10DIV onwards [251] it is logical to hypothesise that trans-synaptic oligomeric hTauP301L transmission seems to be an important event for hTauP301L aggregation process. As already discussed, to test investigate the importance of the trans-synaptic transmission, microfluidic polydimethylsiloxane chambers could be used [248] as well as the manipulation of events at the synapse level (e.g., exocytosis and endocytosis) could point out some answers [249, 250]. However, the

"short" model does not provide a good paradigm to study such phenomenon. On the other hand, the "long" model appears better suited to address questions dependable on mature synapses. In other words, in the "long" model K18P301L seeding only occurs on the 10DIV and, consequently, mature synapses are already present from the beginning of the K18P301L incubation. Despite that, the "short" model might provide a good paradigm to study non-synaptic related forms of hTauP301L oligomeric spreading, as there is an initial window (between the 3-10DIV) in which there are not great amounts of mature synapses and hence, if oligomeric transmission is already present, it would be enriched for non-synaptic related during such window. Indeed, it would be interesting to check for the presence of exosomes containing hTauP301L in the medium or even for the presence of hTauP301L directly on the medium as there are several secretory pathways potentially involved in Tau secretion that are not related to synaptic activity [247]. Indeed, as mentioned before, Tau secretion has been associated to non-conventional secretory pathways in several cell lines as seen by the observations that the secretion of endogenous and overexpressed Tau was insensitive to brefeldin A, a drug that blocks the conventional secretory pathway [247].

Given that in humans the extent of Tau pathology correlates with cognitive decline [214, 252], and in animal models of AD reducing Tau levels attenuates neuronal dysfunction [69, 214, 253], there is a growing interest in defining the degradative pathways that remove Tau from the cell. Indeed, the bulk of clearance of both physiological and pathological forms of Tau is mediated by the UPS and autophagy [214, 221]. The contribution of each of these pathways in the turnover of Tau, and which forms of Tau are degraded by each pathway, is an area of significant interest. For this reason, delineating how these pathways may be influenced in Tau aggregation models and how this contributes to Tau pathology is of great importance and could have significance for investing into new therapeutic approaches. In light of these observations, we discuss here the first set of data created characterizing along time UPS and autophagy activity in a primary neuronal model of Tau aggregation.

Proteasome activity in AD brain is lower than that in control brain, and this lowered activity is independent of the expression of proteasome subunits [254]. Proteasomes express three distinct catalytic sites - trypsin-like, chymotrypsin-like and peptidyl-glutamyl-hydrolysing (caspase-like) activities [176] -, each with unique substrate specificity. Although the contribution of these sites to overall proteolysis remains unclear, chymotrypsin-like activity associated to the proteasome has been previously associated to physiological Tau [176] and to misfolded Tau clearance [255]. In our time-course characterization of the proteasome activity, it can be seen that the chymotrypsin-like activity associated to the catalytic 20S core of the proteasome have a significant increase in the 6DIV that continues until the 7DIV - moment in which its maximum peak of activity is achieved (80% increase in comparison to wild-type neuronal UPS activity; adjusted p value <0,0001; alpha=0,05) upon K18P301L seeding (Results 3.2.3.1.; Figure 30a). This peak was followed by oscillations in which there is a drop on the 8DAS with a rescue on the 9DAS (reaching statistical significance) and with final levels on the 10DAS and 11DAS within wild-type neuronal activity (baseline proteasome activity – negative control). Importantly, UPS activity of neurons overexpressing hTauP301L not seeded with K18P301L remained within the baseline levels along the whole studied window with a non-significant increase in the 7DAS (Figure 30a). Despite that, when comparing the UPS activity of neurons overexpressing hTauP301L seeded and not with K18P301L in the 7DAS, there is a statistically significant difference between

them, indicating that even on such time-point there is a specific effect on the UPS activity related to K18P301L seeding in neurons overexpressing hTauP301L. Importantly, when comparing this UPS activity profile (Figure 30a) with the aggregation alphaLISA curve (Figure 25b; Material and Methods 2.8.), it can be observed that the 7DAS proteasome activity peak in neurons in aggregating conditions corresponds to the 10DIV and, therefore, the day that a statistical significant hTauP301L aggregation increase can be detected by the alphaLISA (Material and Methods 2.8.; Figure 45). Considering the progression of Tau aggregation that goes from soluble dimers and oligomers towards insoluble aggregates [163] and that those levels should change in function of the other, by the 10DIV its likely that the ratio between soluble hTauP301L forms and insoluble hTauP301L entities on this time-point would indicate higher levels of soluble hTauP301L in comparison to the insoluble fraction. Therefore, in the 7DAS (10DIV), UPS induction might be related to soluble hTauP301L species (Figure 45). Indeed, soluble proteins are the ideal substrate for the proteasome as UPS proteolysis is preceded by protein unfolding and stretching [254]. Besides, soluble Tau degradation by the UPS has been reported [176]. Therefore, to check for the possibility of the involvement of soluble hTauP301L aggregates conformations in the proteasome activity on the 7DAS, it would be important to perform a sarkosyl extraction and compare the levels associated with aggregated hTauP301L in the soluble and insoluble fractions by using the T22 antibody that specifically detects soluble oligomeric hTau [256]. Additionally, pulling-down the 20S catalytic core of the proteasome by immunoprecipitation with posterior assessments hTauP301L interaction with the UPS would be of a major interest. By that, one could probe which hTauP301L species would be specifically associated to the 20S catalytic UPS core, and a further characterization of their phosphorylation levels and/or ubiquitination levels could also be conducted. For the next few days *in vitro,* although with a signal variation, the chymotrypsin-like UPS activity of neurons in aggregative state displayed a gradual decline to baseline levels. By analysing the hTau10/hTau10 alphaLISA and AT8 western blot (Material and Methods 2.7. and 2.8.; Results 3.2.2.1. and 3.2.2.3.; Figures 25b and 28c) data on such time-point (corresponding to 12DIV), hTauP301L aggregation levels are already significantly increased when measured by alphaLISA, and statistical significant differences between neurons overexpressing hTauP301L not seeded with K18P301L and neurons overexpressing hTauP301L seeded with K18P301L can be seen by AT8 probing western blotting (Material and Methods 2.7.). Importantly, this difference correlates to the appearance of a higher molecular weight migrating band that, in our *in vitro* model, seems to be related to the hTauP301L hyperphosphorylated insoluble Tau [166] (Figure 28b). Hence, increasing levels of hTauP301L insoluble aggregates and/or higher nature soluble hyperphosphorylated hTauP301L conformations could be related to a partial blockage and/or dysfunction of the UPS, leading to a decrease of the UPS activity to the baseline levels (wild-type neurons) on the subsequent days, with a trend towards even lower activity levels (Figure 45). Indeed, it is known that aggregated and/or truncated proteins *per se* can impair proteasome functioning [215, 254, 255, 257], specifically NFTs [215], and truncated Tau species have been associated to chymotrypsin-like proteasome activity suppression [255]. Therefore, it is plausible that hTauP301L aggregated entities might be related to such changes (Figure 45). To address such hypothesis, it would be important to pull-down the 20S catalytic core of the proteasome by immunoprecipitation with posterior assessments hTauP301L interaction with the UPS between the 8DAS and 11DAS. By that, one could probe which hTauP301L species would be specifically associated to the 20S catalytic UPS core, and a further characterization of their phosphorylation levels and/or ubiquitination levels could also be conducted. If hTauP301L species are associated to the 20S catalytic UPS core within those

days, one could also isolate those and test in a cell-free *in vitro* assay whether such specific species are leading to UPS activity blockage or activity reduction. Lastly, although chymotrypsin-like UPS activity was associated to Tau [176, 255], trypsin-like UPS activity seems to be modulated by phosphorylated Tau in HEK293 cells [219]. Consequently, it is of interest to address the questions above observing also the caspase-like and trypsin–like UPS-associated activities, as well as to characterize such activities along time as we did with the chymotrypsin-like activity in primary neurons upon induction of hTauP301L aggregation. Consequently, hints on the contribution of each of these proteasome-associated enzymatic activities in the turnover of hTauP301L, and which forms of hTauP301L are degraded by each of them would be highlighted. Of note is that it would be important to further confirm such results with another read-out, that is, using another luminogenic substrates and/or by making use of total Ubiquitin probing western blot along time.

Autophagic processes in AD's brain are suggested to be compromised either as a result of decreased levels of macroautophagy regulatory proteins such as Beclin-1 [258], or impaired clearance of autophagic vacuoles by lysosomes [259]. Additionally, there is evidence that pharmacological enhancement and blocking of autophagy can lead to Tau clearance and Tau aggregates formation, respectively [198, 217]. In our primary neuronal model of hTauP301L aggregation autophagy induction in neurons overexpressing hTauP301L, can be observed upon seeding with K18P301L already on the 3 days after seeding (3DAS), and also on the 9DAS when comparing to wild-type neurons autophagy levels of activity (results obtained based in two independent quantifications – on the number of autophagolysosomes and on the intensity of the autophagosomes staining; Results 3.2.4.1.; Figures 32; 33 a and b). Neurons overexpressing soluble hTauP301L not seeded with the fibrils also show induction of autophagy, but on the 9DAS and 10DAS (results obtained based in two independent quantifications –on the number of autophagolysosomes and on the intensity of the autophagosomes staining – and in comparison to wild-type neurons levels of activity; Results 3.2.4.1.; Figures 32; 33 a and b). On those days, such induction levels on neurons in non-aggregative state are higher than the levels in the neurons seeded with K18P301L. When comparing both conditions - neurons overexpressing hTauP301L seeded with K18P301L and neurons overexpressing hTauP301L that were not seeded with the fibrils both - on the 3DAS, day in which neurons in aggregative conditions displayed autophagy induction, there is a statistical significant difference between the autophagy activity of neurons overexpressing hTauP301L seeded with K18P301L and neurons overexpressing hTauP301L in non-aggregative conditions (Figures 33 a and b). Similarly on the 9DAS, day in which neurons overexpressing hTauP301L seeded and not seeded displayed autophagy induction, statistical difference is also observed when comparing both conditions (Figures 33 a and b). Importantly, such differences indicate an effect related to K18P301L seeding. The early, 3DAS, autophagy induction in neurons incubated in aggregative conditions (transduced with AAV6hTauP301L and seeded with K18P301L; Material and Methods 2.2. and 2.5.) is intriguing and we hypothesize whether such induction is a direct response to K18P301L seeding (Figure 45). Indeed, the uptake of *in vitro* pre-aggregated Tau fibrils have been shown to be regulated by non-receptor mediated endocytosis [260, 261]. Wu et al. suggested that in HeLa cells the internalized aggregates are transported via endosomal vesicles and trafficked through the endosomal pathway to lysosomes [261], and hence these aggregates can be forwarded to lysosomes and be immediately degraded by autophagy-lysossomal system (Figure 45). Indeed, if this is the case an early induction could be expected. To address such hypothesis, one could perform a short time-course between the 0-4DAS making use of an indirect ELISA with a primary antibody against the Myc

tag present in the K18P301L fibrils (see Material and Methods 2.4.) with the conditions of wild-type rat primary neurons, AAV6hTauP301L transduced neurons, AAV6hTauP301L transduced neurons and K18P301L seeded, AAV6hTauP301L transduced neurons treated with rapamycin and AAV6hTauP301L transduced neurons and K18P301L seeded treated with rapamycin. Consequently, if the K18P301L fibrils are being forwarded to the autophagy-lysossomal system with the rapamycin treatment a further induction on the autophagy levels should occur and clearance of the fibrils should be seen in such paradigm. When focusing on the last days of the experiment, the autophagy induction in neurons overexpressing hTauP301L in the absence of K18P301L on the 9DAS and 10DAS, suggests that autophagy is enhanced in such time-points due to soluble hTauP301L overexpression levels (Figure 45). In fact, soluble Tau has been linked to autophagical degradation [197] and as in our *in vitro* model on the 9DAS and 10DAS (12DIV and 13DIV) soluble hTauP301L levels are on their highest levels in a plateau phase, as assessed by alphaLISA (Results 3.2.2.1., Figure 25a; Figure 45; Material and Methods 2.8.), it is plausible that high overexpression levels of soluble hTauP301L might be triggering autophagy in such time-point (Figure 45). Interestingly, on the 9DAS (equivalent to 12DIV) on the AT8 western blot (Material and Methods 2.7.) time-course a difference between samples from neurons overexpressing hTauP301L in aggregative conditions non-aggregative conditions that seems to correlate to the appearance of a higher molecular weight migrating band possibly related to the hTauP301L insoluble fraction [166] was observed (Figure 28b and c). Therefore, when inspecting neurons in aggregative conditions (i.e., in the presence of K18P301L) the shift to lower levels but still significant autophagy levels in comparison to neurons overexpressing hTauP301L not seeded with K18P301L might suggest that the presence of the soluble and/or insoluble aggregates could be leading to diminution in autophagy levels when comparing these two conditions (AAV6hTauP301L transduced neurons in the presence and absence of K18P301L fibrils; Figure 45). As a matter of fact, autophagical dysfunction with autophagolysossomes accumulation is present in AD brains with Tau pathology [259], and several others neurodegenerative proteinopathies display lysosome-related dysfunctions [262]. Interestingly, alpha-synuclein induces lysosomal rupture in neuronal cell lines [263] and Tau has been shown to disrupt synthetic lipid bilayers [264]. Hence, it is conceivable that Tau may also induce lysosomal

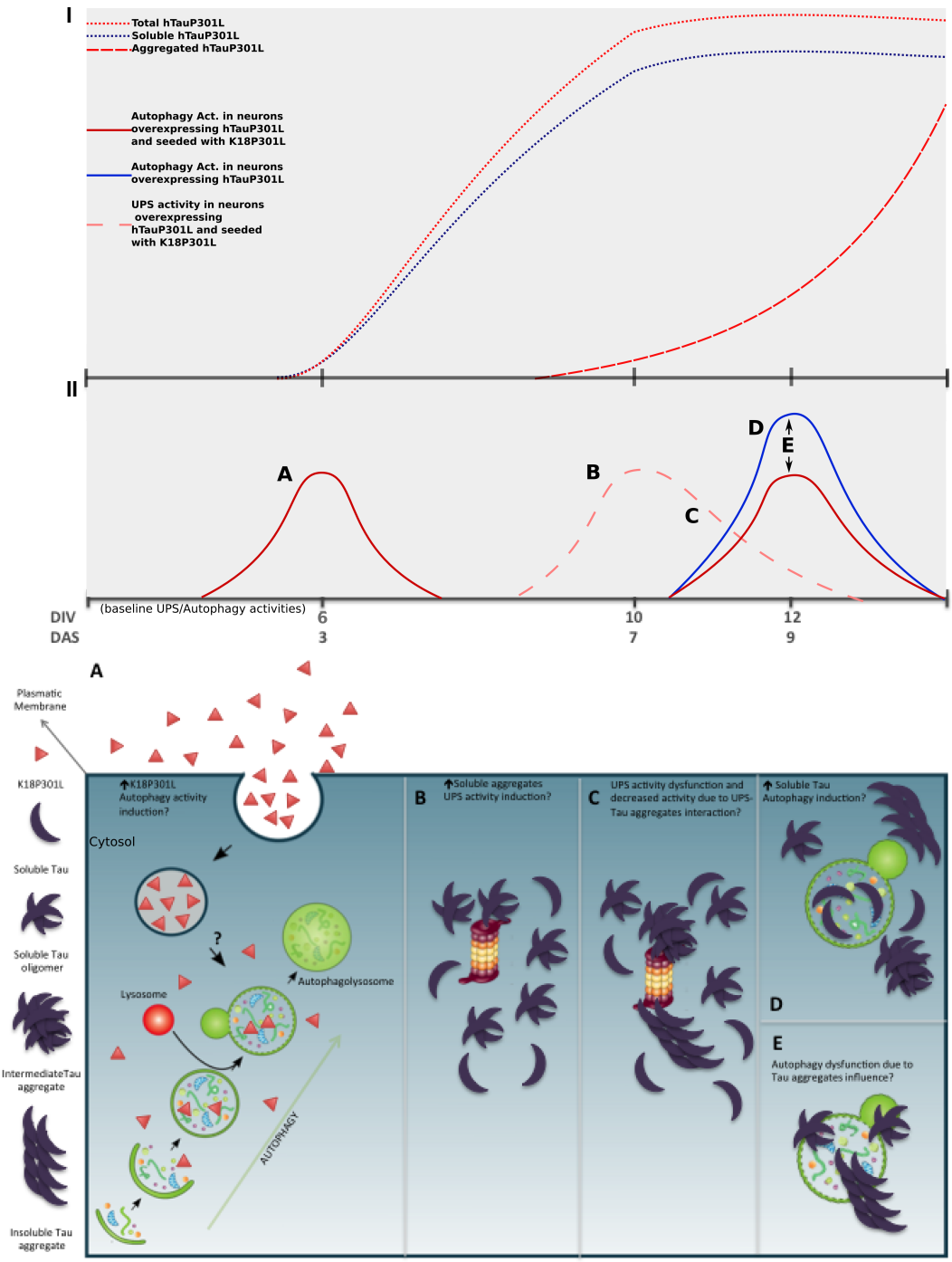

Figure 45: Hypothetical model of hTauP301L interplay with the UPS and autophagy in primary neurons. I) Representation of hTauP301L soluble, total and aggregated levels along time based on the alphaLISA results 3.2.2.1.. Total is represented with higher levels then soluble due to the epitopes shielding hypothesis. II) Representation of the UPS and autophagy activities along time based on the results 3.2.3. and 3.2.4. UPS activity of neurons in non-aggregative conditions is absent on the model as it remained on baseline levels along the studied temporal window. a) Autophagy induction in neurons overexpressing hTauP301L, can be observed upon seeding with K18P301L already on the 3DAS. Such induction is intriguing and we hypothesize whether such induction is a direct response against the K18P301L incubation. Indeed, the uptake of *in vitro* pre-aggregated Tau fibrils has been shown to be regulated by non-receptor mediated endocytosis [260, 261]. Wu et al. suggested that in HeLa cells the internalized aggregates are transported via endosomal vesicles and trafficked through the endosomal pathway to lysosomes [261]. Therefore, these aggregates can be forwarded to lysosomes and be immediately degraded by autophagy-lysossomal system. b) UPS induction in neurons in aggregative conditions can be observed on the 7DAS. When linking this UPS activity profile with the aggregation alphaLISA curve, it can be observed that this 7DAS proteasome activity peak in neurons in aggregating conditions corresponds to the 10DIV and, therefore, the day that a statistical significant hTauP301L aggregation increase can be detected by the alphaLISA (Material and Methods 2.8.). Considering the progression of amyloid aggregation that goes from soluble dimers and oligomers towards insoluble aggregates [163] and that those levels should change in function of the other, by the 10DIV its likely that the ratio between soluble hTauP301L forms and insoluble hTauP301L entities on this time-point would indicate higher levels of soluble hTauP301L in comparison to the insoluble fraction. Therefore, in the 7DAS (10DIV), UPS induction might be related to soluble hTauP301L species. c) For the next few days *in vitro* in our model, the chymotrypsin-

↵**Figure 45 (continuation):** like UPS activity of neurons in aggregative state displayed a gradual decline to baseline levels (wild-type neuronal UPS activity). By analysing the hTau10/hTau10 alphaLISA and AT8 western blot (Material and Methods 2.7. and 2.8.) data on such time-point (corresponding to 12DIV), hTauP301L aggregation levels are already significantly increased when measured by alphaLISA, and statistical significant differences between neurons in aggregative conditions and non-aggregative conditions can be seen by AT8 probing western blotting (data not plotted on the model; see results 3.2.2.3.). Importantly, this difference correlates to the appearance of a higher molecular weight migrating band that, in our *in vitro* model, seems to be related to the hTauP301L hyperphosphorylated insoluble fraction [166]. It is known that aggregated and/or truncated proteins *per se* can impair proteasome functioning [215, 254, 255, 257], specifically NFTs [215], and truncated Tau species have been associated to chymotrypsin-like proteasome activity suppression [255]. Therefore, increasing levels of hTauP301L insoluble aggregates and/or higher nature soluble hyperphosphorylated hTauP301L conformations could be related to a partial blockage and/or dysfunction of the UPS, leading to a decrease of the UPS activity to the baseline levels (wild-type neurons). d) When focusing on the last days of the experiment, the autophagy induction in neurons overexpressing hTauP301L and not seeded with K18P301L on the 9DAS and 10DAS that is higher than in neurons in aggregative conditions together with the observation that in our *in vitro* model on the 9DAS and 10DAS (12DIV and 13DIV) soluble hTauP301L levels are on their highest levels in a plateau phase, as assessed by alphaLISA (Results 3.2.2.1., Figure 25a), it is plausible that high overexpression levels of soluble hTauP301L might be triggering autophagy in such time-point. Indeed, soluble Tau has been linked to autophagical degradation [197]. e) When inspecting neurons in aggregative conditions (i.e., in the presence of K18P301L) there is a shift to lower levels but still significant autophagy levels in comparison to neurons overexpressing hTauP301L not seeded with K18P301L. Additionally, on the 9DAS (equivalent to 12DIV) on the AT8 western blot time-course a difference between samples from neurons overexpressing hTauP301L in aggregative conditions non-aggregative conditions that seems to correlate to the appearance of a higher molecular weight migrating band possibly related to the hTauP301L insoluble fraction [166] was observed. Considering that autophagical dysfunction with autophagolysossomes accumulation is present in AD brains with Tau pathology [259], several others neurodegenerative proteinopathies display lysosome-related dysfunctions [262], Tau pathology has been associated to oxidative stress, and that Tau may also induce lysosomal rupture and consequently autophagical dysfunction with lysosome enzymes leakage, It is possible that the presence of the soluble and/or insoluble aggregates could be leading to diminution in autophagy levels when comparing neurons in aggregative conditions to non-aggregative conditions.

rupture and consequently autophagical dysfunction with lysosome enzymes leakage (e.g. cathepsins) to the cytosol, which in turn could work as a positive feedback for Tau aggregation due to truncated Tau forms formation. Additionally, Tau pathology has been associated to oxidative stress which in turn leads to mitochondria dysfunction and less ATP production [265], which would likely influence vacuolar H(+)-ATPase that is responsible for the acidification of the lysosomes. Considering such background, a possible net outcome of Tau pathology could be lysosomal and autophagy dysfunction due to less acidification of the lysosomes. Therefore, it is possible that soluble hTauP301L might be related to autophagy induction and hTauP301L aggregates dysfunctional autophagy (Figure 45). Consequently, to address the soluble Tau degradation by autophagy hypothesis, the use of the same adeno-associated viral delivery of hTauP301L but with hTauP301L tagged with red fluorescent protein with a posterior autophagy probing with the same Cyto-ID® Autophagy detection reagent (Material and Methods 2.11.) could be used to check for co-localization of hTauP301L and the autophagolysossomes by live imaging and hence confirmation of this possible interaction. For the possibility of Tau aggregation induction of lysosome dysfunction, a comparison between neurons in aggregative state and non-aggregative state could be done making use of a pH sensitive probe (e.g., LysoSensor Green DND-189 probe, Molecular Probes Inc.) that would allow one to compare lysosome function in both cases. Of note is that repeating the discussed time-course including two other additional controls to assure the specific effect of hTauP301L overexpression and aggregation on activity of autophagy would be important. The following controls would be adequate: primary neurons transduced with a AAV6 adeno-associated virus leading to overexpression of other protein unrelated to Tau in the absence and the same neurons seeded with K18P301L. Lastly, to further confirm such time-course results they could be repeated with another read-out, for instance by immunocytochemistry detecting LC3-II levels (which would also allow for co-localization inspection of hTauP301L and autophagy vacuoles) or by LC3-II probing western blot.

Compelling evidence for significant and extensive interplay between the autophagy and proteasomal systems has been highlighted recently [214]. Consequently, intriguing implications for disease processes and specifically Tau degradation in Tauopathies emerged. In view of the updated scientific opinion that autophagy

and UPS have substrate specificity, a particular substrate that under normal conditions may be degraded by the proteasome, in the moment that this system is impaired and/or there is an excess of that substrate present, it may be degraded in a compensatory manner by autophagy [214]. Additionally, post-translational modifications can lead to shuttling of a particular substrate from one degradative pathway to the other. Indeed, Tau, as a monomer, it is natively unfolded and hence a likely a proteasomal substrate, however when oligomerized or aggregated Tau might be preferentially degraded by autophagy. This is supported by evidence that full-length Tau, is cleared by the UPS while caspase-cleaved Tau, which is more aggregate prone, goes through autophagy [266]. Also, aggregated Tau can be cleared by inducing autophagy [197, 267]. We therefore investigated soluble, total and aggregated hTauP301L degradation in neurons *in vitro* using three complementary pharmacological approaches. Hence, MG132, a potent reversible proteasome inhibitor [224] that is also known to induce autophagy [225]; Lactacystin, an specific and irreversible proteasome inhibitor [224]; and Rapamycin, a canonical allosteric inhibitor of the mammalian target of rapamycin (mTOR) kinase that strongly induce autophagy *in vitro* [226] were chosen. By chosing such compounds, we could isolate the specific contribution of an inhibition of the proteasome alone (lactacystin treatment) and the specific contribution of an activation of autophagy alone (rapamycin treatment) in the hTauP301L aggregation, as well as, these two factors acting together in the hTauP301L aggregation *in vitro* (MG132 treatment). As Tau overexpression and aggregation as well as autophagy and UPS activities are strongly temporal dependent as seen by time-course results, five time-points were chosen to treat the neurons: -1DAS, 0DAS, 3DAS, 4DAS and 7DAS. Consequently, based on our data, hTauP301L soluble, total and aggregated levels upon an early inhibition of the UPS or inhibition on its highest induction peak on our time-course – 7DAS (Results 3.2.3.) – was addressed. Regarding autophagy, we aimed at a very early activation before its induction observed in time-course - -1DAS and 0DAS -, sustained activation of its first peak – 3DAS and 4DAS – and induction right before its second peak and in the UPS highest peak – 7DAS (autophagy induction on the time course was seen on the 9DAS and UPS on the 7DAS; Results 3.2.3. and 3.2.4.).

By our alphaLISA (Material and Methods 2.8.) results it is clear that hTauP301L is not mainly degraded by the UPS. In fact, when inhibiting specifically the 20S catalytic core of the proteasome, hTauP301L soluble, total and aggregated levels were not increased (Results 3.3.). Instead, only unexpected decreases on the soluble (treatment with 500nM and 100nM) levels were observed when neurons were treated with lactacystin on the 4DAS when comparing to DMSO treated neurons (Results 3.3.2.1.; Figures 37a). Interestingly, although lactacystin is a specific inhibitor of the UPS, it has been shown to induce the activation of caspase-3 [268, 269] and caspase-6 [269] in cell lines. Importantly, there are evidences that Tau is cleaved in the C-terminus by several caspases including caspase-3 and caspase- 6 [270-272]. Caspase-6 was also shown to cleave the N-terminus of Tau *in vitro* [273]. More recently, Dolan and Johnson experimentally showed that cleaved forms of Tau are preferentially degraded by autophagy [266]. Consequently, such caspases might be involved in the degradation of soluble hTauP301L or might be leading to the shuttling of hTauP301L to autophagy degradation. It is important to notice that the 4DAS lactacystin treatment was performed only once and with low number of replicates (n=4), hence it should be repeated. It would be important to check in these conditions the levels of hTauP301L by phospho-dependent and independent antibodies to understand what hTauP301L species is degraded; the immunoreactivity of total ubiquitin and/or of Ser33/37- Thr41-phosphorylatedβ-catenin (a well-known UPS substrate) to further confirm the UPS inhibition; and lastly the

LC3-II levels to check a possible involvement of autophagy in such degradation by western blotting. In case of confirmation of the discussed results, a simultaneous treatment with lactacystin and caspase inhibitors could be tested to assure the caspase role in this context.

Further confirming the observation that the UPS does not seem to be the main degradative pathway for hTauP301L in our neuronal *in vitro* model, are the MG132 treatments results. By inspecting the alphaLISA (Material and Methods 2.8.) measurements, effects on hTauP301L levels could only be observed on the 4DAS and 7DAS MG132 treatments (Results 3.3.2.2. and 3.3.2.3.; Figures 37 a; b and c; and 38 a; b and c). MG132 neuronal treatment when comparing to DMSO treated neurons at 4DAS lead to reduction on soluble and total hTauP301L levels with all MG132 concentrations tested, but no difference could be seen in the aggregated levels with the exception of the 100nM MG132 treated neurons in which an increase was observed. However, considering the HT7/hTau10 total and soluble results of the 4DAS MG132 treatment where hTauP301L reductions were seen, for all concentrations – 100nM, 50nM and 10nM -, the alphaLISA data on the MG132 neuronal treatments on -1DAS, 0DAS, 3DAS where no effect could be observed for any of the concentrations and conditions tested and the 7DAS where soluble hTauP301L reductions were seen for the treated neurons with 100nM and 50nM, this panorama strongly suggests that the increase on the 100nM concentration mentioned before is an artefact, possibly related to the alphaLISA assay (Material and Methods 2.8.) and/or measurement. On the other hand the soluble and total hTauP301L differences on this 4DAS treatment, suggest that the reduction in the total hTauP301L levels are consequence of a reduction in the soluble hTauP301L levels as the hTauP301L aggregation levels were not overall altered. On the MG132 neuronal treatment on the 7DAS (Figures 38 a; b and c), similar results to the discussed above were observed, where soluble hTauP301L reductions were observed for the tested MG132 concentrations (100nM and 50nM). Reductions can also be observed in the total levels of the hTauP301L (neurons overexpressing hTauP301l in the presence of K18P301L), which were likely a reflection of the soluble hTauP301L signal reduction described above. Regarding levels of aggregated hTauP301L there are significant differences when comparing the compound treatments with 50nM and 10nM final concentrations when comparing to neurons treated with the vehicle, however, as 100nM of MG132 treatment of neurons showed no statistical difference in comparison to the DMSO treated neurons and as there is a higher reduction in the treatment with the lowest MG132 concentration, such results are likely to account for a random biological variation or a technical artefact. Interestingly and agreeing with our data is that upon MG132 treatment, overexpressed mutant Tau ΔK280 (FTDP-17 mutation) degradation was observed in neuroblastoma N2a cell line [197]; full-length Tau degradation was described in immortalized CN1.4 mouse cortical neurons (CN) that stably express full-length Tau (containing four microtubule repeats and no N-terminal inserts) and endogenous soluble Tau degradation has also been previously described in human neuroblastoma SH-SY5Y cell line [274] and rat primary cortical neurons [197]. Of particular notice is that MG132 has been associated to autophagy induction [225] and, indeed, it seems that in our *in vitro* model it increases the LC3-II levels (Results 3.3.1.) and induces autophagy (assay controls of Results 3.2.4.). Interestingly, MG132 has been linked to the transcription factor nuclear factor-erythroid 2-related factor 2 (Nrf2) - a transcription factor activated in response to oxidative stress - upregulation in mice [275]. Additionally, in an interesting recent study, Chulman et al. observed that nuclear dot protein 52 kDa (NDP52), which is an autophagy adaptor that contains an LC3-interacting region (LIR), is induced by Nrf2 and seems to play an important role in directing Tau,

particularly phosphorylated Tau, to the autophagic degradative pathway [241]. These observations were made by a combination of strategies and correlating results form human AD brain samples, rat primary cortical neurons, mouse cortical CN1.4 immortalized cells and *in vivo* wild-type and knockdown Nrf2-/- C57BL/6J mice [241]. Of particular note is that MG132 was shown to lead to increased levels of forkhead O (FOXO) transcription factors, and these transcription factors are linked to oxidative stress responses [276] and in neurons to autophagy induction [190]. Hence, it would be of interest to check whether FOXO transcription factors and/or Nrf2 are upregulated in our MG132 treatments and, if so, to address the questions whether MG132 is leading FOXO-mediated autophagy induction and/or to Nfr2 mediated hTauP301L or phospho-hTauP301L autophagical targeting in our experimental settings. In light of this possible phosphorylation-dependent Tau degradation, it would be also important to perform an alphaLISA in order to detect hTauP301L soluble, total and aggregated phospho-dependent levels by the use of different antibody sandwiches (e.g., for soluble and total HT7/AT8 and aggregated AT8/AT8 sandwiches) in the experimental settings discussed above. It would be important to include in such experiment samples for western blot to check for the levels of hTauP301L by phospho-dependent and independent antibodies to confirm hTauP301L degradation; the immunoreactivity of Ser33/37- Thr41-phosphorylatedβ-catenin (a well-known UPS substrate) or to total ubiquitin to further confirm the UPS inhibition and lastly the LC3-II levels to confirm the possible involvement of autophagy in such degradation. It is important to notice that the treatments at 4DAS and 7DAS were done once and with a low number of replicates (n=4), different from the treatments on -1DAS, 0DAS and 3DAS that were performed twice each with an n=8 per experiment. Hence, to further confirm the alphaLISA results on the 4DAS and 7DAS, it would be important to repeat the experiments with higher number of replicates.

Corroborating our hypothesis that autophagy is related to hTauP301L degradation in neurons *in vitro* are the rapamycin treatments data (Results 3.3.3.3.). Interestingly, rapamycin neuronal treatment only on the -1DAS significantly reduced soluble, total and aggregates phospho-independent levels for almost every rapamycin concentration tested when in comparison to DMSO treated neurons with the exception of 0.0001μM for total and soluble levels (Figures 42a; b and c). Such data further emphasizes the link between soluble Tau and aggregation in our experimental settings and it is in agreement with the fact that in Tau aggregation, modulating the aggregation substrate results in aggregation levels modulation [163]. It is important to highlight that in addition to the soluble levels reduction, K18P301L clearance upon its uptake is likely to be accounting for the reduced levels of aggregation as well. Indeed, Eisenberg and Jucker previously described that the amount of this fribrilogenic material is proportional to the aggregates levels formation and speed of formation in amyloid aggregation systems [244]. Additionally, if one analyses the data of the autophagy time-course upon K18P301L seeding, it can be observed an early autophagical induction peak on the 3DAS, hence it is possible that inducing autophagy even before the seeding may have rendered, upon K18P301L uptake by endocytosis, in direct targeting of the K18P301L seeds to the autophagic-lysosomal pathway, as previously described in HeLa cells [261]. Performing the indirect ELISA time-course previously mentioned when discussing the autophagy time-course results should indicate whether such premise is true or not. Despite that, autophagy degradation of endogenous Tau in rat cortical primary neurons was indeed observed upon trehalose autophagy induction [197]. Aggregated oveerexpressed mutant Tau ($Tau_{RD}\Delta K280$) was also shown to be cleared by autophagy in N2a cell Tet-On induclible cell model [41]. Additionally,

rapamycin has been previously shown to attenuate the progression of Tau pathology in P301S Tau transgenic mice [277]. Interestingly, in an *in vivo* parallel paradigm of our early *in vitro* rapamycin treatment (on the -1DAS), Majumder and collegues showed that inducing autophagy by rapamycin in 3xTg-AD mice before, but not after, the formation of plaques and tangles ameliorates cognitive deficits [278]. Altogether, these data suggests that autophagy induction via rapamycin may represent a valid therapeutic strategy in Tauopathies when administered early in the disease progression. Despite that, it would still be valid to repeat this experiment with the treatment time-points of 4DAS and 7DAS as in such moments, treatments with MG132 and Lactacystin resulted in soluble hTauP301L reductions. An important observation is that autophagy is up regulated upon oxidative stress [279, 280] and oxidative stress is interlinked with Tau pathology [265]. Indeed, it was previously shown that the cells overexpressing Tau protein had increased susceptibility against oxidative stress, perhaps due to the depletion of peroxisomes [281] and that in cortical neurons derived from a transgenic rat model expressing a human truncated variant form of Tau protein, it was observed that the levels of ROS were increased when compared to control nontransgenic neurons [265]. In addition to that, advanced glycation end-products (AGEs) are found in AD brains associated with NFTs and when AGE-recombinant Tau was introduced into the cytoplasm of SH-SY5Y neuroblastoma cells, oxidative stress was induced [282]. Hence, it would be interesting to address in our *in vitro* model whether oxidative stress is present and if so whether the FOXO and/or if the Nrf2 transcription factors, that are related to such kind of stress, are upregultated because, as mentioned above, such signalling molecules are related to autophagy induction and phospho-Tau targeting to autophagy, respectively. Consequently, in our model, upon treatment with rapamycin, such mechanisms might render a positive feedback loop further enhancing Tau targeting to autophagy and its degradation. Lastly, focusing on rapamycin's specific means of action, it is important to highlight that this compound is a canonical allosteric inhibitor of mTOR kinase which in its turn functions as nexus of protein kinase signalling, receiving inputs from numerous upstream signalling pathways and delivering instructions to a variety of downstream kinases, such as cAMP-dependent protein kinase (PKA) [283], Akt [284], glycogen synthase kinase-3b (GSK-3b) [285], cyclin-dependent kinase (CdK) [286] and mitogen activated protein kinases (MAPKs)[287] and mTOR inhibition culminates in autophagy induction [279]. Importantly, the PI3K/Akt/mTOR signalling pathway have been shown to regulate Tau phosphorylation at many sites by controlling the GSK-3-dependent phosphorylation of Tau [288-290] and rapamycin have been linked to decreased Tau phosphorylation at Ser214 through regulation of cAMP-dependent kinase [291]. In fact excessive activation of mTOR can also induce the occurrence of Tau-phosphorylated proteins in the hippocampal tissue of rats with type 2 diabetes and that models AD [292]. Importantly, a link between Tau phosphorylation, by GSK3, and the formation of Tau aggregates has been established in certain mouse models [92, 293]. Therefore, it is also conceivable that rapamycin might modulate Tau aggregation kinetics *in vitro* by influencing Tau phosphorylation levels. Therefore, a simultaneous treatment with rapamycin and autophagy inhibitors could be tested to check for the hypothesis that rapamycin may also be attenuating the process of hTauP301L hyper-phosphorylation by modulation of MAPK signalling as well as probing the phosphorylation levels of known Tau-related kinases by western blotting. In light of these possible phosphorylation-dependent Tau outcomes, it would be important to perform an alphaLISA in order to detect hTauP301L soluble, total and aggregated phospho-dependent levels by the use of different antibody sandwiches (e.g., for soluble and total HT7/AT8 and aggregated AT8/AT8 sandwiches) in the experimental settings discussed above to check the influences of this compound on

phospho-Tau species. It would be important to include in such experiment samples for western blot to check for the levels of hTauP301L by phospho-dependent making use of antibodies that detect different Tau phosphorylation epitopes (e.g., AT8, 12E8 and PHF1 antibodies, that detects hTau phosphorylated at Ser202/Thr205 [206], Ser262/Ser356 and Ser396/Ser404, respectively [241]) providing a more broad view of the subject, and independent antibodies to confirm hTauP301L degradation. Additionally to that, it would be important to check for the immunoreactivity of Ser33/37- Thr41-phosphorylatedβ-catenin (a well-known UPS substrate) or total ubiquitin to further confirm the UPS inhibition and lastly the LC3-II levels to confirm the involvement of autophagy in such degradation. Finally, autophagy inhibitors, such as chloroquine that inhibits an overall autophagic degradation, and 3-Methyladenine (3-MA) that inhibits autophagolysomes formation that is related to macroautophagy could be used to get insights into which autophagy process (see Introduction 1.5.2. for more details) is more related to hTauP301L levels control.

In summary, this pharmacological approach display soluble hTauP301L reduction when the UPS is inhibited and autophagy functional (lactacystin treatment), soluble hTauP301L levels reduction when UPS is inhibited and autophagy induced (MG132 treatment) and soluble and aggregated hTauP301L reduction when the UPS is functional and autophagy enhanced (rapamycin treatment) – Figure 46. Therefore such data underscores a role of autophagy in hTauP301L soluble and aggregates build-up in primary neurons. Indeed the data discussed here show that an early, when hTauP301L overexpression levels are still low and before aggregation induction (on the -1DAS), autophagy induction by rapamycin is able to reduce hTauP301L soluble, total and aggregates levels. Explanations for that outcome might come from the sum of autophagy induction with a possible K18P301L seeds efficient clearance due to the early treatment time-point, as well as, from a modulation of hTauP301L phosphorylation levels that could influence the hTauP301L aggregation kinetics. However, such data also highlights that autophagy was only able to effectively reduce hTauP301L aggregates levels when in presence of a functional UPS (Figure 46). Therefore, although our data points-out to autophagy as a central player in soluble hTauP301L clearance *in vitro*, they might also suggest that, in our experimental settings, UPS might be secondary, but still only on its functional presence a reduction in aggregates could be seen. Therefore, in these settings, UPS might be related to soluble hTauP301L clearance that summing up to the autophagy effects influenced the hTauP301L aggregates by substantially reducing their aggregative substrate, or could even be working directly on hTauP301L aggregates levels. Hence, in addition to the complementary experiments suggested above, it would be interesting to check the effect of an activation of the UPS in the soluble and aggregated hTauP301L levels in the presence of functional autophagy, induced autophagy and inhibited autophagy. When the amounts of intracellular abnormal proteins are increased, the 20S catalytic core of the UPS can assemble with proteasome activators (PA) and recently it was demonstrated that gene transfer of the PA subunits of the UPS can enhance abnormal protein degradation leading to improved function and survival of cells in Huntington's disease [294]. Hence, the overexpression of the proteasome activator (PA) subunit PA28 or PA700 could provide a good paradigm to study the effect of UPS activation in the hTauP301L *in vitro* levels.

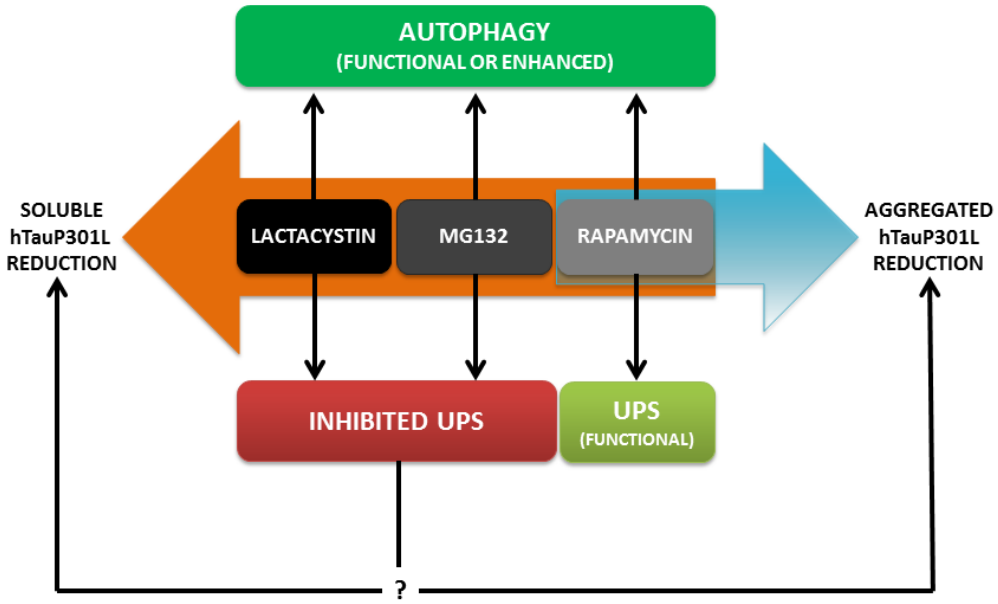

Figure 46: Schematic summary of the pharmacological treatments of rat cortical primary neurons. By this pharmacological approach it could be observed soluble hTauP301L reduction when the UPS is inhibited and autophagy functional (lactacystin treatment), soluble hTauP301L levels reduction when UPS is inhibited and autophagy induced (MG132 treatment) and soluble and aggregated hTauP301L reduction when the UPS is functional and autophagy enhanced (rapamycin treatment). This data underscores an autophagical role in soluble hTauP301L clearance, but also highlights the fact that hTauP301L aggregates were only reduced in the presence of a functional UPS. Therefore, is UPS related to such results? If so, is it clearing hTauP301L soluble and thus decreasing the aggregative substrate or is it directly acting on hTauP301L aggregates?

As mentioned above, a microarray exercise from the host laboratory in which compared primary neurons overexpressing hTauP301L and neurons overexpressing and aggregating hTauP301L identified genes which expression was altered due to Tau seeding. Of particular notice is that some of these genes are known to be related to the UPS and autophagy systems (data not shown). Moreover, previous experiments from our group identified that deubiquitinating enzymes (DUBs) interact with Tau in mouse brain, namely the DUBs OTUB1, USP5 and USP7 [11]. As a consequence, they stood out as possible targets to manipulate and in this way affect levels of aggregated Tau. A set of lentiviruses that encode shRNAs to downregulate each of the targets, with different but target-specific sequences, were used (Table 1) in order to assess the role of these DUBs in clearing human Tau *in vitro*.

Our results show that the overall phenotype displayed by treatments with different shRNAs targeting OTUB1 and USP5 point to no significant reductions on hTauP301S. Indeed, only two out of five shRNAs targeting OTUB1 (OTUB1 shRNA #2 and #4) and only one out of three shRNAs targeting USP5 (USP5 shRNA #2) displayed hTauP301L reductions (Results 3.4.3.; Figures 44 a; b; c; d; e; f; g; h and i). Hence, such positive results are likely to account for off-target effects on hTauP301S levels. As a consequence one cannot conclude that the downregulation of OTUB1 and USP5 have a specific effect on hTauP301S levels. Importantly, OTUB1 was previously identified as a K48 linkage-specific deubiquitinating enzyme [192] and indeed biochemical analysis revealed that OTUB1 has a preference for cleaving K48-linked polyubiquitin chains over K63-linked polyubiquitin chains [295]. Such results strongly suggest that this DUB

enzyme is related to positive regulation of proteins by editing their K48-linked polyubiquitin chains and hence inhibiting their targeting to the proteasome (K48-linked polyubiquitin chains are canonical signals to protein targeting to UPS; see Introduction 1.5.1.). Interestingly, Tau and NFTs has been previously associated to K48-linked polyubiquitin chains [296] and its interaction with OTUB1 showed in previous experiments from the host laboratory [11] suggested a possible involvement of this DUB in inhibiting Tau targeting to the UPS. As previously discussed in the pharmacological approach, UPS does not seem to be pivotal in degrading hTauP301L in our primary neurons *in vitro* model of hTauP301L aggregation and overexpression. Interestingly and agreeing with such data, even downregulating OTUB1, hTauP301S seems not to have its levels altered, which might suggest that it is not being targeted to the UPS. Although such premise is conceivable, this data might reflect a functional redundancy between OTUB1's and other DUBs or even that OTUB1 interaction with Tau might be related to functions other than deubiquitination as it was previously described for the OTUB1 p53-mediated stabilization and activation *in vitro* [297]. Although five (5) shRNAs against OTUB1 were used which strongly suggests that the Tau-related phenotype observed is related to OTUB1 downregualtion, to confirm such results this experiment should be repeated as it was only performed once including a western blot to check OTUB1 protein levels and a real-time PCR to assess OTUB1 mRNA expression levels to compare with neurons not transduced with the lentivirus encoding the shRNA and assure the downregulation of OTUB1. Despite these results, it would still be important to address whether the overexpression of OTUB1 in primary neurons could lead to hTauP301L and/or hTauP301S soluble, total and aggregates levels increase due to polyubiquitin chain editing and stabilization of hTauP301L protein. OTUB1 has been recently shown to positively regulate p53 levels in a non-canonical way (not related to its deubiquitinating functions) [297, 298] and to be localized within the nucleus in porcine derived cell line PK-15 [299]. Interestingly, p53 activation when in the nucleus has been shown to transactivate pro-autophagic genes [300]. Hence it would be also of interest to address whether the overexpression of OTUB1 in primary neurons could lead to autophagy induction and hTauP301L and/or hTauP301S levels reduction in rat primary neurons overexpressing hTauP301L and in Ps19hTauP301S Tg mice primary neurons respectively. If so, assessing the involvement of p53, FOXO and Nrf2 transcription factors on such process could point out to the signalling pathways involved in such scenario and hence interesting insights on the subject could be highlighted.

USP5 most characterized function is to recognize and recycle the unanchored polyUb chain to keep the free Ub pool stable *in vivo* [301]. The K63-, K48-, K11-, K29- linked and linear polyUb chains are all hydrolyzed by USP5 [301]. As mentioned above Tau and NFTs has been previously associated to K48-linked polyubiquitin chains [296] and its interaction with USP5 showed in previous experiments from the host laboratory [11] suggested a possible involvement of this DUB in regulating Tau levels. Indeed, due to its catalytic nature and shown interaction with Tau, USP5, could be stabilizing Tau by removing K48-linked chains from this protein, or could be regulating Tau targeting both, to UPS or to autophagy by editing the polyubiquitin chains attached to Tau. Besides, an effective turnover of the polyUb chains by USP5 logically should favour the ubiquitination of several proteins, including Tau, by increasing the availability of free Ub substrate. Interestingly, our results indicate that USP5 downregulation does not seem to influence hTauP301L overall levels, which is highlighted by the fact that only one out of three shRNA targeting USP5 (USP5 shRNA #2) led to decreased levels (soluble, total and aggregates) of hTauP301S *in vitro*. Considering a

hypothetical panorama in which the interaction of USP5 stabilizes Tau, one possible explanation for the lack of hTauP301S degradation when USP5 is ablated could be a similar mechanism that was proposed by Dayal et al, for the p53 not degradation in the absence of USP5 [171]. In their work, it was proposed a model in which the free polyubiquitin chains that accumulate as a result of the lack of USP5 catalytic function could compete with p53 as a substrate for the UPS and hence p53 degradation would be affected [171]. Therefore, in the hypothetical panorama that USP5 stabilizes Tau, the downregulation of USP5 could render in increased levels of polyubiquitin free chains that would compete with Tau as an UPS substrate and consequently the negative results obtained could be a possible outcome. Additionally, it was recently demonstrated that in *Drosophila* deleting USP5 gene led to JNK MAPK pathway activation [184] and suppression of USP5 in human melanoma-derived cell lines induced p53 activation [171]. Interestingly, JNK has been reported as a potent negative regulator of FOXO-dependent autophagy in neurons [190], and p53 activation is associated to autophagy suppression and induction dependent on its subcellular localization [300]. Hence it would be of interest to assess JNK, FOXO and p53 activation levels as well as p53 localization in our USP5 knockdown model, as they might be related to the negative results observed. Additionally, one cannot exclude that other DUBs could have overcome the downregulation of USP5 due to a functional redundancy between them. However, as USP5 is believed not to prematurely deubiquitinate a polyubiquitinated protein [182], the nature of the USP5 interaction with Tau might not be related to its USP5's catalytic capacity (deubiquitination functions) and hence with Tau targeting to the UPS and/or autophagy degradative systems. Indeed, considering such information its interaction with Tau is likely to be a more complex protein-protein interaction that remains to be elucidated. Of particular notice is that this experiment was only performed once it would be important to repeat it including a higher number of shRNAs targeting USP5 to have a better power of analysis to identify possible off-target effects on Tau; a western blot to check USP5 protein levels and a real-time PCR to assess USP5 mRNA expression levels to compare with neurons not transduced with the lentivirus encoding the shRNA to assure the downregulation of USP5. However, it is very likely that the results observed indeed reflect USP5's downregulation effects as the efficacy of those three (3) shRNAs were previously tested in N2a cells (data not shown). In case of different and positive results, the co-localization of LC3-II and hTauP301S and the co-localization of proteasome 20S C2 subunit and hTauP301S by immunocytochemistry could be performed to try to understand by which of the systems Tau levels are being influenced. Additionally, another paradigm that should be tested is the overexpression of USP5 in primary neurons. An overexpression of USP5 could possibly increase the turnover of polyUB chains, increasing the availability of free UB substrate and hence it could favour the ubiquitination of several proteins, including Tau. Such possible Tau ubiquitination could target it both to UPS or autophagy depending on the ubiquitin chain added to it (see Introduction 1.5.). If that would be the case, it would be interesting to check whether USP5 overexpression could favour the appearance of K48-linked polyubiquitin chains or K63-linked polyubiquitin chains (or even others) by western blot in addition to the alphaLISA hTauP301S assessments, USP5 western blot levels mentioned for the repetition of the knockdown paradigm, as well as the co-localization of LC3-II and hTauP301S and the co-localization of proteasome 20S C2 subunit and hTauP301S by immunocytochemistry to check which of the proteolitic systems were related to such hypothetical results.

USP7 is a cysteine protease that was originally identified as a binding partner for the Herpes simplex viral (HSV) protein infected cell protein 0 (ICP0/Vmw110) [187]. Afterwards, numerous proteins have been identified as potential substrates/binding partners of USP7, which play crucial roles by controlling their ubiquitin levels, for instance, in tumour suppression, DNA repair, immune responses, viral replication, and epigenetic control [187]. Indeed, as mentioned above, previous experiments from the host laboratory identified that deubiquitinating enzymes (DUBs) interact with Tau, amongst them USP7 [11]. Interestingly, in our study, USP7 downregulation by both shRNAs used (Table 1) displayed similar hTauP301S phenotypes with increases in the hTauP301S aggregates levels (Results 3.4.3.; Figures 44 j; k and l), which suggests a possible involvement of this DUB in hTauP301S aggregation levels modulation. It is important to highlight that because of the reduced number of shRNAs targeting USP7 used it is difficult to exclude possible off-target effects. However, the downregulation potency of these two shRNAs had been previously confirmed in N2a cells (data not shown). Interestingly, USP7 has also been linked to regulation of important autophagy-related proteins, namely phosphatase and tensin homologue (PTEN), FOXO transcription factors and p53 [187]. Indeed, monoubiquitination was shown to control PTEN and FOXO subcellular localization [187]. Specifically, monoubiquitinated PTEN and FOXO translocate to the nucleus and USP7 antagonizes this nuclear localization by deubiquitinating these proteins and it was suggested that inhibition of USP7 could lead to nuclear accumulation of these proteins [187]. Remarkably, PTEN reduction levels were shown to be correlated to AD patient's brains where a dramatically increased concentration of phospho-Tau at Ser-214 in NFTs was found, and in COS-7 cells expressing a PTEN mutant without its phosphatase domain led to Tau aggregation [302]. Therefore, one could hypothesize that knocking-down USP7 might strongly favour PTEN nuclear localization and hence reducing its cytosolic levels, which could in turn could be reflected in Tau aggregation levels. Interestingly, genetic blockage of USP7 seems to result in upregulation of p53 [187]. This tumour suppressor protein has been shown to be upregulated in AD patients brains and it was found to induce phosphorylation of human 2N4R Tau at the Tau-1/AT8 epitope in HEK293a cells [303]. As a consequence, it is conceivable that by ablating USP7, Tau phosphorylation might be induced resulting in a higher aggregation predisposition. PTEN and p53 might be on the onset of the increased aggregation levels observed in our knockdown of USP7 in PS19hTauP301S primary neurons (Results 3.4.3.; Figures 44 j; k and l). Therefore, to address this question it would be important to check for the subcellular localization of PTEN and p53 activation upon USP7 knockdown while controlling hTauP301L phospho-dependent and independent levels. Another interesting fact is that USP7 is activated by Pin1, which is altered in AD and co-localizes with Tau in the same disease [304]. USP7 Pin1-mediated activation culminates in reduced FOXO4 transcriptional activity, likely due to its shuttling to the cytosol that is regulated by the removal of monoubiquitin from FOXO4 by USP7 [187]. Additionally, Pin1 overexpression exacerbated the Tauopathy phenotype in P301L Tau mice [305]. Thus, as FOXO transcription factors are related to autophagy induction in neurons [190], it is possible that such Pin1 FOXO4-dependent localization mechanism might be antagonizing autophagy induction in addition to its Tau isomerization functions that might be exacerbating the pathological condition in the presence of mutated Tau. Hence, it would be of particular interest to assess in our knockdown model the subcellular localization of PTEN as already mentioned and Pin1, FOXO4, as well as, the co-localization of LC3-II, Pin1 and hTauP301L and the co-localization of proteasome 20S C2 subunit, Pin1 and hTauP301L. These assessments might provide useful mechanistic information that could help in the understanding of hTauP301S levels quantification upon downregulation of USP7. However, as

this experiment was only performed once it would be important to repeat it including a western blot to check USP7 protein levels and a real-time PCR to assess USP7 mRNA expression levels to compare with neurons not transduced with the lentivirus encoding the shRNA to assure the downregulation of USP7, as well as the just mentioned suggestions. Additionally, another paradigm that should be tested is the overexpression of USP7 in primary neurons, in which the same aforementioned assessments (alphaLISA, western blotting and immunocytochemistry) could be performed.

5 CONCLUDING REMARKS

Data accumulated from over the years led to a better understanding of the role of Tau in the pathogenesis of many neurodegenerative disorders [1, 2, 16, 44, 45]. These data highlighted the complex biology of this protein and showed that Tau contributes to toxicity by multiple mechanisms and at different stages of the diseases [1, 2, 16, 44, 45]. Given that increases in aberrant forms of Tau play a role in the neurodegeneration process in tauopathies, there is growing interest in understanding the degradative pathways that remove Tau from the cell, and the selectivity of these different pathways for various forms of Tau. Therefore evaluating the roles of the ubiquitin-proteasome system and autophagy in the clearance of aggregated Tau *in vitro* is of major importance.

Aiming to contribute to such described panorama, in this thesis we optimized a neuronal Tau aggregation cellular model wherein synthetic pre-aggregated fibrils made from recombinant protein (K18P301L) introduced in cell cultures can recruit soluble endogenous Tau into insoluble fibrillar aggregates, making it more suitable for future High Throughput Screens. Such model was then used as a platform to kinetically characterize the UPS and autophagy activities in primary neurons upon Tau aggregation. Interestingly, we show that Tau aggregation induces temporal-dependent UPS and autophagy inductions. We further then validated the role of these degradative processes in Tau clearance by means of use of reference compounds known to inhibit UPS activity and to induce autophagy activity namely: MG132, Lactacystin and Rapamycin. By such pharmacological approach we could observe that autophagy seems to play a pivotal role in clearing soluble Tau species when induced early, before Tau aggregation induction. Our results also suggest that UPS seems to be a secondary mechanism, in Tau clearance, but might be working together with autophagy resulting in aggregates clearance. This hypothesis requires further investigation. Lastly, by knockingdown the deubiquitinating enzymes OTUB1, USP5 and USP7 that were shown to be interacting with Tau in the mouse brain [11], our preliminary results indicate that neither OTUB1 nor USP5 seem to influence Tau levels *in vitro*. On the other hand, USP7 ablation resulted in further Tau aggregation indicating a possible role of such DUB in regulating Tau degradation in primary neurons *in vitro*.

Although this study made an important initial step toward elucidating the role of UPS and autophagy in Tau degradation *in vitro*, further studies that better gauge the contribution of each degradative pathway will be necessary. In view of this observation, *in vitro* studies that can tightly control for variables including Tau modifications and proteolytic pathway function will likely be instrumental due to the complexity of the cellular environment. Fundamentally, a more complete understanding of the differential contribution of various proteolytic and degradative pathways will provide critical opportunities for therapeutically addressing the Tau pathology associated with neurodegeneration in tauopathies.

6 REFERENCES

1. Lee, G. and C.J. Leugers, *Tau and tauopathies.* Prog Mol Biol Transl Sci. **107**: p. 263-93.
2. Lee, V.M., M. Goedert, and J.Q. Trojanowski, *Neurodegenerative tauopathies.* Annu Rev Neurosci, 2001. **24**: p. 1121-59.
3. Williams, D.R., *Tauopathies: classification and clinical update on neurodegenerative diseases associated with microtubule-associated protein tau.* Intern Med J, 2006. **36**(10): p. 652-60.
4. Mizushima, N., *Autophagy: process and function.* Genes Dev, 2007. **21**(22): p. 2861-73.
5. Petrucelli, L., et al., *CHIP and Hsp70 regulate tau ubiquitination, degradation and aggregation.* Hum Mol Genet, 2004. **13**(7): p. 703-14.
6. Wang, Y. and E. Mandelkow, *Degradation of tau protein by autophagy and proteasomal pathways.* Biochem Soc Trans. **40**(4): p. 644-52.
7. Park, C. and A.M. Cuervo, *Selective Autophagy: Talking with the UPS.* Cell Biochem Biophys.
8. Haglund, K. and I. Dikic, *The role of ubiquitylation in receptor endocytosis and endosomal sorting.* J Cell Sci. **125**(Pt 2): p. 265-75.
9. Grune, T., et al., *Tau protein degradation is catalyzed by the ATP/ubiquitin-independent 20S proteasome under normal cell conditions.* Arch Biochem Biophys. **500**(2): p. 181-8.
10. Pritchard, S.M., et al., *The toxicity of tau in Alzheimer disease: turnover, targets and potential therapeutics.* J Cell Mol Med. **15**(8): p. 1621-35.
11. Moechars, D., et al., *Identification of the tau interactome in mouse brain.* Alzheimer's & Dementia: The Journal of the Alzheimer's Association, 2011. **7**(4).
12. Thies, W. and L. Bleiler, *2013 Alzheimer's disease facts and figures.* Alzheimers Dement. **9**(2): p. 208-45.
13. international, A.s.d., *World Alzheimer Report 2009.* World Alzheimer Report, 2009.
14. Organization, W.H., *Dementia: a public health priority.* WHO reports, 2012.
15. Sosa-Ortiz, A.L., I. Acosta-Castillo, and M.J. Prince, *Epidemiology of dementias and Alzheimer's disease.* Arch Med Res. **43**(8): p. 600-8.
16. Buee, L., et al., *Tau protein isoforms, phosphorylation and role in neurodegenerative disorders.* Brain Res Brain Res Rev, 2000. **33**(1): p. 95-130.
17. Arriagada, P.V., et al., *Neurofibrillary tangles but not senile plaques parallel duration and severity of Alzheimer's disease.* Neurology, 1992. **42**(3 Pt 1): p. 631-9.
18. Prince, M., et al., *Ageing and dementia in low and middle income countries-Using research to engage with public and policy makers.* Int Rev Psychiatry, 2008. **20**(4): p. 332-43.
19. Citron, M., *Alzheimer's disease: strategies for disease modification.* Nat Rev Drug Discov. **9**(5): p. 387-98.
20. Perrin, R.J., A.M. Fagan, and D.M. Holtzman, *Multimodal techniques for diagnosis and prognosis of Alzheimer's disease.* Nature, 2009. **461**(7266): p. 916-22.
21. Price, D.L. and S.S. Sisodia, *Mutant genes in familial Alzheimer's disease and transgenic models.* Annu Rev Neurosci, 1998. **21**: p. 479-505.

22. Price, D.L., et al., *Alzheimer's disease: genetic studies and transgenic models.* Annu Rev Genet, 1998. **32**: p. 461-93.
23. Buckner, R.L., J.R. Andrews-Hanna, and D.L. Schacter, *The brain's default network: anatomy, function, and relevance to disease.* Ann N Y Acad Sci, 2008. **1124**: p. 1-38.
24. Imahori, K. and T. Uchida, *Physiology and pathology of tau protein kinases in relation to Alzheimer's disease.* J Biochem, 1997. **121**(2): p. 179-88.
25. Tanzi, R.E., *A genetic dichotomy model for the inheritance of Alzheimer's disease and common age-related disorders.* J Clin Invest, 1999. **104**(9): p. 1175-9.
26. Dartigues, J.F., et al., *Early prevention at public health issue.* J Nutr Health Aging, 2008. **12**(1): p. 84S-5S.
27. Ballatore, C., V.M. Lee, and J.Q. Trojanowski, *Tau-mediated neurodegeneration in Alzheimer's disease and related disorders.* Nat Rev Neurosci, 2007. **8**(9): p. 663-72.
28. Imahori, K., *The biochemical study on the etiology of Alzheimer's disease.* Proc Jpn Acad Ser B Phys Biol Sci. **86**(1): p. 54-61.
29. Conrad, C., et al., *Genetic evidence for the involvement of tau in progressive supranuclear palsy.* Ann Neurol, 1997. **41**(2): p. 277-81.
30. Morris, H.R., et al., *The tau gene A0 polymorphism in progressive supranuclear palsy and related neurodegenerative diseases.* J Neurol Neurosurg Psychiatry, 1999. **66**(5): p. 665-7.
31. Di Maria, E., et al., *Corticobasal degeneration shares a common genetic background with progressive supranuclear palsy.* Ann Neurol, 2000. **47**(3): p. 374-7.
32. Dickson, D.W., *Pick's disease: a modern approach.* Brain Pathol, 1998. **8**(2): p. 339-54.
33. Munoz-Garcia, D. and S.K. Ludwin, *Classic and generalized variants of Pick's disease: a clinicopathological, ultrastructural, and immunocytochemical comparative study.* Ann Neurol, 1984. **16**(4): p. 467-80.
34. Murayama, S., et al., *Immunocytochemical and ultrastructural studies of Pick's disease.* Ann Neurol, 1990. **27**(4): p. 394-405.
35. Iwatsubo, T., M. Hasegawa, and Y. Ihara, *Neuronal and glial tau-positive inclusions in diverse neurologic diseases share common phosphorylation characteristics.* Acta Neuropathol, 1994. **88**(2): p. 129-36.
36. Probst, A., et al., *Pick's disease: hyperphosphorylated tau protein segregates to the somatoaxonal compartment.* Acta Neuropathol, 1996. **92**(6): p. 588-96.
37. Rademakers, R., M. Neumann, and I.R. Mackenzie, *Advances in understanding the molecular basis of frontotemporal dementia.* Nat Rev Neurol. **8**(8): p. 423-34.
38. Simon, D., F. Hernandez, and J. Avila, *The involvement of cholinergic neurons in the spreading of tau pathology.* Front Neurol. **4**: p. 74.
39. Weingarten, M.D., et al., *A protein factor essential for microtubule assembly.* Proc Natl Acad Sci U S A, 1975. **72**(5): p. 1858-62.
40. Lee, G., N. Cowan, and M. Kirschner, *The primary structure and heterogeneity of tau protein from mouse brain.* Science, 1988. **239**(4837): p. 285-8.
41. Wang, Y., et al., *Tau fragmentation, aggregation and clearance: the dual role of lysosomal processing.* Hum Mol Genet, 2009. **18**(21): p. 4153-70.
42. Martin, L., X. Latypova, and F. Terro, *Post-translational modifications of tau protein: implications for Alzheimer's disease.* Neurochem Int. **58**(4): p. 458-71.

43. Ballatore, C., et al., *Microtubule stabilizing agents as potential treatment for Alzheimer's disease and related neurodegenerative tauopathies.* J Med Chem. **55**(21): p. 8979-96.
44. Avila, J., et al., *Role of tau protein in both physiological and pathological conditions.* Physiol Rev, 2004. **84**(2): p. 361-84.
45. Morris, M., et al., *The many faces of tau.* Neuron. **70**(3): p. 410-26.
46. Johnson, G.V. and W.H. Stoothoff, *Tau phosphorylation in neuronal cell function and dysfunction.* J Cell Sci, 2004. **117**(Pt 24): p. 5721-9.
47. Sultan, A., et al., *Nuclear tau, a key player in neuronal DNA protection.* J Biol Chem. **286**(6): p. 4566-75.
48. Biernat, J., et al., *Phosphorylation of Ser262 strongly reduces binding of tau to microtubules: distinction between PHF-like immunoreactivity and microtubule binding.* Neuron, 1993. **11**(1): p. 153-63.
49. Drewes, G., et al., *Microtubule-associated protein/microtubule affinity-regulating kinase (p110mark). A novel protein kinase that regulates tau-microtubule interactions and dynamic instability by phosphorylation at the Alzheimer-specific site serine 262.* J Biol Chem, 1995. **270**(13): p. 7679-88.
50. Biernat, J. and E.M. Mandelkow, *The development of cell processes induced by tau protein requires phosphorylation of serine 262 and 356 in the repeat domain and is inhibited by phosphorylation in the proline-rich domains.* Mol Biol Cell, 1999. **10**(3): p. 727-40.
51. Timm, T., et al., *Structure and regulation of MARK, a kinase involved in abnormal phosphorylation of Tau protein.* BMC Neurosci, 2008. **9 Suppl 2**: p. S9.
52. Litersky, J.M., et al., *Tau protein is phosphorylated by cyclic AMP-dependent protein kinase and calcium/calmodulin-dependent protein kinase II within its microtubule-binding domains at Ser-262 and Ser-356.* Biochem J, 1996. **316 (Pt 2)**: p. 655-60.
53. Scott, C.W., et al., *Phosphorylation of recombinant tau by cAMP-dependent protein kinase. Identification of phosphorylation sites and effect on microtubule assembly.* J Biol Chem, 1993. **268**(2): p. 1166-73.
54. Sironi, J.J., et al., *Ser-262 in human recombinant tau protein is a markedly more favorable site for phosphorylation by CaMKII than PKA or PhK.* FEBS Lett, 1998. **436**(3): p. 471-5.
55. Fanara, P., et al., *Changes in microtubule turnover accompany synaptic plasticity and memory formation in response to contextual fear conditioning in mice.* Neuroscience. **168**(1): p. 167-78.
56. Qiang, L., et al., *Tau protects microtubules in the axon from severing by katanin.* J Neurosci, 2006. **26**(12): p. 3120-9.
57. King, M.E., et al., *Tau-dependent microtubule disassembly initiated by prefibrillar beta-amyloid.* J Cell Biol, 2006. **175**(4): p. 541-6.
58. Takei, Y., et al., *Defects in axonal elongation and neuronal migration in mice with disrupted tau and map1b genes.* J Cell Biol, 2000. **150**(5): p. 989-1000.
59. Caceres, A., S. Potrebic, and K.S. Kosik, *The effect of tau antisense oligonucleotides on neurite formation of cultured cerebellar macroneurons.* J Neurosci, 1991. **11**(6): p. 1515-23.
60. Caceres, A. and K.S. Kosik, *Inhibition of neurite polarity by tau antisense oligonucleotides in primary cerebellar neurons.* Nature, 1990. **343**(6257): p. 461-3.

61. Harada, A., et al., *Altered microtubule organization in small-calibre axons of mice lacking tau protein.* Nature, 1994. **369**(6480): p. 488-91.
62. Dawson, H.N., et al., *Inhibition of neuronal maturation in primary hippocampal neurons from tau deficient mice.* J Cell Sci, 2001. **114**(Pt 6): p. 1179-87.
63. Sayas, C.L., J. Avila, and F. Wandosell, *Regulation of neuronal cytoskeleton by lysophosphatidic acid: role of GSK-3.* Biochim Biophys Acta, 2002. **1582**(1-3): p. 144-53.
64. Dixit, R., et al., *Differential regulation of dynein and kinesin motor proteins by tau.* Science, 2008. **319**(5866): p. 1086-9.
65. Ishihara, T., et al., *Age-dependent emergence and progression of a tauopathy in transgenic mice overexpressing the shortest human tau isoform.* Neuron, 1999. **24**(3): p. 751-62.
66. Tatebayashi, Y., et al., *Role of tau phosphorylation by glycogen synthase kinase-3beta in the regulation of organelle transport.* J Cell Sci, 2004. **117**(Pt 9): p. 1653-63.
67. Takashima, A., et al., *Presenilin 1 associates with glycogen synthase kinase-3beta and its substrate tau.* Proc Natl Acad Sci U S A, 1998. **95**(16): p. 9637-41.
68. Kampers, T., et al., *Assembly of paired helical filaments from mouse tau: implications for the neurofibrillary pathology in transgenic mouse models for Alzheimer's disease.* FEBS Lett, 1999. **451**(1): p. 39-44.
69. Ittner, L.M., et al., *Dendritic function of tau mediates amyloid-beta toxicity in Alzheimer's disease mouse models.* Cell. **142**(3): p. 387-97.
70. Reynolds, C.H., et al., *Phosphorylation regulates tau interactions with Src homology 3 domains of phosphatidylinositol 3-kinase, phospholipase Cgamma1, Grb2, and Src family kinases.* J Biol Chem, 2008. **283**(26): p. 18177-86.
71. Jenkins, S.M. and G.V. Johnson, *Tau complexes with phospholipase C-gamma in situ.* Neuroreport, 1998. **9**(1): p. 67-71.
72. Hwang, S.C., et al., *Activation of phospholipase C-gamma by the concerted action of tau proteins and arachidonic acid.* J Biol Chem, 1996. **271**(31): p. 18342-9.
73. Perez, M., et al., *Tau--an inhibitor of deacetylase HDAC6 function.* J Neurochem, 2009. **109**(6): p. 1756-66.
74. Barreda, E.G. and J. Avila, *Tau regulates the subcellular localization of calmodulin.* Biochem Biophys Res Commun. **408**(3): p. 500-4.
75. Rapoport, M., et al., *Tau is essential to beta -amyloid-induced neurotoxicity.* Proc Natl Acad Sci U S A, 2002. **99**(9): p. 6364-9.
76. Roberson, E.D., et al., *Reducing endogenous tau ameliorates amyloid beta-induced deficits in an Alzheimer's disease mouse model.* Science, 2007. **316**(5825): p. 750-4.
77. Gendron, T.F. and L. Petrucelli, *The role of tau in neurodegeneration.* Mol Neurodegener, 2009. **4**: p. 13.
78. Khlistunova, I., et al., *Inducible expression of Tau repeat domain in cell models of tauopathy: aggregation is toxic to cells but can be reversed by inhibitor drugs.* J Biol Chem, 2006. **281**(2): p. 1205-14.
79. Wittmann, C.W., et al., *Tauopathy in Drosophila: neurodegeneration without neurofibrillary tangles.* Science, 2001. **293**(5530): p. 711-4.
80. Engel, T., et al., *A mouse model to study tau pathology related with tau phosphorylation and assembly.* J Neurol Sci, 2007. **257**(1-2): p. 250-4.
81. Santacruz, K., et al., *Tau suppression in a neurodegenerative mouse model improves memory function.* Science, 2005. **309**(5733): p. 476-81.

82. Bretteville, A. and E. Planel, *Tau aggregates: toxic, inert, or protective species?* J Alzheimers Dis, 2008. **14**(4): p. 431-6.
83. Gura, T., *Hope in Alzheimer's fight emerges from unexpected places.* Nat Med, 2008. **14**(9): p. 894.
84. Wischik, C.M., et al., *Selective inhibition of Alzheimer disease-like tau aggregation by phenothiazines.* Proc Natl Acad Sci U S A, 1996. **93**(20): p. 11213-8.
85. Schirmer, R.H., et al., *"Lest we forget you--methylene blue...".* Neurobiol Aging. **32**(12): p. 2325 e7-16.
86. O'Leary, J.C., 3rd, et al., *Phenothiazine-mediated rescue of cognition in tau transgenic mice requires neuroprotection and reduced soluble tau burden.* Mol Neurodegener. **5**: p. 45.
87. Greenwood, J.A. and G.V. Johnson, *Localization and in situ phosphorylation state of nuclear tau.* Exp Cell Res, 1995. **220**(2): p. 332-7.
88. Liou, Y.C., et al., *Role of the prolyl isomerase Pin1 in protecting against age-dependent neurodegeneration.* Nature, 2003. **424**(6948): p. 556-61.
89. Steinhilb, M.L., et al., *S/P and T/P phosphorylation is critical for tau neurotoxicity in Drosophila.* J Neurosci Res, 2007. **85**(6): p. 1271-8.
90. Arrasate, M., M. Perez, and J. Avila, *Tau dephosphorylation at tau-1 site correlates with its association to cell membrane.* Neurochem Res, 2000. **25**(1): p. 43-50.
91. Cuchillo-Ibanez, I., et al., *Phosphorylation of tau regulates its axonal transport by controlling its binding to kinesin.* FASEB J, 2008. **22**(9): p. 3186-95.
92. Noble, W., et al., *Inhibition of glycogen synthase kinase-3 by lithium correlates with reduced tauopathy and degeneration in vivo.* Proc Natl Acad Sci U S A, 2005. **102**(19): p. 6990-5.
93. Peineau, S., et al., *LTP inhibits LTD in the hippocampus via regulation of GSK3beta.* Neuron, 2007. **53**(5): p. 703-17.
94. Kimura, T., et al., *GSK-3beta is required for memory reconsolidation in adult brain.* PLoS One, 2008. **3**(10): p. e3540.
95. Ciechanover, A., *Intracellular protein degradation: from a vague idea thru the lysosome and the ubiquitin-proteasome system and onto human diseases and drug targeting.* Cell Death Differ, 2005. **12**(9): p. 1178-90.
96. Rubinsztein, D.C., *The roles of intracellular protein-degradation pathways in neurodegeneration.* Nature, 2006. **443**(7113): p. 780-6.
97. Iqbal, K. and I. Grundke-Iqbal, *Ubiquitination and abnormal phosphorylation of paired helical filaments in Alzheimer's disease.* Mol Neurobiol, 1991. **5**(2-4): p. 399-410.
98. Iqbal, K., et al., *Mechanisms of neurofibrillary degeneration and the formation of neurofibrillary tangles.* J Neural Transm Suppl, 1998. **53**: p. 169-80.
99. Novak, P., M. Prcina, and E. Kontsekova, *Tauons and prions: infamous cousins?* J Alzheimers Dis. **26**(3): p. 413-30.
100. de Calignon, A., et al., *Caspase activation precedes and leads to tangles.* Nature. **464**(7292): p. 1201-4.
101. Claeysen, S., et al., *Alzheimer culprits: cellular crossroads and interplay.* Cell Signal. **24**(9): p. 1831-40.
102. Luan, K., J.L. Rosales, and K.Y. Lee, *Viewpoint: Crosstalks between neurofibrillary tangles and amyloid plaque formation.* Ageing Res Rev. **12**(1): p. 174-81.

103. Bates, K.A., et al., *Clearance mechanisms of Alzheimer's amyloid-beta peptide: implications for therapeutic design and diagnostic tests.* Mol Psychiatry, 2009. **14**(5): p. 469-86.
104. Tseng, B.P., et al., *Abeta inhibits the proteasome and enhances amyloid and tau accumulation.* Neurobiol Aging, 2008. **29**(11): p. 1607-18.
105. Oh, S., et al., *Amyloid peptide attenuates the proteasome activity in neuronal cells.* Mech Ageing Dev, 2005. **126**(12): p. 1292-9.
106. Shimura, H., et al., *CHIP-Hsc70 complex ubiquitinates phosphorylated tau and enhances cell survival.* J Biol Chem, 2004. **279**(6): p. 4869-76.
107. Garwood, C.J., et al., *Astrocytes are important mediators of Abeta-induced neurotoxicity and tau phosphorylation in primary culture.* Cell Death Dis. **2**: p. e167.
108. Dubey, M., et al., *Tau inhibits anterograde axonal transport and perturbs stability in growing axonal neurites in part by displacing kinesin cargo: neurofilaments attenuate tau-mediated neurite instability.* Cell Motil Cytoskeleton, 2008. **65**(2): p. 89-99.
109. Brandt, R., J. Leger, and G. Lee, *Interaction of tau with the neural plasma membrane mediated by tau's amino-terminal projection domain.* J Cell Biol, 1995. **131**(5): p. 1327-40.
110. Sharma, V.M., et al., *Tau impacts on growth-factor-stimulated actin remodeling.* J Cell Sci, 2007. **120**(Pt 5): p. 748-57.
111. Terry, R.D., et al., *Physical basis of cognitive alterations in Alzheimer's disease: synapse loss is the major correlate of cognitive impairment.* Ann Neurol, 1991. **30**(4): p. 572-80.
112. DeKosky, S.T. and S.W. Scheff, *Synapse loss in frontal cortex biopsies in Alzheimer's disease: correlation with cognitive severity.* Ann Neurol, 1990. **27**(5): p. 457-64.
113. Yoshiyama, Y., et al., *Synapse loss and microglial activation precede tangles in a P301S tauopathy mouse model.* Neuron, 2007. **53**(3): p. 337-51.
114. Eckermann, K., et al., *The beta-propensity of Tau determines aggregation and synaptic loss in inducible mouse models of tauopathy.* J Biol Chem, 2007. **282**(43): p. 31755-65.
115. Iqbal, K., et al., *Defective brain microtubule assembly in Alzheimer's disease.* Lancet, 1986. **2**(8504): p. 421-6.
116. Alonso, A.C., et al., *Role of abnormally phosphorylated tau in the breakdown of microtubules in Alzheimer disease.* Proc Natl Acad Sci U S A, 1994. **91**(12): p. 5562-6.
117. Alonso, A.D., et al., *Abnormal phosphorylation of tau and the mechanism of Alzheimer neurofibrillary degeneration: sequestration of microtubule-associated proteins 1 and 2 and the disassembly of microtubules by the abnormal tau.* Proc Natl Acad Sci U S A, 1997. **94**(1): p. 298-303.
118. Alonso, A.C., I. Grundke-Iqbal, and K. Iqbal, *Alzheimer's disease hyperphosphorylated tau sequesters normal tau into tangles of filaments and disassembles microtubules.* Nat Med, 1996. **2**(7): p. 783-7.
119. Butler, D., et al., *Microtubule-stabilizing agent prevents protein accumulation-induced loss of synaptic markers.* Eur J Pharmacol, 2007. **562**(1-2): p. 20-7.
120. Brunden, K.R., et al., *The characterization of microtubule-stabilizing drugs as possible therapeutic agents for Alzheimer's disease and related tauopathies.* Pharmacol Res. **63**(4): p. 341-51.

121. Brunden, K.R., et al., *Epothilone D improves microtubule density, axonal integrity, and cognition in a transgenic mouse model of tauopathy.* J Neurosci. **30**(41): p. 13861-6.
122. Divinski, I., et al., *Peptide neuroprotection through specific interaction with brain tubulin.* J Neurochem, 2006. **98**(3): p. 973-84.
123. Vulih-Shultzman, I., et al., *Activity-dependent neuroprotective protein snippet NAP reduces tau hyperphosphorylation and enhances learning in a novel transgenic mouse model.* J Pharmacol Exp Ther, 2007. **323**(2): p. 438-49.
124. Gozes, I., et al., *Addressing Alzheimer's disease tangles: from NAP to AL-108.* Curr Alzheimer Res, 2009. **6**(5): p. 455-60.
125. Vershinin, M., et al., *Multiple-motor based transport and its regulation by Tau.* Proc Natl Acad Sci U S A, 2007. **104**(1): p. 87-92.
126. Ebneth, A., et al., *Overexpression of tau protein inhibits kinesin-dependent trafficking of vesicles, mitochondria, and endoplasmic reticulum: implications for Alzheimer's disease.* J Cell Biol, 1998. **143**(3): p. 777-94.
127. Morel, M., et al., *Glycogen synthase kinase-3beta and the p25 activator of cyclin dependent kinase 5 increase pausing of mitochondria in neurons.* Neuroscience. **167**(4): p. 1044-56.
128. Ittner, L.M., Y.D. Ke, and J. Gotz, *Phosphorylated Tau interacts with c-Jun N-terminal kinase-interacting protein 1 (JIP1) in Alzheimer disease.* J Biol Chem, 2009. **284**(31): p. 20909-16.
129. Chen, B.S. and K.W. Roche, *Regulation of NMDA receptors by phosphorylation.* Neuropharmacology, 2007. **53**(3): p. 362-8.
130. De Felice, F.G., et al., *Abeta oligomers induce neuronal oxidative stress through an N-methyl-D-aspartate receptor-dependent mechanism that is blocked by the Alzheimer drug memantine.* J Biol Chem, 2007. **282**(15): p. 11590-601.
131. Karch, C.M., A.T. Jeng, and A.M. Goate, *Extracellular Tau levels are influenced by variability in Tau that is associated with tauopathies.* J Biol Chem. **287**(51): p. 42751-62.
132. Kalia, L.V., J.R. Gingrich, and M.W. Salter, *Src in synaptic transmission and plasticity.* Oncogene, 2004. **23**(48): p. 8007-16.
133. Chin, J., et al., *Fyn kinase induces synaptic and cognitive impairments in a transgenic mouse model of Alzheimer's disease.* J Neurosci, 2005. **25**(42): p. 9694-703.
134. Chin, J., et al., *Fyn kinase modulates synaptotoxicity, but not aberrant sprouting, in human amyloid precursor protein transgenic mice.* J Neurosci, 2004. **24**(19): p. 4692-7.
135. Moreno, H., et al., *Blocking Effects of Human Tau on Squid Giant Synapse Transmission and Its Prevention by T-817 MA.* Front Synaptic Neurosci. **3**: p. 3.
136. Jucker, M. and L.C. Walker, *Pathogenic protein seeding in Alzheimer disease and other neurodegenerative disorders.* Ann Neurol. **70**(4): p. 532-40.
137. Rhein, V., et al., *Amyloid-beta and tau synergistically impair the oxidative phosphorylation system in triple transgenic Alzheimer's disease mice.* Proc Natl Acad Sci U S A, 2009. **106**(47): p. 20057-62.
138. Coppede, F. and L. Migliore, *DNA damage and repair in Alzheimer's disease.* Curr Alzheimer Res, 2009. **6**(1): p. 36-47.
139. Rutten, B.P., et al., *The aging brain: accumulation of DNA damage or neuron loss?* Neurobiol Aging, 2007. **28**(1): p. 91-8.
140. Vossel, K.A., et al., *Tau reduction prevents Abeta-induced defects in axonal transport.* Science. **330**(6001): p. 198.

141. Holmes, B.B. and M.I. Diamond, *Cellular mechanisms of protein aggregate propagation.* Curr Opin Neurol. **25**(6): p. 721-6.
142. Cushman, M., et al., *Prion-like disorders: blurring the divide between transmissibility and infectivity.* J Cell Sci. **123**(Pt 8): p. 1191-201.
143. Pooler, A.M., et al., *Physiological release of endogenous tau is stimulated by neuronal activity.* EMBO Rep. **14**(4): p. 389-94.
144. Kfoury, N., et al., *Trans-cellular propagation of Tau aggregation by fibrillar species.* J Biol Chem. **287**(23): p. 19440-51.
145. Pooler, A.M., et al., *Dynamic association of tau with neuronal membranes is regulated by phosphorylation.* Neurobiol Aging. **33**(2): p. 431 e27-38.
146. Rajendran, L., et al., *Alzheimer's disease beta-amyloid peptides are released in association with exosomes.* Proc Natl Acad Sci U S A, 2006. **103**(30): p. 11172-7.
147. Emmanouilidou, E., et al., *Cell-produced alpha-synuclein is secreted in a calcium-dependent manner by exosomes and impacts neuronal survival.* J Neurosci. **30**(20): p. 6838-51.
148. Fevrier, B., et al., *Cells release prions in association with exosomes.* Proc Natl Acad Sci U S A, 2004. **101**(26): p. 9683-8.
149. Saman, S., et al., *Exosome-associated tau is secreted in tauopathy models and is selectively phosphorylated in cerebrospinal fluid in early Alzheimer disease.* J Biol Chem. **287**(6): p. 3842-9.
150. Wang, W., et al., *Immunotherapy for Alzheimer's disease.* Acta Biochim Biophys Sin (Shanghai). **44**(10): p. 807-14.
151. Asuni, A.A., et al., *Immunotherapy targeting pathological tau conformers in a tangle mouse model reduces brain pathology with associated functional improvements.* J Neurosci, 2007. **27**(34): p. 9115-29.
152. Boutajangout, A., D. Quartermain, and E.M. Sigurdsson, *Immunotherapy targeting pathological tau prevents cognitive decline in a new tangle mouse model.* J Neurosci. **30**(49): p. 16559-66.
153. Rosenmann, H., et al., *Tauopathy-like abnormalities and neurologic deficits in mice immunized with neuronal tau protein.* Arch Neurol, 2006. **63**(10): p. 1459-67.
154. Miller, Y., B. Ma, and R. Nussinov, *Synergistic interactions between repeats in tau protein and Abeta amyloids may be responsible for accelerated aggregation via polymorphic states.* Biochemistry. **50**(23): p. 5172-81.
155. Guo, J.P., et al., *Abeta and tau form soluble complexes that may promote self aggregation of both into the insoluble forms observed in Alzheimer's disease.* Proc Natl Acad Sci U S A, 2006. **103**(6): p. 1953-8.
156. Giasson, B.I., et al., *Initiation and synergistic fibrillization of tau and alpha-synuclein.* Science, 2003. **300**(5619): p. 636-40.
157. Lee, V.M., T.K. Kenyon, and J.Q. Trojanowski, *Transgenic animal models of tauopathies.* Biochim Biophys Acta, 2005. **1739**(2-3): p. 251-9.
158. Lewis, J., et al., *Neurofibrillary tangles, amyotrophy and progressive motor disturbance in mice expressing mutant (P301L) tau protein.* Nat Genet, 2000. **25**(4): p. 402-5.
159. Takeuchi, H., et al., *P301S mutant human tau transgenic mice manifest early symptoms of human tauopathies with dementia and altered sensorimotor gating.* PLoS One. **6**(6): p. e21050.

160. Oddo, S., et al., *Triple-transgenic model of Alzheimer's disease with plaques and tangles: intracellular Abeta and synaptic dysfunction.* Neuron, 2003. **39**(3): p. 409-21.
161. Santana, S., E.P. Rico, and J.S. Burgos, *Can zebrafish be used as animal model to study Alzheimer's disease?* Am J Neurodegener Dis. **1**(1): p. 32-48.
162. Trojanowski, J.Q. and V.M. Lee, *Transgenic models of tauopathies and synucleinopathies.* Brain Pathol, 1999. **9**(4): p. 733-9.
163. Lee, S.J., et al., *Protein aggregate spreading in neurodegenerative diseases: problems and perspectives.* Neurosci Res. **70**(4): p. 339-48.
164. Noble, W., D.P. Hanger, and J.M. Gallo, *Transgenic mouse models of tauopathy in drug discovery.* CNS Neurol Disord Drug Targets. **9**(4): p. 403-28.
165. Guo, J.L. and V.M. Lee, *Seeding of normal Tau by pathological Tau conformers drives pathogenesis of Alzheimer-like tangles.* J Biol Chem. **286**(17): p. 15317-31.
166. Marreiros, R.M.G., *Validation of Tau aggregation model in HEK cells and cortical rat neurons.* Tese de Mestrado em Biologia Cellular e Molecular, Universidade de Coimbra, 2013.
167. Calafate, S.S.C., *Tauopathy seeding models as a platform for Tau aggregation and clearance study.* Tese de Mestrado em Biologia Cellular e Molecular, Universidade de Coimbra, 2012.
168. McClellan, A.J., et al., *Protein quality control: chaperones culling corrupt conformations.* Nat Cell Biol, 2005. **7**(8): p. 736-41.
169. Eletr, Z.M. and K.D. Wilkinson, *Regulation of proteolysis by human deubiquitinating enzymes.* Biochim Biophys Acta. **1843**(1): p. 114-28.
170. Stanisic, V., et al., *OTU Domain-containing ubiquitin aldehyde-binding protein 1 (OTUB1) deubiquitinates estrogen receptor (ER) alpha and affects ERalpha transcriptional activity.* J Biol Chem, 2009. **284**(24): p. 16135-45.
171. Dayal, S., et al., *Suppression of the deubiquitinating enzyme USP5 causes the accumulation of unanchored polyubiquitin and the activation of p53.* J Biol Chem, 2009. **284**(8): p. 5030-41.
172. Dickey, C.A., et al., *Deletion of the ubiquitin ligase CHIP leads to the accumulation, but not the aggregation, of both endogenous phospho- and caspase-3-cleaved tau species.* J Neurosci, 2006. **26**(26): p. 6985-96.
173. Tan, J.M., et al., *Lysine 63-linked ubiquitination promotes the formation and autophagic clearance of protein inclusions associated with neurodegenerative diseases.* Hum Mol Genet, 2008. **17**(3): p. 431-9.
174. Salminen, A., et al., *Hsp90 regulates tau pathology through co-chaperone complexes in Alzheimer's disease.* Prog Neurobiol. **93**(1): p. 99-110.
175. Sahara, N., et al., *In vivo evidence of CHIP up-regulation attenuating tau aggregation.* J Neurochem, 2005. **94**(5): p. 1254-63.
176. David, D.C., et al., *Proteasomal degradation of tau protein.* J Neurochem, 2002. **83**(1): p. 176-85.
177. Lee, B.H., et al., *Enhancement of proteasome activity by a small-molecule inhibitor of USP14.* Nature. **467**(7312): p. 179-84.
178. Han, K.J., et al., *Ubiquitin-specific protease 9x deubiquitinates and stabilizes the spinal muscular atrophy protein-survival motor neuron.* J Biol Chem. **287**(52): p. 43741-52.
179. Rott, R., et al., *alpha-Synuclein fate is determined by USP9X-regulated monoubiquitination.* Proc Natl Acad Sci U S A. **108**(46): p. 18666-71.

180. Luo, W., et al., *Roles of heat-shock protein 90 in maintaining and facilitating the neurodegenerative phenotype in tauopathies.* Proc Natl Acad Sci U S A, 2007. **104**(22): p. 9511-6.
181. Dang, L.C., F.D. Melandri, and R.L. Stein, *Kinetic and mechanistic studies on the hydrolysis of ubiquitin C-terminal 7-amido-4-methylcoumarin by deubiquitinating enzymes.* Biochemistry, 1998. **37**(7): p. 1868-79.
182. Reyes-Turcu, F.E., K.H. Ventii, and K.D. Wilkinson, *Regulation and cellular roles of ubiquitin-specific deubiquitinating enzymes.* Annu Rev Biochem, 2009. **78**: p. 363-97.
183. Reyes-Turcu, F.E., et al., *The ubiquitin binding domain ZnF UBP recognizes the C-terminal diglycine motif of unanchored ubiquitin.* Cell, 2006. **124**(6): p. 1197-208.
184. Fan, X., et al., *Drosophila USP5 controls the activation of apoptosis and the Jun N-terminal kinase pathway during eye development.* PLoS One. **9**(3): p. e92250.
185. Nakajima, S., et al., *Ubiquitin-specific protease 5 is required for the efficient repair of DNA double-strand breaks.* PLoS One. **9**(1): p. e84899.
186. Yoshioka, Y., et al., *Ubiquitin-specific peptidase 5, a target molecule of vialinin A, is a key molecule of TNF-alpha production in RBL-2H3 cells.* PLoS One. **8**(12): p. e80931.
187. Nicholson, B. and K.G. Suresh Kumar, *The multifaceted roles of USP7: new therapeutic opportunities.* Cell Biochem Biophys. **60**(1-2): p. 61-8.
188. Huang, Z., et al., *Deubiquitylase HAUSP stabilizes REST and promotes maintenance of neural progenitor cells.* Nat Cell Biol. **13**(2): p. 142-52.
189. Huang, Z., W. Zhou, and S. Bao, *Role of deubiquitylase HAUSP in stem cell maintenance.* Cell Cycle. **10**(8): p. 1182-3.
190. Xu, P., et al., *JNK regulates FoxO-dependent autophagy in neurons.* Genes Dev. **25**(4): p. 310-22.
191. Marino, G. and C. Lopez-Otin, *Autophagy: molecular mechanisms, physiological functions and relevance in human pathology.* Cell Mol Life Sci, 2004. **61**(12): p. 1439-54.
192. Wiener, R., et al., *The mechanism of OTUB1-mediated inhibition of ubiquitination.* Nature. **483**(7391): p. 618-22.
193. Levine, B. and G. Kroemer, *Autophagy in the pathogenesis of disease.* Cell, 2008. **132**(1): p. 27-42.
194. Stevens, J.B., et al., *Heterogeneity of cell death.* Cytogenet Genome Res. **139**(3): p. 164-73.
195. Cao, Y. and D.J. Klionsky, *Physiological functions of Atg6/Beclin 1: a unique autophagy-related protein.* Cell Res, 2007. **17**(10): p. 839-49.
196. Li, L., X. Zhang, and W. Le, *Autophagy dysfunction in Alzheimer's disease.* Neurodegener Dis. **7**(4): p. 265-71.
197. Kruger, U., et al., *Autophagic degradation of tau in primary neurons and its enhancement by trehalose.* Neurobiol Aging. **33**(10): p. 2291-305.
198. Hamano, T., et al., *Autophagic-lysosomal perturbation enhances tau aggregation in transfectants with induced wild-type tau expression.* Eur J Neurosci, 2008. **27**(5): p. 1119-30.
199. Kaushik, S., et al., *Chaperone-mediated autophagy at a glance.* J Cell Sci. **124**(Pt 4): p. 495-9.
200. Ferreira, J.V., et al., *STUB1/CHIP is required for HIF1A degradation by chaperone-mediated autophagy.* Autophagy, 2013.

201. Wright, S.P., *Adjusted P-Values for Simultaneous Inference* Biometrics, 1992: p. 1005-1013.
202. Westfall, P.H., et al., *Multiple Comparisons and Multiple Tests Text and Workbook Set*. 2000: SAS Publishing.
203. Luk, K.C., et al., *Exogenous alpha-synuclein fibrils seed the formation of Lewy body-like intracellular inclusions in cultured cells.* Proc Natl Acad Sci U S A, 2009. **106**(47): p. 20051-6.
204. Hanisch, K., et al., *Analysis of human tau in cerebrospinal fluid.* J Proteome Res. **9**(3): p. 1476-82.
205. Teng, J., et al., *Synergistic effects of MAP2 and MAP1B knockout in neuronal migration, dendritic outgrowth, and microtubule organization.* J Cell Biol, 2001. **155**(1): p. 65-76.
206. Augustinack, J.C., et al., *Specific tau phosphorylation sites correlate with severity of neuronal cytopathology in Alzheimer's disease.* Acta Neuropathol, 2002. **103**(1): p. 26-35.
207. Blazquez-Llorca, L., V. Garcia-Marin, and J. Defelipe, *Pericellular innervation of neurons expressing abnormally hyperphosphorylated tau in the hippocampal formation of Alzheimer's disease patients.* Front Neuroanat. **4**: p. 20.
208. Zhang, Y.H., et al., *Recombinant Apoptin multimers kill tumor cells but are nontoxic and epitope-shielded in a normal-cell-specific fashion.* Exp Cell Res, 2003. **289**(1): p. 36-46.
209. Gonzalez-Arenas, A., et al., *Expression pattern of Tau in the rat brain during pregnancy and the beginning of lactation.* Brain Res Bull. **89**(3-4): p. 108-14.
210. McMillan, P., et al., *Tau isoform regulation is region- and cell-specific in mouse brain.* J Comp Neurol, 2008. **511**(6): p. 788-803.
211. Whiteman, I.T., et al., *Activated actin-depolymerizing factor/cofilin sequesters phosphorylated microtubule-associated protein during the assembly of alzheimer-like neuritic cytoskeletal striations.* J Neurosci, 2009. **29**(41): p. 12994-3005.
212. Clavaguera, F., et al., *Transmission and spreading of tauopathy in transgenic mouse brain.* Nat Cell Biol, 2009. **11**(7): p. 909-13.
213. Ebrahimi-Fakhari, D., L. Wahlster, and P.J. McLean, *Protein degradation pathways in Parkinson's disease: curse or blessing.* Acta Neuropathol. **124**(2): p. 153-72.
214. Chesser, A.S., S.M. Pritchard, and G.V. Johnson, *Tau clearance mechanisms and their possible role in the pathogenesis of Alzheimer disease.* Front Neurol. **4**: p. 122.
215. Keck, S., et al., *Proteasome inhibition by paired helical filament-tau in brains of patients with Alzheimer's disease.* J Neurochem, 2003. **85**(1): p. 115-22.
216. Dickey, C.A., et al., *Pharmacologic reductions of total tau levels; implications for the role of microtubule dynamics in regulating tau expression.* Mol Neurodegener, 2006. **1**: p. 6.
217. Rodriguez-Navarro, J.A., et al., *Trehalose ameliorates dopaminergic and tau pathology in parkin deleted/tau overexpressing mice through autophagy activation.* Neurobiol Dis. **39**(3): p. 423-38.
218. Tan, C.C., et al., *Autophagy in aging and neurodegenerative diseases: implications for pathogenesis and therapy.* Neurobiol Aging. **35**(5): p. 941-57.
219. Ren, Q.G., et al., *Effects of tau phosphorylation on proteasome activity.* FEBS Lett, 2007. **581**(7): p. 1521-8.

220. Wang, Y., et al., *Synergy and antagonism of macroautophagy and chaperone-mediated autophagy in a cell model of pathological tau aggregation.* Autophagy. **6**(1): p. 182-3.
221. Lee, M.J., J.H. Lee, and D.C. Rubinsztein, *Tau degradation: the ubiquitin-proteasome system versus the autophagy-lysosome system.* Prog Neurobiol. **105**: p. 49-59.
222. Cardozo, C. and C. Michaud, *Proteasome-mediated degradation of tau proteins occurs independently of the chymotrypsin-like activity by a nonprocessive pathway.* Arch Biochem Biophys, 2002. **408**(1): p. 103-10.
223. Zhang, J.Y., et al., *Microtubule-associated protein tau is a substrate of ATP/Mg(2+)-dependent proteasome protease system.* J Neural Transm, 2005. **112**(4): p. 547-55.
224. Lee, D.H. and A.L. Goldberg, *Selective inhibitors of the proteasome-dependent and vacuolar pathways of protein degradation in Saccharomyces cerevisiae.* J Biol Chem, 1996. **271**(44): p. 27280-4.
225. Ge, P.F., et al., *Inhibition of autophagy induced by proteasome inhibition increases cell death in human SHG-44 glioma cells.* Acta Pharmacol Sin, 2009. **30**(7): p. 1046-52.
226. Boland, B., et al., *Autophagy induction and autophagosome clearance in neurons: relationship to autophagic pathology in Alzheimer's disease.* J Neurosci, 2008. **28**(27): p. 6926-37.
227. Yew, E.H., et al., *Proteasome inhibition by lactacystin in primary neuronal cells induces both potentially neuroprotective and pro-apoptotic transcriptional responses: a microarray analysis.* J Neurochem, 2005. **94**(4): p. 943-56.
228. Garat, C.V., et al., *Platelet-derived growth factor BB induces nuclear export and proteasomal degradation of CREB via phosphatidylinositol 3-kinase/Akt signaling in pulmonary artery smooth muscle cells.* Mol Cell Biol, 2006. **26**(13): p. 4934-48.
229. Droggiti, A., et al., *Targeted disruption of neuronal 19S proteasome subunits induces the formation of ubiquitinated inclusions in the absence of cell death.* J Neurochem. **119**(3): p. 630-43.
230. Liu, J., et al., *Proteasome inhibitor MG132 enhances the antigrowth and antimetastasis effects of radiation in human nonsmall cell lung cancer cells.* Tumour Biol.
231. Fletcher, L., et al., *Rapamycin treatment improves neuron viability in an in vitro model of stroke.* PLoS One. **8**(7): p. e68281.
232. Hershko, A. and A. Ciechanover, *The ubiquitin system.* Annu Rev Biochem, 1998. **67**: p. 425-79.
233. Meiners, S., et al., *Ubiquitin-proteasome pathway as a new target for the prevention of restenosis.* Circulation, 2002. **105**(4): p. 483-9.
234. Tydlacka, S., et al., *Differential activities of the ubiquitin-proteasome system in neurons versus glia may account for the preferential accumulation of misfolded proteins in neurons.* J Neurosci, 2008. **28**(49): p. 13285-95.
235. Barth, S., D. Glick, and K.F. Macleod, *Autophagy: assays and artifacts.* J Pathol. **221**(2): p. 117-24.
236. Hyman, B.T., et al., *National Institute on Aging-Alzheimer's Association guidelines for the neuropathologic assessment of Alzheimer's disease.* Alzheimers Dement. **8**(1): p. 1-13.

237. Davis, K.L. and A.C. Neuropsychopharmacology, *Neuropsychopharmacology: The Fifth Generation of Progress : an Official Publication of the American College of Neuropsychopharmacology*. 2002: Lippincott Williams & Wilkins.
238. Hoover, B.R., et al., *Tau mislocalization to dendritic spines mediates synaptic dysfunction independently of neurodegeneration.* Neuron. **68**(6): p. 1067-81.
239. Cochran, J.N., A.M. Hall, and E.D. Roberson, *The dendritic hypothesis for Alzheimer's disease pathophysiology.* Brain Res Bull. **103**: p. 18-28.
240. Santa-Maria, I., et al., *Paired helical filaments from Alzheimer disease brain induce intracellular accumulation of Tau protein in aggresomes.* J Biol Chem. **287**(24): p. 20522-33.
241. Jo, C., et al., *Nrf2 reduces levels of phosphorylated tau protein by inducing autophagy adaptor protein NDP52.* Nat Commun. **5**: p. 3496.
242. Guzman-Martinez, L., G.A. Farias, and R.B. Maccioni, *Tau oligomers as potential targets for Alzheimer's diagnosis and novel drugs.* Front Neurol. **4**: p. 167.
243. Cowan, C.M., S. Quraishe, and A. Mudher, *What is the pathological significance of tau oligomers?* Biochem Soc Trans. **40**(4): p. 693-7.
244. Eisenberg, D. and M. Jucker, *The amyloid state of proteins in human diseases.* Cell. **148**(6): p. 1188-203.
245. Friedhoff, P., et al., *Rapid assembly of Alzheimer-like paired helical filaments from microtubule-associated protein tau monitored by fluorescence in solution.* Biochemistry, 1998. **37**(28): p. 10223-30.
246. Braak, H. and E. Braak, *Neuropathological stageing of Alzheimer-related changes.* Acta Neuropathol, 1991. **82**(4): p. 239-59.
247. Mohamed, N.V., et al., *Spreading of tau pathology in Alzheimer's disease by cell-to-cell transmission.* Eur J Neurosci. **37**(12): p. 1939-48.
248. Millet, L.J. and M.U. Gillette, *Over a century of neuron culture: from the hanging drop to microfluidic devices.* Yale J Biol Med. **85**(4): p. 501-21.
249. Ioannou, M.S. and A.L. Marat, *The role of EHD proteins at the neuronal synapse.* Sci Signal. **5**(221): p. jc1.
250. Lee, S.J., et al., *Cell-to-cell transmission of non-prion protein aggregates.* Nat Rev Neurol. **6**(12): p. 702-6.
251. Ichikawa, M., et al., *Formation and maturation of synapses in primary cultures of rat cerebral cortical cells: an electron microscopic study.* Neurosci Res, 1993. **16**(2): p. 95-103.
252. Guillozet, A.L., et al., *Neurofibrillary tangles, amyloid, and memory in aging and mild cognitive impairment.* Arch Neurol, 2003. **60**(5): p. 729-36.
253. Roberson, E.D., et al., *Amyloid-beta/Fyn-induced synaptic, network, and cognitive impairments depend on tau levels in multiple mouse models of Alzheimer's disease.* J Neurosci. **31**(2): p. 700-11.
254. Sorokin, A.V., E.R. Kim, and L.P. Ovchinnikov, *Proteasome system of protein degradation and processing.* Biochemistry (Mosc), 2009. **74**(13): p. 1411-42.
255. Opattova, A., et al., *Intracellular degradation of misfolded tau protein induced by geldanamycin is associated with activation of proteasome.* J Alzheimers Dis. **33**(2): p. 339-48.
256. Lasagna-Reeves, C.A., et al., *Identification of oligomers at early stages of tau aggregation in Alzheimer's disease.* FASEB J. **26**(5): p. 1946-59.
257. Bence, N.F., R.M. Sampat, and R.R. Kopito, *Impairment of the ubiquitin-proteasome system by protein aggregation.* Science, 2001. **292**(5521): p. 1552-5.

258. Pickford, F., et al., *The autophagy-related protein beclin 1 shows reduced expression in early Alzheimer disease and regulates amyloid beta accumulation in mice.* J Clin Invest, 2008. **118**(6): p. 2190-9.
259. Nixon, R.A., et al., *Extensive involvement of autophagy in Alzheimer disease: an immuno-electron microscopy study.* J Neuropathol Exp Neurol, 2005. **64**(2): p. 113-22.
260. Frost, B., R.L. Jacks, and M.I. Diamond, *Propagation of tau misfolding from the outside to the inside of a cell.* J Biol Chem, 2009. **284**(19): p. 12845-52.
261. Wu, J.W., et al., *Small misfolded Tau species are internalized via bulk endocytosis and anterogradely and retrogradely transported in neurons.* J Biol Chem. **288**(3): p. 1856-70.
262. Boya, P., *Lysosomal function and dysfunction: mechanism and disease.* Antioxid Redox Signal. **17**(5): p. 766-74.
263. Freeman, D., et al., *Alpha-synuclein induces lysosomal rupture and cathepsin dependent reactive oxygen species following endocytosis.* PLoS One. **8**(4): p. e62143.
264. Jones, E.M., et al., *Interaction of tau protein with model lipid membranes induces tau structural compaction and membrane disruption.* Biochemistry. **51**(12): p. 2539-50.
265. Zhao, Y. and B. Zhao, *Oxidative stress and the pathogenesis of Alzheimer's disease.* Oxid Med Cell Longev. **2013**: p. 316523.
266. Dolan, P.J. and G.V. Johnson, *A caspase cleaved form of tau is preferentially degraded through the autophagy pathway.* J Biol Chem. **285**(29): p. 21978-87.
267. Wong, E.S., et al., *Autophagy-mediated clearance of aggresomes is not a universal phenomenon.* Hum Mol Genet, 2008. **17**(16): p. 2570-82.
268. Pasquini, L.A., et al., *Lactacystin, a specific inhibitor of the proteasome, induces apoptosis and activates caspase-3 in cultured cerebellar granule cells.* J Neurosci Res, 2000. **59**(5): p. 601-11.
269. Yamada, Y., et al., *Lactacystin activates FLICE (caspase 8) protease and induces apoptosis in Fas-resistant adult T-cell leukemia cell lines.* Eur J Haematol, 2000. **64**(5): p. 315-22.
270. Fasulo, L., et al., *The neuronal microtubule-associated protein tau is a substrate for caspase-3 and an effector of apoptosis.* J Neurochem, 2000. **75**(2): p. 624-33.
271. Gamblin, T.C., et al., *Caspase cleavage of tau: linking amyloid and neurofibrillary tangles in Alzheimer's disease.* Proc Natl Acad Sci U S A, 2003. **100**(17): p. 10032-7.
272. Chung, C.W., et al., *Proapoptotic effects of tau cleavage product generated by caspase-3.* Neurobiol Dis, 2001. **8**(1): p. 162-72.
273. Horowitz, P.M., et al., *Early N-terminal changes and caspase-6 cleavage of tau in Alzheimer's disease.* J Neurosci, 2004. **24**(36): p. 7895-902.
274. Feuillette, S., et al., *Tau is not normally degraded by the proteasome.* J Neurosci Res, 2005. **80**(3): p. 400-5.
275. Cui, W., et al., *Potential role for Nrf2 activation in the therapeutic effect of MG132 on diabetic nephropathy in OVE26 diabetic mice.* Am J Physiol Endocrinol Metab. **304**(1): p. E87-99.
276. Salih, D.A. and A. Brunet, *FoxO transcription factors in the maintenance of cellular homeostasis during aging.* Curr Opin Cell Biol, 2008. **20**(2): p. 126-36.
277. Ozcelik, S., et al., *Rapamycin attenuates the progression of tau pathology in P301S tau transgenic mice.* PLoS One. **8**(5): p. e62459.

278. Majumder, S., et al., *Inducing autophagy by rapamycin before, but not after, the formation of plaques and tangles ameliorates cognitive deficits.* PLoS One. **6**(9): p. e25416.
279. Jung, C.H., et al., *mTOR regulation of autophagy.* FEBS Lett. **584**(7): p. 1287-95.
280. Hariharan, N., P. Zhai, and J. Sadoshima, *Oxidative stress stimulates autophagic flux during ischemia/reperfusion.* Antioxid Redox Signal. **14**(11): p. 2179-90.
281. Stamer, K., et al., *Tau blocks traffic of organelles, neurofilaments, and APP vesicles in neurons and enhances oxidative stress.* J Cell Biol, 2002. **156**(6): p. 1051-63.
282. Yan, S.D., et al., *Glycated tau protein in Alzheimer disease: a mechanism for induction of oxidant stress.* Proc Natl Acad Sci U S A, 1994. **91**(16): p. 7787-91.
283. Jacinto, E. and A. Lorberg, *TOR regulation of AGC kinases in yeast and mammals.* Biochem J, 2008. **410**(1): p. 19-37.
284. Rodrik-Outmezguine, V.S., et al., *mTOR kinase inhibition causes feedback-dependent biphasic regulation of AKT signaling.* Cancer Discov. **1**(3): p. 248-59.
285. Vigneron, F., et al., *GSK-3beta at the crossroads in the signalling of heart preconditioning: implication of mTOR and Wnt pathways.* Cardiovasc Res. **90**(1): p. 49-56.
286. Vaysberg, M., et al., *Rapamycin inhibits proliferation of Epstein-Barr virus-positive B-cell lymphomas through modulation of cell-cycle protein expression.* Transplantation, 2007. **83**(8): p. 1114-21.
287. Li, X., et al., *Mammalian target of rapamycin inhibition in macrophages of asymptomatic HIV+ persons reverses the decrease in TLR-4-mediated TNF-alpha release through prolongation of MAPK pathway activation.* J Immunol. **187**(11): p. 6052-8.
288. Meske, V., F. Albert, and T.G. Ohm, *Coupling of mammalian target of rapamycin with phosphoinositide 3-kinase signaling pathway regulates protein phosphatase 2A- and glycogen synthase kinase-3 -dependent phosphorylation of Tau.* J Biol Chem, 2008. **283**(1): p. 100-9.
289. C, O.N., *PI3-kinase/Akt/mTOR signaling: impaired on/off switches in aging, cognitive decline and Alzheimer's disease.* Exp Gerontol. **48**(7): p. 647-53.
290. Nemoto, T., et al., *Homologous posttranscriptional regulation of insulin-like growth factor-I receptor level via glycogen synthase kinase-3beta and mammalian target of rapamycin in adrenal chromaffin cells: effect on tau phosphorylation.* Neuropharmacology. **58**(7): p. 1097-108.
291. Liu, Y., et al., *Rapamycin decreases tau phosphorylation at Ser214 through regulation of cAMP-dependent kinase.* Neurochem Int. **62**(4): p. 458-67.
292. Ma, Y.Q., D.K. Wu, and J.K. Liu, *mTOR and tau phosphorylated proteins in the hippocampal tissue of rats with type 2 diabetes and Alzheimer's disease.* Mol Med Rep. **7**(2): p. 623-7.
293. Perez, M., et al., *Chronic lithium treatment decreases mutant tau protein aggregation in a transgenic mouse model.* J Alzheimers Dis, 2003. **5**(4): p. 301-8.
294. Seo, H., et al., *Proteasome activator enhances survival of Huntington's disease neuronal model cells.* PLoS One, 2007. **2**(2): p. e238.
295. Edelmann, M.J., et al., *Structural basis and specificity of human otubain 1-mediated deubiquitination.* Biochem J, 2009. **418**(2): p. 379-90.

296. Cripps, D., et al., *Alzheimer disease-specific conformation of hyperphosphorylated paired helical filament-Tau is polyubiquitinated through Lys-48, Lys-11, and Lys-6 ubiquitin conjugation.* J Biol Chem, 2006. **281**(16): p. 10825-38.
297. Sun, X.X., K.B. Challagundla, and M.S. Dai, *Positive regulation of p53 stability and activity by the deubiquitinating enzyme Otubain 1.* EMBO J. **31**(3): p. 576-92.
298. Sun, X.X. and M.S. Dai, *Deubiquitinating enzyme regulation of the p53 pathway: A lesson from Otub1.* World J Biol Chem. **5**(2): p. 75-84.
299. Shan, T.L., et al., *Partial molecular cloning, characterization, and analysis of the subcellular localization and expression patterns of the porcine OTUB1 gene.* Mol Biol Rep, 2009. **36**(6): p. 1573-7.
300. Maiuri, M.C., et al., *Autophagy regulation by p53.* Curr Opin Cell Biol. **22**(2): p. 181-5.
301. Zhang, Y.H., et al., *Domain analysis reveals that a deubiquitinating enzyme USP13 performs non-activating catalysis for Lys63-linked polyubiquitin.* PLoS One. **6**(12): p. e29362.
302. Zhang, X., et al., *Tumor-suppressor PTEN affects tau phosphorylation, aggregation, and binding to microtubules.* FASEB J, 2006. **20**(8): p. 1272-4.
303. Hooper, C., et al., *p53 is upregulated in Alzheimer's disease and induces tau phosphorylation in HEK293a cells.* Neurosci Lett, 2007. **418**(1): p. 34-7.
304. Ramakrishnan, P., D.W. Dickson, and P. Davies, *Pin1 colocalization with phosphorylated tau in Alzheimer's disease and other tauopathies.* Neurobiol Dis, 2003. **14**(2): p. 251-64.
305. Lim, J., et al., *Pin1 has opposite effects on wild-type and P301L tau stability and tauopathy.* J Clin Invest, 2008. **118**(5): p. 1877-89.